Performance Investigation of Integrated Gasification Combined Cycle Power Plant for Polygeneration

zur Erlangung des akademischen Grades Doktor–Ingenieur (Dr.-Ing.)
Genehmigte Dissertation von M.Eng. Ammar Ahmad Jamil Bany Ata
aus Ajloun, Jordanien
Tag der Einreichung: 22.10.2021, Tag der Prüfung: 01.02.2022

1. Gutachten: Prof. Dr.-Ing. Bernd Epple
2. Gutachten: Prof. Dr.-Ing. habil. Andreas Richter
Darmstadt

TECHNISCHE UNIVERSITÄT DARMSTADT

Mechanical Engineering Department

Institute for Energy Systems and Technology

TECHNISCHE UNIVERSITÄT DARMSTADT

Performance Investigation of Integrated Gasification Combined Cycle Power Plant for Polygeneration

Vom Fachbereich Maschinenbau
an der Technischen Universität Darmstadt
zur
Erlangung des akademischen Grades
Doktor–Ingenieur (Dr.-Ing.)

Genehmigte

D I S S E R T A T I O N

von

M.Eng. Ammar Ahmad Jamil Bany Ata

aus Ajloun, Jordanien

Erstgutachter:	Prof. Dr.-Ing. Bernd Epple
Zweitgutachter:	Prof. Dr.-Ing. habil. Andreas Richter
Tag der Prüfung:	01.02.2022

Darmstadt 2021

D 17

Performance Investigation of Integrated Gasification Combined Cycle Power Plant for Polygeneration

Genehmigte Dissertation von M.Eng. Ammar Ahmad Jamil Bany Ata

Erstgutachter:	Prof. Dr.-Ing. Bernd Epple
Zweitgutachter:	Prof. Dr.-Ing. habil. Andreas Richter

Tag der Einreichung:	22.10.2021
Tag der Prüfung:	01.02.2022

Darmstadt, Technische Universität Darmstadt

URN: urn:nbn:de:tuda-tuprints-206699

Jahr der Veröffentlichung der Dissertation auf TUprints: 2022

Preface

The work of the present doctoral thesis “Performance Investigation of Integrated Gasification Combined Cycle Power Plant for Polygeneration” started in October 2018 and was carried out at the Institute of Energy Systems and Technology (EST), Department of Mechanical Engineering, Technical University of Darmstadt. Three years and a half of full-time work and deep research made this work possible. This work came out in its final form through the support of many people. The main supervision was done by **Prof. Dr.-Ing. Bernd Epple** and the co-supervision was done by **Prof. Dr.-Ing. habil. Andreas Richter**.

A team of qualified supervisors has taken on the task of guiding me through my doctoral thesis. At the head of this team is **Prof. Dr.-Ing. Bernd Epple**, whose scientific experience is greatly appreciated. My gratitude goes to **Priv.-Doz. Dr.-Ing. habil. Falah Alobaid**, for spending much of his valuable time helping me with step-by-step suggestions and comments on my research. I am especially grateful for the feedback and modeling support provided by **Dr.-Ing. Christian Heinze** and **M.Sc. Jens Kaltenmorgen.** Moreover, I want to thank all of the **EST staff**, for making my time at the institute a memorable and valuable experience.

Last but not least, I would like to express my deepest feelings to **my family** for their continuous encouragement, understanding, and support. My god bestows health and happiness to all of them.

I dedicate this work to my beloved family.

Ammar Bany Ata

Erklärung

Hiermit erkläre ich, dass ich die vorliegende Arbeit, abgesehen von den in ihr ausdrücklich genannten Hilfen, selbständig verfasst habe.

Darmstadt, den 22.10.2021

Ammar Ahmad Jamil Bany Ata

Abstract

Energy and environment are playing an important role in shaping the world at present and the path ahead into the future. Both affect the aspects of the economy, politics, health, and welfare. In addition, the growth of wind and photovoltaic plants has greatly increased the demand for flexible generation or storage options in the electricity market due to their fluctuation. The Integrated Gasification Combined Cycle (IGCC) with carbon capture for polygeneration of power and chemicals features the advantages of flexible power generation that has low CO_2 emissions, alongside essential chemicals for the industry or even production of fuels that for storage and then to be utilized during the peak time. Moreover, the ability to use biomass and Refuse Derived Fuel (RDF) as feedstock for IGCC contributes to waste management and better use of the resources.

In the scope of this work, a process simulation model of an IGCC using Aspen Plus was developed based on a pilot-scale 0.5 MW_{th} HTW gasifier and gas purification plant installed at TU Darmstadt. The gasification and purification pilot plant model was scaled up and then integrated with a CCPP for power generation. For the power generation part, a process simulation model of Combined Cycle Power Plant (CCPP) was built based on a 360 MW_{el} General Electric (GE) STAG 109FA CCPP located at Prai in Malaysia. For chemical production, a methanol synthesis unit was also modeled and integrated with the IGCC model to enable polygeneration of electricity and methanol in an IGCC plant.

To improve the performance of the IGCC, heat integration between the heat recovery steam generator (HRSG) and the syngas production process (gasification and purification) was applied. Additionally, an acid gas removal (AGR) process was adopted for the IGCC model. In this respect, three process simulation models for AGR were developed using three different solvents (Selexol, Rectisol, and a-MDEA) and then evaluated seeking a better performance of the IGCC. Furthermore, co-gasification of coal and refuse derived fuel in different mixing ratios were used and investigated.

The evaluation of the developed IGCC power plant model for flexible polygeneration using HTW gasification technology shows a promising electrical efficiency of about 37.48% with a carbon capture rate of 90%. Also, the comparison between the three AGR processes shows that the Selexol process is the most efficient. Therefore, this process was used in the final configuration of the IGCC plant. Finally, a thermo-economic evaluation under volatile selling prices of IGCC products was executed to investigate the production regime and to make better decisions for production.

Kurzfassung

Die Themen Energie und Umwelt spielen eine wichtige Rolle bei der Gestaltung der gegenwärtigen Welt sowie für die Entwicklung der Zukunft. Beide Aspekte beeinflussen die Wirtschaft, der Politik, der Gesundheit und des Wohlstandes. Darüber hinaus hat das Wachstum von Wind- und Photovoltaikanlagen die Nachfrage nach flexiblen Erzeugungs- oder Speicheroptionen auf dem Strommarkt aufgrund ihrer Fluktuation stark erhöht. Der Gas- und Dampf-Kombiprozess mit integrierter Vergasung (IGCC-Prozess)mit Kohlenstoffabscheidung zur Polygeneration von Strom und Chemikalien bieten neben einer flexiblen Stromerzeugung bei geringen CO_2-Emissionen den Vorteil der Produktion von wichtigen Chemikalien für die Industrie oder von Kraftstoffen, die gespeichert und dann in Spitzenzeiten verwendet werden können. Darüber hinaus trägt die Möglichkeit, Biomasse und Ersatzbrennstoffe (RDF) als Ausgangsmaterial für IGCC zu verwenden, zu einem optimierten Abfallmanagement und zur besseren Nutzung von Ressourcen bei.

Im Rahmen dieser Arbeit wurde ein Prozesssimulationsmodell eines IGCC-Prozesses mit Aspen Plus auf der Grundlage einer 0,5 MW_{th} HTW-Vergasungs- und Gasreinigungsanlage im Pilotmaßstab an der TU Darmstadt entwickelt. Das Modell der Pilot-Vergasungs- und Gasreinigungsanlage wurde hochskaliert und dann in ein GuD-Kraftwerk zur Stromerzeugung integriert.Für die Stromerzeugung wurde ein Prozesssimulationsmodell eines Gas- und Dampfturbinenkraftwerks (GuD) auf der Grundlage eines 360 MW_{el} General Electric (GE) STAG 109FA GuD-Kraftwerks in Prai in Malaysia erstellt. Für die Synthese wurde eine Methanolsyntheseeinheit modelliert und in das IGCC-Modell integriert, um die Simulation der Polygeneration von Strom und Methanol in einer IGCC-Anlage zu ermöglichen.

Zur Verbesserung der Leistung des IGCC-Prozesss wurde eine Wärmeintegration zwischen dem Abhitzedampferzeuger (HRSG) und dem Syngasproduktionsprozess (Vergasung und Gasreinigung) durchgeführt. Darüber hinaus wurde für das IGCC-Modell ein Verfahren zur Entfernung saurer Gase (AGR) angenommen. In diesem Zusammenhang wurden drei Prozesssimulationsmodelle für AGR unter Verwendung von drei verschiedenen Lösungsmitteln (Selexol, Rectisol und a-MDEA) entwickelt und anschließend mit Ziel einer besseren Leistung von IGCC bewertet. Darüber hinaus wurde die Co-Vergasung von Kohle und RDF in verschiedenen Mischungsverhältnissen angewendet und untersucht.

Die Bewertung des entwickelten IGCC-Kraftwerksmodells für flexible Polygeneration unter Verwendung der HTW-Vergasungstechnologie zeigt einen vielversprechenden elektrischen Wirkungsgrad von etwa 37,48 % mit einer Kohlenstoffabscheidungsrate von 90 %. Auch der Vergleich zwischen den drei AGR-Verfahren zeigt, dass das Selexol-Verfahren das effizienteste Verfahren ist. Daher wurde dieses Verfahren in der endgültigen Konfiguration der IGCC-Anlage verwendet. Schließlich wurde eine thermo-ökonomische Bewertung unter Berücksichtigung der schwankenden Verkaufspreise von IGCC-Produkten durchgeführt, um das Produktionssystem zu untersuchen und bessere Entscheidungen für die Produktion treffen zu können.

Table of Contents

Preface ... iii
Erklärung ... v
Abstract ... vii
Kurzfassung ... viii
Table of Contents ... ix
List of Tables ... xiii
List of Figures ... xv
Nomenclatures ... xix
Symbols ... xix
Greek Symbols ... xix
Subscripts ... xix
Abbreviations and Acronyms ... xx
Chapter 1: Introduction ... 1
1.1 Background and Motivation ... 1
1.2 IGCC with Polygeneration Concept ... 4
1.3 Literature Review ... 5
1.3.1 IGCC Power Plant with Carbon Capture ... 5
1.3.2 Pre-combustion Acid Gas Removal Process ... 7
1.3.3 Pilot Plants for the Material Utilization ... 9
1.3.4 Process Modeling of Polygeneration ... 10
1.4 Research Aim and Objectives ... 11
1.5 Outline of the Thesis ... 11
Chapter 2: State of the Art of the IGCC ... 13
2.1 Gasification ... 13
2.1.1 Moving-bed Gasifier ... 14
2.1.2 Fluidized-bed Gasifier ... 16
2.1.3 Entrained-flow Gasifier ... 19
2.2 Feedstock Pretreatment and Drying ... 20
2.3 Syngas Cleaning and Treatment ... 21
2.3.1 Syngas Cooling ... 21
2.3.2 Solid Particles Removal ... 22

2.3.3 Chloride Scrubbers....22
2.3.4 BTX Scrubber....22
2.3.5 Water-gas Shift....24
2.3.6 COS Hydrolysis....27
2.3.7 Acid Gas Removal....27
2.4 Power Generation....31
2.5 Synthesis....33
Chapter 3: Process Simulation of the IGCC Power Plant....39
3.1 Introduction....39
3.2 Description of Reference Plants....41
3.2.1 Gasification and Purification....41
3.2.2 Combined Cycle Power Plant....45
3.3 Process Simulation Software....47
3.3.1 Property Calculation and Estimation....47
3.4 Simulation of Pilot Plant....50
3.4.1 Filtration....53
3.4.2 Raw Gas Scrubbing....54
3.4.3 Compression....55
3.4.4 Water-gas Shift and Hydrolysis....56
3.4.5 BTX Scrubber....56
3.4.6 Amine Scrubber....58
3.4.7 Synthesis Test Rig....60
3.4.8 Mobile Washing Test Rig....61
3.5 Simulation of Industrial Scale....62
3.5.1 Coal Pre-treatment....62
3.5.2 Gasification....63
3.5.3 Syngas Treatment....65
3.5.4 Water-gas Shift and Hydrolysis....65
3.5.5 Acid Gas Removal (AGR)....67
3.6 Simulation of Power Generation....75
3.6.1 Gas Turbine Simulation....76
3.6.2 HRSG Simulation....77
3.7 Heat Integration....82
3.8 Simulation of Methanol Synthesis....84

Chapter 4: Results and Discussion....87
4.1 Pilot Plant Simulation Results....87
4.2 Enhancement of Predefined Extractions....89
4.2.1 Enhancement of Dryer Extraction....90
4.2.2 Enhancement of Gas Preheating and Acid Gas Removal Extractions....90
4.2.3 Enhancement of Gasifier and WGS Extractions....90
4.2.4 Modification of the Intermediate Pressure System....91
4.2.5 Variation of the Gasifier and WGS Extractions....92
4.2.6 Enhancement the Heat Input of the Raw Gas Cooler....92
4.2.7 Enhanced Model....93
4.2.8 Assessment of the Improvements....93
4.3 Evaluation of Acid Gas Removal (AGR) Process....96
4.3.1 Variation of the Design Parameters....98
4.4 Thermo-economic Evaluation of Polygeneration....103
4.4.1 Energy Analysis....104
4.4.2 Energy Analysis for Polygeneration....105
4.4.3 Economic Analysis for Polygeneration....106
Chapter 5: Conclusion and Outlook....113
5.1 Heat Integration Enhancement....113
5.2 AGR Evaluation....114
5.3 Energy and Economical Analysis....115
Bibliography....117

List of Tables

Table 2.1 Basic gasification reactions [29,71] 14
Table 2.2 Characteristics of acid gas removal process solvents [101,111] 31
Table 2.3 Direct synthesis products from synthesis gas [71,122] 33
Table 3.1 Raw gas scrubber inlet and outlet streams 42
Table 3.2 Technical data of the HRSG of the reference CCPP 45
Table 3.3 Feedstock characteristics (Mass fractions on dry basis) 51
Table 3.4 Raw syngas parameters 52
Table 3.5 Amine scrubbing reactions [157–161] 59
Table 3.6 Simulation results of gasifier model for different feedstocks 64
Table 3.7 Simulation results of the three different cases 65
Table 3.8 Mass balance of water-gas shift [101] 67
Table 3.9 Design Specifications of the Selexol Process 72
Table 3.10 Performance parameters of Rectisol Process 74
Table 3.11 Parameters of the gas turbine process models 77
Table 3.12 Parameters at the outputs of HPHT-SH at different load cases 79
Table 3.13 Parameters at the outputs of HT-RH at different load cases 80
Table 3.14 Parameters at the outputs of LP-SH at different load cases 80
Table 3.15 Comparison of Steam turbine power [MW_{el}] 81
Table 3.16 The outputs of the steam turbine combined with synthetic GT and natural gas GT [MW_{el}] 81
Table 3.17 Heat and steam integration for the steam power process 82
Table 3.18 Power of the steam turbine of the reference case in all load cases 84
Table 3.19 Results of Methanol Synthesis model [101] 85
Table 4.1 Heat and material balance of the pilot plant simulation 88
Table 4.2 The Output of Steam Turbine with new WTA dryer mass flow rate 90
Table 4.3 Output of ST with the synthesis gas turbine before and after pressure modification [MW_{el}] 91
Table 4.4 Steam turbine output in all load cases after optimization [MW_{el}] 93
Table 4.5 Characteristics of Syngas streams entering the WGS and AGR 96
Table 4.6 Simulation result on each process 97
Table 4.7 Scenarios of polygeneration 103
Table 4.8 Electricity and methanol market price scenarios 104
Table 4.9 IGCC power plant performance indicators 104

List of Figures

Figure 1.1 Historical CO_2 emissions from 1750 to 2020 [13] 1
Figure 1.2 CO_2 emissions by sectors in 2019 [19] 2
Figure 1.3 Regional electricity generation by fuel type in 2020 [25] 3
Figure 1.4 Schematic of Polygeneration concept 4
Figure 2.1 Feedstock and product flexibility of gasification [71] 13
Figure 2.2 Illustration of Moving-bed Gasifier (Sasol-Lurgi) [71] 15
Figure 2.3 (a) Lurgi FBDB and (b) BGL gasifier [71] 15
Figure 2.4 Illustration of the Fluidized-bed gasifier [71] 16
Figure 2.5 Fluidized-bed Regimes [71] 17
Figure 2.6 Schematic of HTW Gasifier [71] 18
Figure 2.7 Illustration of Entrained-flow Gasifier (a) Top-fired coal-water slurry feed slagging (b) Side-fired dry coal feed slagging [71] 20
Figure 2.8 Syngas treatment process for a Polygeneration plant 21
Figure 2.9 Process flow diagram of the OLGA process [71] 24
Figure 2.10 Multi-stage water-gas conversion with water quench for intercooling [98] 26
Figure 2.11 Multi-stage water-gas conversion with multi-stage steam injection [99] 26
Figure 2.12 Basic flow diagram of solvent-based processes 28
Figure 2.13 Relative solvent loading of chemical and physical solvents [103] 29
Figure 2.14 Structural formula of MDEA, MEA, and DEA [101] 30
Figure 2.15 permissible fuel mixture ratios in gas turbines [113] 32
Figure 2.16 Mega-methanol process developed by Lurgi [134] 36
Figure 3.1 Schematic of IGCC with polygeneration 40
Figure 3.2 Process Flow Diagram of BTX-Scrubber 43
Figure 3.3 Acid gas removal process flow diagram 44
Figure 3.4 Schematic diagram of Prai CCPP 46
Figure 3.5 Intermolecular forces between molecule 1 and 2, 1 and 1, and molecule 2 and 2 [150] 50
Figure 3.6 All possible intermolecular forces between molecule a and m, a and c, c and m, and m and m. [151] 50
Figure 3.7 Block flow diagram of the pilot plant at TU Darmstadt 52
Figure 3.8 Syngas treatment simulation block flow diagram 53
Figure 3.9 Block flow diagram of the filtration process 53
Figure 3.10 Block diagram of raw gas scrubbing simulation flow sheet 54
Figure 3.11 Temperature and pressure profile of the gas scrubbing column 55
Figure 3.12 Block flow sheet of the compression process 55

Figure 3.13 Block flow diagram of the process simulation of WGS and Hydrolysis 56
Figure 3.14 Block flow diagram of the process simulation of BTX-removal section.....57
Figure 3.15 Block flow diagram of the process simulation of BTX-desorption 58
Figure 3.16 schematic of the absorption process.....58
Figure 3.17 Block flow diagram of the Amine scrubbing Process simulation.....59
Figure 3.18 Block flow diagram of the synthesis test rig 60
Figure 3.19 Block flow diagram of the washing test rig.....61
Figure 3.20 Schematic process description of the innovative washing procedure 62
Figure 3.21 Gasifier model flowsheet.....64
Figure 3.22 Water-gas shift flowsheet.....66
Figure 3.23 Process flow diagram of dual-stage Selexol process for AGR.....69
Figure 3.24 Rectisol process flow diagram.....73
Figure 3.25 Process flow diagram of a-MDEA acid gas removal process 75
Figure 3.26 Simplified schematic diagram of Combined Cycle Power Plant 76
Figure 3.27 Gas Turbine process flow diagram.....77
Figure 3.28 Aspen Plus flowsheet of HRSG model 78
Figure 3.29 Steam power process with tapping and heat integration. ((1) Water-gas shift; (2) raw gas cooler and methanol synthesis; (3) HTW gasifier; (4) WTA drying; (5) Acid Gas Removal). 83
Figure 3.30 Methanol synthesis process flow diagram.....84
Figure 4.1 Block flow diagram of the pilot plant simulation.....87
Figure 4.2 The output deviations of the different extractions at the three load cases.....94
Figure 4.3 Specific electrical energy content of steam taps.....95
Figure 4.4 Correlation between Power deviation and steam exergy 95
Figure 4.5 Electrical and thermal energy consumption on each process.....97
Figure 4.6 Comparison results of total solvent flow rate against WGS conversion rate.....98
Figure 4.7 Comparison result of reboiler heat duty of AGR with WGS conversion rate.....98
Figure 4.8 Electric energy consumption depending on WGS conversion rate.....99
Figure 4.9 Hydrogen loss of each process relation with WGS conversion rate 99
Figure 4.10 Solvent loss of each process relation with WGS conversion rate 100
Figure 4.11 Relation of total solvent circulation flow rate depending on CO_2 capture rate 100
Figure 4.12 Relation of reboiler heat duty depending on CO_2 capture rate 101
Figure 4.13 Electric energy consumption depending on CO_2 capture rate 101
Figure 4.14 Hydrogen loss depending on CO_2 capture rate 102
Figure 4.15 Comparison result for solvent loss of each case depending on CO_2 capture rate 102
Figure 4.16 Power and methanol production at a different CO_2 capture rate 105
Figure 4.17 Selling price of the IGCC products at different shares of syngas for methanol production and different availability levels of the IGCC.....106

Figure 4.18 Effect of market price change at 100% availability of IGCC 108
Figure 4.19 Effect of market price change at 85% availability of IGCC 109
Figure 4.20 Effect of market price change at 70% availability of IGCC 110
Figure 4.21 Effect of market price change at 55% availability of IGCC 111

Nomenclatures

Symbols

A	Area	[m^2]
D	Diameter	[m]
ΔH^o_R	Standard reaction enthalpy	[MJ/kmol]
H_i	Henry coefficient of component or species i	[-]
ṁ	Mass flowrate	[kg/s]
p	Pressure	[bar]
P_c	Pressure at the critical point	[bar]
p_i	Partial Pressure	[bar]
$\dot{Q}$	Heat	[MW_{th}]
R	Gas constant	[-]
SR	Stoichiometric ratio	[-]
T	Temperature	[°C]
T_c	Temperature at the critical point	[°C]
v	molar volume	[m^3/mol]
W_n	Weight fraction of hydrocarbon molecules	[-]
$\tilde{x}_i$	Gas concentration	[-]
Z	Universal correction factor	[-]

Greek Symbols

α	Chain growth probability	[-]
δ	differential	[-]
Δ	Difference	[-]
η	Efficiency	[-]
ρ	Density	[kg/m^3]
Σ	Summation operator	[-]

Subscripts

amb	Ambient
aq	Aqueous
av	Average
c	Critical point

CP	Condensate pump
e	Exit
el	Electric
ex	Exergy
f	Liquid
FWP	Feedwater pump
g	Gas
GT	Gas turbine
n	chain length (carbon atoms)
i	Component or species i
in	Inlet
R	Reaction
s	Solid
ST	Steam turbine
th	Thermal

Abbreviations and Acronyms

AGR	acid gas removal
ASU	air separation unit
BASF	German federal office for economic affairs and export control
BGL	British Gas Lurgi
BTX	Benzene, toluene, xylene
CCGT	Combined Cycle Gas Turbine
CCS	Carbon Capture and Storage
CCU	carbon capture and utilization
COT	combustor outlet temperature
DEA	Diethanolamine
DEA	di-ethanolamine
DEPG	dimethyl ether polyethylene glycol
DME	Dimethyl Ether
DOE	U.S. Energy Information Association
ECN	Energy Research Centre of the Netherlands
ECO	economizer
ECUST	East China University of Technology

EOR	enhanced oil recovery
EVAP	evaporator
FBDB	Fixed Bed Dry Bottom
FSC	fixed-site-carrier
FT	Fischer-Tropsch
GE	General Electric
GEE	General Electric Energy
GT	gas turbine
HP	high pressure
HRSG	heat recovery steam generator
HT	high temperature
HTW	High Temperature Winkler
IEA	International Energy Agency
IGCC	Integrated Gasification Combined Cycle
IP	intermediate pressure
IPCC	Intergovernmental Panel on Climate Change
IT	Intermediate temperature
LEG	Lignite Energy Grained
LP	low pressure
LT	low temperature
MDEA	Monoethylamine
MEA	monoethanolamine
NETL	U.S. National Energy Technology Laboratory
NGCC	natural gas combined cycle
NMP	n-methyl-pyrrolidone
OMB	Opposed Multi Burner
PC-SAFT	perturbed chain statistical association fluid theory
PEM	proton exchange membrane
RDF	refuse-derived fuel
RH	reheater
RKS-BM	Redlich-Kwong-Soave with Boston-Matthias alpha function
RME	Rapeseed methyl ester
SCPC	Supercritical Pulverized Coal
SH	superheater

SNG	synthetic natural gas
ST	Steam Turbine
STIG	Steam Injected Gas Turbine
TIT	turbine inlet temperature
TKIS	ThyssenKrupp Industrial Solutions
TOT	turbine outlet temperature
TTD	terminal temperature difference
USC	ultra-supercritical
WGS	water-gas shift
WTA	Fluidized-bed drying process

Chapter 1: **Introduction**

In this chapter, the background and motivation for investigating the performance of integrated gasification combined cycle (IGCC) power plants are presented. Furthermore, the objectives of the study and the methodology applied are explained, as well as a literature review. Finally, the outlines of the dissertation are mentioned.

1.1 Background and Motivation

The energy sector is one of the most influential factors in driving political, economic, and social change in the world and contributing to the shaping of the new world order [1–3]. The energy demand is growing globally, driven by industrial operations and progress in both developing and developed countries [4–7]. This demand is primarily met at present by burning oil, natural gas, and coal, with the trend toward using these non-renewable fossil fuels continuing to grow due to the fact that global energy demand is growing faster than renewables [8,9]. The global environment has also been significantly affected by the continuous emission of greenhouse gases, mainly carbon dioxide, resulting from the combustion of fossil fuels [10].

As a consequence of increasing carbon dioxide emissions, as shown in Figure 1.1, limiting carbon dioxide emissions has become a political and social strategy. The political response to the growth of carbon dioxide emissions was a United Nations agreement in 1997, the Kyoto Protocol. An extension of this was made in 2015 by the Paris Agreement to limit global warming to 2 or 1.5 °C compared to the pre-industrial era through appropriate measures [11,12]. Accordingly, reducing greenhouse gas emissions in all sectors (transport, energy, industry, and households) is one of the most important goals.

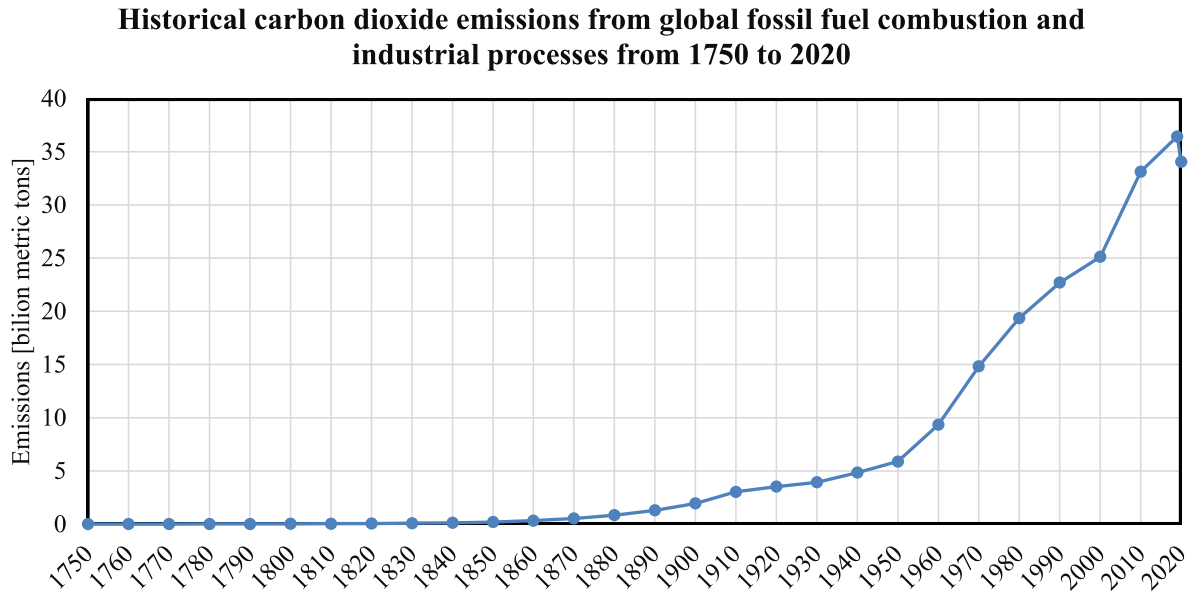

Figure 1.1 Historical CO_2 emissions from 1750 to 2020 [13]

According to recent evaluations, the current measures taken by governments worldwide are not sufficient to prevent global warming of more than 3 °C by the end of this century, with an increase of 4 or even 6 °C not excluded [14,15]. Thus, it is important to use technologies that generate electricity without harming the environment. The Intergovernmental Panel on Climate Change (IPCC) regularly summarizes the scientific state of research on climate change. In this context, possible measures to reduce CO_2 emissions are listed. In the field of energy supply, the list includes low-carbon power generation from renewable energy sources (wind, solar, and biomass), nuclear energy, and natural gas, as well as CO_2 capture and storage from fossil and biomass-fueled power plants. According to the report of the global institute concerning bioenergy and carbon capture and storage (BECCS) [16], the latter option, in particular, plays an essential role in achieving negative CO_2 emissions in the power sector to offset unavoidable CO_2 emissions in other sectors in the future. In the industrial sector, recycling is considered to have an essential role, alongside the reduction of waste materials [17]. Efforts are aimed at a closed carbon cycle operation where carbon, once used, is made available for subsequent products at the end of the product's life through innovative processes [18].

In Figure 1.2, CO_2 emissions are shown by sector, including electricity and heat generation (14 Gt CO_2), transport (8.2 Gt CO_2), industry (6.3 Gt CO_2), buildings (2.8 Gt CO_2), and other (0.6 Gt CO_2). All these sectors are considered separately from electricity and heat [19].

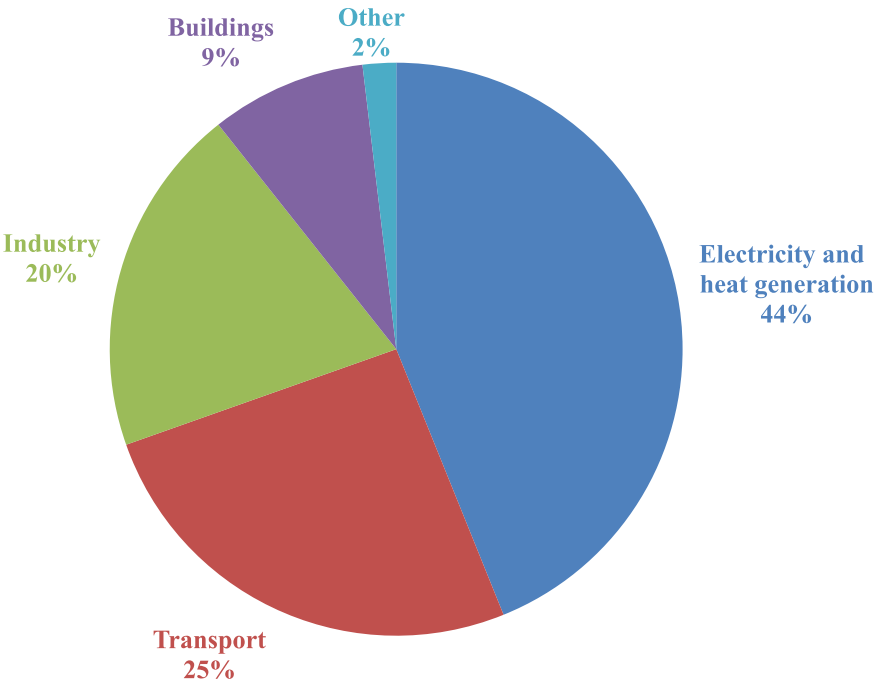

Figure 1.2 CO_2 emissions by sectors in 2019 [19]

Renewable energy is expected to make a significant contribution to the carbon reduction needed to meet European and global climate change targets [11,20]. The European Union and its member states plan to increase the share of renewable energy in gross final energy consumption to at least 32% by 2030. The measures include the advancement of renewable energy sources for electricity generation and the possible electrification of heating and transport. However, the cost price of renewable energy should be low enough to be competitive with other power generation technologies. Consequently, the processing of renewable energy sources and the development of contemporary types of power plants are becoming increasingly important.

The growth of wind and photovoltaic plants has greatly increased the demand for flexible generation or storage options in the electricity market due to their fluctuation [21–23]. As a result, renewable energies are becoming increasingly important as a supplement to conventional ones. The share of electricity generated in thermal power plants remains dominant worldwide at over 80% and is expected as well to play a key role in the foreseeable future. [24]. Figure 1.3 demonstrates electricity generation by fuel type, i.e., coal, natural gas, nuclear, oil, renewables, and other energy sources [25].

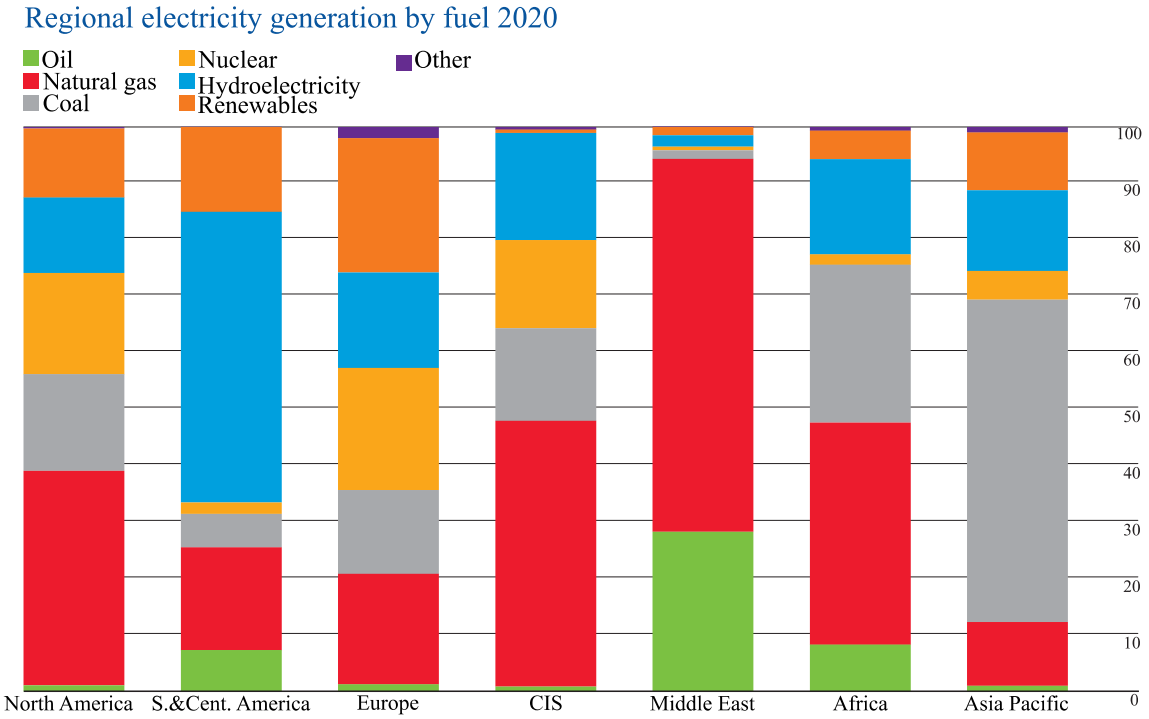

Figure 1.3 Regional electricity generation by fuel type in 2020 [25]

The use of fossil resources is increasingly being restricted, but these are not needed exclusively for power generation and energy supply. In the chemical and petrochemical industries, natural gas and oil continue to be indispensable raw materials for the production of a wide range of products, e.g. plastics, fertilizers, and pharmaceuticals, which release large quantities of CO_2. Furthermore, fossil fuels are a limited resource with a total potential of about 580,000 EJ. Coal accounts for the largest share at around 88%. The current reserves of fossil fuels, i.e., the deposits that can currently be used economically and technically, amount to about 40,000 EJ and compare with a current consumption or extraction of about 525 EJ per year. Even with increasing demand for coal, oil, and natural gas, the known reserves will be able to meet demand in the coming years, although bottlenecks in oil supply cannot be ruled out in the medium term. [26]

Besides fossil resources, the disposal of the CO_2 released during their use also plays a decisive role. Currently, fossil fuels are used to generate electricity or are thermally recycled after material use. For example, only about 14% of plastics are recycled, mostly into low-grade products [27]. This means that the carbon content of the fossil resources used ends up in the atmosphere as CO_2 after use. Therefore, new concepts must be considered, developed, tested, and implemented to ensure the future security of electricity supply and the provision of raw materials for the chemical

industry under these conditions. In this context, attractive opportunities are opening up, especially for integrated gasification combined cycle power plants (IGCC) with carbon capture for polygeneration of electricity and chemicals. This offers the benefits of flexible power generation with low CO_2 emissions, as well as the production of important chemicals for industry or even fuels that can be stored and then used at peak times. Additionally, the ability to use municipal waste as feedstock for IGCC contributes to waste management and better use of our resources.

1.2 IGCC with Polygeneration Concept

The IGCC is a promising concept for flexible polygeneration processes, which utilizes biogenic, anthropogenic resources and/ or fossil fuels to generate electricity and raw materials for the chemical industry. The polygeneration process considered in this work is characterized by a combination of an IGCC process and a synthesis plant for the production of chemical feedstocks, as shown in Figure 1.4.

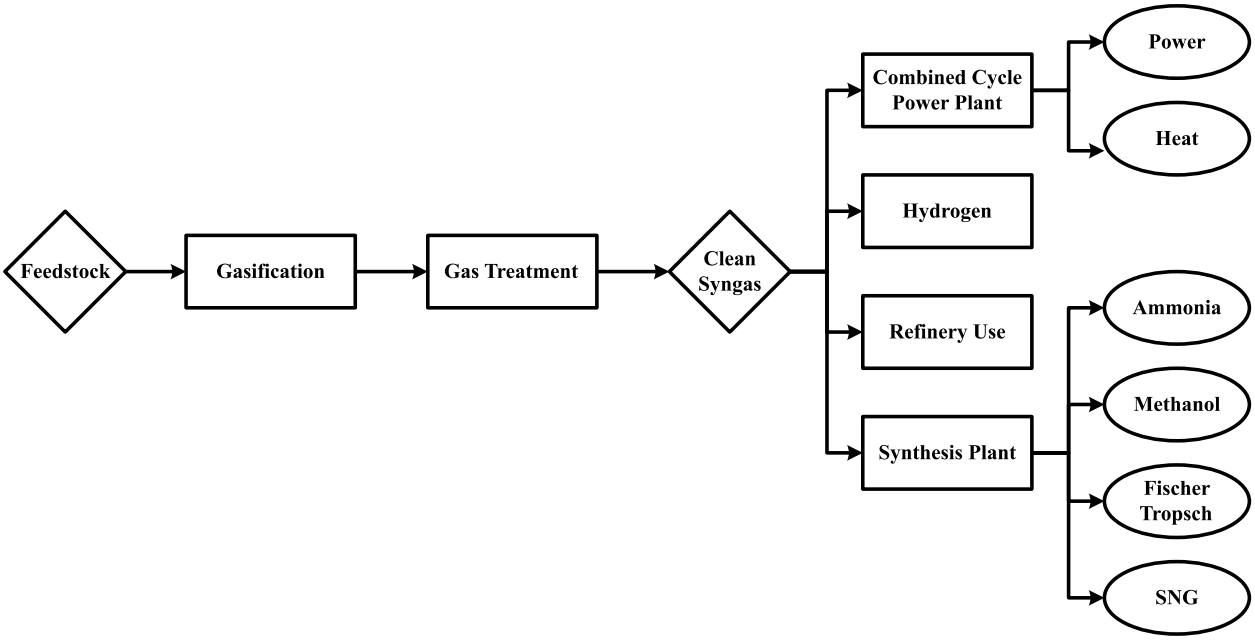

Figure 1.4 Schematic of Polygeneration concept

IGCC plants consist of a gasification plant to convert solid fuels into combustible gas and a combined cycle process, to convert this gas into electric power. In the gasification process, the feedstock is converted into a combustible product gas by partial oxidation. In the purification steps of the gas treatment process, the gas is conditioned for subsequent energy use. In the combined cycle process, the calorific value of the gas is used energetically to generate electricity and, if necessary, heat. Such plants can achieve higher efficiencies than conventional thermal power plants [19–21]. When CO_2 capture is considered in the power plant process, the efficiency advantage increases further, since IGCC plants can use the more energetically efficient pre-combustion capture technologies [22]. Another advantage of the IGCC process is the fuel flexibility and the high efficiencies that can be achieved even with biomass and waste, as has already been demonstrated in various plants [21].

The high efficiency of IGCC plants leads to low variable operating costs. Due to the plant complexity and the associated high investment costs, however, the fixed operating costs are comparatively high. Thus, IGCC plants fit into the electricity market as base-load power plants

[28]. The expansion of renewable energy generation, primarily photovoltaic plants and wind turbines, leads to a highly fluctuating residual load in the power grid. For the foreseeable future, this residual load is expected to be met by highly efficient thermal power plants, while the demand for base-load power plants is declining. Pure IGCC plants are therefore initially not a good choice for the changing electricity market. If, on the other hand, these are expanded to include synthesis plants, large parts of the plant, namely fuel pretreatment, gasification, and gas processing, can be operated at nominal load permanently. By producing electricity and chemical feedstocks on demand, such plants can respond flexibly to changing electricity demand. The purified product gas, which is not used energetically to generate electricity, is converted in these plants into various chemical feedstocks, such as ammonia, methanol, methane, or Fischer-Tropsch products [29]. These chemical feedstocks and intermediates can be converted into high-value chemicals or fuels. In terms of the carbon cycle, long-lived carbon-containing products are of particular interest here, as they sequester carbon for a correspondingly long time and thus reduce CO_2 emissions from the feedstock. For such products, the generation of the carbonaceous feedstocks from CO of the syngas is more favorable than the use of CO_2 from carbon capture plants due to the specific binding energy or oxidation number of the carbon [30].

To be able to function as a building block in the secure supply of electricity in a power grid with a high regenerative share, plant flexibility plays an essential role. On the one hand, the question arises as to how far the load or the electricity production can be reduced compared to the nominal power and, on the other hand, with which gradient this is possible. In the case of negative electricity prices, the use of hydrogen electrolysis to provide O_2 for the gasifier and hydrogen for the synthesis gas can also be interesting.

1.3 Literature Review

Intensive research has been carried out since the beginning of the 20th century on processes of gasification or utilizing syngas as a material or for power generation. Current studies on these topics focus primarily on the optimization and detailed investigation of individual process steps. In the following, relevant publications of works on IGCC for the polygeneration approach with carbon capture are discussed, which deal with parallel energetic and material utilization.

1.3.1 IGCC Power Plant with Carbon Capture

In IGCC with carbon capture, the acid gases are removed prior to the power generation or synthesis process. The technology of carbon capture pre-combustion is classified into physical and chemical absorption, depending on the absorption specifications of the solvents. Physical absorption technology is preferred over chemical absorption in the IGCC process because the power plants are operated at high pressures, resulting in high partial pressures of CO_2 in the syngas [31]. Consequently, extensive research has been conducted on physical absorption for IGCC in the pre-combustion process. Berstad et al. [32] demonstrated that using the Pneumatic feeding method is more practical than slurry feeding particularly in Selexol process technology in the gasification procedure. In order to assess the performance of Selexol process efficiency for hybrid electric power, they developed a dynamic simulator. This method will provide the operating characteristics.

In terms of electricity generation costs and CO_2 mitigation costs, the impact of pre-combustion CO_2 capture rate using Selexol technology was considered [33].

Descamps et al. [34] investigated the usage of chemical absorption and Rectisol solvent by applying these technologies in the study of an IGCC power plant as a pre-combustion method. They concluded that the use of Rectisol in one stage is more effective than chemical absorption. Padurean et al. [35] extended their research to different solvents such as Selexol, Rectisol, and Purisol for IGCC power plants with a capacity of 435 and 450 MW_{el}. Coal with biomass was used as fuel, the findings confirmed that using Selexol as a solvent is the most effective among other solvents in terms of energy savings.

In terms of fuel source, the majority of previous studies have focused on high-quality coal [36–41], while there are few studies on low-quality coal [38,42,43]. Lee et al. [38] used high-grade coal in an IGCC power plant, and the results showed that CO_2 concentration was higher than using low-grade coal, while H_2 was higher with high-grade coal. Nevertheless, the power generated with low-grade coal was low compared to high-grade coal when the same amount of fuel was used. Also, the efficiency of power plants is 3.5% higher when using high-grade coal than when using low-grade coal [44]. Li et al. [45] concluded that using lignite coal reduced the electricity cost by 24.4%. Mondol et al. [43] illustrated that the integration of gasification with regeneration is more beneficial in terms of efficiency increase and cost reduction compared to the conventional IGCC process. However, this procedure might increase the existence of H_2S in the Pure CO_2 product. Majoumerd et al. [44] investigated three types of power plants in their study, natural gas combined cycle (NGCC), super critical pulverized coal (SCPC), and IGCC. They were trying to demonstrate the performance of these power plants in terms of efficiency, electric cost, and CO_2 cost. The results confirmed that NGCC is the highest in efficiency while SCPC has the lowest among other plants.

Bonalumi et al. [46] have shown that using an air-cooled system instead of a refrigeration system is productive as it reduces the energy required for CO_2 capture and increases efficiency by up to 0.7%. A reduction in CO_2 emissions can be achieved by co-firing 60% biomass with coal. In the Australian black coal power plant, the effect of co-firing biomass was investigated with and without CO_2. The results confirmed that when the biomass percentage is 10, CO_2 emission can be reduced by 9% without any profound impact on the performance of the power plant. The findings that were obtained in Australian power plants were in agreement with the Puertollano IGCC power plant [47]. Their results showed that adding a small amount of biomass has no effect on IGCC performance, while the trend led to a linear decrease in CO_2 emissions when the biomass fraction was increased to 60%, which results in a 50% decrease in CO_2 emissions while the net power generated is decreased to 20% [48]. Other studies focused on an increase in the percentage of biomass up to 70% in IGCC power plant (253 MW_{el}) [49]. It was noted that high LHV fuel blend utilization can provide this capacity with 41.5% electrical efficiency. The capacity of IGCC depends on several parameters such as quality of coal, moisture and ash content, mercury contents, the amount of volatile components, and char reactivity [38].

In polygeneration plants, the impact of increasing hydrogen output was considered by Cormos [36,50]. They found that the electric efficiency and emissions were reduced. However, the overall efficiency is increased for the provided hydrogen and electricity. Zhang et al. [51] demonstrated the polygeneration of electricity and liquid fuels. They showed that the percentage of carbon

capture was 60% for storage and 19% for liquid fuel production. While the remaining CO_2 was emitted into the atmosphere or waste. Also, it was found that the use of low-temperature carbon capture increased the efficiency of the power plant compared to Selexol. While by using MDEA, it was found that the efficiency decreased by 9.5% at 87% carbon capture. Descamps et al. [34] investigated the effect of changing CO_2 Capture levels. From this suggestion, it was noted that there is an increase in the thermal regeneration penalty when the carbon capture level is high. Hence, it will reduce the efficiency and IGCC power plant output. However, this impact is not significant in the case of post-combustion carbon capture plants. Kanniche and Bouallou [52] studied the impact of different solvents such as methanol, Selexol, and MDEA and investigate their effects on plant efficiency. In the study, the power consumption which is related to gross power plant output was investigated. It was noticed that using methanol as an absorbent has higher efficiency among Selexol and MDEA which has the lowest electric power.

Cau et al. [53] utilized two technologies for power generation USC steam plant and conventional IGCC with pre-combustion (400 and 500 MW_{el}). They carried out the simulation through Aspen Plus and Gate-cycle. Furthermore, NO_X and SO_X were reduced through pre-treatment. They conducted technical performance analysis including power generation and consumption for 70 and 90% CO_2 capture. Furthermore, the results showed that the performance of USC is better than IGCC power plants because the efficiency of USC was 44.8% compared to IGCC which is 43.9%. Nevertheless, the IGCC has lower energy consumption when it is integrated with CO_2 removal and compression. The net efficiency of IGCC with CO_2 removal is higher than with USC (35.3 versus 34.2%). Therefore, they stated that IGCC is known as more affordable than USC although it is highly expensive and lower reliable than the former. Also, it can be effectively integrated with pre-combustion carbon capture to reduce the target of CO_2.

1.3.2 Pre-combustion Acid Gas Removal Process

A few previous studies have investigated, the simulation and modeling of CPPs for IGCC power plants using different solvents such as 2-Amino-2-Methyl-1-Propanol (AMP), Selexol, Rectisol, Methyl diethanolamine (MDEA), K_2CO_3, Membrane, Monoethanolamine (MEA), Methanol, and Ammonia. These studies were categorized under three classifications; performance [35,54,55], economic [35,55–58], and exergy analysis [54,57,58]. Performance analysis was carried out including the analysis of power generation, consumption, and technical efficiency. Asif et al. [54] studied the performance of an IGCC power plant using a blend of AMP with Ammonia to figure out the power plant with/without pre-combustion and post-combustion. The results indicated that this blend can be applied to both combustions whether it is pre or post. However, retrofitting to post-combustion is more efficient than pre-combustion because the energy penalty is 1.1% with post-combustion which is less than 4.3% in pre-combustion. Power generated of IGCC with post-combustion was 576 MW_{el} which is larger than when the power is connected with pre-combustion (560 MW_{el}). The energy efficiency results showed that 8.3% higher of pre-combustion than post-combustion.

Padurean et al. [35] simulated pre-combustion carbon capture with different solvents using Aspen Plus. They utilized coal and biomass as fuel for the IGCC power plants. The results indicated that dimethyl ether polyethylene glycol (DEPG), known commercially as Selexol, was the most energy-

efficient among the other chemical and physical solvents. Analytical results presented that Selexol has high energy consumption compared to other solvents but it has the lowest thermal energy which indicated that this solvent might become a promising solvent also its efficiency was 70, 80, and 90% which was investigated. The capital cost with CO_2 capture rises 19.55%, 20.91%, and 22.55% compared to the capital cost without carbon capture.

Cormos [50] performed the simulation of an IGCC power plant (400 and 450 MW_{el}) with pre-combustion carbon capture using Aspen Plus. As part of the study, technical analysis and evaluation of steam, electricity, and refrigerant utilization was conducted. In addition, the economic performance with and without carbon capture was investigated. While Field and Brasington [59] executed the simulation of 464 MW_{el} IGCC with pre-combustion at 90% efficiency. They estimated the solubility of Selexol by PC-SAFT. Kanniche and Bouallou [52] performed the simulation of IGCC, pre-combustion, CO_2 compression, and TEG dehydration. Also, the efficiency of CO_2 capture that was considered is 77, 81, 85, and 88%. However, the results showed that 85% as efficiency is classified as the maximum due to losses during the process. They conducted different solvents but the most promising finding is Rectisol as it required lower energy for regeneration. Kapetaki et al. [60] performed two schemes consisting of integrated and nonintegrated Selexol with 464 MW_{el} IGCC through UniSim. The finding showed that 95% efficiency was found for an integrated scheme but it had higher energy consumption. Kunze et al [57] performed the IGCC with methanol solvent through Aspen Plus conducting technical analysis and exergy efficiency where they found that the efficiency of IGCC with carbon capture was 40%. Regarding the exergy, they figured out that the most exegetical destructions were from the combined cycle, gasifier, water-gas shift reactor (WGSR), and acid gas removal unit (AGRU).

Moioli et al. [61] performed dual-stage MDEA with IGCC (250 MW_{el}) through Aspen Plus. They conducted IGCC with and without pre-combustion by analytical performance including power generation and power consumption. In terms of energy penalty, the IGCC with 87% efficiency of carbon capture showed a 9.5% energy loss than without carbon capture. Ordorica et al. [56] executed the simulation of IGCC (577 MW_{el}) and NGCC (488 MW_{el}) through Aspen Plus. Also, they carried out with and without CO_2 Capture using Selexol in which the efficiency was 60, 80% respectively. Regarding CO_2 capture cost for 80% efficiency, the CO_2 removal cost was 28 USD/ton CO_2 for IGCC while 30 USD/ton CO_2 for NGCC.

Siefert and Litster [58] simulated different fossil fuels power plants consisting of IGCC and IGFC in which membrane processes were used for CO_2 capture. Moreover, capital and operating costs were conducted as evaluation tests where the consequence was IRR and LCOE has to be suggested. Their finding focused on the improved coal process. Therefore, studies that highlight the research of advanced H_2 and O_2 separation membranes and pressurized SOFCs play a vital role in low-cost load development if the electricity continuously rises above 50 USD/MWh. Skorek et al. [62] also performed a membrane process, which might be a promising technology to reduce the energy losses in IGCC processes, which could reduce the efficiency loss compared to chemical absorption. The results showed that the separation method using a polymer membrane with solid support was 15 times lower than chemical absorption using amine solvents such as MEA. Urech et al. [55] executed a systematic comparison for IGCC power plants integrated with pre-combustion technologies such as chemical absorption using amines (MDEA) and hot potassium carbonate (K_2CO_3), Physical absorption using Selexol as well. The research assesses the performance of

IGCC (440, 540 MW_{el}) with and without pre-combustion. Their results notified that the efficiency of IGCC was 45.02% while integrated with pre-combustion, was 36.39% and 36.42% for MDEA and Selexol, respectively. Regarding the hot potassium carbonate process, the efficiency was a bit higher which 37.33% is. In terms of improvement for the IGCC with hot potassium carbonate, multi-objective optimization was conducted for different variables, resulting in an increase in the efficiency of 39.31%.

1.3.3 Pilot Plants for the Material Utilization

In line with the long development time of gasification technologies, a large number of laboratory and pilot-scale test plants exist for the gasification of solid feedstocks. Three important plants are presented here which, in addition to coal, have also been designed for the use of alternative feedstocks and also serve to investigate the necessary pretreatment or gas treatment steps.

At the ECN in the Netherlands, an integrated test facility for investigating biomass gasification was already commissioned in 2003 [63]. The gasifier used is a 500 kW_{th} fluidized bed gasifier, which has already been operated with wood, straw, refuse-derived fuels, sewage sludge, and manure. Downstream is a three-stage, air-cooled gas cooler, which is used to investigate corrosion and erosion behavior. In the next process step, hot gas filtration is performed using sintered metal filter cartridges or through a cyclone. Plants for tar separation were set up, both a water-based process and a pilot plant for the OLGA process described in Section 2.3.4. After a wash column with water for ammonia separation, the pressure is increased and the synthesis gas is made available for test stands that further utilize the synthesis gas. These include gas engines, gas turbines, fuel cells, and synthesis plants for FT products, SNG, and alcohols [63].

Since 2013, a pilot plant has been operating in Karlsruhe to investigate the so-called bioliq process. The bioliq process involves decentralized pretreatment and pyrolysis of biomass. The pyrolysis oil produced is called bioSyncrude and is transported to a central gasification plant. The associated pilot plant consists of a 5 MW_{th} entrained-flow gasifier operating at 80 bar. Downstream, a hot gas cleaning system is used to investigate high-temperature cleaning steps to preserve the sensible heat of the gas as much as possible and to suffer only low exergy losses. The hot gas filter operates at up to 800 °C. The removal of trace gases HCl, H_2S, and COS, as well as alkali components, is done with fixed bed sorption at 500 °C. In addition, a catalytic conversion stage is used to break down ammonia, hydrogen cyanide, and hydrocarbons. After conventional CO_2 capture and water-gas conversion, the synthesis gas is converted to Dimethyl Ether (DME) [64].

The BioTfuel project follows a similar approach to the bioliq process. Biomass is also pretreated locally in this process and synthesis gas is then produced in a central entrained-flow gasifier for the synthesis of new hydrocarbons. For the demonstration of the BioTfuel process, all process steps were set up in Dunkirk, France. Commissioning is currently underway. The pretreatment in BioTfuel is done by torrefaction. This makes the straw used easier to grind and greatly increases the volumetric energy content. The 15 MW_{th} PRENFLO gasifier produces the syngas. In the downstream syngas processing unit, 20 to 30% of the syngas are further processed. A water gas conversion unit and a sour gas scrubbing unit are provided for this purpose. To meet the high purity requirements of the FT catalyst, a chemical sorption unit is used. Finally, a small partial stream of

the purified synthesis gas is used for FT synthesis. The FT products are then further processed into middle distillates (diesel and kerosene) by hydrocracking and hydro isomerization [65].

1.3.4 Process Modeling of Polygeneration

The possible concepts for designing a polygeneration plant are very diverse. For example, Buttler et al [66] investigated an approach in which hard coal is converted to syngas using entrained-flow gasification and converted to electricity or SNG on demand. When electricity demand is high, the stored SNG can be converted into additional electrical energy using the CCPP process. When there is an oversupply of electricity, additional hydrogen can be produced by electrolysis and fed into the synthesis process to increase the efficiency of synthesis. In addition, oxygen produced by the air separation unit can be stored to briefly increase the electrical output of the unit during peak demand periods. The maximum overall efficiency when SNG is used as a storage medium and recycled through the CCPP process is reported to be 40.1% by Buttler et al. [66].

A concept comparable to Buttler et al. was investigated by Meermann et al. [67,68]. The main difference to the polygeneration approach of Buttler et al. is the broader spectrum of feedstocks and products. Biomass, coal, heavy oil, and natural gas were investigated as feedstocks. Electricity, methanol, urea, and Fischer-Tropsch products were identified as possible products. For this purpose, this approach does not include the coupling of excess electricity by means of electrolysis and also does not provide for the return of electricity from the chemicals produced. The electrical efficiency determined is between 38 and 40%, depending on the feedstock. Meermann et al. also studied their polygeneration approach economically. They find that feedstock flexibility incurs less additional cost and makes sense even with small fluctuations in the price of CO_2 allowances and coal and biomass. In contrast, the production of FT products for further processing into diesel or gasoline is not profitable compared to conventional production paths. The production of urea or methanol from synthesis gas is also assessed as uneconomical.

Furthermore, Wolfersdorf et al. [69] presented the so-called annex concept. It provides for a pulverized coal-fired power plant to be extended by a smaller entrained-flow gasifier unit including gas processing and SNG or methanol production. The integration of an electrolysis unit, as in Buttler et al. [66], was also investigated as an option. In this concept, when excess electricity is produced, the gasifier and synthesis unit can be used as an energy sink for steam and electricity from the coal-fired power plant. In addition, the addition of an electrolysis unit for hydrogen production allows the power plant's demand to be further increased. In this way, the minimum load can be reduced from 50 to about 33% compared to an autonomous coal-fired power plant. In contrast, when electricity demand is high, the output of the coal-fired power plant is increased by a good 50% above the nominal load by feeding synthesis gas into the boiler. At very high electricity demand, the products generated, methanol or natural gas, can be reused for electricity generation in external plants.

The load gradients and their influence on the individual process steps of an IGCC plant have so far only been investigated by Todd et al. [70] and in particular, the gas cleaning with the complex absorption-desorption systems has been identified as a bottleneck. The assessments are mainly based on expert interviews as well as the limited operational experience with load transients. Experimental studies on load transient capability have not yet been found in the literature.

The existing studies concentrate on the technical evaluation of the concepts and the economics of predefined operating points. In particular, the question of when which operating mode in a flexible plant makes economic sense and which technical challenges arise for gasification and gas cleaning has not been the focus of attention so far.

1.4 Research Aim and Objectives

This study aims to investigate the performance of an integrated gasification combined cycle power plant with carbon capture for polygeneration, which was achieved through the following objectives:

1) Process modeling and simulation of an IGCC power plant:
    a) Model development and validation of gasification and gas treatment at pilot-scale that installed at the Technical University of Darmstadt.
    b) Scale-up of gasification and gas treatment to match a 360 MW_{el} combined cycle power plant.
    c) Model development and validation of a 360 MW_{el} combined cycle power plant located in Malaysia.
    d) Heat integration implemented between the Heat Recovery Steam Generator (HRSG), Gasification, gas treatment, and synthesis process.
2) Performance evaluation of the Acid Gas Removal (AGR) process using three different solvents, i.e., Selexol, Rectisol, and a-MDEA.
3) Conducting a thermo-economic assessment of the IGCC power plant for polygeneration based on co-gasification of lignite and Refuse Derived Fuel (RDF) at different blend ratios, considering variable prices for electricity and methanol.

1.5 Outline of the Thesis

The outlines of this study are as follows:

Chapter 1 Introduction. This chapter presented the background and motivation for studying the performance of integrated gasification combined cycle (IGCC) power plants. In addition, a literature review was conducted. Finally, the objectives of the study were stated and the outline of the thesis was presented.

Chapter 2 State of the Art of the IGCC. This chapter has provided an overview of the IGCC process and its components, including a summary of the different feedstocks for IGCC as well as the different components of the syngas treatment process in terms of their characteristics and their variants. Furthermore, it includes a summary of the different carbon capture and absorption technologies.

Chapter 3 Process Simulation of the IGCC Power Plant. This chapter included a brief description of the reference plants on which this study is based. Subsequently, a process simulation model of the IGCC power plant for polygeneration was developed using Aspen Plus software. This

model was developed by three steps outlined in this chapter. First, a process simulation model of the pilot gasification and gas processing plant was built according to the design data and specifications of the 0.5 MW_{th} pilot plant at TU Darmstadt. Second, the pilot-scale model was scaled up to an industrial scale based on a combined cycle power plant with a capacity of 360 MW_{el}. Third, a process simulation model was developed for the combined cycle power plant in Malaysia based on the plant's operating data.

Chapter 4 Results and Discussion. This chapter reported and discussed the results of the process simulation. The syngas composition in the main streams of the pilot plant process simulation model was presented. Then, an evaluation of the three different AGR processes was performed. Finally, a techno-economic assessment was carried out for the IGCC power plant for polygeneration of electricity and methanol under various availabilities and variable product prices.

Chapter 5 Conclusion and Outlook. This chapter summarizes the conclusions and recommendations from this thesis and provides an outlook for future research.

Chapter 2: **State of the Art of the IGCC**

In this chapter, an overview of the IGCC process and its components, including a summary of the different feedstocks for IGCC as well as the different components of the syngas treatment process in terms of their characteristics and their variants. Furthermore, it includes a summary of the different carbon capture and absorption technologies.

2.1 Gasification

Gasification is the transformation of carbonaceous fuels into a highly energetic gas with a useful calorific value, otherwise known as synthesis gas or syngas. It offers particular product flexibility; Power, chemicals, substitute natural gas (SNG) and transport fuels can all be generated from syngas. Furthermore, the gasification feedstock is extremely flexible, as almost all organic fuels like coal, oil, biomass, and wastes can be gasified as shown in Figure 2.1.

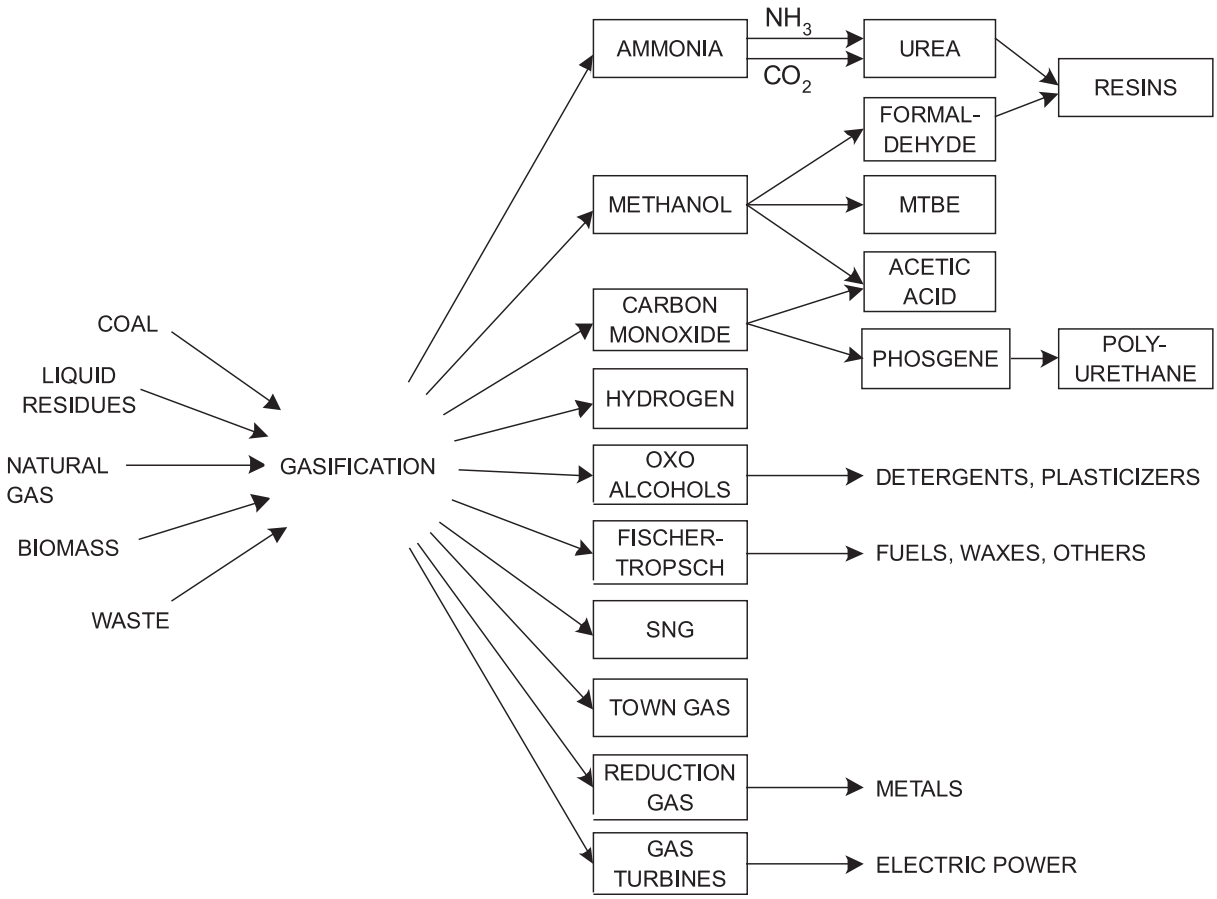

Figure 2.1 Feedstock and product flexibility of gasification [71]

The most common gasification technology basically includes pyrolysis, which is the addition of heat to fuel in the absence of oxygen, partial oxidation, and hydrogenation with hydrogen at high temperatures (800-1800 °C) and pressures of (10-100 bar) [71]. This produces a gaseous mixture with substances such as elemental carbon, carbon monoxide, carbon dioxide, hydrogen, water, and methane. The exact gasification temperature is set depending on the deployed feedstock. The main

issue to be considered when choosing the gasification operation temperature is the melting point of the feedstock ash. This work is concerned with gasification in the sense of partial oxidation of solid carbonaceous fuels, although pyrolysis of the fuel also occurs as an intermediate step in the technical processes considered for partial oxidation. Steam, O_2, or air is usually used as the oxidant in partial oxidation to produce a synthesis gas containing hydrogen and CO as the product gas.

During the gasification of solid fuels, several chemical reactions can occur simultaneously. These reactions can be classified into exothermic or endothermic reactions, depending on whether heat is released or absorbed, respectively. Furthermore, the gasification reactions can be subdivided according to their reaction educts states into homogenous and heterogeneous reactions. For homogenous reactions, the educts have the same state of matter (mostly gaseous state), while in the heterogeneous reactions the educts differ in phase states. A set of simplified major global reactions, the most relevant reactions during the gasification process are summarized in Table 2.1 where reactions heat (ΔH^o_R) are based on 298K and 1 atm.

Table 2.1 Basic gasification reactions [29,71]

Heterogeneous reactions	ΔH^o_R [MJ/kmol]		
$C_{(s)} + ½O_2 \rightarrow CO$	–110.5	Partial oxidation reaction	R 2.1
$C_{(s)} + CO_2 \rightleftarrows 2CO$	+172.0	Reverse Boudouard reaction	R 2.2
$C_{(s)} + H_2O_{(g)} \rightarrow CO + H_2$	+131.4	Steam-Char Gasification	R 2.3
$C_{(s)} + 2H_2 \rightarrow CH_4$	–87.4	Hydrogasification, Direct Methanation	R 2.4
Homogeneous reactions	ΔH^o_R [MJ/kmol]		
$CO + ½O_2 \rightarrow CO_2$	–283.1	Carbon monoxide oxidation	R 2.5
$CO + H_2O_{(g)} \rightleftarrows CO_2 + H_2$	–41.0	Water-gas shift	R 2.6
$CO + 3H_2 \rightleftarrows CH_4 + H_2O$	–205.7	Methanation	R 2.7
$CH_4 + ½ O_2 \rightarrow CO + 2H_2$	–35.7	Volatiles gasification via CH_4	R 2.8
$C_2H_2 + O_2 \rightarrow 2CO + H_2$	–447.83	Volatiles gasification via C_2H_2	R 2.9
$H_2 + ½O_2 \rightarrow H_2O$	–242	Hydrogen oxidation	R 2.10

Since fuels usually contain traces of other substances, like sulfur and elemental nitrogen, further secondary chemical reactions can take place in the gasifier. The fuel-bound sulfur tends to react with other syngas components into H_2S and COS, whereas nitrogen is prone to conversion into molecular nitrogen, NH_3, or HCN [71].

The established gasifier technologies can be divided into Moving-bed, Fluid-bed, and Entrained-flow gasifiers. These technologies are suitable for different fuels, especially concerning particle size, ash composition, and the associated ash melting behavior as well as reactivity.

2.1.1 Moving-bed Gasifier

In moving-bed gasifiers (also called fixed bed gasifiers), the feedstock is fed at the top of the bed and falls slowly by gravity as it is being heated by a high-temperature blast in co-, counter-, or cross-current. A counter-current blast is generally preferred since it allows for better heat transfer. As depicted in Figure 2.2, three vertical heat transfer regions are distinguished when operating a counter-current moving bed gasifier. Coal is burnt in the lower regions, providing sufficient heat for the gasification of the coal in the middle region. The residual heat of the rising gases serves to dry the coal of the upper region that had just been introduced. Examples of commercially successful moving-bed gasifiers are the Lurgi fixed-bed gasifier from AirLiquide (Lurgi FBDB) and the

British Gas/Lurgi (BGL) gasifier from Zemag GmbH. The basic design of these two gasifiers is shown in Figure 2.3.

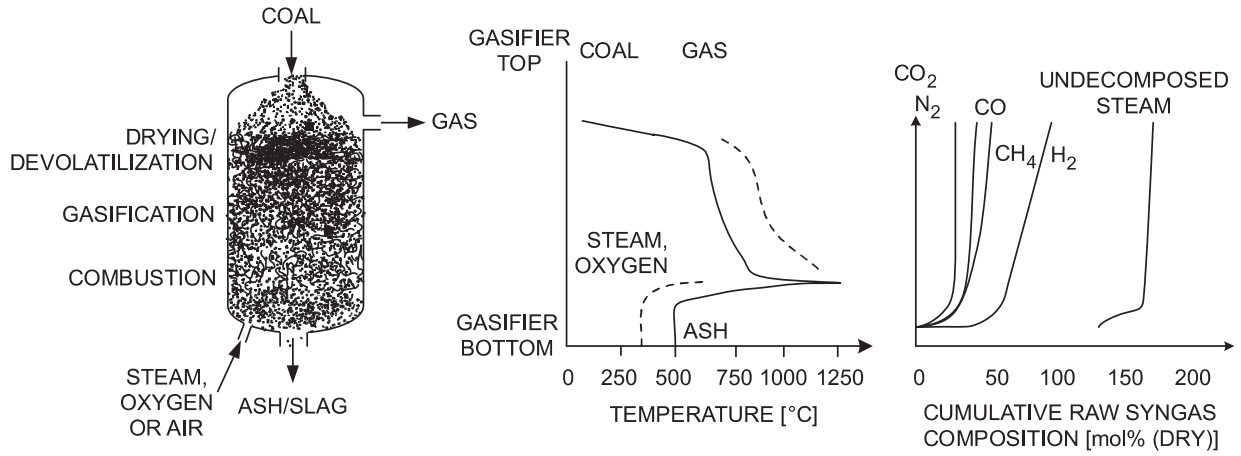

Figure 2.2 Illustration of Moving-bed Gasifier (Sasol-Lurgi) [71]

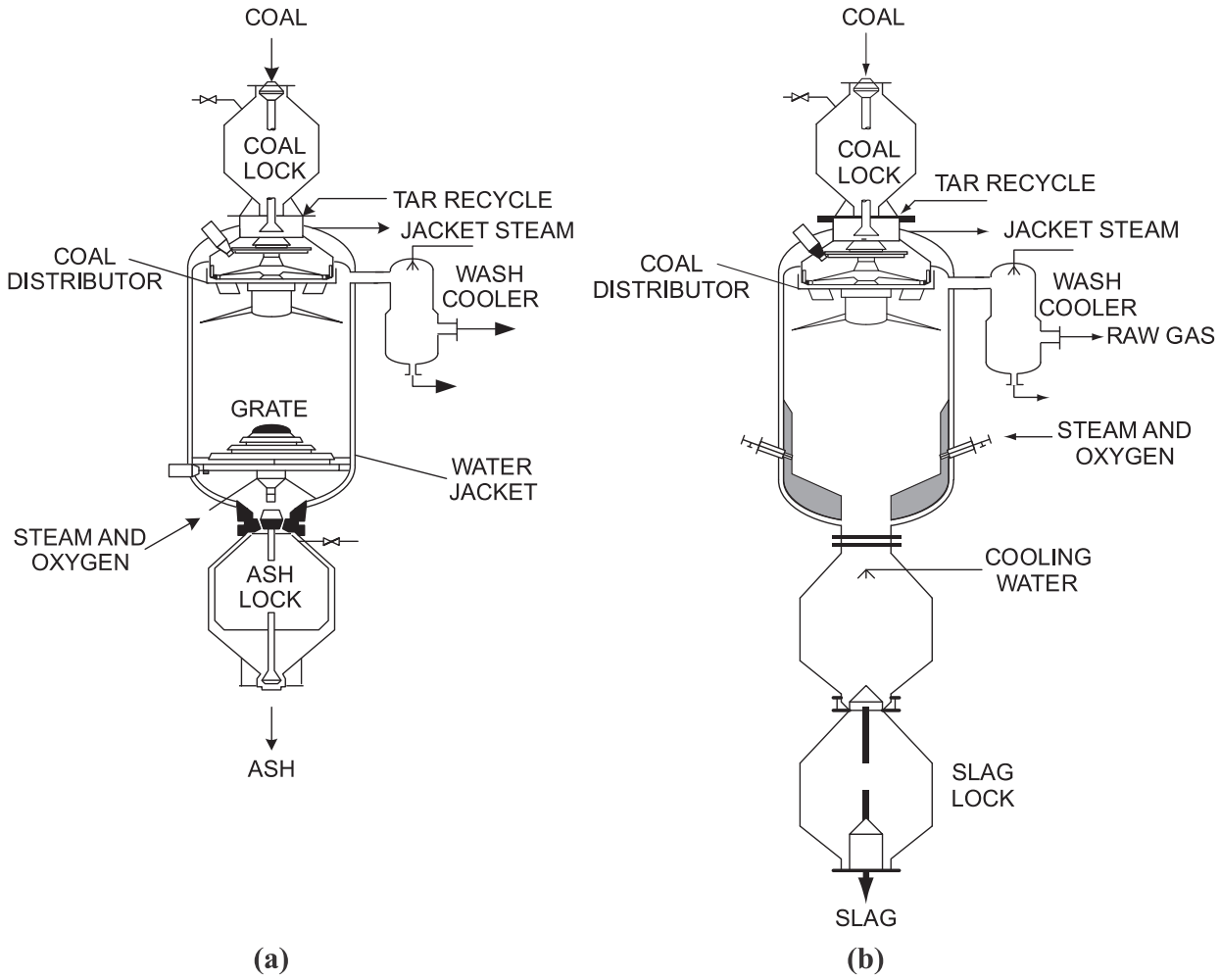

Figure 2.3 (a) Lurgi FBDB and (b) BGL gasifier [71]

Before the gasification, the feedstock is generally crushed in grinding mills to coarse granulates of 6-50 mm. Then gasified in a reactor whose temperature reaches 700-1200 °C in the co-current reactor and 700-900 °C in the counter-current reactor, producing a syngas of 420-650 °C [72]. The syngas typically contains a relatively high methane content that can range from 10 to 15% [73]. The moving bed processes stand out by their very high cold gas efficiency, which is frequently around 90% [73].

The main drawback of the moving bed gasifiers is the relatively high fraction of tar in the syngas. Hence, the entrained tar is capable of condensing during syngas cooling [73]. For this reason, coke and anthracite are the recommended feedstocks for this gasification process, given that they contain lower levels of tar [71].

2.1.2 Fluidized-bed Gasifier

The Fluidized-bed (also called fluid-bed) gasification is based on the fluidization of solid feedstocks. In fluidized-beds, the feedstock is fluidized with liquid or gaseous media, i.e. flowed through from below, to create a so-called fluid-bed (see Figure 2.4). For fluidization to occur, the pressure drop across the fluid-bed must exceed the weight and holding forces of the particles. After exceeding this limit point, the so-called minimum fluidization, a stationary fluid-bed initially forms. In this, mixing of the particles occurs, but not yet entrainment. If the fluidization velocity is increased further, the pressure drop across the fluidized-bed initially remains constant and the height of the fluidized-bed and its porosity increase. Only when the fluidization velocity is increased further does a discharge of the particles from the fluid-bed occur from a point, the discharge point. From this speed, the pressure drop increases again. If the discharge point is exceeded, particles are entrained and have to be separated from the gas phase in a cyclone and returned to the bed. Such fluidized-beds are called circulating fluidized-beds. If the fluidization velocity is further increased to well above the discharge point, the fluid-bed disintegrates and all particles are immediately pneumatically transported further after entry into the reactor (see Figure 2.5) [74]. The fluidized-bed generated by fluidization is characterized by very good mixing and fluid-like properties in terms of heat and mass transfer.

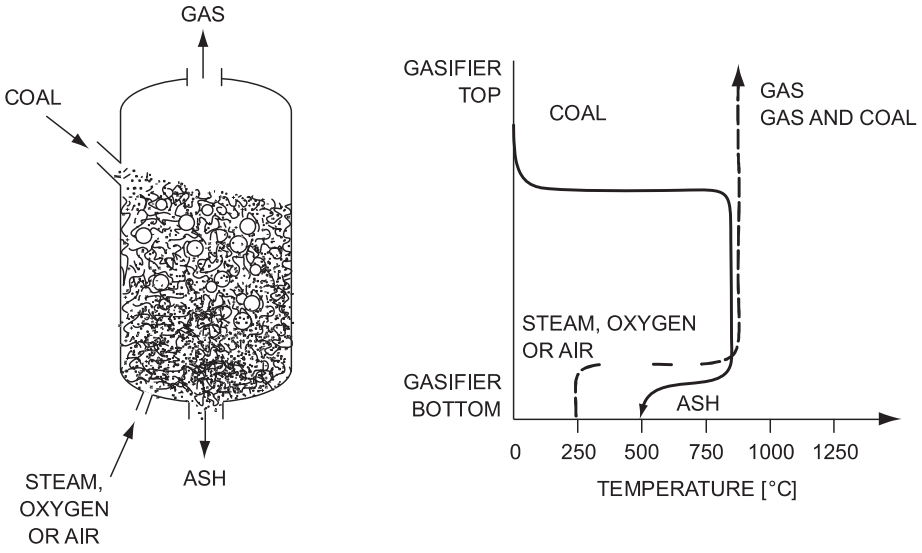

Figure 2.4 Illustration of the Fluidized-bed gasifier [71]

The first commercial, large-scale use of fluidized bed reactors was as gasifiers for the Winkler process [74]. Therefore, the development of fluidized bed technology is also closely related to gasifier development. fluid-beds are suitable for particle sizes less than10 mm to achieve their optimal fluidization. The typical operating temperature of the fluid-bed processes ranges between 950-1100 ℃. This temperature interval shouldn't be exceeded to avoid the softening point of the ash, which leads to the formation of agglomerations. The operation temperature shouldn't be dropped below 950 ℃ for coals and about 800 ℃ for biomasses either, otherwise, the tar content in the syngas would increase considerably [71]. In order to achieve sufficient reactivity despite the lower temperatures, reactive coals, i.e. lignite, or biomasses are preferably used as feedstocks. Typical carbon conversion rates for fluid bed processes range from 95 to 97%, whereas the cold gas efficiency is about 85% [73].

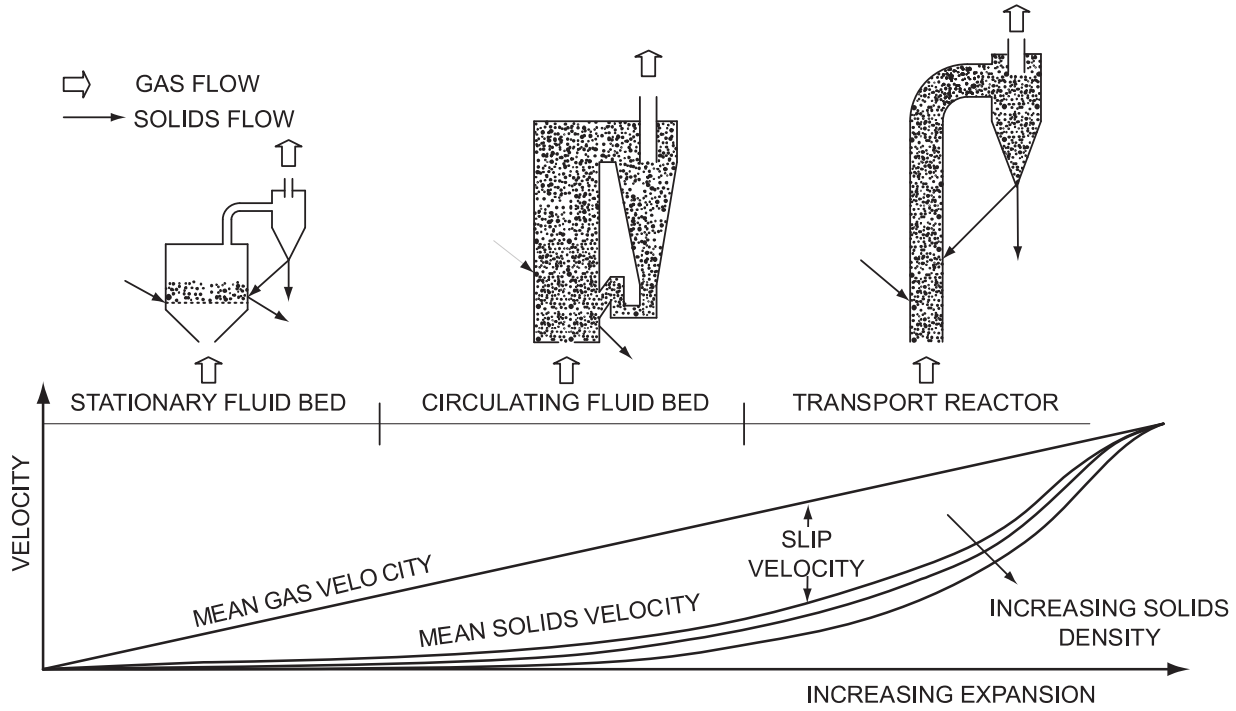

Figure 2.5 Fluidized-bed Regimes [71]

2.1.2.1 **High-Temperature Winkler Process (HTW)**

High-temperature Winkler process (HTW process), which is a particular configuration of fluidized-bed gasifiers, as a further development of the Winkler process from 1920 and the Kellogg, Brown, & Root (KBR) Transport Gasifier (also known as TRIG Transport Integrated Gasification) [71]. In the field of biomass gasification, the two-bed fluidized-bed gasification should be mentioned, as it was used for wood in Güssing, Austria from 2002 to 2016 [75]. Another commercially available gasification process is the Enerkem process for gasification of household waste, which uses a bubbling fluidized-bed and has been used in Edmonton, Canada since 2011 [76].

The focus of this work is on the HTW gasifier. This fluid-bed gasifier is a further development of the atmospherically operated Winkler gasifier and differs from the latter mainly in the increased process pressure and the use of a gasification zone with elevated temperatures to reduce the

hydrocarbon content in the product gas [77]. The basic design of the gasification reactor can be seen in Figure 2.6.

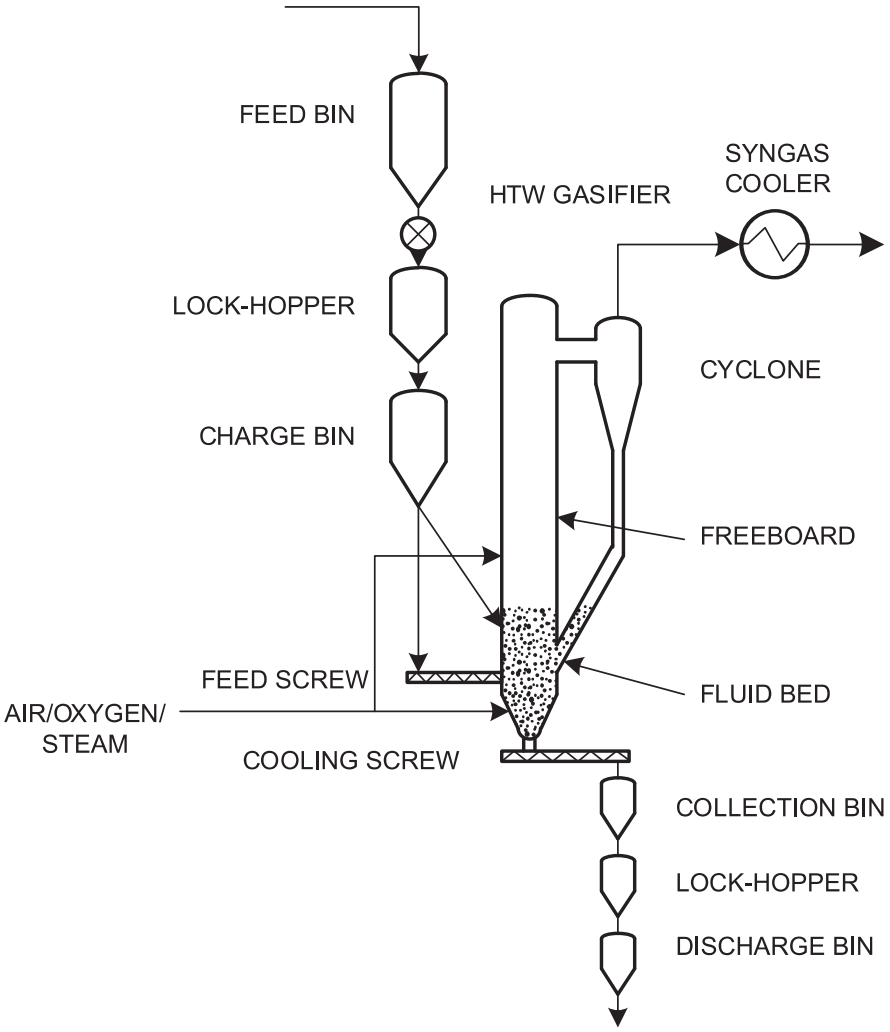

Figure 2.6 Schematic of HTW Gasifier [71]

In the HTW process, the raw product gas is cooled through a raw gas cooler, which is designed either as a shell-and-tube heat exchanger or as a flue tube cooler. The design with water- and steam-carrying tube bundles is more expensive, but allows higher steam parameters and is thus particularly interesting for applications in connection with an integrated gas and steam power plant. The design with a flue tube cooler is less expensive, but can only produce saturated steam up to about 150 bar [78]. A special form of the flue tube cooler is the Schmidt'sche Schack design with a double tube and oval collector [79]. In these, the cooling water is guided at a high velocity in an annular gap around the flue tubes, thus improving the heat transfer compared to classical flue tube heat exchangers. Headers consisting of oval tubes are used because they achieve similar strength to normal headers with a smaller wall thickness. The lower wall thickness improves the resilience of the raw gas cooler to temperature fluctuations [80].

The HTW process is suitable and proven for a wide range of feedstocks, which makes it very interesting for use in polygeneration concepts that are also intended to use waste streams as feedstocks. The most extensive operational experience with HTW technology has been gained for the use of lignite or peat. In particular, the HTW gasifier in Berrenrath, which was operated by

Rheinbraun/RWE from 1986 to 1997, should be mentioned here. This plant had a thermal output of 160 MW with a throughput of 720 t of lignite per day. The operating pressure of the plant was 10 bar [77]. In addition to lignite, co-gasification with pelletized municipal waste was also investigated in this plant in three test campaigns. Up to 50% of the lignite was replaced by domestic waste without any restrictions in operation and syngas quality [81]. Further experience with gasification of waste in an HTW gasifier was gained in Niihama in Japan. In an HTW demonstration plant, 20 t of domestic waste per day was converted into an atmospherically operated gasifier from 1999 onward [81]. In Oulu, Finland, an HTW gasifier with 10 bar operating pressure produced 300 Nm^3/h of ammonia from 30 t/h of peat from 1988 to 1990 [80]. Higher operating pressures, requiring a more elaborate sluice system for solids input and output, have also been investigated. For this purpose, a pilot plant in Wesseling was operated from 1989 to 1992 at various pressures up to 25 bar [71,77].

2.1.3 Entrained-flow Gasifier

Entrained-flow gasifiers utilize pulverized fuel by converting it at high temperatures of usually more than 1400 °C to sometimes more than 2000 °C [71]. In so-called "slurry-type" gasifiers, the fine-grained fuel is emulsified in water. Due to the high temperatures in entrained flow gasifiers, the gas species in the product gas are in thermodynamic equilibrium and thus free of hydrocarbons. In addition to the high-quality, methane-free product gas, the high temperatures in the reactor also lead to melting of the ash and almost complete conversion of the coke and lead to a higher oxygen demand than in moving-bed and fluid-bed gasifiers. However, it is suitable for almost all sorts of solid fuels, including those with high moisture levels and low reactivity [71,73]. The technical designs of entrained-flow gasifiers are very diverse and differ, among other things, in terms of the feed system (dry or slurry) and the design of the reactor wall (lined or water-cooled membrane wall). The arrangement of the nozzles and burners can be tangential, axial, or radial (so-called boxer firing) (see Figure 2.7), and the cooling of the hot product gas can be done by quench or through a raw gas cooler [29,71]. The most commercially successful entrained-flow gasifiers are the GE Energy Process (GEE; formerly Texaco) and the Shell and Prenflo gasifiers, both of which are based on the Koppers-Totzek process [29,71]. The GEE process uses a lined reactor and is top-fired with a slurry, or coal-water emulsion [71]. Shell and Prenflo diaphragm-wall cooled gasifiers are fired with dry pulverized coal through burners located radially on the reactor in the lower section in a boxer design [71]. Another now very successful process is the OMB gasifier developed at East China University of Technology (ECUST), which uses coal slurry as fuel through four radially arranged burners in the upper region of the lined reactor [29,82,83].

In the entrained-flow gasifiers, a major portion of the ash particles achieves their melting point and phase transition. About 60% of the ash leaves the reactor bottom in a liquid state, as slag. The remaining 40% is entrained with the gas and separated in the following steps. Because of the extremely high reactor temperature, the inside walls of the gasifier are generally coated with fireproof material. The cold gas efficiency of the process is generally below 85%, and the carbon conversion lies at more than 99%. [73]

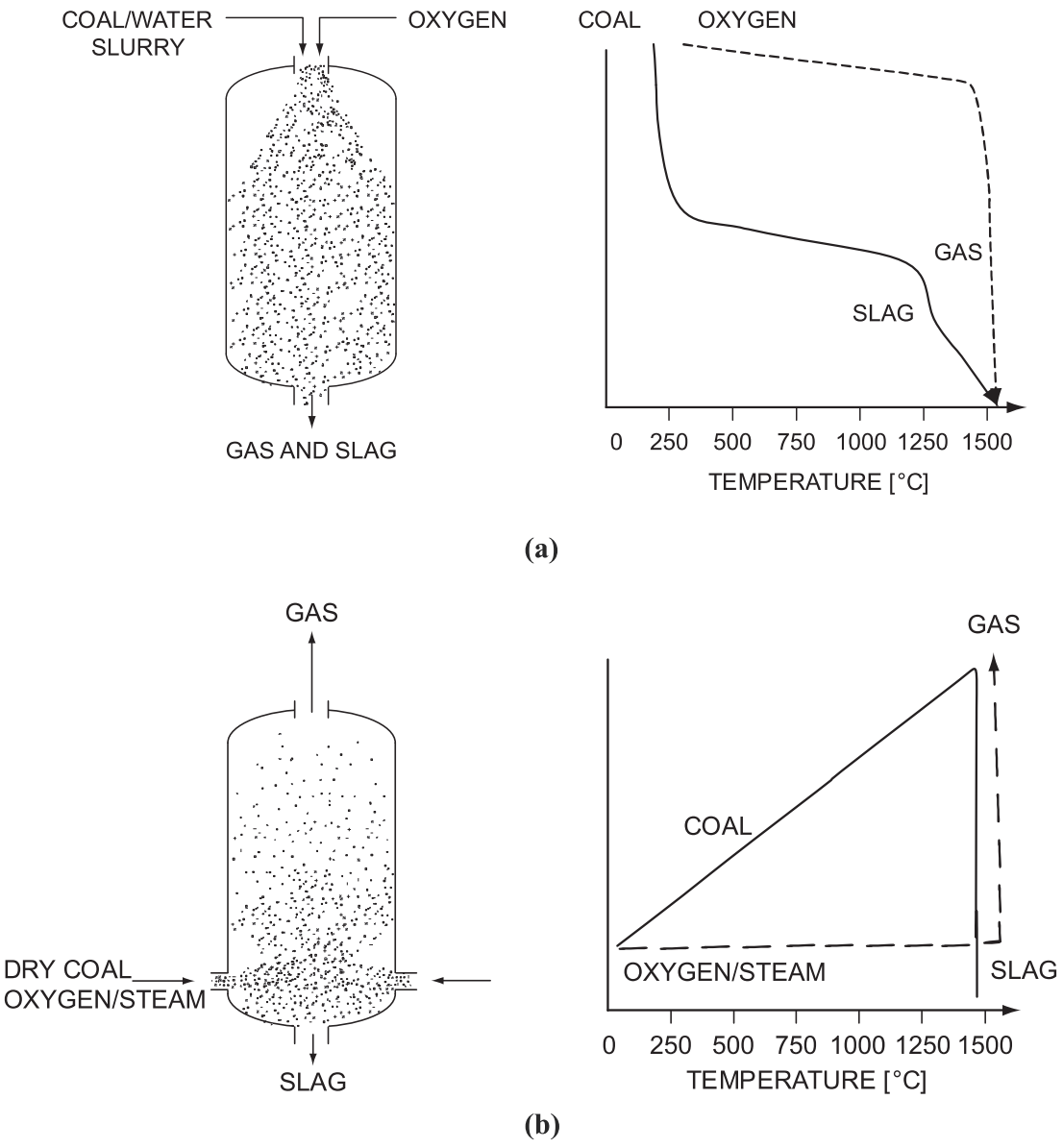

Figure 2.7 Illustration of Entrained-flow Gasifier (a) Top-fired coal-water slurry feed slagging (b) Side-fired dry coal feed slagging [71]

2.2 Feedstock Pretreatment and Drying

Pretreatment is necessary before using the feedstocks in gasification, depending on the gasification process and the feedstock, in order to obtain the necessary fuel characteristics. The main fuel characteristics that are influenced in the pretreatment are the fuel moisture and the grain size or particle size distribution. In this work, the focus is on gasification using the HTW fluidized bed process. An average particle size of less than 10 mm is desirable [71,81].

The moisture content of the feedstock has a significant influence on the efficiency of gasifiers since a higher fuel moisture content implies a higher energy input into the gasifier to evaporate the water. In high-temperature gasifiers, which draw the necessary heat for the gasification process from the fuel, the higher energy requirement reduces the cold gas efficiency, i.e. the ratio of chemical energy of the feedstock to the chemical energy of the product gas. Residual moisture can be removed by mechanical and thermal drying, i.e., without phase change of the water in the fuel, and thermal

drying, i.e., by evaporation or evaporation of the water [29]. In the field of large-scale lignite utilization, only thermal drying has become established, due to the high adhesive forces of the water in the coal [84]. Thermal drying is also preferably used in the field of refuse-derived fuels (RDF), e.g. by belt and drum dryers for the preparation of wood for pelletization [85].

2.3 Syngas Cleaning and Treatment

Syngas cleaning is an essential process of a gasification system. Cleaning eliminates the impurities and other undesired compounds from the product gas. This treatment follows, according to the polygeneration process, a defined arrangement (see Figure 2.8). First, a major part of the syngas heat is extracted in a syngas cooler. This heat is generally recovered by producing steam, which generates power using a turbine. Then, the syngas follows several stages of scrubbers and separators that reduce the syngas' pollutants content to adequately sustainable levels. These remove solid particles, halides, benzene, naphthalene, Carbonyl sulfide, and acid gases. The hydrogen-carbon monoxide ratio in the syngas should also be adjusted, depending on the production target. That is generally achieved with steam in a water gas shift reactor.

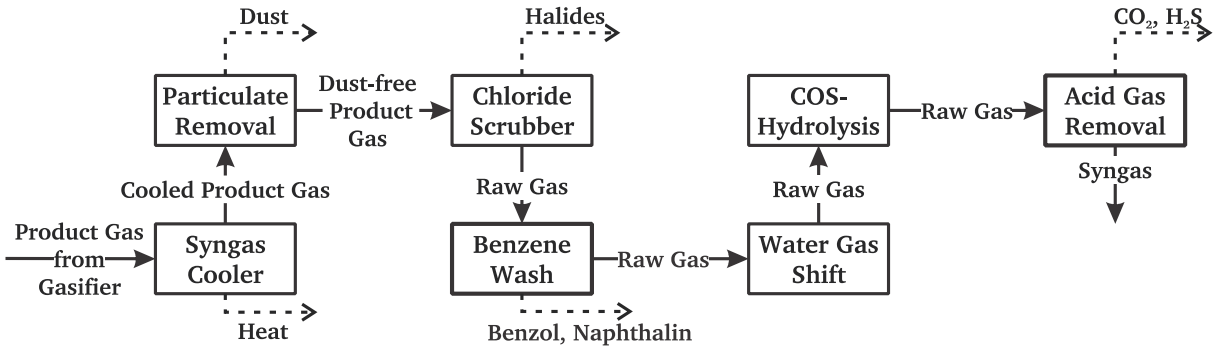

Figure 2.8 Syngas treatment process for a Polygeneration plant

2.3.1 Syngas Cooling

Syngas is produced at high temperature using the gasification reactor, ranging from 500 to 1600 °C in accordance with the selected technology [86]. The raw syngas at this high temperature, if this raw syngas could be burned directly in the gas turbine (GT), all of the heat generated in the gasifier that wasn't consumed by the endothermic gasification reactions would have been saved and effectively used by the GT to produce power. Nevertheless, because of the contaminants and undesired compounds in the raw syngas, it has to be cleaned to be suitable for final use, as fuel or as a chemical feedstock. On the other hand, the syngas treatment and cleaning process require a lower temperature than that of the gasifier. It will also in most circumstances be desired to employ the sensible heat in the gas, e.g. through steam generation, which could be used in the syngas treatment process or by using it with the HRSG in the IGCC process. Thus, the syngas must continually be cooled. On the other hand, changes in contamination varying from feed to feed as well as the features of the various processes of gasification itself lead to a wide selection of cooling solutions for syngas.

2.3.2 Solid Particles Removal

Solid particles removal is the second step of syngas treatment. A common solution able to remove solid particles from syngas at elevated temperatures is candle filtration. It is generally deployed after a cyclone separator removes the heaviest particles from the syngas. The candle filters are mostly composed of ceramic material. At the microscopic level, the solid particles are rejected and only the gas phase passes. The deposited particles fall to the bottom of the filter vessel, from where they are evacuated by a lock-hopper. Candle filters are generally operated at temperatures of 340-500 °C [29]. They can principally afford higher temperatures. This would, however, raise the partial pressure of some ash components dramatically, enough to allow substantial transport through the filters.

2.3.3 Chloride Scrubbers

After the filtration process, the warm product gas still usually contains a small concentration of solid particles and a considerable fraction of chlorides. Most of the chlorine is found as part of hydrogen chloride molecules (HCL). Upon contact with metal, hydrogen chloride can react to metal chlorides. These substances can be very hazardous for heat exchangers since they could lead to fouling. Chlorides are often considered as catalyst poison, especially for catalysts that are used for methanol synthesis, COS hydrolysis, and low-temperature water-gas shift. For these reasons, chlorine substances are usually separated at an early stage. A common method able to remove most chloride components as well as the small amounts of solid particles is water scrubbing. [29,87,88]

Water scrubber for chloride separation generally consists of water quench and washing column. The water quench occurs in a vessel containing water in its bottom, and a submerged dip pipe. The syngas is blown via the dip pipe below the vessel's liquid level, settling the majority of chlorides and solid impurities. During this quench, the syngas evaporates and entrains a considerable amount of water. The syngas leaves this stage in a saturated state. The vessel is continuously fed with fresh water, so its chloride concentration on a mass basis doesn't exceed 500 ppm. After the quench, the syngas is introduced in a washing column, where further chlorine particles are removed. A demister stands at the top of the washing column to prevent liquid water droplets from being entrained by the purified syngas.

2.3.4 BTX Scrubber

In fixed-bed and fluidized-bed gasifiers, the product gas contains relevant proportions of tar-like hydrocarbons. This includes all hydrocarbon compounds with a molar mass of 78 g/mol or more, corresponding to the molar mass of benzene [89]. They are subdivided into primary, secondary, and tertiary tars. Primary tars are released directly during pyrolysis. Higher temperatures and residence times lead to the volatilization of further components from the tars, from which secondary tars, i.e. phenols and olefins, and finally tertiary tars, the polycyclic aromatic hydrocarbons, are formed. In fluidized-bed gasifiers, (polycyclic) aromatics such as benzene and naphthalene and their derivatives are released in particular [90]. These components, usually grouped under the abbreviation BTX (Benzene, Toluene, Xylene), can condense out in the gas cleaning process and thus lead to clogging and blocking of pipelines, clogging and deactivation of catalysts, and negative influence on washes, especially foaming of the detergent. Effective

separation of these condensable hydrocarbons is therefore of great importance for the high availability and performance of gasification plants.

In gasification processes with low tar loading, the BTX components can be condensed out at cold points in the process and removed together with the aqueous condensate. Condensed out at cold points in the process and removed together with the aqueous condensate. In addition, two basic approaches exist for removing the condensable hydrocarbons from the gasifier product gas stream: catalytic cracking of the compound and separation using a scrubbing oil [71]. In catalytic cracking, the hydrocarbons are decomposed over a catalyst. The range of possible catalysts is wide, ranging from precious metals to nickel to natural ores, such as dolomite, magnesite, or calcite [71]. Comparatively, high temperatures of about 750 to 900 °C are required [71]. Due to the high temperatures required, catalytic treatment of the hydrocarbons must usefully precede raw gas cooling. Current research on such hot gas purification is taking place at the BioLiq™ plant in Karlsruhe, Germany, among others, with operating temperatures exceeding 500 °C [64]. An interesting approach to catalytic cracking is to combine it with particle separation. Ceramic filter cartridges, which have been vaporized or impregnated with a catalyst, are used here [71].

The removal of hydrocarbons with oil has already been successfully employed in the two-bed fluid-bed gasification of biomass in Güssing, Austria. Here, biodiesel, i.e. fatty acid methyl esters obtained from rapeseed, was used as a scrubbing oil. The loaded oil was not regenerated in this process but used as fuel for the fluid-bed used as a combustion chamber [71,75]. The so-called OLGA process is also commercially available. This was developed by ECN and uses mineral oil as the scrubbing liquid [91]. The OLGA process exploits the different dew points of the components for the separation of the tars and is operated above the dew point of the water contained in the syngas. A simplified flow diagram is shown in Figure 2.9. The syngas is first cooled in the collector and the heavy tars are condensed out in the mineral oil used for cooling. The mineral oil is recycled, and the heavy tar components are removed from the process using a separator. After the collector, the pre-cleaned syngas is passed through a wet electrostatic precipitator into the absorber. The electrostatic precipitator separates aerosols from the collector and feeds them to the mineral oil of the collector. In the absorber, the light tar components are absorbed with the mineral oil. Regeneration of the scrubbing oil is done with steam or air. Both the heavy and light tars can be returned to the gasifier for thermal conversion [91].

Another approach based on scrubbing oil was developed by Thielert et al. [92]. In this approach, absorption is carried out at a lower temperature of about 30 °C and thus below the dew point of the water in the synthesis gas. In addition, instead of mineral oil, rapeseed methyl ester (RME) is used as a solvent for the BTX fractions in the synthesis gas. The advantage over the OLGA process is the better separation of the BTX fraction and the lower viscosity and higher heat capacity of the scrubbing oil [92,93]. Therefore, this approach is particularly interesting when no energy, but a material use of the synthesis gas is intended. A disadvantage is that a way must be found to deal with the aqueous condensate from the synthesis gas.

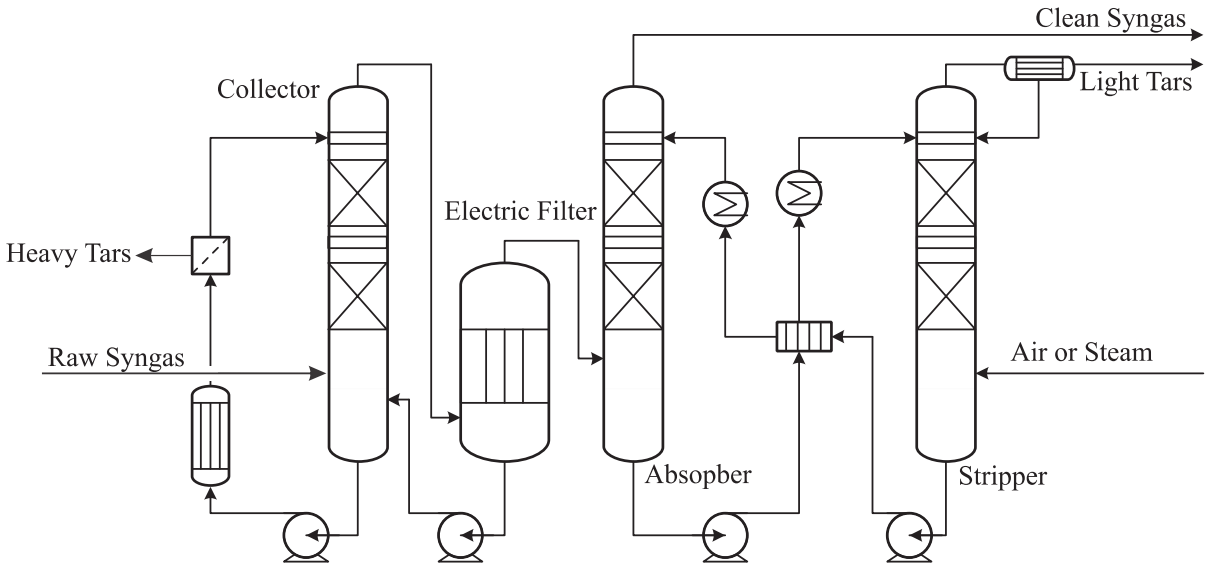

Figure 2.9 Process flow diagram of the OLGA process [71]

2.3.5 Water-gas Shift

The optimal syngas composition varies depending on the targeted product. Whereas an optimal molar H_2/CO ratio of one is generally appropriate for the production of oxo alcohols, a molar ratio of about two is desired for methanol and Fischer-Tropsch products. For the production of ammonia and hydrogen, or even for power generation, the CO fraction in the syngas should be preferably decreased as low as possible [71]. In order to reduce CO-fractions to the desired level, a water gas shift reactor is normally deployed. In this reactor, carbon monoxide is reacted with steam to carbon dioxide, producing more hydrogen (R 2.6).

The water-gas shift reaction is exothermic and requires the use of an appropriate catalyst. The shift reactor temperature shall be kept at a relatively low temperature that ranges between 200 °C and 500 °C, to promote the extent of reaction. Besides, the shift reaction is independent of pressure, given that the reactants and products involved are stoichiometrically equimolar. In water gas shift technologies, a basic distinction can be made between the high-temperature process, the low-temperature process, and acid conversion.

The high-temperature process, developed by BASF in 1914, runs from 300 to 500 °C and can reduce the CO concentration to about 3% with the iron-chromium catalyst. The deactivation of the catalyst mainly occurs due to unavoidable sintering processes during startup and operation. Temperature control is also of particular relevance during operation and aims at avoiding temperatures above 500 °C in order not to further favor the sintering processes. These temperature peaks can occur, among other things, due to excessive concentrations of hydrogen in the gas mixture supplied to the reactor and the resulting highly exothermic reduction of iron oxide to elemental iron. Under normal operating conditions, the steam/hydrogen ratio should be greater than 0.4 and the CO_2/CO ratio greater than 1.2 [94]. Measures to control the temperature in the reactor include gas-to-gas heat exchangers integrated into the reactor in the Lurgi/Air Liquide and Casale processes, injection of condensate into the reactor, and a high steam-to-gas ratio. The iron-chromium catalyst can also be used with sulfur-containing synthesis gases, but in the presence of sulfur, it is sulfided according to (R 2.11), which leads to a sharp reduction in the activity.

Therefore, for sulfur-containing synthesis gases, either the sulfur components should be removed before conversion or a high vapor partial pressure should be run [95]. A high steam fraction shifts the equilibrium of the conversion to hydrogen and CO_2 and improves the kinetics of the reaction over the iron-chromium catalyst. Energetically, a high steam fraction is not desirable because it reduces the efficiency of the overall system. If the amount of steam is too low, there is a risk of iron carbides forming, which catalyze the formation of hydrocarbons [94,95].

$$Fe_3O_4 + 3H_2S + H_2 \rightleftarrows 3FeS + 4H_2O \quad \Delta H^\circ_R = -75 \text{ MJ/kmol} \qquad \text{R 2.11}$$

The low-temperature process developed in the 1960s operates in the 200 °C to 250 °C range using a copper-zinc catalyst [96]. Due to its high activity in the low-temperature range, this catalyst can be used to produce shifted gas with less than 0.3% CO [94]. The main application of this process is ammonia plants using hydrogen from steam reforming. Here, the purity of the hydrogen produced has a high influence on the ammonia production in terms of yield and necessary purge gas quantity [71]. Apart from sintering processes above 300 °C, the catalyst is deactivated mainly by chlorine and lowest sulfur concentrations < 0.1 ppm [94]. Use in the field of gasification of coal, oil, or petroleum coke is therefore unusual. In addition, there are the pyrophoric properties of the catalyst, very high sensitivity to capillary condensation when operating near the dew point, and high sensitivity to local temperature peaks [94–96].

When gasifying feedstocks containing sulfur, such as coal or oil, a sulfur-tolerant conversion process is desirable because it eliminates the need for a two-stage acid gas removal and all acidic components must be removed only after CO shift [71]. The sour shift process uses cobalt-molybdenum catalysts, which must be sulfided with sulfur-containing gases. Accordingly, minimum sulfur content is required for the operation of the catalyst, which is in the order of 300 ppm [94]. With sufficient activation prior to operation, the catalyst can also be used with sulfur contents as low as about 35 ppm [94]. The sour shift process is operated at temperatures between 250 °C and 350 °C, which is why it can achieve significantly lower CO concentrations than the iron-chromium catalyst in the high-temperature process [95]. In addition, lower steam-to-gas ratios are also required, since the reduction of cobalt and molybdenum sulfides and associated potential synthesis of hydrocarbons are not expected [97].

Conversion plants for syngas from coal gasification are usually of two- or multi-stage design, with preheating and intercooling. The first stage is operated at higher temperatures to benefit from the higher reaction rates. The other stages are designed for low temperatures to obtain the lowest possible residual CO in the syngas [73]. Depending on the process pressure, the necessary moisture before the first conversion stage can be present from quench or halide scrubbing alone or can be achieved by adding saturated steam. The gas is preheated to approximately 300-350 °C and directed to the first stage [71]. The first conversion stage is usually equilibrium limited and reaches CO contents of about 5%. The gas is then cooled and fed to the further conversion stages, which are often kinetically limited due to the lower temperatures. Depending on the design of the reactor, CO contents < 0.5 % can be achieved there [71].

The energetic efficiency of the water-gas conversion is essentially determined by the steam requirement or the possible steam generation within the conversion. If the unconverted syngas already has sufficient moisture for the desired conversion, there is no need for an additional steam

feed before the first conversion stage. If a higher steam fraction is required for conversion operation, there are several innovative approaches to reduce the requirement for medium pressure steam. As an example, two concepts by Carbo et al. [98] and Martelli et al. [99] are shown in Figure 2.10 and Figure 2.11, respectively. The approach of Carbo et al. [98] provides that only a part of the synthesis gas is fed into the first conversion reactor, and thus the steam demand for this reactor is also reduced. The intercooling between the stages is done with a water quench, as well as the supply of further synthesis gas. The approach of Martelli et al. [99] is comparable, but instead of a water quench, it uses steam injection and heat exchangers for cooling between the conversion reactors. Both approaches can reduce the demand for steam compared to the conventional approach with two sequential conversion reactors at the expense of higher investment costs.

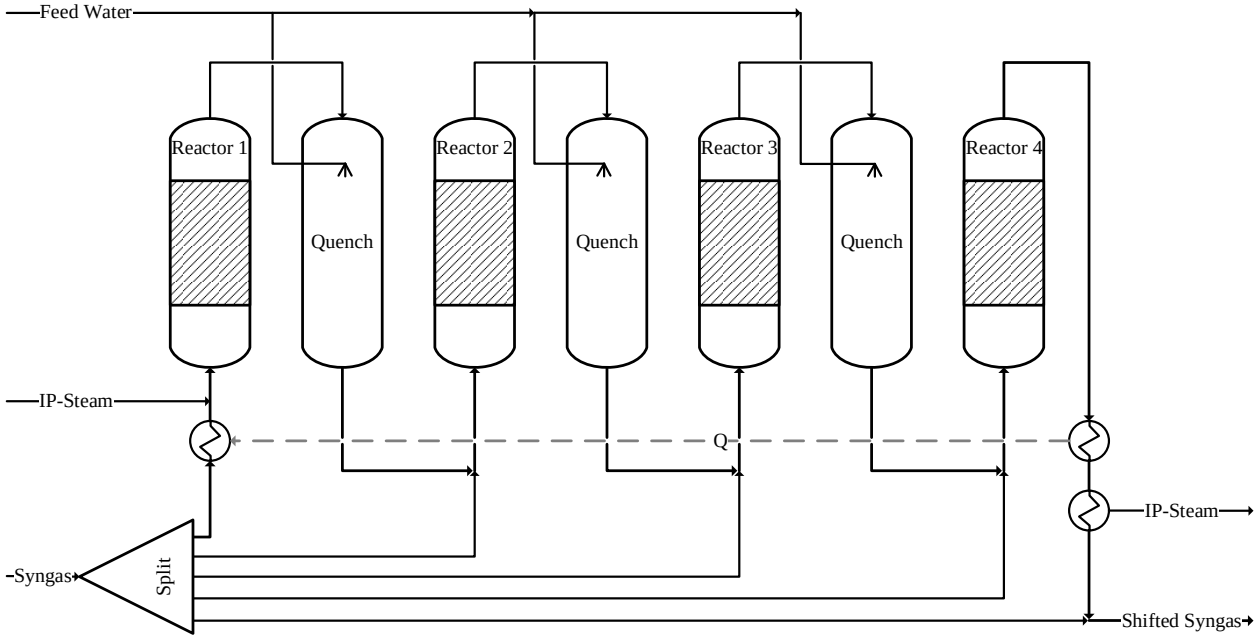

Figure 2.10 Multi-stage water-gas conversion with water quench for intercooling [98]

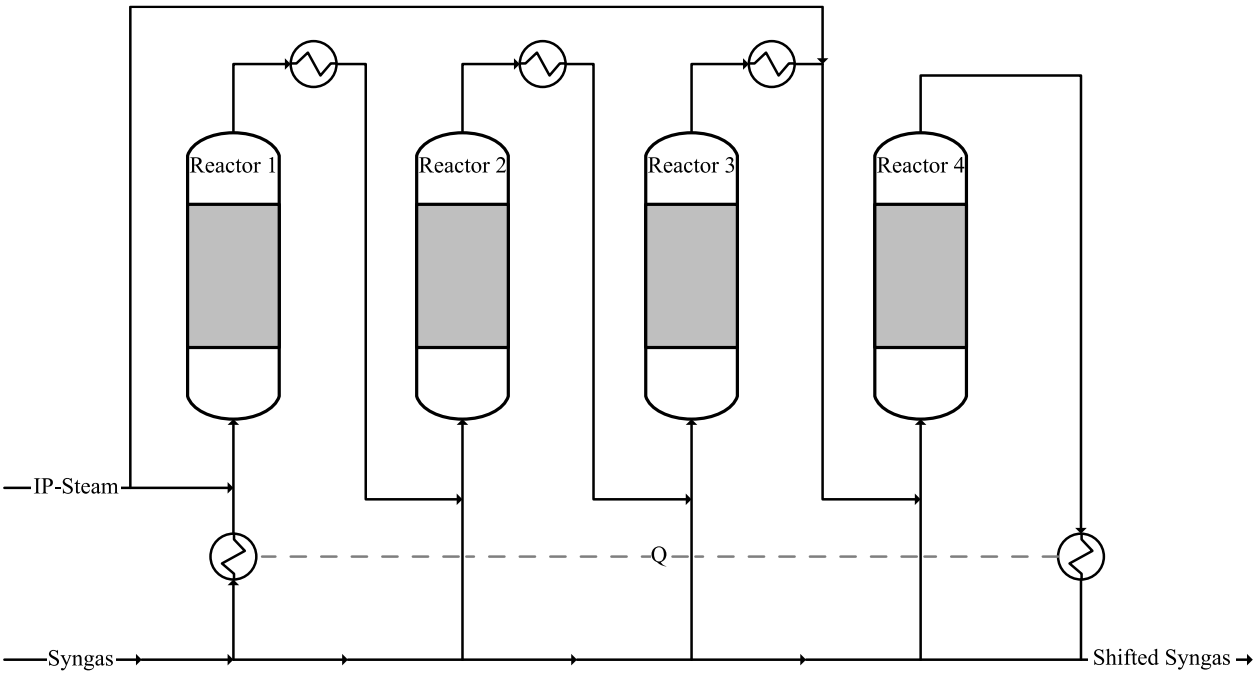

Figure 2.11 Multi-stage water-gas conversion with multi-stage steam injection [99]

In the flexible use of power plants for polygeneration of electricity and fuels, the flexibility of water-gas shift can play a critical role in switching between electricity production with as complete CO_2 capture as possible and hydrocarbon production. In electricity production, the complete unconverted syngas stream would be passed through the conversion. In the production of Fischer-Tropsch products or methanol, on the other hand, depending on the CO/H_2 ratio of the gasifier product gas, about half of the unconverted syngas is not converted, and the conversion load is reduced by 50% accordingly. Partial load conditions have no significant effect on the performance of the conversion. The load cycling capability has not been studied intensively but is more than 2% per minute without negative effects on the catalyst [67].

2.3.6 COS Hydrolysis

Sulfur components are considered poisonous for the catalysts and equipment usually employed for chemical synthesis. 90% of the sulfur components released by coal gasification are H_2S, which tends to be separated in the acid gas removal unit (AGR). The remaining Sulfur is bound in molecules of carbonyl sulfide (COS). To make the COS particles easily separable in the AGR unit, they are usually converted into H_2S molecules through hydrolysis. The chemical equation (R 2.12) dictates the hydrolysis of COS [71,73].

$$COS + H_2O \rightleftarrows H_2S + CO_2 \qquad \Delta H^o_R = -30 \text{ MJ/kmol} \qquad \text{R 2.12}$$

Typically, COS hydrolysis takes place in a reactor with the presence of an appropriate catalyst at a temperature of 160-300 °C. Appropriate catalysts include chromium oxide-alumina, pure activated alumina, or titanium oxide. The deployment of a Rectisol process for the acid gas removal can make the COS hydrolysis procedure obsolete since this method can separate COS from other acid gases [71,73].

2.3.7 Acid Gas Removal

Despite the several previous scrubbing stages, the syngas still contains a high amount of acid gases with critical environmental damage potentials. These acid gases, which essentially include hydrogen sulfide (H_2S) and carbon dioxide (CO_2), possess very low water solubility. Due to this fact, they are generally not or only slightly separated during the previous washing processes. To deplete the syngas of acid gases before the combustion, acid gas removal (AGR) is required.

There are numerous processes for AGR. For sour gas treatment of gasifier product gas, mainly solvent-based processes are used on a commercial scale. The basic flow diagram of all solvent-based processes can be seen in Figure 2.12. In an absorber column, the gas to be purified is brought into contact with the solvent and the gas components to be dissolved pass into the solvent. The purified gas leaves the top of the column for further use. The enriched solvent is regenerated by raising the temperature using a reboiler, by lowering the pressure, or by using a stripping gas in the stripper, and then fed back to the absorber [100].

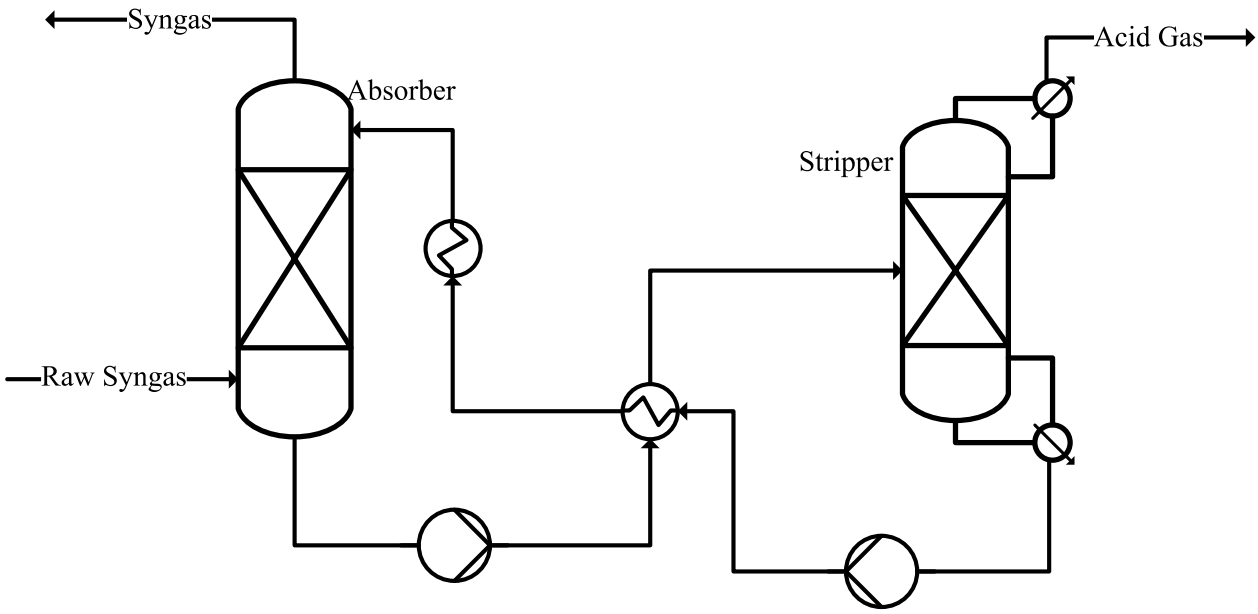

Figure 2.12 Basic flow diagram of solvent-based processes

The solvent-based processes can be divided into chemical and physical absorption processes. Physical solvents exploit Henry's law (equation 2.1), which describes the proportional relationship between partial pressure p_i of a gas and its concentration in a solvent $\tilde{x}_i$. The temperature-dependent Henry coefficient H_i takes into account the activity coefficient between solvent and solute. For high partial pressures in the gas phase, the activity coefficient approaches 1 and Henry's law simplifies to Dalton's law (equation 2.2) [101].

$$\tilde{x}_i = \frac{p_i}{H_i(T)} \tag{2.1}$$

$$\tilde{x}_i = p_i \tag{2.2}$$

On the other hand, chemical solvents chemically bind the components to be removed. Therefore, chemical solvents can bind large portions of the gas to be dissolved even at low partial pressures but are limited when the stoichiometric ratio of solvent to the component to be dissolved is reached. In contrast, the capacity of physical solvents continues to increase almost proportionally as the partial pressure of the component to be dissolved increases. This relationship between the partial pressure of the gas to be dissolved and the loading of the solvent is shown qualitatively for physical and chemical solvents in Figure 2.13. Therefore, physical solvents are suitable for high partial pressures, i.e., in the field of CO_2 separation, especially in pre-combustion processes due to the higher pressures prevailing there compared to post-combustion processes [102–104]. In addition, physical solvents are characterized by a significantly higher dissolving capacity for the acid gases compared to chemical solvents, which leads to low solvent flows and thus also to a lower specific energy requirement.

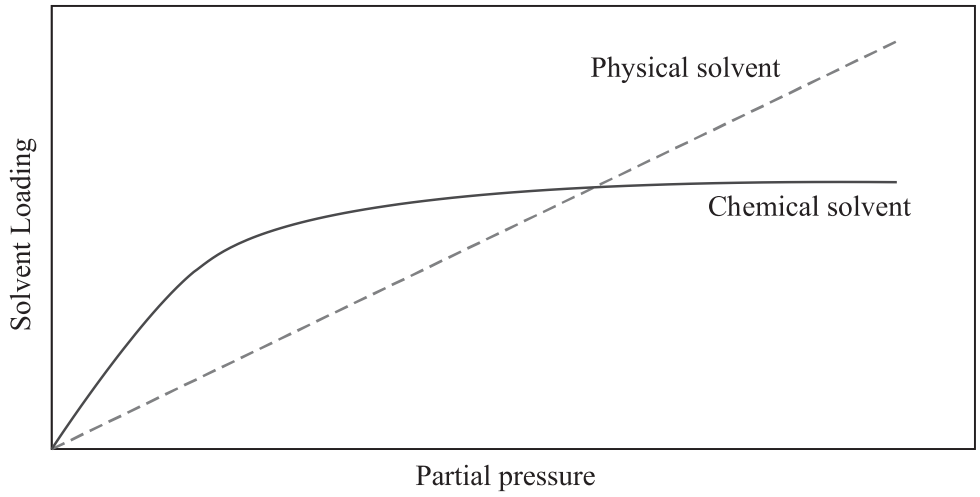

Figure 2.13 Relative solvent loading of chemical and physical solvents [103]

Solvents that absorb gases by both physical and chemical effects are referred to as hybrid solvents. These are classified between physical and chemical solvents in terms of the capacity and purity of the gas. The regeneration of physical solvents can take place by pressure reduction alone, thus requiring little or no thermal energy to raise the temperature. Thermal regeneration must only be applied if a high H_2S purity is required. Lastly, physical solvents are usually non-corrosive, so stainless steel can be dispensed with for the system components [102–105].

The physical AGR processes for pre-combustion capture or gasifier product gas treatment include well-proven solutions, i.e. the dimethyl ether of polyethylene glycol (DEPG) based Selexol process, the methanol-based Rectisol process, and the n-methyl-pyrrolidone (NMP) based Purisol. On the other hand, the chemical solvents include amines solutions, like monoethanolamine (MEA), diethanolamine (DEA), and methyldiethanolamine (MDEA) [103,104].

The Selexol Process is an absorption process that uses a physical solvent of DEPG, to absorb the acid gases H_2S, COS, and CO_2 selectively from syngas at relatively high pressure (20 - 120 bar) [106]. The process was developed by Allied Chemical Corporation in the 1950s with the formula $[CH_3(CH_2CH_2O)_nCH_3]$, where n is 3–9 [103], but now DEPG solvents are licensed and/or produced by many manufacturers including Coastal Chemical Company (as Coastal AGR), Dow (Selexol) and UOP Solvents (Selexol). Similar solvents are offered by other process providers including Clariant GmbH from Germany. The solvent Clariant is a series of dialkyl ethers of polyethylene glycol, under the brand Genosorb [107]. The optimal temperature range for operation is 5−40 °C. The ability to work in this temperature range significantly reduces expenses by eliminating the need for cooling [108]. The process could be set up to deliver a rich H_2S feed to the Claus unit along with large capacity CO_2 removal. To achieve selective H_2S and deep CO_2 removal, the process requires a two-stage with two absorption and regeneration columns [108].

The Rectisol process is an absorption process that uses a physical solvent of methanol, which differs greatly from other solvents in terms of its process conditions, as it has a comparatively high vapor pressure and thus a large solvent loss occurs at ambient temperatures. Therefore, the Rectisol process is operated at very low temperatures, usually in the range of -40 to -60 °C. In this

temperature range, the solubility of H_2S, COS, and CO_2 is very high. However, the Rectisol process also has some disadvantages. For example, due to the very low temperatures, about 5% of a Rectisol plant must be stainless steel, even though it is a physical solvent [107]. Also, compared to other acid gas scrubbing systems, the plants are procedurally complex and thus have high investment and operating costs, also due to the necessary cryogenic process [50,107]. For processes where H_2S is to be selectively removed from a CO_2-containing gas stream, the Selexol process and the Purisol process are more suitable [107]. The reason for this is the solubility of H_2S compared to CO_2 under normal process conditions [100].

Alkanolamines, organic derivatives of ammonia (NH_3), form an important group of chemical solvents for acid gas scrubbing. Depending on how many hydrogen atoms of the ammonia have been exchanged for organic molecular groups, the alkanolamines are divided into primary, secondary, and tertiary amines. Examples of these compounds relevant in practice are MEA (monoethanolamine), DEA (diethanolamine), and MDEA (methyldiethanolamine) (see Figure 2.14).

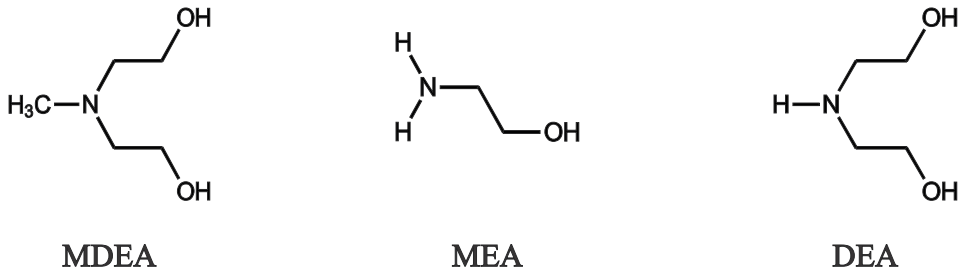

Figure 2.14 Structural formula of MDEA, MEA, and DEA [101]

Most pre-combustion capture plants rely on the tertiary amine MDEA as a solvent in acid gas scrubbing, as it is energetically more favorable than other amines due to its low heat capacity and low heat of reaction with CO_2. Thus, the specific energy requirement per kg CO_2 is about 3100 – 3700 MJ, which is lower than other amine-based scrubbing but higher than physical scrubbing [58]. MDEA also has low vapor pressure and is not corrosively compared to MEA, which allows it to be used in high solution concentrations from 35 wt% to 60 wt%. It is also chemically and thermally stable. The disadvantages of MDEA are the relatively high viscosity of the detergent, the lack of absorption of COS, and the low kinetic absorption rate for CO_2. The low viscosity of the detergent must be covered by the column design. The lack of ability to separate COS requires upstream COS hydrolysis as a catalytic conversion step [101,102,109]. The reason for the low kinetic absorption rate of CO_2 can be found in the reaction mechanism. Since MDEA is a tertiary amine, no carbonate formation can occur. Accordingly, the absorption is kinetically limited by the hydrolysis of CO_2. The absorption of H_2S, on the other hand, proceeds extremely rapidly. This effect can be used for selective capture of H_2S. If selectivity is not desired or if the aim is to achieve the most complete CO_2 capture possible, an activator, such as piperazine in the a-MDEA process developed by BASF, or the primary amine MEA, can be added. Activation exploits, on the one hand, the fact that the added amine can react directly with the CO_2 without prior hydrolysis. On the other hand, the amine is regenerated by a reaction with MDEA and can thus absorb significantly more CO_2 than would be the case with an aqueous solution containing only piperazine or MEA

[101,110]. Table 2.2 compares the characteristics of MDEA and the two physical AGR processes Selexol and Rectisol.

Table 2.2 Characteristics of acid gas removal process solvents [101,111]

Parameter		Unit	MDEA	Selexol	Rectisol
Density at 20°C		[kg/m³]	1040	~1030	785
Molar Mass		[g/mol]	119	~280	32
Boiling point	at 100 kPa	[°C]	247	~240	65
	at 6.7 kPa	[°C]	164	~200	9
Vapor pressure	at 20 °C	[Pa]	1.3	~0.1	14700 (110 at –40 °C) (11 at –60 °C)
Evaporation enthalpy		[kJ/kg]	519	~1350	1150
Mean heat of solution		[kJ/kgCO_2]	1337	~51	152
Dynamic viscosity		[mPa s]	13	~5,8	0.6
Heat capacity		[kJ/kg K]	3.4	~2.05	2.33
Typical Concentration		[wt%]	20 - 50	~100	100

The process selection depends principally on three main criteria: target gas purity, raw gas composition, and process selectivity. Indeed, the required gas purity can strongly vary depending on the intended application. For power generation, H_2S content of 40 ppmv in the syngas is generally satisfying. However, for chemical applications like ammonia, methanol, or Synthetic Natural Gas (SNG), the H_2S content has to be lower than 0.1 ppmv since H_2S can be poisonous for the catalysts are usually used in the chemical synthesis. Besides, a high syngas purity of CO_2 can be claimed, in some applications, like in the ammonia synthesis, where a CO_2 content of 10 ppmv or lower is commonly required. The raw gas composition should be seriously considered since eventual undesirable interactions between the solvent and the syngas components must be prevented. The process selectivity is also important to figure out whether H_2S and CO_2 have to be released separately. [71,103,104]

2.4 Power Generation

The energetic utilization of the high-calorific purified syngas can be carried out using various prime movers or direct electrochemical conversion in fuel cells. Due to the necessary size of gasifier plants, the use of combined cycle power plant (CCPP) processes has become well established [112–114]. An overview of commercial as well as demonstration plants has been compiled by Wolfersdorf et al. [115]. In the design, construction, and operation of these plants, broad experience in the field of natural gas-fired combined cycle plants can be drawn upon. However, the use of syngas instead of natural gas as a feedstock presents many challenges in the design and construction of gas turbines. The turbines must be designed for a wide range of possible syngas compositions depending on the type of gasifier and the upstream gas cleaning system, in addition to usually still being suitable for natural gas as an alternate fuel [113]. In addition, mixtures containing substantial amounts of hydrogen and CO have higher flame speeds, higher adiabatic combustion temperatures, a wider ignition range, low ignition energy, and lower density than

natural gas, which is essentially methane. As a result, the risk of blowout and burn-back is higher [116]. The increased flame temperature increases the amount of NO_x formed. In natural gas turbines, a greatly increased air ratio and lower temperature in the combustion chamber are achieved by premixing the fuel gas to reduce the formation of NO_x [117]. This is not possible with hydrogen-fired turbines because hydrogen already reacts spontaneously with air at the conditions at the compressor outlet and thus no controlled combustion can take place in the combustion chamber. Accordingly, only diffusion combustors are used when synthesis gas or hydrogen is used. To control the flame temperature, the fuel gas is diluted with inert gases, i.e., nitrogen or steam [117]. The use of nitrogen leads to a lower efficiency loss in the gas turbine but requires higher investment costs due to an additional compressor. On the other hand, when steam is used as an inert gas, the steam turbine in a downstream steam power process can be smaller with higher water requirements for the overall plant [116,117].

Turbines intended to operate with hydrogen or syngas are always started with natural gas for safety reasons. Some models also allow continuous operation with a fuel mix of natural gas and synthesis gas or hydrogen in order to cover a wide range of operating cases [112]. There are usually restrictions on the permissible mixtures in the turbine map and the minimum load, as shown in Figure 2.15 [113].

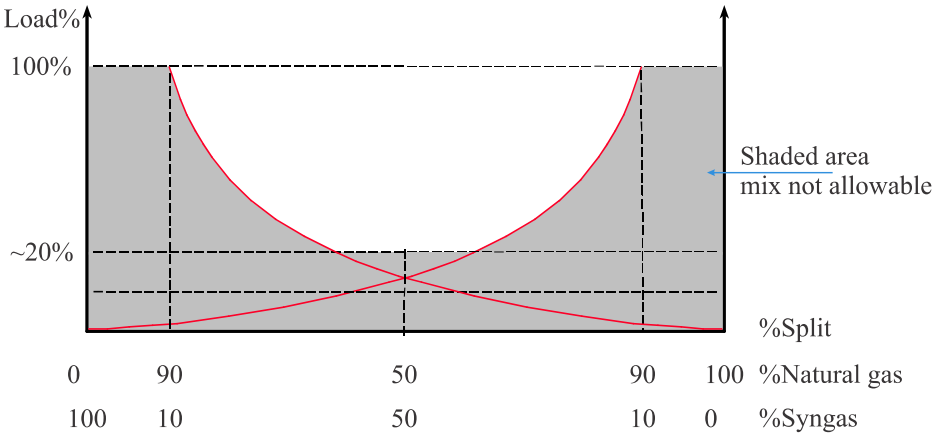

Figure 2.15 permissible fuel mixture ratios in gas turbines [113]

The downstream steam power process in IGCC plants does not differ in its basic design from that of a natural gas-fired combined cycle power plant. In a heat recovery steam generator, the hot flue gas from the gas turbine is used, which can be raised to higher temperatures by auxiliary firing if necessary, to preheat, evaporate and superheat water at various pressure levels. The steam generated in the steam power process is expanded in steam turbines. In IGCC plants, heat flows from the gasification process and gas cleaning is coupled for high efficiency. In polygeneration plants with an exothermic synthesis, where steam power plant and synthesis are operated simultaneously, the heat flows from the synthesis can also be integrated. With this integration, a balance must be maintained at all times between increased efficiency and the associated increase in complexity in the plant. On the one hand, the higher complexity can reduce the operability and system stability, while increasing the investment and operating costs as well. However, a high degree of integration between the gasifier, gas cleaning, and the water-steam cycle is necessary for high efficiency [29,118].

In addition to the combined cycle power plant, some approaches dispense with the steam power process and increase the efficiency of the gas turbine through other measures. These include the so-called steam injected gas turbine (STIG) process, in which the exhaust heat from the gas turbine is used to produce steam. The steam is then injected into the gas turbine's combustor to increase the gas mass flow and thus the turbine's output [119]. Other variants provide for intercooling during compression of the combustion air, either by injecting water or by indirect cooling with water and production of additional steam for the combustor [120].

Load cycling has not been a primary consideration in the design and operation of IGCC plants. However, in principle, power generation in an IGCC plant can have the same load cycling capability as CCPP plants, since IGCC plants run on natural gas during startup and ramp-up anyway. The load cycling capability of CCPP has long been the subject of research and development. Meanwhile, a hot start-up of the plant can reach full load in less than 30 min and run load changes at 60% of rated capacity per minute. The minimum load is usually from 40 to 50% but can be reduced to 20% with sequential firing in the turbine [121].

2.5 Synthesis

A large variety of chemical base materials up to specialty chemicals can be obtained from the synthesis gas consisting of hydrogen and CO. Products that can be synthesized directly from synthesis gas are listed in Table 2.3, together with the CO/H_2 ratio required in each case. The most relevant in terms of quantity here are ammonia and methanol, most of which are merely intermediates in further processing [71]. The production of liquid or gaseous energy carriers in the form of Fischer-Tropsch (FT) products or SNG from coal was originally the main driver for the development of many gasification technologies. Currently, the economic importance is limited with only the Sasol complex in South Africa for the coal-to-liquid (CtL) process and one plant SNG production in Beulah, North Dakota in the United States of America outside China is low [71]. In China, only 8% of the energy demand is met by natural gas due to its low availability [26]. Therefore, there exists a great interest in China to convert the abundant coal into more easily transportable gaseous and also liquid energy sources.

Table 2.3 Direct synthesis products from synthesis gas [71,122]

Synthesis products	Reaction	CO/H_2 ratio	
Ammonia	$N_2 + 3H_2 \rightleftarrows 2NH_3$	1/∞	R 2.13
Methane	$CO + 3H_2 \rightleftarrows CH_4$	1/3	R 2.14
Methanol	$CO + 2H_2 \rightleftarrows CH_3OH$	1/2	R 2.15
Fischer-Tropsch products	$nCO + (2n + 1)H_2 \rightleftarrows C_nH_{2n+2} + nH_2O$	<1/2 (depending on chain length)	R 2.16
Acetic acid	$2CO + 2H_2 \rightleftarrows CH_3COOH$	1/1	R 2.17
Methyl formate	$2CO + 2H_2 \rightleftarrows HCOOCH_3$	1/1	R 2.18
Ethanol	$2CO + 4H_2 \rightleftarrows C_2H_5OH + H_2O$	1/2	R 2.19
Propanol	$3CO + 6H_2 \rightleftarrows C_3H_7OH + 2H_2O$	1/2	R 2.20
Ethylene glycol	$2CO + 3H_2 \rightleftarrows C_2H_4(OH)_2$	2/3	R 2.21
Isobutanol	$4CO + 8H_2 \rightleftarrows C_4H_9OH + 3H_2O$	1/2	R 2.22
Ethylene	$2CO + 4H_2 \rightleftarrows C_2H_4 + 2H_2O$	1/2	R 2.23

Ammonia is one of the most synthesized chemicals, with an annual production of about 150 million tons [71]. More than 80% of ammonia is required for the production of fertilizers, in the form of ammonium nitrate or urea [101]. Synthesis is carried out almost exclusively using the Haber-Bosch process, developed at the beginning of the 20th century. The feedstock used is predominantly natural gas, which is reacted with steam in a primary reformer according to the reverse of Methanation reaction R 2.7. In the secondary reformer, the remaining methane is partially oxidized with atmospheric oxygen according to reaction R 2.24. By using atmospheric oxygen, the necessary nitrogen is simultaneously supplied to the process. The CO from the steam reforming is converted to CO_2 in a water gas conversion, which is then washed out together with the steam through a gas scrubber. The actual ammonia synthesis according to reaction R 2.25 takes place over an iron catalyst at pressures around 200 bar and temperatures between 400 and 500 °C. The process releases large amounts of CO_2 from the gas scrubbing as well as from the heat input in the primary reformer, which is typically fired by natural gas. Some of CO_2 can be recaptured during the production of urea according to reaction R 2.26. Nevertheless, ammonia synthesis is fundamentally not suitable for capturing CO_2 from the feedstock in relevant quantities [101].

$$CH_4 + 2O_2 \rightarrow CO_2 + H_2O_{(g)} \qquad \Delta H^o_R = -802.3 \text{ MJ/kmol} \qquad \text{R 2.24}$$

$$N_2 + 3H_2 \rightleftarrows 2NH_3 \qquad \Delta H^o_R = -92.4 \text{ MJ/kmol} \qquad \text{R 2.25}$$

$$2NH_3 + CO_2 \rightarrow CO(NH_2)_2 + H_2O_{(g)} \qquad \Delta H^o_R = -89.1 \text{ MJ/kmol} \qquad \text{R 2.26}$$

Substitute or Synthetic natural gas (SNG) in the form of methane has been widely considered in the past as an energy carrier. In the 1970s and 1980s, for example, the steam reformation of methane using heat from a nuclear reactor and methanation at the heat consumer were investigated at the Juelich Nuclear Research Center as a possible cycle for efficient heat transport over long distances [123]. Currently, an intensively discussed approach is the generation of methane from the electrolysis of hydrogen, which in turn is increasingly available from surplus electricity due to fluctuating power generation [124]. In all approaches, including syngas from gasification, SNG is generated via a nickel catalyst according to reactions R 2.7 and R 2.27. However, the commercial importance of generating SNG from solid fuels via gasification is low, as already described above. In addition, any CO_2 that is stored in the product during SNG production is released again during the primarily energetic use and is not permanently bound.

$$CO_2 + 4H_2 \rightleftarrows CH_4 + 2H_2O \qquad \Delta H^o_R = -165.0 \text{ MJ/kmol} \qquad \text{R 2.27}$$

Fischer-Tropsch synthesis (FT synthesis) allows the production of a wide range of aliphatic hydrocarbons, both unbranched and branched, as well as oxygenated hydrocarbons from synthesis gas. FT synthesis is an essential process step in "coal liquefaction", i.e., the provision of liquid fuels from coal, which is being intensively studied, particularly in China [125–127]. Cobalt, ruthenium, and iron can be used as catalysts. Iron is popular due to its lower price as well as good water-gas conversion activity and shows high selectivity to olefins. Cobalt is more expensive than iron by a factor of more than 200. On the other hand, cobalt catalysts can achieve the highest conversion rates and the longest catalyst lifetimes. However, cobalt catalysts mainly produce linear kerosenes [128].

In principle, the Fischer-Tropsch synthesis proceeds in five steps. First, the reactants are adsorbed on the catalyst surface. This is followed by chain initiation by dissociation of the CO and hydrogenation of the carbon to form a methyl group. In the third step, chain growth occurs, in which a methyl monomer reacts with the chain, initially also just a monomer. This growth continues until chain termination and eventual desorption of the product. Chain termination is a statistical event. Thus, chain lengths are subject to probability distributions, which can be described by the Anderson-Schulz-Flory distribution (equation 2.3) where W_n is the weight fraction of hydrocarbon molecules, n is chain length (carbon atoms) and α is the chain growth probability. An increase in temperature and a decrease in pressure both lead to a decrease in the growth probability and thus to a smaller chain length [129].

$$W_n = n(1-\alpha)^2\alpha^{n-1} \qquad (2.3)$$

Fischer-Tropsch products still have to be processed after synthesis and separated according to chain length. The gaseous products can be used as SNG (C1, C2) and as liquid gas (C3, C4). Chain lengths from C5 to C11 can be used as gasoline, C10 to C16 as kerosene in aviation, and C12 to C20 as diesel. Diesel produced in this way is particularly interesting as an alternative to diesel from mineral oil since FT products contain few aromatics but oxygenated hydrocarbons, thus reducing soot, CO, and hydrocarbon emissions when used in diesel engines [130]. Even longer chain length, up to C120, can also be converted to diesel by mild hydrocracking. Alternatively, these waxes can serve as a base for lubricants and pharmaceutical products.

This work focuses on the material utilization of synthesis gas via methanol synthesis. Methanol has been intensively discussed since the beginning of the 21st century as the central feedstock of a "methanol chemistry" or "methanol economy" as an energy source, fuel, and chemical feedstock instead of fossil oil [131]. The synthesis of methanol is mainly governed by the following three equilibrium reactions: the hydrogenation of CO reaction R 2.28, the hydrogenation of CO_2 reaction R 2.29, and the water-gas shift reaction R 2.6.

$CO + 2H_2 \rightleftarrows CH_3OH$ $\quad \Delta H^\circ_R = -90.8$ MJ/kmol R 2.28

$CO_2 + 3H_2 \rightleftarrows CH_3OH + H_2O$ $\quad \Delta H^\circ_R = -49.6$ MJ/kmol R 2.29

The basic reaction mechanism of methanol synthesis has been the subject of scientific debate for a long time. Initially, it was assumed that only CO hydrogenation leads to the formation of methanol and that the production of methanol from CO_2 always proceeds via the intermediate step of WGS. Later, CO_2 hydrogenation was assumed to be the sole or dominant step in the synthesis. It is now clear from isotopic labeling studies that both hydrogenation reactions, as well as WGS, play a role [132].

As the hydrogenation of CO and CO_2 leads to a reduction of the amount of substance towards methanol and both reactions are exothermic, the production of methanol is favored by high pressures and low temperatures. Therefore, catalysts have always been used in industrial processes for an adequate reaction rate. In the high-pressure processes at pressures of 250 – 350 bar and temperatures between 320 and 450 °C that have meanwhile been displaced, ZnO/Cr_2O_3 catalysts were used. These catalysts were characterized by high resistance to catalyst poisons, e.g. in the

form of sulfur compounds. At the same time, high investments in thick-walled reactors, as well as a large energy input for compression, were necessary. The development of effective gas purification processes, in particular for the separation of sulfur compounds, as well as significantly more active $Cu/ZnO/Al_2O_3$ catalysts, has enabled more energetically favorable low-pressure processes to become established. These catalysts operate in a pressure range of 50 – 100 bar and temperatures between 200 and 300 °C [133]. An example of a commercially available methanol process is the mega-methanol process developed by Lurgi shown in Figure 2.16.

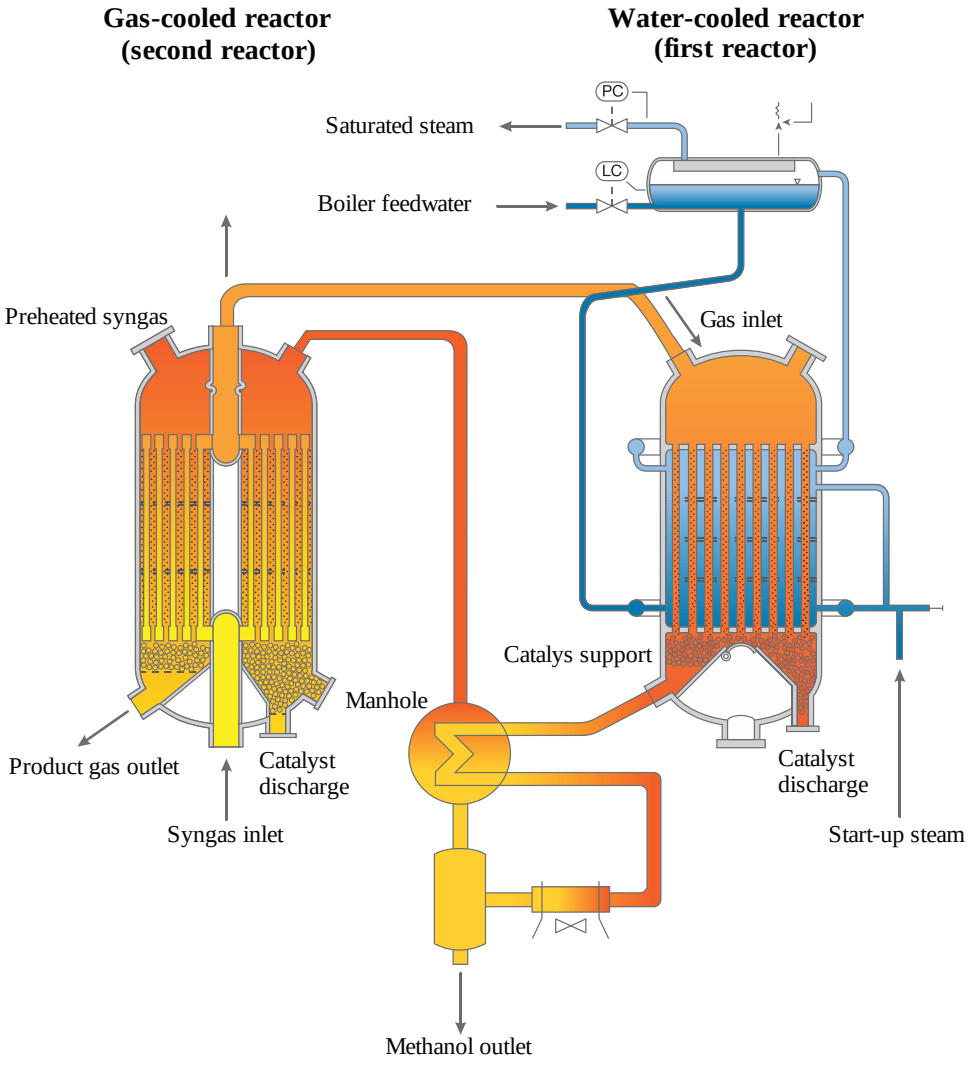

Figure 2.16 Mega-methanol process developed by Lurgi [134]

Two reactors are used in this process. Most of the conversion of synthesis gas to methanol takes place in the water-cooled reactor. The partially converted gas is further converted at lower temperatures in the reactor, cooled with fresh synthesis gas. The heat generated is simultaneously used to preheat the fresh synthesis gas. After the gas-cooled reactor, the stream consisting of methanol and synthesis gas is cooled, and the methanol is separated. The unreacted syngas is recompressed and added to the fresh syngas as recycle stream. A partial stream of the unreacted synthesis gas is withdrawn to prevent the accumulation of inert components (especially methane and nitrogen). The mega-methanol process allows the parallel production of medium-pressure steam in the water-cooled reactor. [135]

The flexible production of methanol from synthesis gas requires more temperature control of the reactors than stationary methanol processes to avoid temperature peaks and the associated coking. Methanol synthesis does have inherent temperature control, since the equilibrium of reactions R 2.28 and R 2.29 shifts toward reactants as the temperature rises. Nevertheless, temperature peaks may occur, for which suitable control strategies must be devised [136].

Chapter 3: **Process Simulation of the IGCC Power Plant**

In this chapter, a brief description of the reference plants on which this study is based was given. Subsequently, a process simulation model of the IGCC power plant for polygeneration was developed using Aspen Plus software. This model was developed by three steps outlined in this chapter. First, a process simulation model of the pilot gasification and gas processing plant was built according to the design data and specifications of the 0.5 MW_{th} pilot plant at TU Darmstadt. Second, the pilot-scale model was scaled up to an industrial scale based on a combined cycle power plant with a capacity of 360 MW_{el}. Third, a process simulation model was developed for the combined cycle power plant in Malaysia based on the plant's operating data. The simulation results, such as the electrical power, pressure, temperature, and mass flow rate, were compared against the actual measurements and showed good agreement, expressing the reliability of the process simulation model in predicting the behavior of the process.

3.1 Introduction

Mathematical modeling is a tool to enhance the understanding of energy systems considering various constraints. The mathematical modeling can be classified as a steady-state simulation and dynamic simulation. The steady-state simulation is typically used in the design and optimization of energy systems based on the mass, momentum, and energy conservation equations along with empirical correlations. However, the steady-state simulation is only performed for a series of steady-state points and does not provide any information during the transients. While, the dynamic simulation is more powerful during transients, load changes, and malfunctions.

This work contributes to evaluating the performance of IGCC with the polygeneration concept of power and chemicals in terms of energy and environment. It is intended to increase the flexibility of the IGCC operation by investigating different operating strategies. For this purpose, an Aspen Plus process simulation model was developed. The model comprises components of the IGCC that consist of fuel pre-treatment and gasification process including raw gas cooler, treatment of the product gas with a hot gas filter, raw gas scrubbing, water gas shifting, and sour gas removal. Furthermore, the syngas is utilized in a CCPP or methanol synthesis and O_2 is provided by an air separation unit. A schematic of the IGCC process is presented in Figure 3.1.

The modeling data inputs and assumptions for the gasification and product gas treatment are based on the pilot plant installed at TU Darmstadt. The modeling data of the power island is based on the reference CCPP installed in Malaysia that has been investigated as part of a published article [137]. The European best practice guidelines for the assessment of CO_2 capture technologies [138] were used also for some assumptions. Where possible, existing, validated, or verified models were used. Otherwise, models were created and verified with data from the literature. The models were also examined individually for various influencing parameters to ensure sufficient robustness for subsequent parameter variation. The models were ultimately transformed into an integrated overall model, which serves as the basis for evaluating and optimizing the IGCC power plants

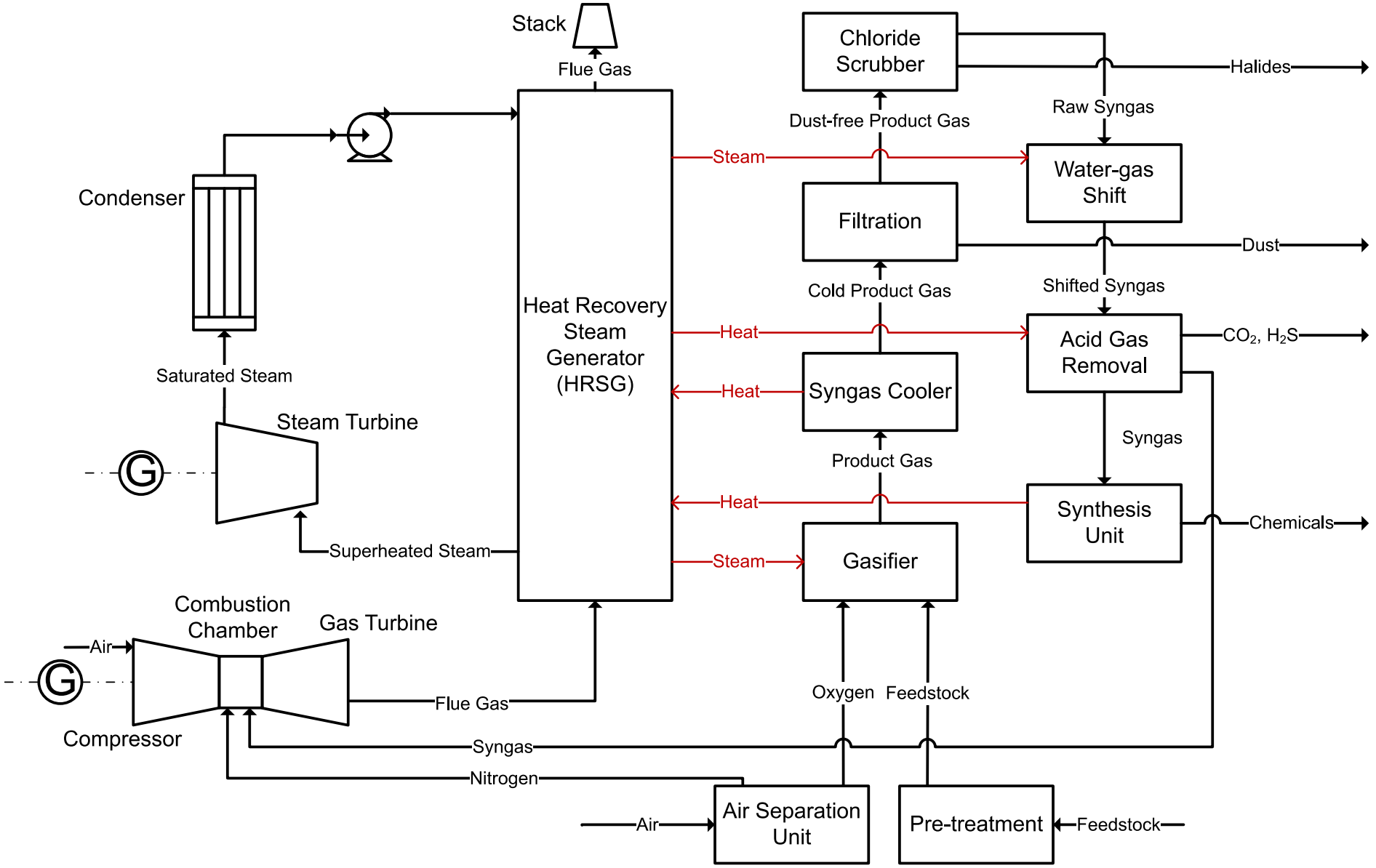

Figure 3.1 Schematic of IGCC with polygeneration

3.2 Description of Reference Plants

In this work, the process simulation of the IGCC power plant for polygeneration is based on the gasification and gas treatment plants installed at TU Darmstadt and the combined cycle power plant installed at Prai in Malaysia. A description of these plants is given in this section.

3.2.1 Gasification and Purification

At the Institute for Energy Systems and Energy Technology at the Technical University of Darmstadt, an atmospheric 0.5 MW_{th} HTW gasifier has been in operation since 2015. The facility was expanded to include the necessary gas purification steps and a synthesis test rig. The HTW pilot plant was built in close cooperation with ThyssenKrupp Industrial Solutions (TKIS) by converting an existing fluidized-bed combustor and was commissioned in 2015 [79]. Several campaigns for the gasification of lignite and hard coal as well as for co-gasification of residues have already been carried out at this plant [79,139].

The gasification part consists of a fluidized-bed gasifier based on HTW technology with a diameter of 0.4 m (the lowest 2 m of the reactor are tapered to a diameter of 0.15 m) and a height of 12.5 m. The reactor can be operated up to 1200 °C if the feedstock permits. The gasification agents O_2, steam, and CO_2 are individually preheated and fed to the reactor via seven nozzle levels. From the head, the gasifier product gas is fed into the cyclone. There, ash and fuel particles are separated and returned to the bed zone via the downcomer. The gas leaves the cyclone in the direction of the raw gas cooler. The raw gas cooler of horizontal double oval tube design from Schmidt'sche Schack. The raw gas cooler with a length of 6.4 m has four tubes with an inner diameter of 70 mm and a total heat transfer surface of 5.63 m². In contrast to the usual design in commercial plants, the raw gas cooler in the pilot plant is not an evaporator but a cooler. The cooling water is provided by a 28 bar cooling system at 205 °C. Here, the synthesis gas is cooled from approx. 900 to 950 °C to approx. 350 °C. The cooling water is supplied by a 28 bar cooling system at 205 °C. The cooled synthesis gas is then fed to the gas treatment process.

The gas treatment part consists of a hot gas filter for particle separation, a raw gas scrubber for cooling the synthesis gas and for the separation of chlorides and other halides as well as ammonia, a raw gas compression, a water-gas shift, a COS hydrolysis, a BTX scrubber based on biodiesel for the separation of condensable hydrocarbons, and an amine-based acid gas scrubber for the separation of CO_2 and H_2S.

Particle removal from the approx. 350 °C hot synthesis gas after raw gas cooling is achieved using a hot gas filter from TREMA made of heat-resistant pressure vessel steel with mineral fiber-based filter cartridges. The dust content in the synthesis gas is to be reduced to < 0.1 mg/m³ over a filter area of approx. 9 m². The filter is located before the raw gas compression, is atmospherically operated, and is designed for operating temperatures of up to 400 °C. The filter is also equipped with a heat tracing system. A trace heating system ensures that the filter has a temperature above 220 °C at all times to avoid condensation of ammonium chloride, associated piping blockage, and valve blockage. On the other hand, using a hot gas filter for dust separation allows the in-situ Claus process to be investigated after raw gas cooling as a second option. For this purpose, a small amount of O_2 is added to the synthesis gas after the raw gas cooler to oxidize the sulfur compounds in the synthesis gas, primarily H_2S, to elemental sulfur and separate them in the hot gas filter. On

a large scale, this process is interesting because less sulfur has to be removed in the sour gas scrubber.

In the raw gas scrubber, the low-dust synthesis gas from the hot gas filter is cooled to approx. 70 °C and the remaining dust and the water-soluble components, essentially HCl and NH_3, are separated. The scrubbing column is made of heat-resistant pressure vessel steel. The column has a height of about 11 m and a diameter of about 250 mm, with a sump area, flared to about 800 mm. The column is supplied with fresh water at the head. The circulating water is withdrawn from the sump of the column and added again in the middle section to improve the absorption of the water-soluble components. The synthesis gas from the hot gas filter is fed via a dip tube into the water receiver in the sump of the column, where it is cooled. The cooled and cleaned syngas leaves the column at the top. The main streams are summarized in Table 3.1. To improve the mass transfer between recycled water and synthesis gas, packed beds of the type Raschig Super Ring #0.7 are installed below the recycled water inlet over a height of 3.9 m. Two sieve trays are used above the recycle water inlet for the contact of fresh water and synthesis gas due to the very low liquid loading. According to the design, the total pressure drop across the raw gas scrubber is about 15 mbar, with about 5 mbar dropping to the packing.

Table 3.1 Raw gas scrubber inlet and outlet streams

Operation point	**Temperature [°C]**		**Mass flow [kg/h]**		**Water content [kg/h]**	
	Inlet	Outlet	Inlet	Outlet	Inlet	Outlet
Fresh water	25	–	134	–	–	–
Circulation water	72	72	112	224	–	–
Synthesis gas	350	69	187	209	33	55

The raw gas compression represents the transition from the atmospherically operated low-pressure section to the high-pressure section of the gas treatment system. The pressure is increased through single-stage compression from 950 mbar to approx. 6 bar. The increased pressure is required in the subsequent conversion stages and washes to achieve sufficient activity or absorption at smaller apparatus diameters and to overcome the pressure loss of the subsequent process steps.

The un-shifted synthesis gas from the raw gas compression is preheated to approx. 210 °C by an electric flow heater. It is then fed to the water-gas shift, which is designed as a single-stage sour gas shift. A multi-stage shift is not necessary, since the desired synthesis products (Fischer-Tropsch products or methanol) require a H_2/CO ratio of about 2/1, which can be easily adjusted with a single-stage shift. Before the shift reactor, the gas is heated to 325 °C in a regenerative heat exchanger using temperature-controlled bypass control, and the water content of the gas is increased to approx. 35% by adding saturated steam. As a result, the H_2/CO ratio of approx. 5/1 can be achieved in the conversion reactor. The gas from the exothermic conversion is finally cooled in the regenerative heat exchanger and another cooler before being mixed with a bypass flow around the conversion stage to obtain the desired H_2/CO ratio for product synthesis.

In the hydrolysis reactor, the hydrolysis of COS and HCN takes place after the conversion according to equations R 3.1 and R 3.2, respectively. Hydrolysis is necessary because the amine-based acid gas scrubbing in the pilot plant cannot absorb COS. After hydrolysis, the converted synthesis gas is cooled to approx. 75 °C and fed to the BTX scrubber.

$COS + H_2O \rightleftarrows H_2S + CO_2$ $\Delta H^o_{R,473\,K} = -34.3$ MJ/kmol R 3.1

$HCN + H_2O \rightleftarrows CO + NH_3$ $\Delta H^o_{R,473\,K} = -50.7$ MJ/kmol R 3.2

To protect the acid gas removal from condensable hydrocarbons, in particular benzene, toluene and xylene, these must be separated in advance. The separation is carried out in the pilot plant employing a novel BTX scrubber based on fatty acid methyl ester/biodiesel developed by Thielert et al [92,140], which takes place at about 30 °C and thus below the dew point of the synthesis gas. The BTX scrubber has a two-stage design for separation of the aqueous condensate as shown in Figure 3.2. The first stage is used for gas cooling and separation of the condensate while the second stage is required for the absorption of the BTX fraction according to the process patented by Thielert et al. In the subsequent regeneration process, the biodiesel is recycled and the BTX components are separated.

In the first stage of the BTX scrubbing, the synthesis gas is cooled from about 75 to 28 °C at 3.2 bar using a mixture of about 50 vol% rapeseed methyl ester (RME) and 50 vol% circulating water. The DN250 stainless steel gas cooler is equipped with two 2 m high type 250Y structured packings for high flexibility in the choice of the operating point. The nominal mixture flow rate is about 2 m³/h, which is about two orders of magnitude above the de-wetting limit of the structured packings [141]. The gas load in the column is about $0.8\sqrt{Pa}$, which is about a factor of 5 below the flooding limit for the nominal liquid load [141].

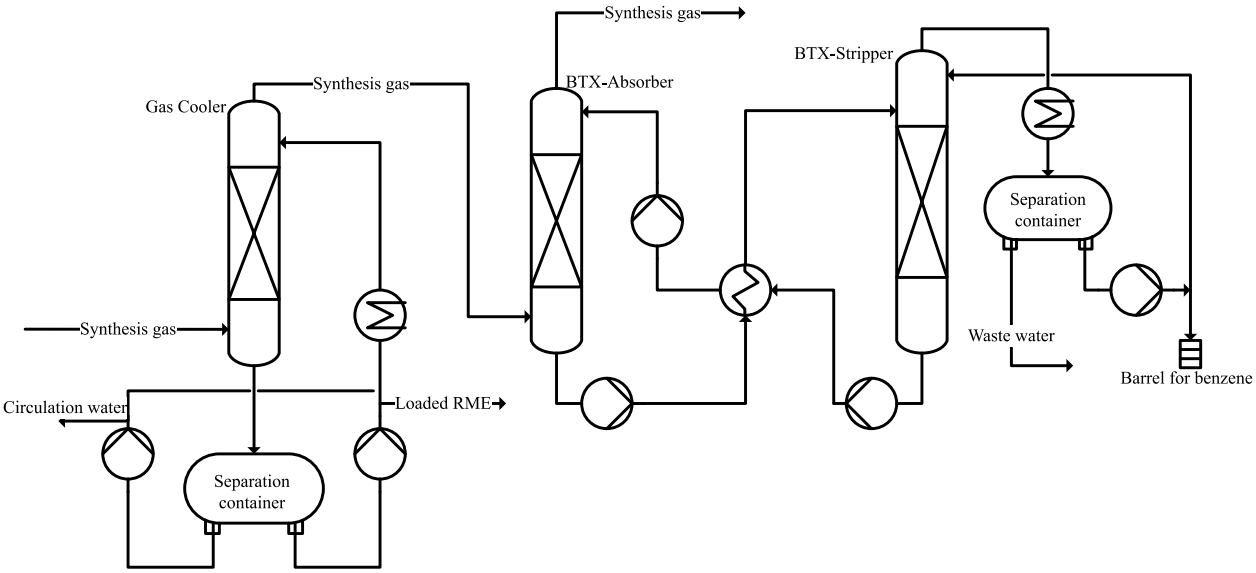

Figure 3.2 Process Flow Diagram of BTX-Scrubber

In the second stage of BTX scrubbing, after gas cooling, absorption takes place with pure RME at a constant temperature of 30 °C. The flow diagram of the second stage including the scrubbing oil regeneration is shown in Figure 3.2. In the absorber, the BTX components that have not yet been condensed in the gas cooler are absorbed. For this purpose, as in the gas cooler, two 2 m high structured packings of type 250Y with a diameter of 250 mm are used. The gas load is slightly lower than in the gas cooler at $0.7\sqrt{Pa}$ due to the lower vapor content. The nominal flow rate of RME as absorbent is 250 L/h, which is about 1 order of magnitude above the de-wetting limit of the packings. The loaded wash oil exits the absorber through the sump and is pumped through a

regenerative heat exchanger and an electric wash oil heater and heated to the boiling point of the enriched wash oil at about 180 °C. Three packings are installed in the subsequent DN100 stripper. From top to bottom, they are 1 m Raschig Wire Pak 500X, 1.6 m Raschig Pak 350X and 1.4 m Raschig Pak 350X. In Raschig Wire Pak 500X, the packing is made of wire mesh, while in Raschig Pak 350X, it is made of stainless steel sheets. The two-phase mixture from the electric wash oil heater is fed into the stripper above the second packing. Stripping steam is added at the bottom of the column to assist desorption, raising the gas load to approximately $0.3\sqrt{Pa}$. The liquid loading for the bottom two packings is similar to the conditions in the gas cooler. At the top of the column, the temperature must be set to approximately 105 °C to retain the wash oil without condensing the stripping vapor. For this purpose, approximately 10 L/h of cold crude benzene are added above the Wire Pak 500X packing in nominal operation under temperature control.

Acid gas removal of CO_2 and H_2S is performed in the pilot plant in an absorber-stripper system using an aqueous solution of MEA-activated MDEA. The flow diagram of the scrubbing is shown in Figure 3.3. CO_2 and H_2S are absorbed in the DN250 absorber via four 3 m high Mellapak 350X packings at approximately 3 bar and 45 °C with the amine solution. Above these four packings is another 1 m high packing in which circulating water is circulated to retain amine aerosols in the synthesis gas stream. The circulating water is continuously replenished with fully demineralized feedwater to compensate for evaporation losses in the sour gas scrubber. For this purpose, the excess water runs into the lower separation stages of the absorber via an overflow at the collector for the circulating water.

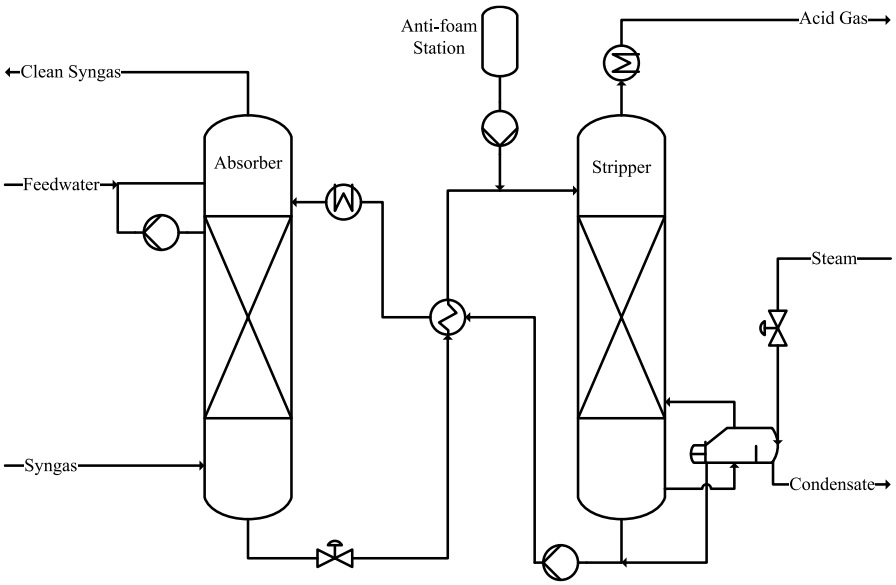

Figure 3.3 Acid gas removal process flow diagram

On the bottom of the absorber, the loaded amine is fed level-controlled through a filter section with two amine filters and an activated carbon filter, as well as through a regenerative heat exchanger. Before entering the stripper, it is possible to add additives to the loaded amine using an anti-foam station. For the first tests, a silicone-based anti-foam agent is provided which, due to its very low surface tension, supports the disintegration of any bubbles and foams that may occur. Then the amine is added at approx. 100 °C and at a slight overpressure of approx. 300 mbarg above three Mellapak 250X packings, each with a height of 3.3 m, in the stripper. The three packings together correspond to about 20 theoretical separation stages. As the packings are passed through, the acid

gases are stripped from the amine with steam. A reboiler heated with 5 bar saturated steam is connected to the sump of the stripper. Here, the water contained in the amine solution is partially evaporated. The reboiler output is controlled to the temperature of 105 °C in the top packing of the output side. The sump of the stripper also acts as a reservoir for the depleted amine, which is fed back to the absorber via a circulation pump through the regenerative heat exchanger and a cooler under volume flow control. A condenser is located at the head of the stripper to cool the acid gas stream to 45 °C and provide the condensate for the booster section of the column with a 1 m high Mellapak 350X. The valves in the outgoing syngas or acid gas stream provide pressure control for the two columns.

3.2.2 Combined Cycle Power Plant

The CCPP (Prai Power Station, located in Malaysia) consists of three General Electric (GE) single-shaft 50 Hz gas turbines (GT) (STAG 109FA), which is connected to three steam generators built by Doosan Heavy Industries and Construction, based on the principle of heat recovery and manufactured by GE. The HRSG, without additional firing, is flowed through the flue exhaust gas with a temperature equal to 628 °C and a flow rate of 587 kg/s from the GT. In the vertical steam generator, the flue gas is diverted by ninety degrees after it leaves the GT and passes through the horizontal heating surfaces positioned in the flue gas duct in an upward direction. The HRSG is vertically orientated, sub-critical, and has triple pressure with a reheater. The high-pressure (HP) system is up to 100 bar. The evaporator path has a forced circulation in the high, intermediate, and low-pressure circuits. The reheater combines the steam flow from the HP turbine exit to the Intermediate-pressure (IP) steam flow.

A schematic diagram of the CCPP is illustrated in Figure 3.4. The HP circuit raises the feedwater temperature to generate superheated steam, which enters the HP steam turbine. The IP circuit raises the feedwater temperature to generate superheated steam that is mixed with the cold reheat steam, then it is admitted to the reheater (RH), afterward, it enters the IP steam turbine. In addition, the IP steam circuit provides steam from the IP economizer to preheat the natural gas fuel. The low-pressure (LP) steam circuit increase the temperature of the feedwater to generate LP steam that flows into the LP steam turbine. The HP and RH steam temperature is controlled and limited by using attemperators before feeding them to the HP and IP steam turbine sections respectively. The LP economizer is operated when the GT fuel has low sulfur content, otherwise, the LP economizer is bypassed. The temperature of the LP economizer inlet is controlled using the recirculation circuit to about 50 °C independently of plant load. The metal temperature of the LP economizer in this case will not fall below the sulfur acid dew point, avoiding the occurrence of corrosion. In this configuration, the LP main steam control valve is fully closed, allowing the LP drum equilibrium pressure to be below the minimum admission pressure. The HRSG technical data for flue gas and water/steam side is introduced in Table 3.2.

Table 3.2 Technical data of the HRSG of the reference CCPP

HRSG outlet steam conditions				Flue gas conditions	GT Power ST Power
HP	**RH/IP**	**LP**	**Condenser**		
p=97,7 bar	p=21.4 bar	p=4.1 bar	p=0.052 bar	$\dot{m}$=587 kg/s	220 MW_{el} 140 MW_{el}
T=567 °C	T=567 °C	T=293 °C	T=35 °C	T_{Inlet}=628 °C	
$\dot{m}$=78.2 kg/s	$\dot{m}$=83.2 kg/s	$\dot{m}$=9.8 kg/s	$\dot{m}$=93 kg/s	T_{Outlet}=81 °C	

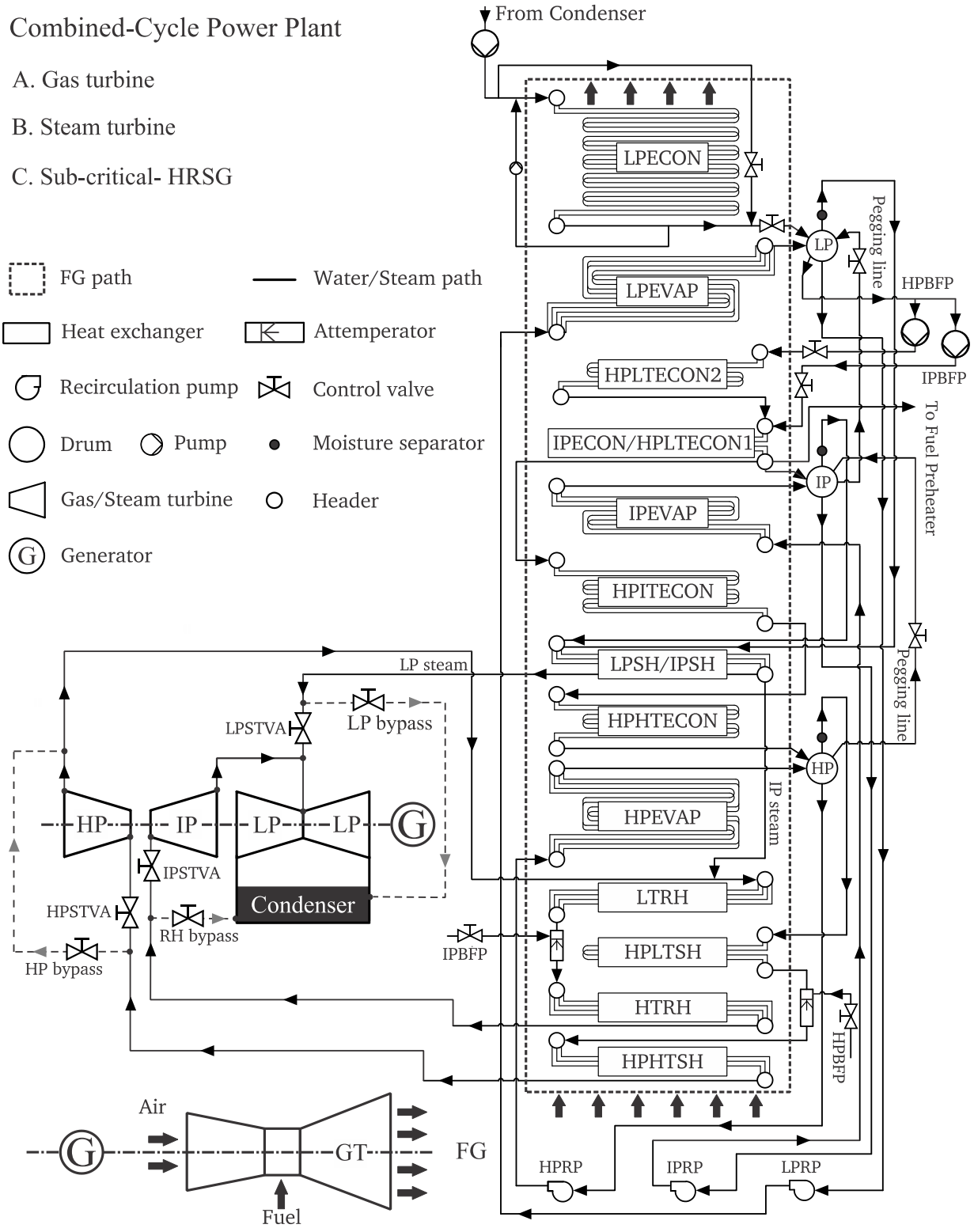

Figure 3.4 Schematic diagram of Prai CCPP

3.3 Process Simulation Software

The process simulations were carried out using Aspen Plus software version 11.1, developed by Aspen Technology Inc. [142]. Aspen Plus is a process simulation tool suitable for the design, optimization, and performance evaluation of a wide range of processes. It conducts mass and energy balances and performs rigorous calculations of process systems. With a large database of pure component and equilibrium data, Aspen Plus can also perform chemical reactions and equilibrium processing. With a large database of pure component and equilibrium data, Aspen Plus can also perform chemical reactions and equilibrium processing. Also, transport phenomena can be integrated, which allows the dimensioning of process equipment such as absorbers. Moreover, the data management and other calculations were conducted using Microsoft Excel [143] software. All simulations and analyses in this work were performed under steady-state conditions.

3.3.1 Property Calculation and Estimation

An important aspect of liquid gas system simulation is the selection of property methods carefully. Aspen Plus has a variety of different property methods, ranging from simple and strong property methods to complex estimators based on molecular structure. Understanding vapor-liquid equilibrium (VLE) theory and the importance of correlations is necessary to make the right selection. The derivation begins with the basic equation of equilibrium and ends with a concrete formulation with special reference to absorption processes and electrolyte systems.

Multiple property methods are used to meet the requirements of the complex IGCC process. The requirements range from sour water systems, which require electrolyte modeling, to high temperature and high-pressure syngas processing, which requires a suitable equation of state model.

An equation of state of Peng-Robinson with the Boston-Mathias alpha function (PR-BM) is used in many sections of the flowsheet. A preference was given to the Boston-Mathias alpha function over the standard Peng-Robinson equation because it is more accurate for the light gases in the system at high reduced temperatures. The STEAMNBS steam tables are used for modeling boiler feed-water heaters, steam boilers, and steam turbine units.

The Gibbs-Duhem (equation 3.1) describes the basic relationship between the states of any two phases. A special case is a relationship between a liquid and its vapor. An equilibrium is reached between two phases when the derivative of entropy is zero:

$$dS = \left(\frac{1}{T'} - \frac{1}{T''}\right) dU' + \left(\frac{P'}{T'} - \frac{P''}{T''}\right) dV' - \sum_{i=1}^{k} \left(\frac{\mu_i{}'}{T'} - \frac{\mu_i{}''}{T''}\right) dn' = 0 \qquad (3.1)$$

The vapor-liquid equilibrium (VLE) is subdivided into mechanical (P), thermal (T), and chemical (μ) equilibrium. There are several conservation laws describing the mechanical and thermal equilibrium, whereas chemical equilibrium requires more complex calculations. Maxwell's relations provide an expression for the chemical potential based on measurable physical quantities. Thus, to calculate the chemical potential, the derivation of the chemical potential concerning pressure is given in equation (3.2).

$$\left(\frac{\delta\mu_i}{\delta P}\right)_{T,n_i} = \mathrm{v}_i \tag{3.2}$$

Assuming an ideal gas, the chemical potential for gases and liquids are calculated according to equations (3.3 and 3.4).

Gas
$$\mu_i^G = \mu_i^{\emptyset} + RTln\left(\frac{P_i}{P^{\emptyset}}\right) \tag{3.3}$$

Liquid
$$\mu_i^L = \mu_i^{\emptyset} + RTln(X_i) \tag{3.4}$$

The chemical potential cannot be measured directly so it is not applicable. G. N. Lewis introduced fugacity in The Law of Physico-Chemical Change [144,145]. It is replacing the chemical potential with another mathematical expression that can be described as an escape tendency (see equation 3.5).

$$\ln\left(\frac{f_i}{y_i P}\right) = \frac{1}{RT}\int_0^P \left(\mathrm{v} - \frac{RT}{P}\right) dP = ln(\varphi) \tag{3.5}$$

Lewis made a revolution in thermodynamic calculations, which both scientists and engineers use today. However, there is a weak point in the calculation of fugacity in the liquid phase. The small derivative of vapor over pressure is sensitive to errors. Therefore, in this simulation, the activity coefficient model is used to calculate the chemical potential of the liquid phase, while the fugacity of the gas phase is correlated via an equation of state. Considering that the simulation contains several absorption processes, an asymmetric approach with the standard condition ($f_i^{\emptyset;x_i=0}$) offers an advantage in calculating the absorption efficiency in a range of ppm.

with
$$f_i^{\emptyset;x_i=0} = H_{ij} \tag{3.6}$$

Henry's Law
$$y_i P = H_{ij} x_i \,, when\ x_i \to 0 \tag{3.7}$$

Where is H_{ij} factor called Henry's constant with gas i and specified solvent j

The simulation uses database access provided by Aspen Plus. However, critical parameters such as Henry's constants are checked or replaced if they are not applicable for this simulation.

3.3.1.1 **Equation of State**

The integral of equation (3.5) is composed of the volume and the pressure. Thus, the ideal gas law is a simplification of the relationship between volume, temperature, and pressure, the compressibility (Z) stands for a universal correction factor. The deviation from 1 indicates the non-ideality of the system.

For low pressure
$$Z(P,T) = \frac{P\mathrm{v}}{RT} \tag{3.8}$$

Non-polar system
$$Z(P,T) = \frac{P\mathrm{v}}{RT} = 1 \tag{3.8 a}$$

Under consideration of the critical point for temperature and pressure, the boundary conditions are set:

$$\left(\frac{\delta P}{\delta \mathrm{v}}\right)_{P_c} = 0 \tag{3.9}$$

and

$$\left(\frac{\delta^2 P}{\delta \mathrm{v}^2}\right)_{P_c} = 0 \tag{3.10}$$

The Van der Waals equation was derived. An improvement is a Redlich-Kwong equation [146–148].

$$P = \frac{RT}{\mathrm{v} - b} - \frac{a}{\mathrm{v}(\mathrm{v} + b)T^{0.5}} \tag{3.11}$$

The solidity of this equation is the reason why it is often used. The increased pressure in some parts of the system leads to a strong non-ideal gas, which is why a more complex equation is used: The Redlich-Kwong-Soave equation (RKS) [147,149]:

$$P = \frac{RT}{\mathrm{v} - b} - \frac{a_c[1 + M(\omega)(1 - T_r^{0.5})]^2}{\mathrm{v}(\mathrm{v} + b)} \tag{3.12}$$

with

$$M(\omega) = (0.48508 + 1.55171\omega - 0.17613\omega^2 \tag{3.12a}$$

$$a_c = \frac{0.42748(RT_c)}{P_c} \tag{3.12b}$$

$$b = \frac{0.08664(RT_c)}{P_c} \tag{3.12c}$$

3.3.1.2 **Activity Coefficient Model**

Similar to the fugacity coefficient, the activity coefficient model is a compensation for the ideal and non-ideal conditions. In equation 3.13, the activity coefficient model is described as excess free energy.

Gibbs

$$G = \sum_{i=1}^{k} n_i \mu_i^{\emptyset} + \sum_{i=1}^{k} n_i RT ln(x_i) + \sum_{i=1}^{k} n_i RT ln(\gamma_i) = G^{id} + G^{e} \tag{3.13}$$

A powerful model was established by Renon and Prausnitz [150]. Their equations take into account the intermolecular forces as seen in Figure 3.5. The factors g_{11}, g_{12}, and g_{22} are parameters that can be fit. In that way, each possible relationship or structure is taken into account. A system with n molecules can be described as given in equation 3.14.

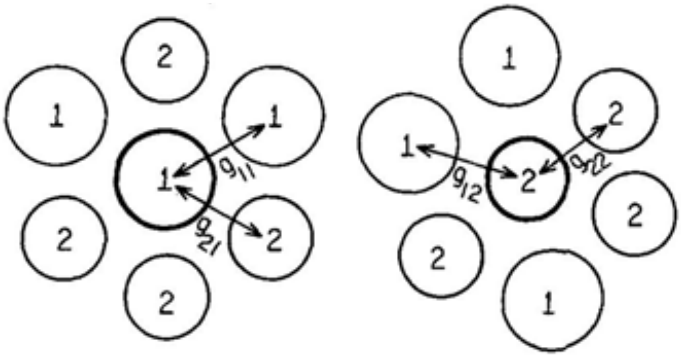

Figure 3.5 Intermolecular forces between molecule 1 and 2, 1 and 1, and molecule 2 and 2 [150]

NRTL
$$\frac{g^e}{RT} = \sum_{i=1}^{k} \frac{x_i \sum_{j=1}^{n} \tau_{ij} G_{ij} x_j}{\sum_{l=1}^{n} G_{li} x_l} \tag{3.14}$$

Chen et al. [151] developed an extended model (equation 3.15) to include the special case of electrolytes. Depending on the electric charge, more cases can be considered as shown in Figure 3.6.

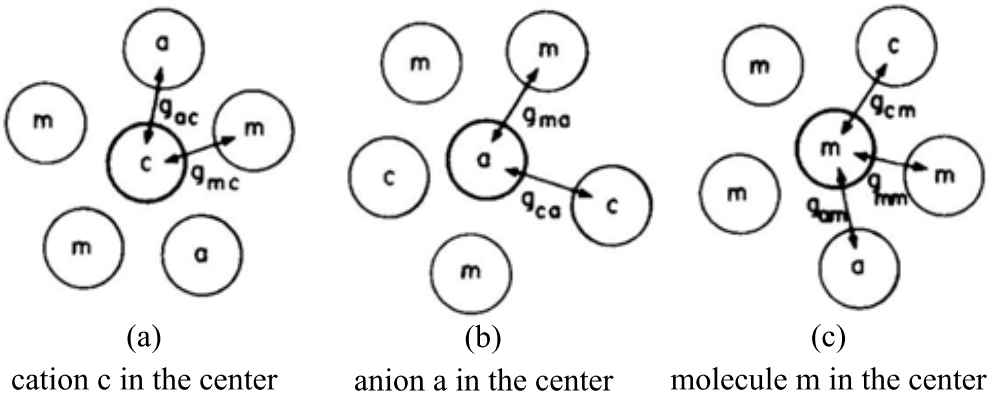

Figure 3.6 All possible intermolecular forces between molecule a and m, a and c, c and m, and m and m. [151]

eNRTL
$$\frac{g^e}{RT} = \sum_{m=1}^{n} \frac{X_m \sum_{j=1}^{n} \tau_{jm} G_{jm} X_j}{\sum_{k=1}^{n} G_{km} X_k} + \sum_{c=1}^{n} X_c \sum_{a\prime=1}^{n} \frac{X_{a\prime} \sum_{j=1}^{n} \tau_{jc,a\prime c} G_{jc,a\prime c}}{\left(\sum_{a''=1}^{n} X_{a''}\right)\left(\sum_{k=1}^{n} G_{kc,a\prime c} X_k\right)} + \sum_{a=1}^{n} X_a \sum_{c\prime=1}^{n} \frac{X_{c\prime} \sum_{j=1}^{n} \tau_{ja,c\prime a} G_{ja,c\prime a}}{\left(\sum_{c''=1}^{n} X_{c''}\right)\left(\sum_{k=1}^{n} G_{ka,c\prime a} X_k\right)} \tag{3.15}$$

3.4 Simulation of Pilot Plant

Co-gasification of lignite and Refuse Derived Fuel (RDF) is used as feedstock for gasification. The evaluation of this co-gasification using HTW is carried out experimentally at TU Darmstadt and the results of this project are published in Savuto et al. [152].

Lignite has high availability as well as low production costs. The RWE operates a bubbling-bed-drier (WTA-drier), which is fed with low-rank lignite and produces a dry WTA lignite with a

moisture content of 12 wt.%. The coal has a typical ash and Sulphur content and is currently used as a substitute fuel in one of the power blocks of the power plant at Niederaußem (Germany) [153].

This dry, low-rank lignite is generally appropriate for HTW gasification [152]. Because the WTA lignite is used for dust firing, it is only available with a small particle size distribution (PSD). The pilot plant at TU Darmstadt needs a bigger PSD therefore, it uses a commercially available high-quality lignite with a suitable PSD. This is called lignite energy grained (LEG). As consequence, two types of lignite were analyzed, WTA lignite for the simulations and business case of the industrial size and the LEG lignite for the gasification test at TU Darmstadt.

Also, the RDF is very suitable for HTW gasification. The main components of the RDF are various plastics, textiles, paper, and wood residues [152].

The characteristics of the considered feedstock to the gasifier is summarized in Table 3.3

Table 3.3 Feedstock characteristics (Mass fractions on dry basis)

Parameter	Unit	WTA Lignite	RDF Pellets	LEG Lignite
Calorific Value	MJ/kg	21.85	26.03	26.69
Moisture	wt.%	12.30	3.30	10.60
Volatile matter		43.21 s	76.30	50.31
Ash		19.20	14.40	3.80
Carbon		56.70	53.70	67.30
Hydrogen		3.95	7.56	4.79
Nitrogen		0.70	0.59	0.84
Chlorine		0.03	1.93	0.02
Sulfur		0.90	0.21	0.35
Biomass		-	42.40	-
Non-Biomass		-	42.80	-

Figure 3.7 shows a simplified block flow diagram of the pilot-scale gasifier and gas treatment at TU Darmstadt. A description of the pilot plant was discussed in section 3.2.1. The streams composition and operational parameters of this simulation of gas treatment in the pilot plant are validated against data and calculations from ThyssenKrupp (TKIS).

The syngas composition produced by the HTW gasifier and enters the gas treatment pilot plant is shown in Table 3.4. The Electrolyte NRTL property method was used, including electrolyte reactions and Henry's law, for liquid phase physical properties calculations in the process. The process simulation is carried out in one Aspen plus flow sheet while each treatment process is simulated using a Hierarchy user model as presented in Figure 3.8.

The simulation includes the main syngas route as well as the auxiliary systems to understand the treatment of solvents regarding accumulations of ions or energy demands. The setup and the simulation can be used for scale-up to estimate OPEX and CAPEX. The structure of the simulation is aligned with the mentioned units of the TU Darmstadt pilot plant. These units are summarized in a hierarchy block shown in Figure 3.8. Details of each unit are described in the individual sub-sections. In addition to the TU Darmstadt pilot-scale setup, a CO-Shift is added to upscale the plant. Each gas treatment step is clustered and is represented by a HIERARCHY block in Aspen

Plus. Each HIERARCHY block has an inlet and outlet stream and contains more Aspen Plus operations. The whole gas cleaning simulation is shown in Figure 3.8.

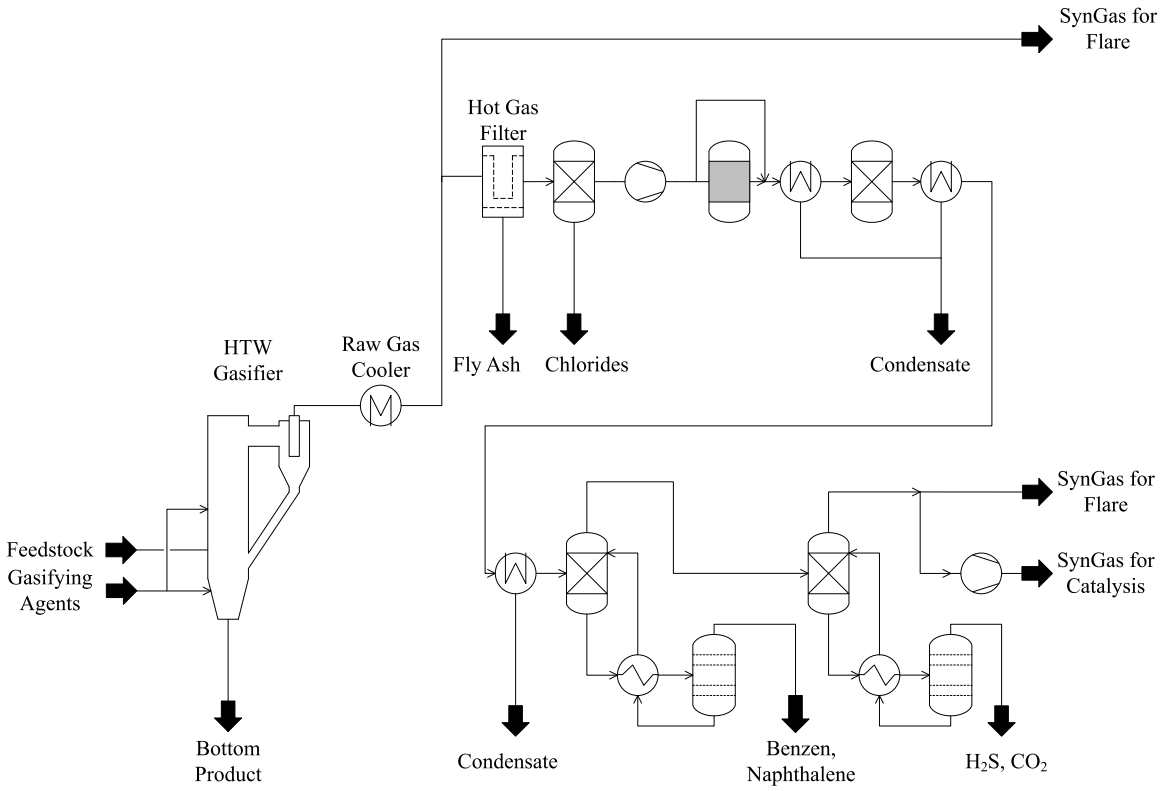

Figure 3.7 Block flow diagram of the pilot plant at TU Darmstadt

Table 3.4 Raw syngas parameters

Parameter		**Unit**	**Value**
Temperature		°C	350
Pressure		bar	1
Flow rate		kg/hr	198.136
Composition	H_2		0.14817
	CO		0.26459
	CO_2		0.29016
	CH_4		0.02646
	H_2O		0.26459
	H_2S	Mole-fraction	0.00115
	COS		0.00011
	NH_3		0.00282
	HCL		0.00001
	Benzene		0.00106
	Naphthalene		0.00088

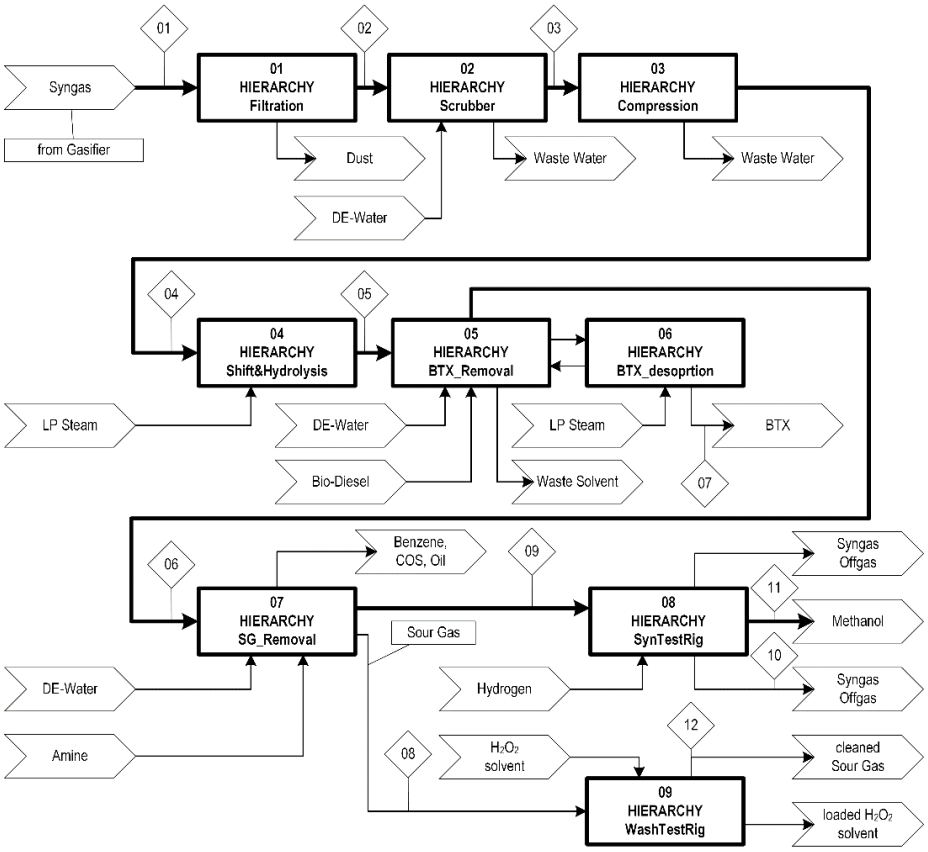

Figure 3.8 Syngas treatment simulation block flow diagram

3.4.1 Filtration

The syngas enters the treatment plant at 350 °C and ambient pressure. The HTW-pilot-gasifier separates the proportion of particles greater than 25 µm with its cyclone. Due to the inertia, the gas flow carries away smaller particles. The first separation deals with the solid phase of the syngas. Dust is a critical process parameter owing to erosion-corrosion, the lifetime of moving equipment and solvents, and in the form of particulate matter even in the deactivation of catalysts. A common way to separate the bulk of the dust is to filter the syngas. To avoid the condensation of tars, trace heaters keep the temperature above 250 °C.

Common PTFE fabric filters are not able to operate at such temperatures. Therefore, ceramic filter candles are used to separate the dust from the syngas. Aspen Plus provides several built-in models to simulate the separation efficiency of the filter. The unit operation “FabFI” calculates the dust removal and the resulting pressure drop. The vendor of the ceramic candles does not provide all the necessary information to calculate both dust removal and the pressure drop. Without the dust removal coefficient of the candles, the efficiency of the filter can be estimated with the assumed pressure drop of about 25 mbar. Figure 3.9 shows the block flow diagram of the filtration process.

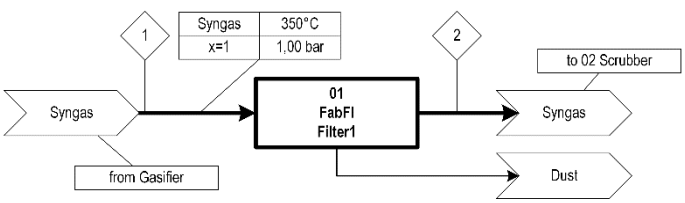

Figure 3.9 Block flow diagram of the filtration process

3.4.2 Raw Gas Scrubbing

After the filtration, recycled and fresh deionized water cools the hot syngas. The temperature drops below the dew point of the syngas. This step is necessary to subsequently compress the syngas. Heavier tars are condensing when they come into contact with the cold water. To avoid the accumulation of acidic components and an organic phase, part of the recovered water is purified. The scrubber removes all residues from the dust.

Simulation of columns is an Aspen Plus specialty. "RadFrac" is the strongest simulation model that Aspen provides and the only one applicable to absorption processes. This operating unit is divided into two different simulation modes. First, assume chemical, thermal and mechanical equilibrium at each stage. Second, rate-based calculation of heat and mass transport as described in the 'Principles of Gas Absorption' by Lewis and Whiteman [154].

Absorption processes are slower compared to thermally driven rectification processes. A single-stage does not equal a theoretical stage. Thus, the rate-based approach is more appropriate and is used in this model. The rate-determining step is assumed to be the diffusion of the substances through the boundary layer of water. Recirculation of the sump reduces the fresh water demand. The block flow diagram is shown in Figure 3.10. In addition to cooling, the scrubber also removes strong acids or alkalis. The combination of hydrogen chloride and ammonia removal causes the process to self-adjust to a pH of about 8.37.

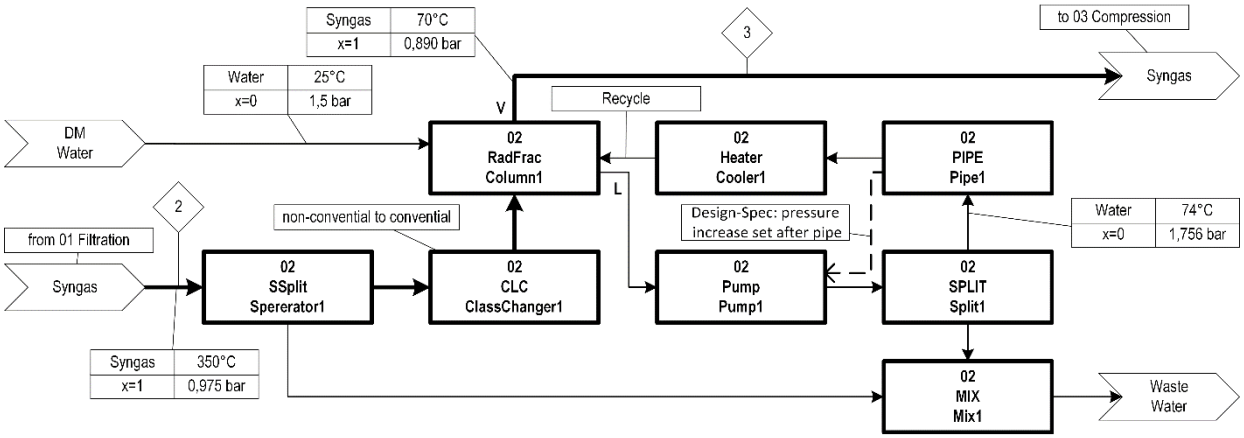

Figure 3.10 Block diagram of raw gas scrubbing simulation flow sheet

The main unit of the scrubbing section is the column (02 Column1). The 25 cm thick column is loaded with a Raschig NO-0.7 packing in a 3.9 m length section. The freshwater enters at the top of the column and passes through two sieve trays. The fresh water and recycle are mixed and flow into the sump in countercurrent with the syngas. The syngas inlet is located directly in the sump beneath the water level. There is no corresponding unit operation that simulates the immersion quench. Another sieve tray replaces this quench as an additional imaginary stage. The height of the sieve is adjusted to affect the proper temperature and pressure drop of the direct contact between water and gas. An assumed equilibrium stage exceeds both the separation efficiency and the temperature drop.

The temperature of the recycle and the outlet temperature of the syngas depend strongly on the amount of evaporating water (02 Column01) and the water removed from the recycle (02 Split1). The pressure drop (02 Column01) results from the correlations for hydrodynamics. Both the

temperature of the liquid and the gas and the pressure of the 02 Column1 operating unit are shown in Figure 3.11. The temperature is immediately cooled down from 350 to 160 °C on stage 10, where the gas dives into the sump. It aligns afterward with the temperature of the water.

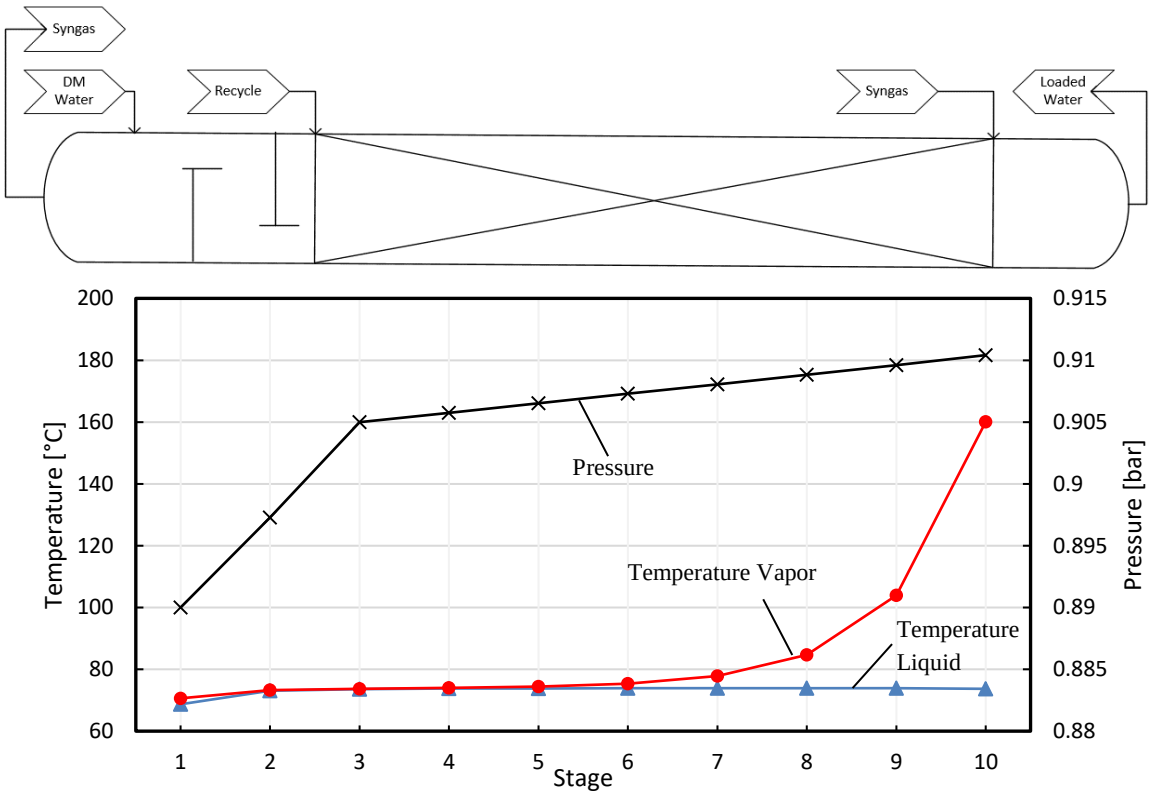

Figure 3.11 Temperature and pressure profile of the gas scrubbing column

3.4.3 Compression

The compressor divides the gas purification process into ambient and high-pressure parts to improve absorption processes. The compressor can handle a temperature of up to 60 °C. A heat exchanger cools the syngas down to 40 °C. A condensate separator removes the liquid that forms from the saturated gas. Water continuously cools the compressor to maintain a constant temperature. Aspen Plus does not have a continuously cooled compressor. With a multi-stage compressor, cooling is divided into six stages. The temperature is set to a specific temperature after each stage. The discharge pressure is 5.4 bar. The block flow diagram of the process simulation is shown in Figure 3.12.

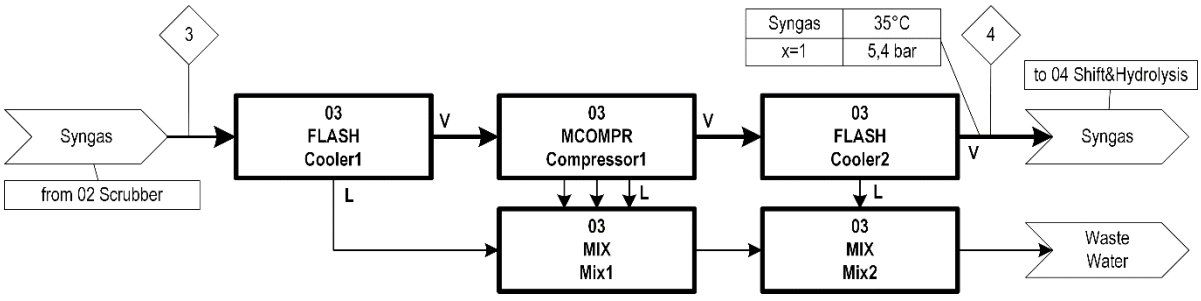

Figure 3.12 Block flow sheet of the compression process

3.4.4 Water-gas Shift and Hydrolysis

In preparation for large-scale syngas purification, CO shifting is also carried out and can be neglected on a pilot-scale according to the current status of the TU Darmstadt. The optimal ratio of H_2/CO for methanol synthesis is 2/1, which promotes synthesis and maximizes conversion. The shift reactor contains an iron-based catalyst. To achieve the 2/1 ratio, a tight control loop is required. The block flow diagram of the process simulation is shown in Figure 3.13. The temperature of the reactor (04 Reactor1) is constant. The turnover of the reactor is not controlled. A bypass (04 Split1) splits the synthesis stream, and the composition of the gas downstream of the merge (04 Mix2) controls the amount of gas that is passed through the bypass (split factor of 04 Split1). Additional steam is needed because the water content of the syngas decreases due to the cooling and heating of the upstream process compared to the industrial process.

The sulfur bound in the fuel reacts during gasification to form hydrogen sulfide and carbonyl sulfide. Sulfur oxides are not formed due to the reductive system. While hydrogen sulfide is an acid gas and can be removed in the acid gas removal, COS reacts with the amine in a one-way reaction and over time lowers the efficiency of acid gas removal. In addition, sulfur is a critical element in methanol and FT synthesis. The sulfur deactivates the catalyst and reacts violently with aluminum. A Co-Zn-catalyst hydrolyzes carbonyl sulfide (reaction R 3.1) and it reacts to form hydrogen sulfide. The same happens with hydrogen cyanide, which reacts to form ammonia (reaction R 3.2).

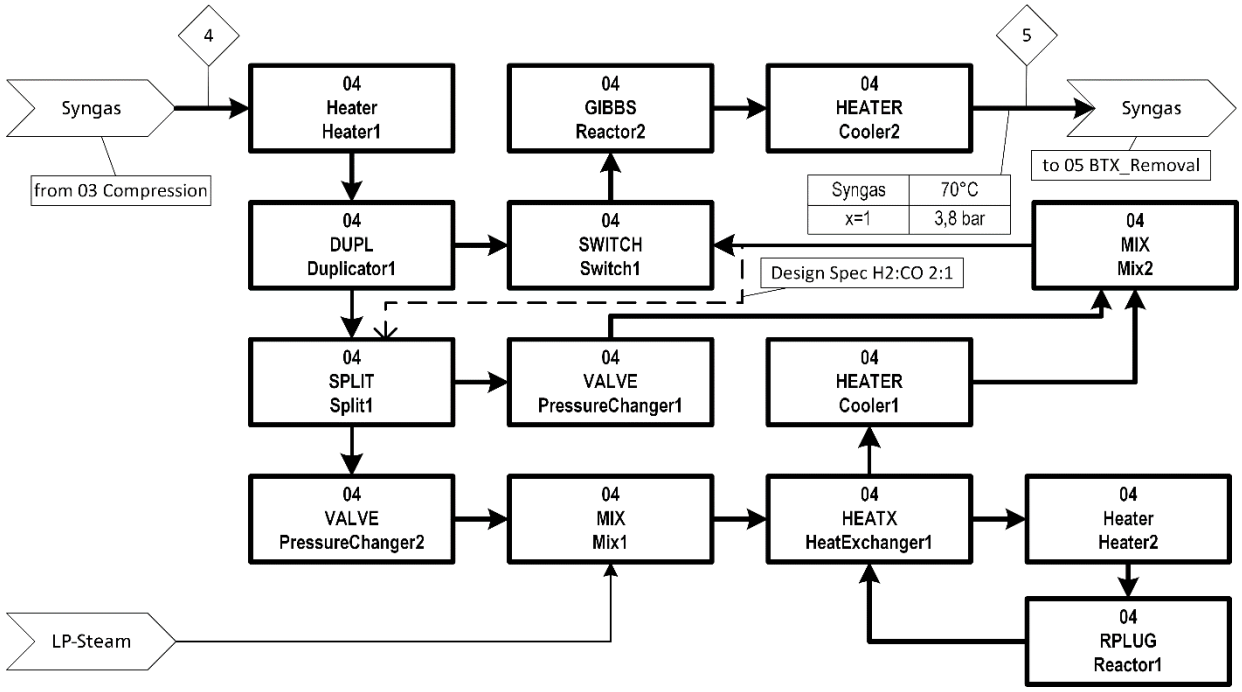

Figure 3.13 Block flow diagram of the process simulation of WGS and Hydrolysis

3.4.5 BTX Scrubber

During pyrolysis, the feedstock releases volatile components and combines them with the bed material. The volatile components vary depending on the feedstock. RDF generally forms more hydrocarbons than LEG. HTW gasification is characterized by the post gasification zone. Molecules with more than 6 carbons present a risk because they can condense and clog valves, dampers, and pumps. The group of tars bundles these types of hydrocarbons. Some acid gas

removal equipment, such as Selexol and Rectisol, is capable of handling tars. While heavy tars (>C12) are easily separated at room temperature, benzene derivatives such as toluene and xylene (abbreviated BTX) condense in a cryogenic environment. Other acid gas removal equipment such as amine scrubbers are unable to treat tars and BTX over time. The result is an accumulation of BTX in the aqueous amine solution. For this reason, ThyssenKrupp Industrial Solutions (TKIS) has developed and patented an innovative concept for BTX removal [92]. By using biodiesel, the thermal stability of the solvent is improved without it decomposing at higher temperatures. The cooling of the syngas causes the decomposition, as do the high temperatures during desorption.

Figure 3.14 shows the block flow diagram of the BTX-removal section, which consists of two absorption columns (05 Column1 and 05 Column2). The first absorber cools the syngas down to room temperature. The steam supplied to operate the CO shift condenses and an oil-water mixture flows in a closed loop. A small amount of regenerated solvent maintains the biodiesel quality at a certain level (05 Mix1) to avoid the infinite solubility of tars. Flow control regulates the water flow (05 Split2). The additional amount of water released by the syngas flows into the wastewater tank. The second absorption column is part of an absorber-desorber configuration. The anhydrous syngas enters the packed column (d=20 cm and 4 m RaschigPak 250Y) at the bottom stage, while the regenerated biodiesel flows into the sump from the top. The solvent absorbs non-polar components due to the Van der Waals force. The quality of the regenerated solvent and the mass ratio of syngas to solvent determine the efficiency of the absorption process.

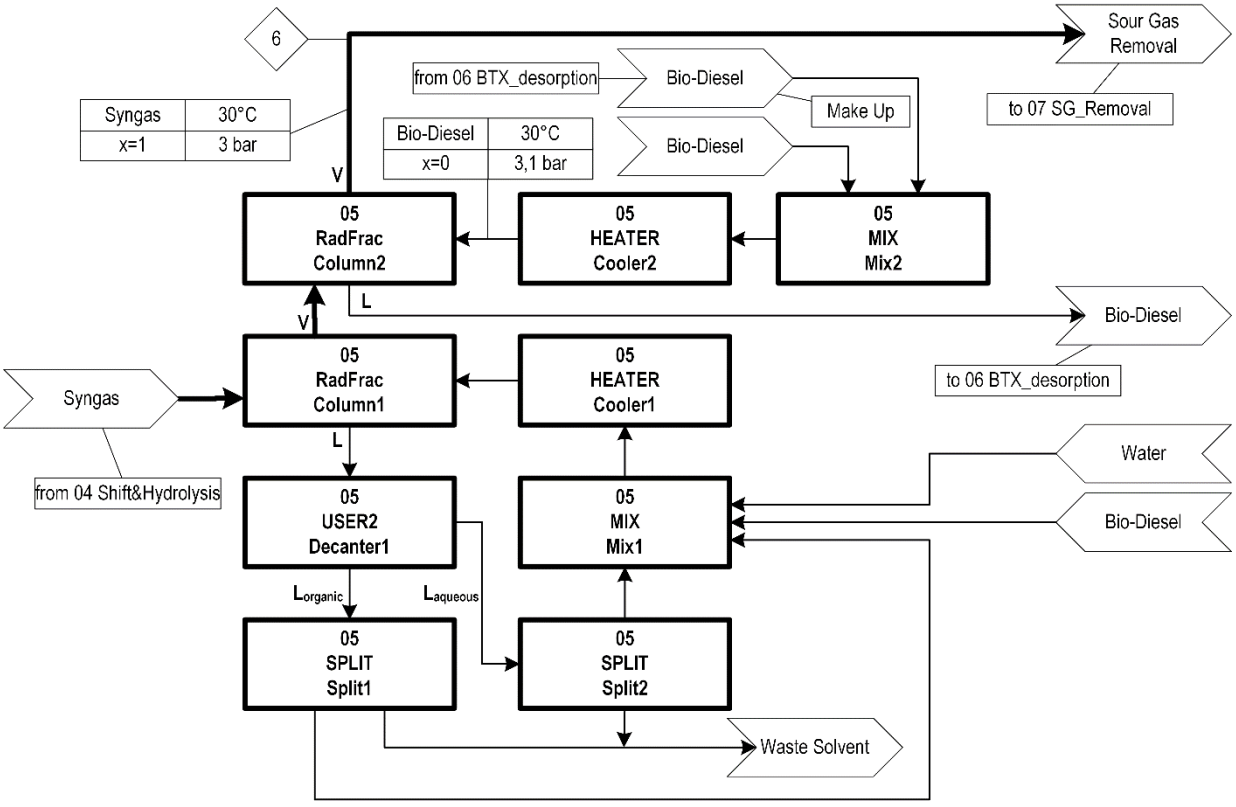

Figure 3.14 Block flow diagram of the process simulation of BTX-removal section

The desorption section is simulated as shown in the block flow diagram in Figure 3.15. Generally, low pressure and high temperature promote desorption processes. The degradation of the biodiesel indicates the upper limit of the preheating (06 Heater1) of the loaded solvent. The inlet of the

loaded solvent divides the column (06 Column1) into a rectification section (d=11 cm and 1 m RaschigPak 500X) and a stripping section (d=11 cm and 3 m RaschigPak 350X). Within the stripping section, a stripping agent absorbs the solvent of the BTX species. In this case, steam is used. In the rectification section, the biodiesel droplets are retained to prevent leakage. A decanter (06 Decanter1) separates the condensates (from 06 Cooler1) into an oily and an aqueous phase. A certain amount of BTX is recycled on the upper stage, while the excess flows into a drum. Adjustable parameters are the amount of steam used, the temperature of the preheated charged solvent, and the BTX reflux.

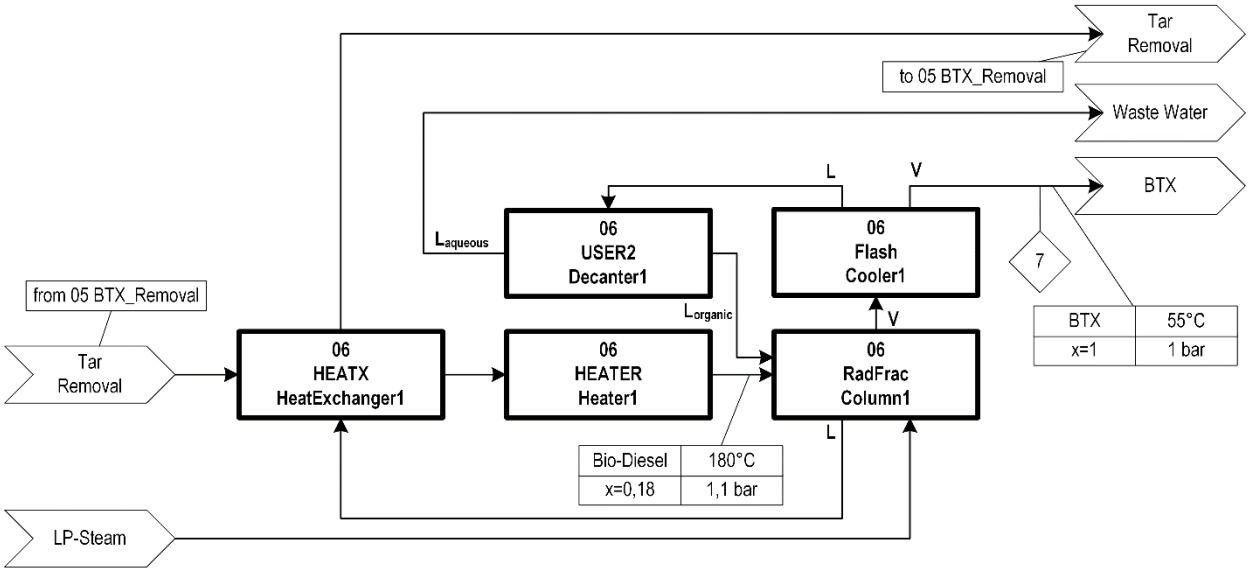

Figure 3.15 Block flow diagram of the process simulation of BTX-desorption

3.4.6 Amine Scrubber

The accurate description of the thermodynamics of amine, water, and acid gases is essential for predicting the separation efficiency of the amine scrubber. The basics have already been discussed in section 3.3.1. Equilibrium constants describe reactions that occur instantaneously, while time controls kinetic reactions. Figure 3.16 shows a schematic representation of the absorption process, divided into a physical layer, the corresponding correlations, and the required data.

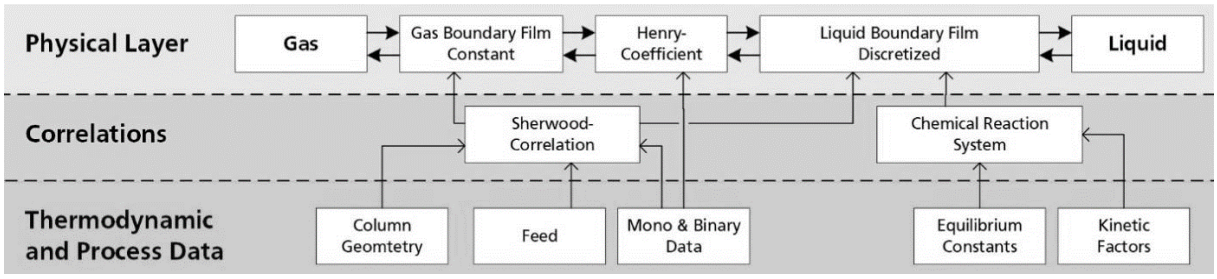

Figure 3.16 schematic of the absorption process

Amine scrubbing is a well-known technology and has been used since 1930 [155,156]. The improvement of the technical process and amine solvent promotes the development of amine scrubbers. TU Darmstadt uses a combination of the tertiary amine Methyl-Di-Ethanol-Amine (MDEA) as the main solvent and Mono-Ethanol-Amine (MEA) as an additive to combine low

regeneration cost with high removal efficiency. The equilibrium and kinetic reactions are listed in Table 3.5.

Table 3.5 Amine scrubbing reactions [157–161]

Equilibrium reaction	**K_1**	**K_2**	**K_3**	**K_4**	
$2H_2O \rightleftarrows H_3O^+ + OH^-$	132.899	-13445.9	-22.4773	0	R 3.3
$HCO_3^- + H_2O \rightleftarrows CO_3^{2-} + H_3O^+$	216.049	-12431.7	-35.4819	0	R 3.4
$H_2S + H_2O \rightleftarrows HS^- + H_3O^+$	214.582	-12995.4	-33.5471	0	R 3.5
$HS^- + H_2O \rightleftarrows S^{2-} + H_3O^+$	-9.742	-8585.47	0	0	R 3.6
$MEA + H_2O \rightleftarrows MEAH^+ + OH^-$	2.1211	-8189.38	0	-0.07484	R 3.7
$MDEA + H_2O \rightleftarrows MEAH^+ + OH^-$	-9.4165	-4234.98	0	0	R 3.8
$(CO_2)_g \rightleftarrows (CO_2)_{aq}$	159.865	-8741.55	-21.669	0.0011029	R 3.9
$(H_2S)_g \rightleftarrows (H_2S)_{aq}$	181.186	-8982	-25.846	0.012128	R 3.10
Kinetic reaction	**K**	**E [J/mol]**	**Basis**		
$CO_2 + OH^- \rightarrow HCO_3^-$	1.33×10^{17}	55470.9	Π_{xy}		R 3.11
$HCO_3^- \rightarrow CO_2 + OH^-$	6.63×10^{16}	107417	Π_{xy}		R 3.12
$MEA+CO_2+H_2O \rightarrow MECOO^-+H_3O^+$	3.02×10^{14}	41264.3	Π_{xy}		R 3.13
$MECOO^-+H_3O^+ \rightarrow MEA+CO_2+H_2O$	5.52×10^{23}	69157.6	Π_{xy}		R 3.14

Figure 3.17 shows a block flow diagram of the process simulation of amine scrubbing. The absorption process takes place at room temperature and about 3.5 bar. Flow control regulates the reflux of the regenerated solvent. The theoretical minimum molar ratio between amine and acid gas is 1.4:1. To avoid heat buildup in the sump, the TU Darmstadt uses a much higher molar ratio of 4. A countercurrent heat exchanger heats the loaded solvent, which then enters the desorber. Steam rises from the stripping section, which absorbs the acid gas and regenerates the solvent. In the rectification section, the acid gas content is raised, which would otherwise result in a significant loss of amine and water. The temperature of the sump controls the vapor flow of the kettle reboiler. A make-up section adds water and amine to restore the originally desired solvent flow.

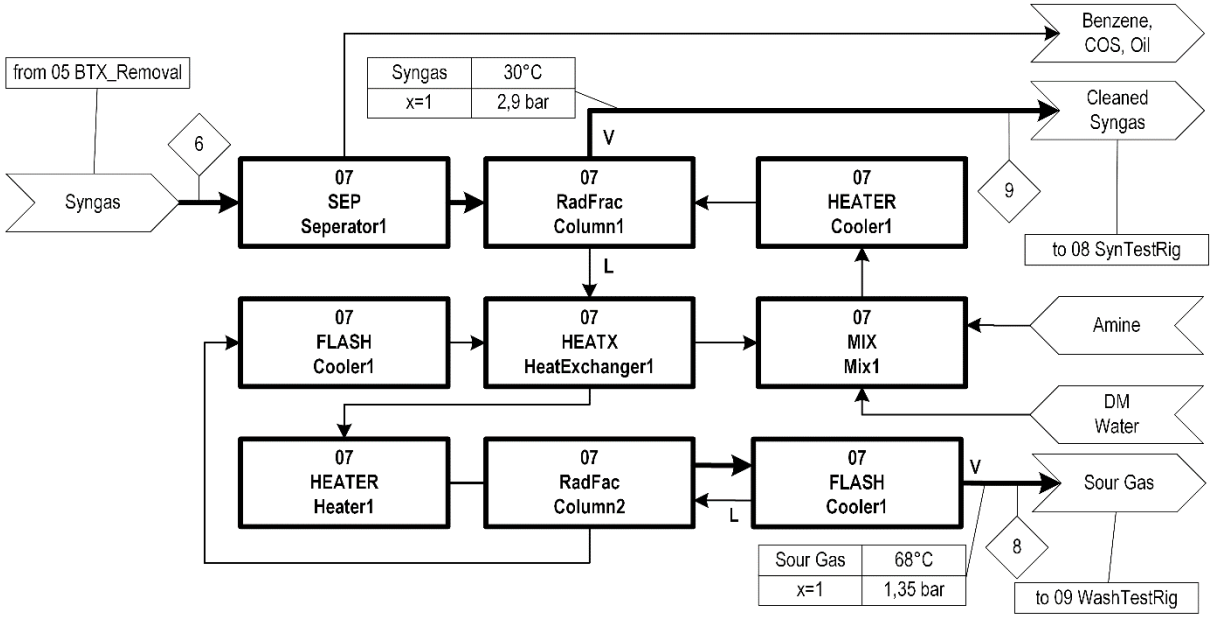

Figure 3.17 Block flow diagram of the Amine scrubbing Process simulation

3.4.7 Synthesis Test Rig

The synthesis gas treatment plant includes all purification processes up to after the amine scrubber. The synthesis gas has almost the quality to perform FT synthesis. RWE provides the synthesis and scrubber trainer to demonstrate the whole chain. A compressor separates a small part of the purified synthesis gas and increases the pressure up to 40 bar. Pipelines conduct the flow into the synthesis test rig, where all sulfur residues are adsorbed in a protective bed in a final purification stage. Figure 3.18 shows the block flow diagram of the synthesis test rig process simulation. Due to the lack of CO shift, hydrogen is added to the synthesis gas (08 Mix1) to achieve the correct CO/H_2 ratio for synthesis. A universal reactor (08 Reactor 1) contains either a modern $Cu/ZnO/Al_2O_3$ methanol catalyst or a Co/Al_2O_3 FT catalyst. The present work focuses on methanol production. Methanol production is an old and still important process. Research is constantly providing new insights into the reaction mechanism, from detailed step-by-step analysis Graaf et al. [162] to trial-and-error Lim et al. [163].

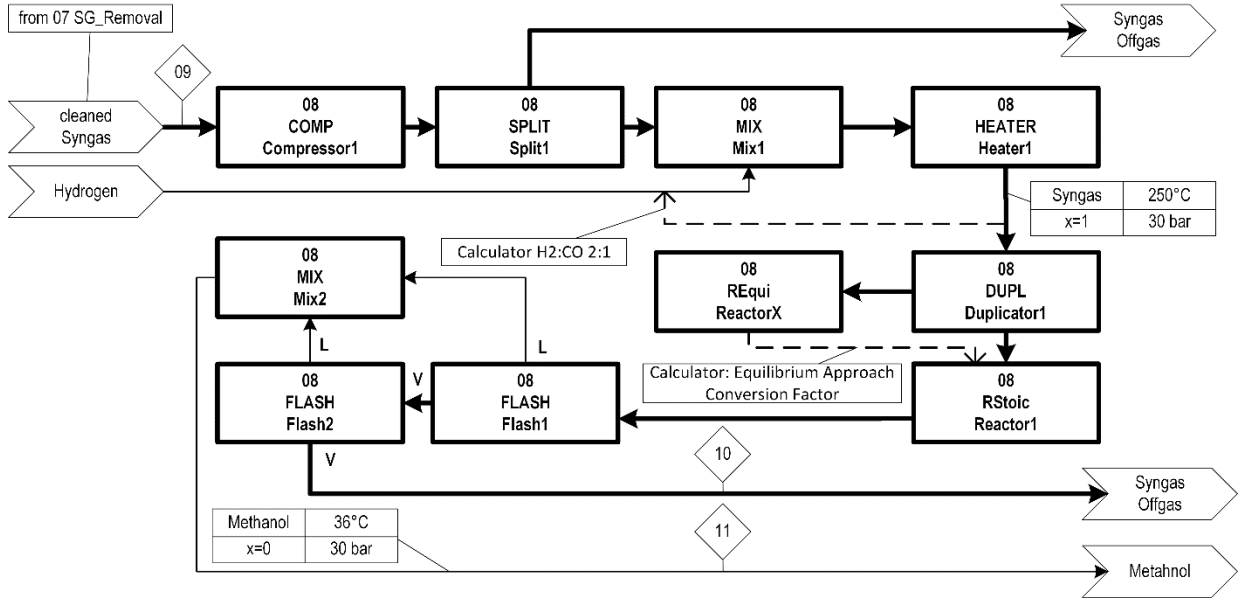

Figure 3.18 Block flow diagram of the synthesis test rig

The reactor is a stainless steel vessel with a length of 900 mm and an inner diameter of 32 mm. The target temperature (08 Heater01) is 230 to 250 °C. Following Le Chatelier's principle, the higher the pressure the better the conversion is. The synthesis test rig's process design limits the pressure to 30 bar. The reactions (R 2.6, R 2.28, and R 2.29) take place here.

In general, there are two options to simulate the reaction. First, the equilibrium approach is built on the minimization of the free Gibbs energy under a given temperature, pressure, and inlet. A Gibbs-reactor model (08 ReactorX) determines the maximum conversion of the reaction independent of the geometry and type of catalyst. A multiplier of the maximum conversion between 0 and 1 (Calculator Equilibrium Approach) determines the catalyst's efficiency, while 0 means no conversion at all and 1 theoretical equilibrium. The second option is to use a kinetic plug flow model. Although there is much data in the literature, the transfer of kinetic factors is limited. Hence, depending on the geometry of the bead, the exact composition of the catalyst, and the process conditions, the kinetic plug flow model is not applicable without further investigation of the catalyst.

Therefore, the Aspen Plus simulation uses the equilibrium approach. The multiplier is a function of pressure and temperature. A cooler reduces the temperature of the product gas down to 50 °C (08 Flash1) and 25 °C (08 Flash2) while methanol condensates partially. The non-synthesized syngas is given to the exhaust.

3.4.8 Mobile Washing Test Rig

The sour gas treatment mobile washing test rig consists of two basic configurations: the baffle tray column (module 100) and the stirred tanks (module 200). The operation of the mobile washing test rig does not represent a steady-state operation, which is mandatory for an Aspen Plus simulation. In comparison to the hydrogen sulfide flow, hydrogen peroxide is present in excess. While using a stirred tank, the change of hydrogen peroxide is negligible. Therefore, the mobile washing test rig can be considered as a quasi-steady-state process. Module 100 monitors the hydrogen peroxide concentration, which controls the make-up section. Hydrogen peroxide is the second most powerful oxygen-based oxidizing agent. It is not expected that back-reactions take place. The slowly rising concentration of sulfur does not influence the experiments. By considering these factors, the simulation of modules 100 and 200 will be modeled with an open countercurrent process and user-defined function shown in Figure 3.19.

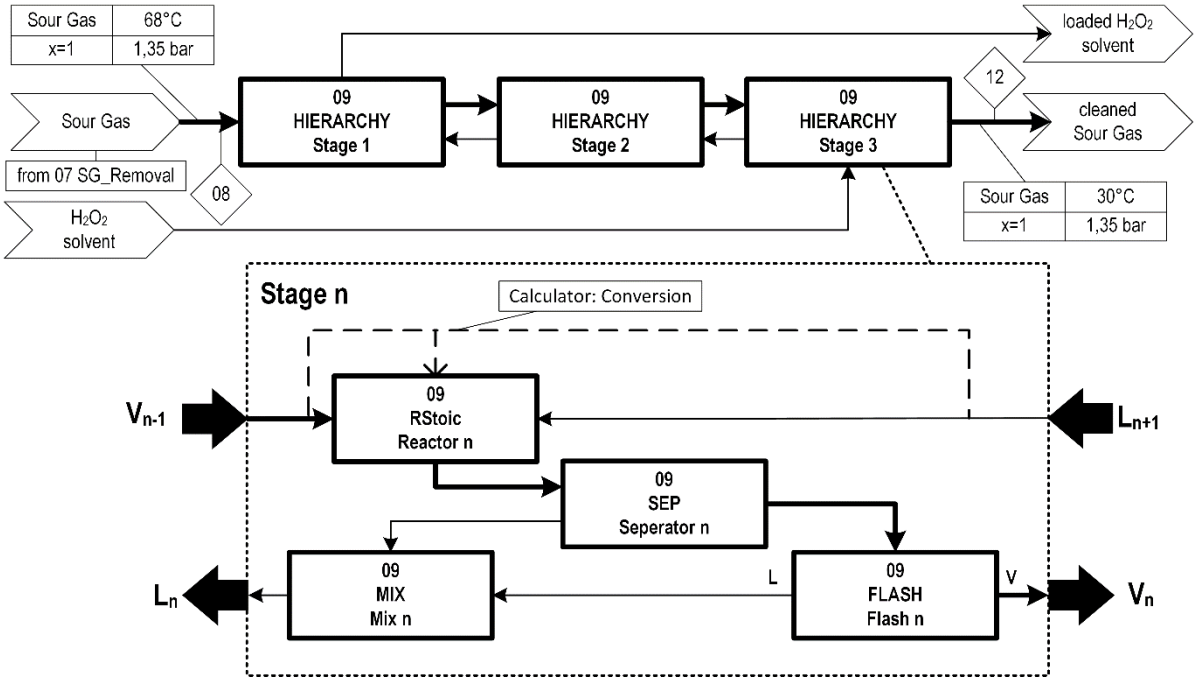

Figure 3.19 Block flow diagram of the washing test rig

The core of the simulation consists of module 200: stirred tanks configuration. Each stirred tank (09 Stage1 to 3) represents a number n of baffle trays in module 100. The baffle tray column is a series connection of multiple stirred tanks following the same procedure. With an experiment, the conversion factor for each stage has to be measured. The setup of the experiments allows measuring the hydrogen sulfide concentration in the sour gas behind and in front of each stirred tank. The second parameter is the number of stirred tanks n that equals combined the performance of the baffle tray column. This technique is comparable to the NTU concept (number of theoretical stages), which is used to specify the effectivity of an absorption.

Even though the reaction is complex and not fully understood, the literature simplifies the mechanism to a single one-way rate-limiting step. This is called the grey-box approach. The pH, the temperature, the concentration of the reactants, and the presence of catalysts influence the conversion of hydrogen sulfide to sulfur. These factors have to be considered in determining the measured conversion. The model takes every step of Figure 3.20 into account. The parameter, which can be adjusted, is the conversion factor of the oxidative reaction.

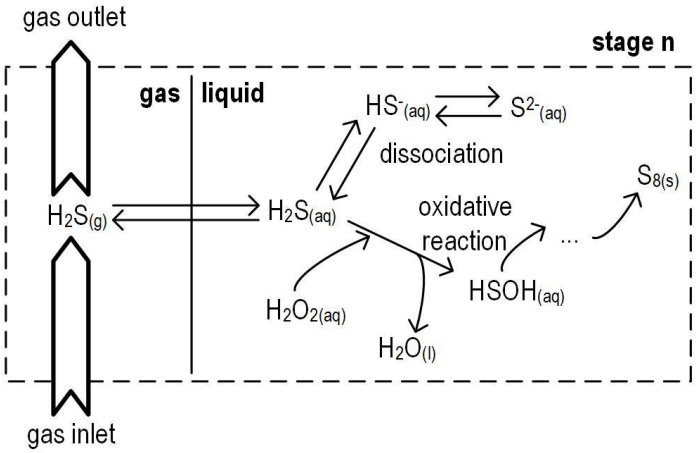

Figure 3.20 Schematic process description of the innovative washing procedure

The conversion factor can be calculated via the different approaches. First, numerical fitting of the known overall conversion. Second, fixed reaction conversion. Third, reaction conversion is dependent on temperature, pH, and H_2O_2 concentration

3.5 Simulation of Industrial Scale

The sizing of the full-scale process is based on the economic feasibility of the entire process chain. Based on ThyssenKrupp's experience, the maximum feasible scale of the gasification unit is 800-900 MW_{th}, depending on the applied mixture of feedstock. It is designed for the maximum capacity of the HTW gasifier. For the gas treatment and synthesis, the operating pressure of the gasifier is chosen to avoid additional compression of the syngas downstream of the gasifier. This means that the decisive factor for the pressure level inside the gasifier is the optimum operating pressure of commercially applied gas treatment and synthesis unit, requiring a minimum pressure of 25 bar. When the pressure drops of the individual process components are taken into account, a gasifier pressure of approx. 30 bar is obtained.

The co-gasification of WTA coal and RDF is applied through this simulation. Three cases are considered of mixing ratio of WTA/RDF, the first case (Case 1) the ratio is 0.8/0.2, the second case (Case 2) is 0.5/0.5, and finally the third case (Case 3) is 02/0.8.

3.5.1 Coal Pre-treatment

The fuel pretreatment of Rhenish lignite by using a WTA drying system is considered in the model. The WTA drying technology is a proven process, and it is already used in many RWE power plants. The WTA process lowers the residual moisture of the coal to a value of about 12% by mass, which is suitable for the gasifier.

The process modeling is based on the experimental results of Buschsieweke [84]. In his work, the author determined the relationship between residual moisture and the temperature of the coal as a function of the saturation temperature at operating pressure for Rhenish lignite as shown in equation 3.16.

$$X_{DryCoal} = (T - T_s)^{-0.75} - 0.02 \tag{3.16}$$

Where T is the fluidized bed temperature and T_s is the saturation temperature at the process pressure in Kelvin.

The process steam parameters including the mass flow as well as the composition and mass flow of the raw coal are specified in the process model. Assuming a gradient of 20 K between the process steam condensate and the raw coal, and operating pressure of the dryer of 1.1 bar, the energy balance for the condensation of the process steam and the heating and drying of the coal is solved as a function of the residual moisture according to equation 3.16. The operating point at which the residual moisture is 15.3% was selected as the reference point of 100% steam flow.

3.5.2 Gasification

The employed gasifier in the IGCC process is an HTW gasifier, which is operated at a pressure of 30 bar and a temperature of about 950 °C at the post gasification zone. A very complicated set of chemical reactions takes place in the gasifier. Thus, a relatively simple approach is used in this model to represent the reactions. It is assumed in the modeling that the gas-phase reactions in the high-temperature gasifier are extremely fast which means that the vapor phase reactions reach equilibrium in the gasifier. Consequently, the key performance indicators are related to carbon conversion, energy balance, oxygen supply, and steam supply.

The gasifier is simulated using two standard Aspen Plus models, RYield and RGibbs. The RYield model serves to convert coal composition details into molecular chemical species, whereas the RGibbs model undertakes the task of determining the equilibrium composition in the gasifier. The Gibbs reactor assumption is a significant simplification. The conversion of hydrocarbons from the pyrolysis of feedstock, especially methane, by steam reforming (R 3.15) or partial oxidation with O_2 (R 3.16), as well as the complete conversion of solid carbon calculated in an equilibrium reactor, will not occur in real plants. Therefore, both carbon conversion and methane formation are externally specified in the model, and the equilibrium of the other components is calculated under this specification. Nevertheless, the other main products of the gasification reaction, CO, H_2, CO_2, and steam, occur close to their chemical equilibrium in an HTW gasifier.

$$CH_4 + H_2O \rightleftarrows CO + 3H_2 \qquad \Delta H^o_R = +205.7 \text{ MJ/kmol} \qquad \text{R 3.15}$$

$$CH_4 + \tfrac{1}{2}O_2 \rightarrow CO + 2H_2 \qquad \Delta H^o_R = -35.7 \text{ MJ/kmol} \qquad \text{R 3.16}$$

Figure 3.21 illustrates the flowsheet of the Gasifier model. The feedstock is introduced to the RYield block, which converts the feedstock to molecular species. The mass yields of H_2O, C, O_2, N_2, S, H_2, Cl_2, and ash are calculated using a calculator block based on the specifications of the feedstock ULTANAL. The decomposed feedstock stream as well as the released decomposition heat are fed into the Gibbs reactor. There, the components of the feedstock are made to react with

each other by calculating the chemical equilibrium of the gas mixture at 30 bar. The chemical equilibrium of a multi-component mixture is reached when its free Gibbs enthalpy is minimized.

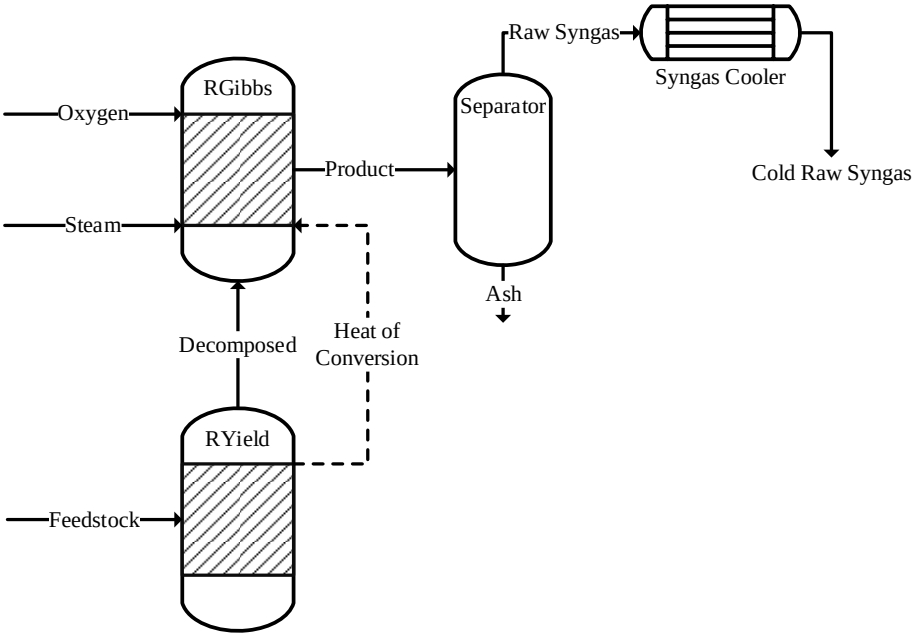

Figure 3.21 Gasifier model flowsheet

The Gibbs reactor is also fed with a steam stream and an oxygen stream. Here, the flow rate of the oxygen stream is controlled using a design spec block to ensure that the temperature of the gasification product is about 950 °C. The solid ash particles are eventually separated from the Gibbs reactor product stream in the separator. The gaseous phase, which forms the raw syngas, leaves the separator from above and is directed into the syngas cooler. The raw gas cooler is modeled as a heat exchanger that cools the hot syngas stream exiting the HTW gasifier. The outlet temperature was set at 350 °C. The produced steam is utilized for the steam power cycle.

Table 3.6 shows an overview of the simulation results obtained with the Aspen Plus gasifier model. It can be seen that high carbon conversion (>93%) is achieved in the gasifier for both feedstocks. Moreover, CO and H_2 are the main species in the raw syngas stream, while slightly higher hydrogen concentrations are achieved for RDF, which can be related to the higher hydrogen content of RDF compared to coal (see Table 3.3). Regardless of feedstock choice, methane concentrations are comparatively low at 6.5 and 6.6 mol% for coal and RDF, respectively.

Table 3.6 Simulation results of gasifier model for different feedstocks

Parameter	Units	Coal	RDF
Carbon conversion	-	0.93	0.99
Water conversion	-	0.49	0.17
Raw syngas	mol/kg_{feed}	107	82
Raw syngas composition			
H_2		28.3	31.1
CO		23.2	20.2
CO_2	mol/mol %	18.2	16.2
CH_4		6.5	6.6
H_2O		23.8	25.9

The characteristics of produced syngas using the simulation model after the raw gas cooling are presented in Table 3.7.

Table 3.7 Simulation results of the three different cases

Parameter	Units	Case 1	Case 2	Case 3
Pressure	bar	29.5	29.5	29.5
Temperature	C	350	350	350
Mass flow	kg/hr	253,883.00	269,976.00	285,676.00
Mole flow	kmol/hr	12,433.87	13,487.07	14,606.59
Raw syngas composition				
H_2	mol/mol %	29.66	30.49	31.66
CO		29.69	28.03	27.25
CO_2		16.15	15.73	14.92
H_2S		0.25	0.17	0.10
COS		0.01	0.01	0.00
HCL		0.12	0.28	0.43
H_2O		18.09	18.96	19.43
N_2		0.28	0.25	0.23
ARGON		0.00	0.01	0.01
CH_4		5.73	6.05	5.96

3.5.3 Syngas Treatment

The HTW gasifier separates the proportion of particles greater than 5 µm with its cyclone. Due to the inertia, the gas flow carries away smaller particles. The first separation deals with the solid phase of the syngas. Dust is a critical process parameter owing to erosion-corrosion, the lifetime of moving equipment and solvents, and in the form of particulate matter even in the deactivation of catalysts. A common way to separate the bulk of the dust is to filter the syngas. To avoid the condensation of tars, trace heaters keep the temperature above 250 °C. Particle removal was simulated in the process model as a pressure drop across the filter.

The raw gas scrubbing to separate the remaining particles, scrub out the water-soluble trace gases, such as HCl and NH_3, and saturate the syngas is modeled as a column with two equilibrium stages. At this column, the syngas stream is enriched with steam before it enters the water-gas shift. The scrubber block uses the Electrolyte NRTL property method. A design spec block is used to adjust the steam flow to operate the scrubber adiabatically. Also, a calculator block is employed to set the scrubber operating temperature 5 °C below the incoming dewpoint.

3.5.4 Water-gas Shift and Hydrolysis

The model uses a sour water-gas conversion to adjust the correct H_2/CO ratio, as this is fundamentally more suitable for treating gasifier product gas containing sulfur (see section 2.3.5). The high-temperature conversion would require either a very high steam/CO ratio or sulfur absorption before conversion, which has a high-cost process in terms of equipment [164].

A three-stage conversion with water quench for intercooling was implemented in Aspen based on the design of Carbo et al. [98] that was presented in Heinze [101]. This has lower steam and energy

requirements compared to simpler configurations, as discussed in Section 2.3.5. The flow diagram of the conversion is presented in Figure 3.22.

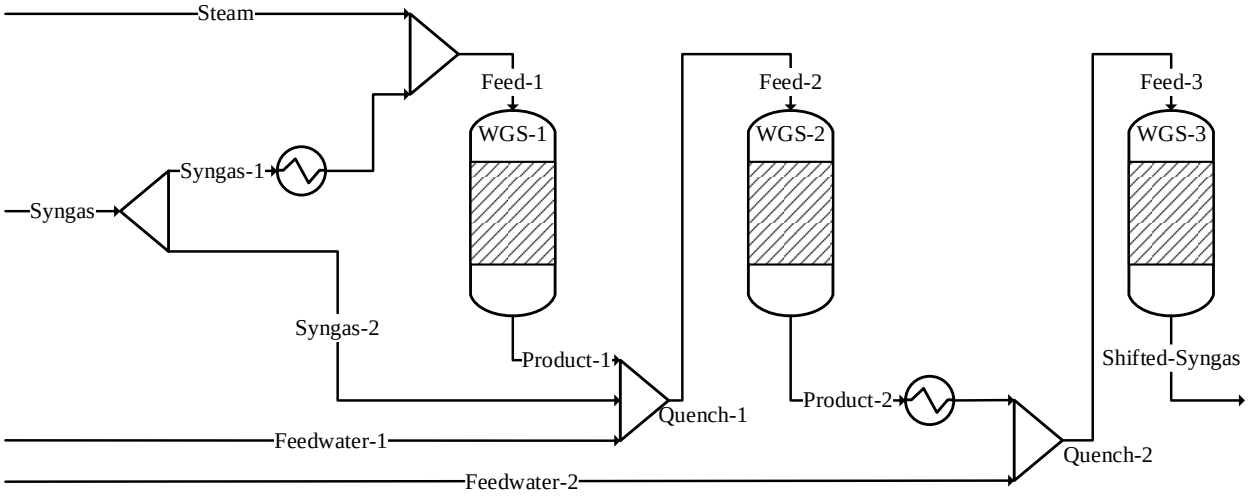

Figure 3.22 Water-gas shift flowsheet

In this process, the un-shifted syngas from the raw gas scrubber is split into two streams at the inlet of the water-gas shift. One stream is preheated with the shifted syngas using a preheater, saturated steam is added, and the stream is shifted to the first conversion stage. Following the first stage, the hot syngas is quenched with feedwater and mixed with the second syngas stream, which has been un-shifted until this point. The total stream is shifted in the second stage, cooled down by the preheater for the incoming stream, and quenched a second time. In the third stage, a final shift reaction takes place. The reactors are modeled as equilibrium reactors for the water-gas shift reaction (R 2.6). The first two reactors are assumed to be equilibrium limited due to the higher temperature and thus higher reaction rate. The last reactor is assumed to be kinetically limited due to the lower temperature by determining equilibrium for a temperature 10 °C higher. For the reference case, the inlet conditions of the conversion stages in terms of temperature and steam/CO ratio were chosen according to Martelli et al. [99].

The adjustment of the desired H_2/CO ratio is not done within the water-gas shift, but it is done by a controlled bypass for un-shifted syngas. The bypass flow around the conversion is thereby controlled to set a stoichiometric ratio (equation 3.17) of 2.03 [71].

$$SR = \frac{p_{H_2} - p_{CO_2}}{p_{CO} + p_{CO_2}} \tag{3.17}$$

Design specs have been implemented in the process simulation to keep the temperature of the first reactor feed about 280 °C and the feed of the second reactor about 250 °C. On the other hand, the supplied saturated steam to CO ratio is selected to be 2/1.

Table 3.8 summarizes the composition of the syngas before and after conversion, as well as the mass and energy balance. The hydrogen content in the gas increases during the water-gas shift and the CO content decreases to about 1%. The streams fed to the water-gas shift were composed of approximately 60% un-shifted syngas and approximately 40% steam and feed-water. The ratio of saturated steam to boiler feedwater as quench water is about 3/2. Due to the increased moisture

and the exothermic conversion reaction, the calorific value of the syngas decreases during conversion. The energy content in the gas decreases by approximately 8%.

Table 3.8 Mass balance of water-gas shift [101]

Parameter	Unit	Un-shifted Syngas	Shifted Syngas	Steam	Feedwater
H_2	Vol.-%	28.50%	39.30%		
H_2O		17.20%	28.30%	100%	100%
CO		38.80%	0.80%		
CO_2		12.10%	29.60%		
CH_4		1.80%	1.10%		
H_2S		0.30%	0.20%		
Ar		0.00%	0.00%		
N_2		0.60%	0.40%		
distribution	mol/mol_{gas}	59.60%	100%	23.80%	16.60%
Calorific value	MJ/kg	9.42	5.6		
Calorific value of flow	$MW/MW_{raw\ gas}$	100%	92.10%		

During gasification, the sulfur bound in the fuel reacts to form hydrogen sulfide and carbonyl sulfide. Sulfur oxides are not formed due to the reductive system. While hydrogen sulfide is an acidic gas and can be removed in the exhaust gas recirculation (EGR) system, COS reacts in a one-way reaction with amine and reduces the efficiency of the EGR over time. In addition, sulfur is a critical element in methanol and FT synthesis. The sulfur deactivates the catalyst and reacts severely with aluminum. A Co-Zn-catalyst hydrolyzes carbonyl sulfide (reaction R 3.1) and it reacts to form hydrogen sulfide. The same happens with hydrogen cyanide, which reacts to form ammonia (reaction R 3.2).

3.5.5 Acid Gas Removal (AGR)

Acid gas removal is one of the most complex and costly processes besides gasification, in terms of both OPEX and CAPEX. As part of this thesis, three different pre-combustion AGR processes have been investigated. First, is the Selexol AGR process. The second is the Rectisol AGR process. Finally, the a-MDEA AGR process.

The AGR performance target of this process simulations are more than 95% of CO_2 product purity, H_2S content less than 20 ppmv in the CO_2 product, recovery of H_2S more than 99.5%, H_2 recovery more than 99%, and overall carbon capture efficiency of 90%.

3.5.5.1 AGR using Selexol Process Simulation

The two-stage Selexol process is one of the preferable technologies used for removing both H_2S and CO_2 out of high-pressure syngas. This process is licensed by UOP LLC. Selexol solvent is a blend of dimethyl ethers of polyethylene glycol (DEPG). Due to the high solubility of acid gases compared to CO and H_2, in addition, H_2S is nine times more soluble than CO_2, thus Selexol is well suited for the separation of H_2S and CO_2 from the syngas. [103,107]

There are many configurations of the Selexol process depending on the AGR targets and the feed syngas. A conventional dual-stage Selexol process for H_2S and CO_2 capture from syngas was

simulated using Aspen Plus. The Perturbed-Chain Statistical Associating Fluid Theory (PC-SAFT) is used as a property method to represent the properties for mixtures of Selexol and the syngas components.

The PC-SAFT model is based on perturbation theory [165]. The main idea is to subdivide the total intermolecular forces into repulsive and attractive contributions. The model applies a hard-chain reference system to account for the repulsive interactions. The attractive forces are further divided into different contributions, which include both dispersion and association. The model's applicability covers fluid systems ranging from small to large molecules, including normal fluids, water and alcohols, polymers and copolymers, and their mixtures. Aspen Tech regressed the VLE data from Selexol on the PC-SAFT model, and these model parameters were used to model the IGCC process [166,167].

The DOE/NETL baseline of cost and performance is taken as a reference for the configuration of the Selexol process simulation of this study [168]. The carbon capture efficiency of an IGCC plant with carbon capture is given in equation 3.18 where the feed syngas is taken after the gasifier [169].

$$Carbon\ Capture\ Efficiency = \frac{Carbon\ in\ the\ Product\ CO_2}{Carbon\ in\ the\ feed\ syngas} \tag{3.18}$$

Whereas the evaluation of carbon capture efficiency should take all carbon spices contained in the CO_2 product stream including CH_4 and CO as well as CO_2. The reason for this is that Selexol can also capture CO and CH_4, but to a lesser extent than CO_2 [107].

The process flow diagram of the dual-stage Selexol process configuration is shown in Figure 3.23. The Selexol configuration commonly consists of two absorbers one serves as an H_2S absorber, which uses a CO_2-rich Selexol to absorb H_2S, and the other one acts as a CO_2 absorber, which uses a lean and semi-lean Selexol to absorb CO_2. In addition to flash drums that regenerate the CO_2-rich Selexol by a multi-pressure drop. H_2S concentrator is used to remove most of CO_2 from the H_2S-rich Selexol stream. Moreover, one stripper is used to regenerate the H_2S-rich Selexol. In addition to other auxiliaries such as heaters, coolers, and pressure changers.

The major distinction between the various two-stage Selexol configurations is the method of vapor recovery management. Both vapor cycles source from the H_2S concentrator and the flashing of the CO_2-rich Selexol.

Although the solubility of H_2 in Selexol to CO_2 is almost a hundred times lower, Selexol's mass flow rate in the CO_2 absorber is sufficient to absorb a considerable amount of H_2. Accordingly, the vapor that comes out of the first flash drum can contain more than 3% of the H_2 extracted from the syngas. As a result, this H_2 content would lead to an unacceptable efficiency loss unless it is recovered. For this reason, the widely used approach is to compress the vapor out of the high-pressure flash drum and feed it into the CO_2 absorber. The H_2 recovery of a dual-stage Selexol process is given by equation 3.19 [169].

$$Recovery\ of\ H_2 = \frac{H_2\ flowrate\ of\ product\ syngas}{H_2\ flowrate\ of\ feed\ syngas} \tag{3.19}$$

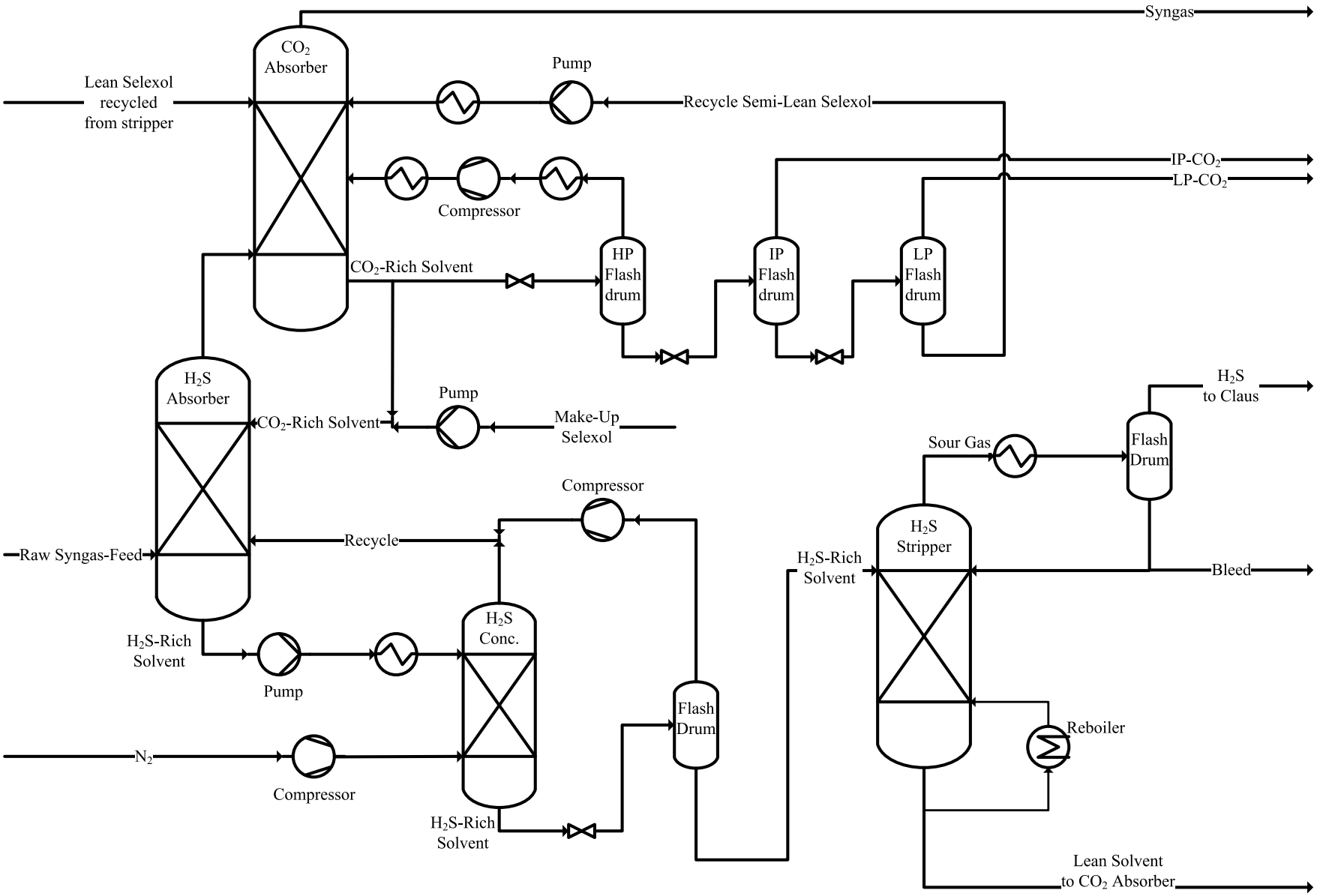

Figure 3.23 Process flow diagram of dual-stage Selexol process for AGR

The vapor from the H_2S concentrator contains significant mole fractions of CO_2 and H_2S. A common configuration for recirculating vapor out of the H_2S concentrator is to return the vapor directly to the H_2S absorber. There are two basic strategies for this recirculation. One is to compress the vapor to return it to the absorber. The other approach is to operate the H_2S concentrator at a higher pressure than the H_2S absorber. Thus, the vapor produced from the H_2S concentrator should not be compressed before it is recirculated to the absorber. Clearly, the N_2 purge still needs to be compressed to the pressure of the H_2S concentrator. However, the energy required to compress the N_2 purge stream is much less than the alternative configuration. In addition to the H_2S concentrator, more CO_2 can be recovered from the H_2S-rich Selexol stream by lowering the pressure of the H_2S-rich Selexol exiting the concentrator. This low-pressure CO_2-rich vapor stream must be compressed and recycled to the absorber. The H_2S recovery of a dual-stage Selexol process is given by equation 3.20 [169].

$$Recovery\ of\ H_2S = \frac{H_2S\ flowrate\ of\ sour\ gas\ leaving\ the\ stripper}{H_2S\ flowrate\ of\ feed\ syngas} \qquad (3.20)$$

Using clean syngas as the purge gas for the H_2S concentrator is an alternative that has been investigated in various studies [60,170]. Where N_2 is required as a diluent for feeding H_2-rich syngas to the gas turbine, N_2 purging is preferred.

As shown in the process flow diagram presented in Figure 3.23. The syngas is fed to the bottom of the H_2S absorber, where the H_2S is selectively absorbed by CO_2-rich solvent coming out from the bottom of the CO_2 absorber. Also, a lean solvent stream feeding the top of the H_2S absorber, while the H_2S-rich solvent leaves from the bottom of the H_2S absorber, and then it enters the top of the H_2S concentrator, which releases most of the absorbed CO_2 in the H_2S-rich solvent by using N_2 as stripping gas that leads to achieving the H_2S recovery target.

The bottom stream of the H_2S concentrator is expanded in a flash drum to the pressure of the H_2S stripper to desorb the CO_2 and H_2 from the H_2S-rich solvent that concentrates the H_2S. The stream out of the top of the flash drum is compressed and mixed with the top stream of the H_2S concentrator, then the total stream is recycled to the H_2S absorber to re-absorb the H_2S from the recycle stream. While the bottom stream of the flash drum is fed to the H_2S stripper that employs steam regeneration of stripping the Selexol solvent to be free of acid gases.

At this stage of the process, the CO_2 and H_2S are stripped from the solvent and flow out from the top of the H_2S stripper. Unless the CO_2 in the H_2S-rich solvent is removed in advance, the acid gas will be significantly diluted by CO_2, which will affect the overall capture efficiency. Consequently, the CO_2 must be desorbed from the H_2S-rich solvent before it is stripped in the H_2S stripper. The lean solvent at the bottom of the H_2S stripper is cooled and pressurized to the pressure of the CO_2 absorber to be recycled back into the CO_2 absorber.

The gas stream that leaves the top of the H_2S absorber is directed into the CO_2 absorber. The CO_2 absorber is operated with two Selexol solvent streams, the lean solvent from the bottom of the H_2S stripper and the semi-lean solvent from the multi-stage flash. The lean solvent is fed into the top of the CO_2 absorber, while the semi-lean solvent enters the middle of the column.

The purified syngas stream leaves the head of the CO_2 absorber, whereas the CO_2-rich solvent is apportioned into two streams: The larger portion is fed to the CO_2 flash section, which is done

through three pressure stages (HP, IP, and LP). The other portion is supplied to the H_2S absorber to trap H_2S and avoid the gas stream carrying H_2S into the CO_2 absorber. This flow rate of CO_2-rich solvent directed to the H_2S absorber is adjusted to ensure that the AGR system is capable of achieving the targeted H_2S capture rate exceeding 99.5%, resulting in a CO_2 product containing less than 20 ppmv of H_2S.

The pressure in the flash drum has to be high enough to achieve the lowest possible energy consumption for the compression of the recycled gas. Simultaneously, its pressure must be low enough to desorb the CO_2 to the required level to achieve good CO_2 recovery and produce a sour gas with a molar H_2S content greater than 0.4 for the Claus plant.

The CO_2-rich solvent includes a substantial fraction of H_2 besides CO_2, even though the solubility of H_2 relative to CO_2 is only 0.013 [107]. To achieve a very high H_2 recovery of more than 99% and CO_2 purity of about 95% simultaneously, the majority of the H_2 in the CO_2-rich solvent should be recovered and recycled to the CO_2 absorber. Therefore, the first flash drum is assigned to recover H_2 from the CO_2-rich solvent. For this study, it was determined that its pressure must be at least 18.5 bar for achieving the H_2 recovery target. As the gas expanded in the first drum has about 50 mol% H_2, it must be recycled to the CO_2 absorber after compression. In case a solvent had a higher CO_2 selectivity with respect to H_2, then the pressure in the first flash drum could be set higher, reducing the power consumption required for the compression of the recycle gas.

The solvent leaned on H_2 is sequentially fed into the second and third flash drums following the first flash drum to recover CO_2 from the solvent. The pressure of the third flash drum is adjusted to a pressure close to ambient pressure maximizing the solvent processing capacity. The second flash drum used a pressure of 3.5 bar because CO_2 product is compressed in the third flash drum at a compression ratio of about 3 and then mixed with CO_2 from the second flash drum. Next, the CO_2 product enters multi-stage compression trains with intercooling. After the CO_2 has liquefied, it is compressed by a pump up to 150 bar.

Pure nitrogen is used as a stripping gas for the H_2S concentrator and is supplied by the air separation unit (ASU). One of IGCC's auxiliary units for supplying oxygen for gasification, the ASU also produces pure nitrogen. A portion of the N_2 is fed to the H_2S concentrator as stripping gas. The majority of the N_2 used as stripping gas ended up in the clean syngas, while a fraction of the N_2 is unavoidably absorbed in the solvent and is contained in the H_2S and CO_2 products. As the fuel gas has to be diluted with the ASU-N_2 for its combustion in any case, the N_2 inclusion in the fuel gas is allowed as long as the quantity of N_2 in the fuel gas is less than the quantity of the N_2 diluent. On the other hand, the N_2 absorbed by the Selexol solvent in the CO_2 absorber should be removed from the CO_2-rich solvent to ensure the purity of the CO_2 product. Most of the N_2 is desorbed from the CO_2-rich solvent in the first flash drum, as well as H_2. Consequently, the CO_2 purity can still be maintained up to 97%. When the ASU-N_2 is adopted as stripping gas in the H2S concentrator, the H_2 purity of the purified syngas decreases from 88% to 82%. However, the 82% H_2 purity is still superior to the H_2 purity of the purified syngas after dilution with ASU-N_2 at the combustor. Nevertheless, if the overall process aims to produce high purity H_2 from syngas rather than electricity, only the purified syngas can be used as stripping gas. This is because the H_2 purity of the purified syngas must be kept as high as possible to improve the performance of a H_2 pressure swing adsorption system downstream of the Selexol process [171].

The Selexol solvent should contain a certain amount of water so that the water can be evaporated by the heat delivered to the stripper reboiler. The heating source of the reboiler is extracted from the LP steam of the HRSG. The water content of a Selexol solvent is not recommended to exceed 5 wt% because the viscosity of the Selexol solvent gradually increases with increasing water content [172].

Table 3.9 shows the design specifications of the Selexol process used throughout the Aspen Plus model.

Table 3.9 Design Specifications of the Selexol Process

Parameter	H_2S Absorber	CO_2 Absorber	H_2S Concentrator	H_2S Stripper
Number of stage	20	30	20	20
Column type	Packed			
Packing type	Norton IMTP			
Packing diameter	50 mm			
Column diameter [m]	1.9	3.45	1.25	1.7
Height [m]	20	32	26	5

3.5.5.2 AGR using Rectisol Process Simulation

The Rectisol AGR process based on methanol (MeOH) as a physical solvent is used for selective capture of H_2S and CO_2 out of high-pressure syngas. The PC-SAFT property method also is considered for representing the properties for mixtures of MeOH and the syngas components [173,174]. The configuration was chosen for this process simulation of the Rectisol process is based on Gatti et al. [175], Munder et al. [176], and Heinze [101]. The process configuration generally consists of two absorbers, one absorbs H_2S whereas the second absorbs the CO_2. In addition to three strippers, two of them work as CO_2 strippers at two stages of pressure (HP and LP), and one for H_2S stripping. The process flow diagram of the Rectisol process configuration is shown in Figure 3.24.

The AGR performance target of this process simulations are more than 95% of CO_2 product purity, H_2S content less than 20 ppmv in the CO_2 product, recovery of H_2S more than 99.5%, H_2 recovery more than 99%, and overall carbon capture efficiency of 90%.

The syngas is fed in at the bottom of the H_2S absorber, which uses CO_2-rich methanol coming out of the bottom of the CO_2 absorber to absorb H_2S, and the other one acts as CO_2 absorber, which uses chilled lean methanol to absorb CO_2. The CO_2–rich solvent leaves the bottom of the CO_2 absorber is split into two streams the majority of it is expanded using two flash drums (HP and LP) to recycle the H_2 and CO_2. While the remaining portion is provided to the top of the H_2S absorber.

The H_2S-rich solvent leaves the bottom of the H_2S absorber is flashed using a flash drum to recover H_2 and CO_2 from the rich solvent and recycle it to the H_2S absorber. The concentrated H_2S-rich solvent is directed to the methanol regeneration section. The regeneration of the rich solvent takes place on two pressure stages in three steps. In the first step, desorption of about 90% of the CO_2 occurs in an HP stripper column. The H_2S-rich solvent is added at the bottom and heated in the reboiler. Condensation of the methanol and recovery of H_2S at the top of the column occurs by feeding the cold-rich solvent from CO_2 absorption. In the next step, desorption of the remaining CO_2 takes place at the LP stripper column with a similar design. Again, heat is added at the base

by means of a reboiler and condensation takes place by feeding CO_2-rich, H_2S-lean solvent from the CO_2 absorption. In the final step, the H_2S is desorbed from the methanol. For this purpose, the methanol is fed into the lower part of the column, which is equipped with a reboiler and a top condenser. An H_2S-rich stream can be removed at the top of the column. At the bottom of the column, the regenerated methanol is discharged. Via a heat exchanger, it preheats the CO_2- and H_2S-rich solvent from the absorption column for regeneration before it is chilled in a second heat exchanger using refrigerant.

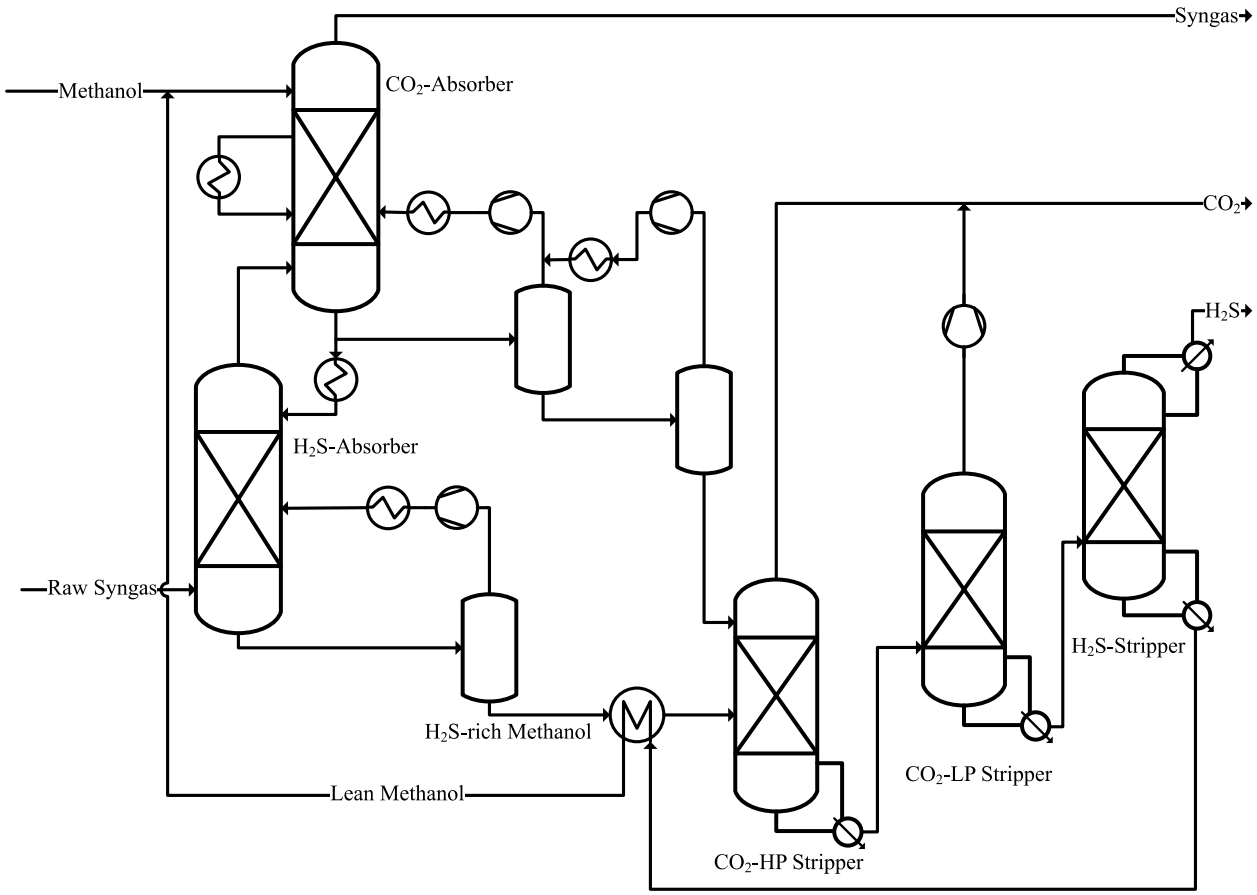

Figure 3.24 Rectisol process flow diagram

The CO_2 desorbed at the LP drum is compressed to the pressure of the HP drum, merged with the CO_2 from the high-pressure desorption, and fed to the CO_2 compression. The modeled CO_2 compression is based on the European best practice guidelines for the assessment of CO_2 capture technologies [138]. The CO_2 is brought to 80 bar via a two-stage compression with intermediate cooling and condensate separation. After further cooling, the non-condensable gas components are separated from the supercritical CO_2 and the CO_2 pressure is increased to 150 bar using a pump.

Table 3.10 summarizes the most important characteristics of the input and output streams for the simulation reference case. The targets set for the process are achieved. Due to the absorption of the inert CO_2, the calorific value of the clean gas is 22.53 MJ/kg, which is significantly higher than before the acid gas removal. In this process, the chemical energy in the clean gas is reduced by approx. 1.4% compared to the raw gas supplied. Two-thirds of the lost chemical energy is found in the H_2S stream to the Claus unit. The last third is the co-absorbed methane, which is conveyed toward CO_2 compression.

Table 3.10 Performance parameters of Rectisol Process

Parameter	Unit	Raw syngas	Clean syngas
H_2	Vol.-%	43.45%	60.24%
CO		22.18%	30.29%
CO_2		28.38%	2.88%
CH_4		5.00%	5.69%
Ar		0.21%	0.30%
N_2		0.43%	0.60%
H_2S		0.34%	0.00%
COS		0.01%	0.00%

3.5.5.3 AGR using a-MDEA Process Simulation

Activated methyldiethanolamine (a-MDEA), using MEA as the activator, is an organic solvent capable of chemically absorbing H_2S when CO_2 is present, particularly where the ratio is very high of CO_2 to H_2S, that is, in coal gasification process products. The flow diagrams employed for this chemical solvent are analogous to those used for the Selexol and Rectisol solvents, with the difference that here the chemical solvent demands much more heat for regeneration because of the chemical reactions involved compared to the physical solvents, thus its regeneration is achieved by elevating the temperature. A simplified process diagram illustrating a process flow diagram for the AGR with chemical solvents is shown in Figure 3.25.

The syngas fed at the bottom of the H_2S absorber is counter-currently exposed to a lean regenerated amine solvent. The clean gas at the top of the H_2S absorber, containing a very small amount of unabsorbed hydrogen sulfide, is sent to the CO_2 absorber for CO_2 capture. At the bottom of the H_2S absorption column, the H_2S-rich amine recovered is fed into a desorption column for regeneration. The regenerator is heated by a reboiler to release the chemically bound H_2S from the solvent. At the top of the desorber, the desorbed H_2S is fed to the Claus unit and an elemental sulfur recovery unit. Following the desulfurization unit, in the second absorption column, the CO_2 is removed. From the packed absorber, the gas flows and comes into contact with the amine, in which the amine chemically reacts with the carbon dioxide. The clean gas obtained at the top of the CO_2 absorption column contains a very small amount of carbon dioxide. The CO_2-rich amine solution obtained at the bottom of the absorption column is fed into the CO_2 stripper. In contrast to absorption, desorption occurs when the temperature is higher and the pressure is lower. The CO_2-rich stream is pressurized and heated with the hot lean solvent coming from the bottom of the desorption column. The temperature profile of the stripper column is sustained using a bottom reboiler. The output of the upper stream is cooled in a heat exchanger to condense the amine and water vapor and then sent to a flash unit from which the condensed water at the bottom and the carbon dioxide stream (greater than 95% CO_2 by volume) at the top are recovered. The resulting carbon dioxide stream is then dried, compressed, and cooled in preparation for transport and storage [100,177,178].

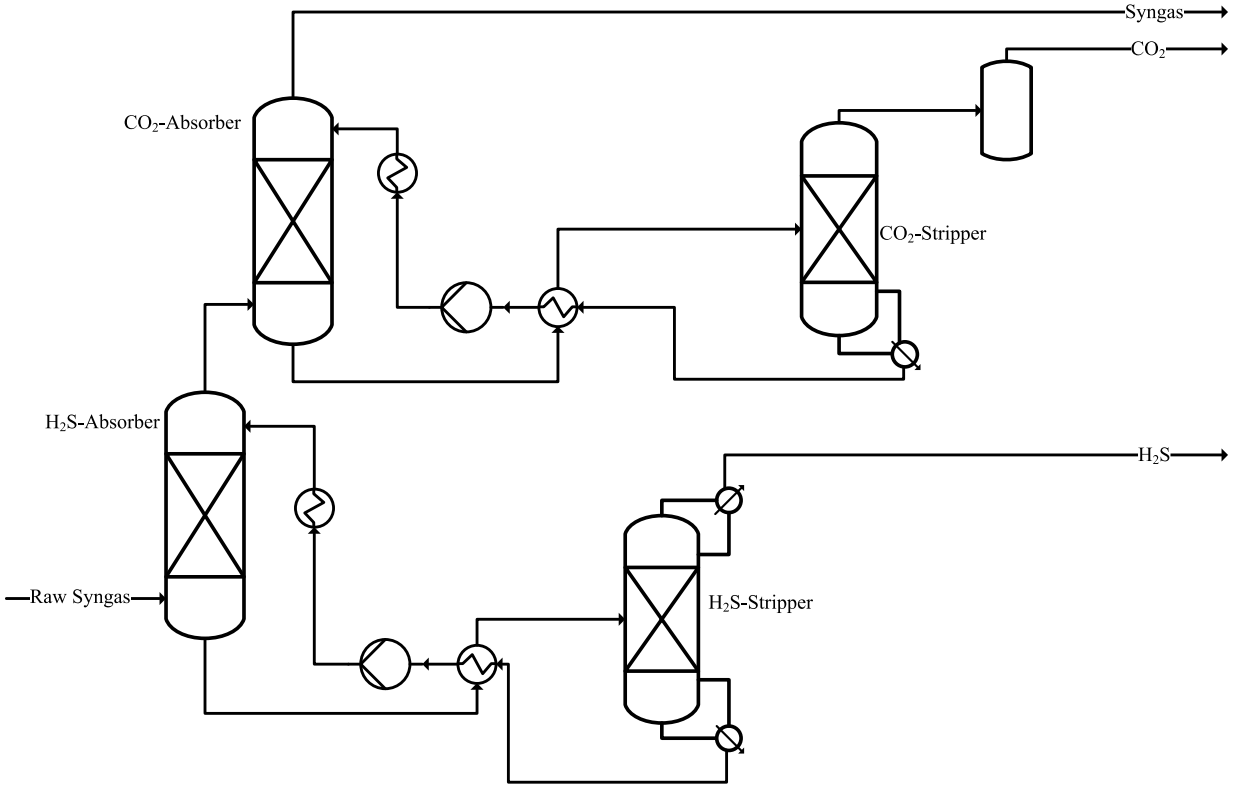

Figure 3.25 Process flow diagram of a-MDEA acid gas removal process

The electrolyte non-random two-liquid model (Electrolyte NRTL), including electrolytic reactions and Henry's law, was used for the calculations of physical properties in the liquid phase in the a-MDEA process. The Soave-Redlich-Kwong (SRK) equation of state was used in the vapor phase and vapor-liquid equilibrium (VLE) to calculate the K value, enthalpy, entropy, and predicted non-idealities of the vapor phase. The equilibrium and kinetic reactions are listed in Table 3.5.

3.6 Simulation of Power Generation

In the polygeneration process model, electricity is generated using a CCPP process that is shown in Figure 3.26 and discussed in section 3.2.2. The syngas is fed into the combustion chamber after the AGR process and diluted with nitrogen. The diluted syngas and the compressed air are mixed in the combustion chamber. After the combustion process, the pressurized flue gas is expanded in the gas turbine. The flue gas then enters the HRSG, which utilizes the heat from the flue gas to generate superheated steam at three pressure levels. The superheated steam is supplied to the steam turbine for power generation.

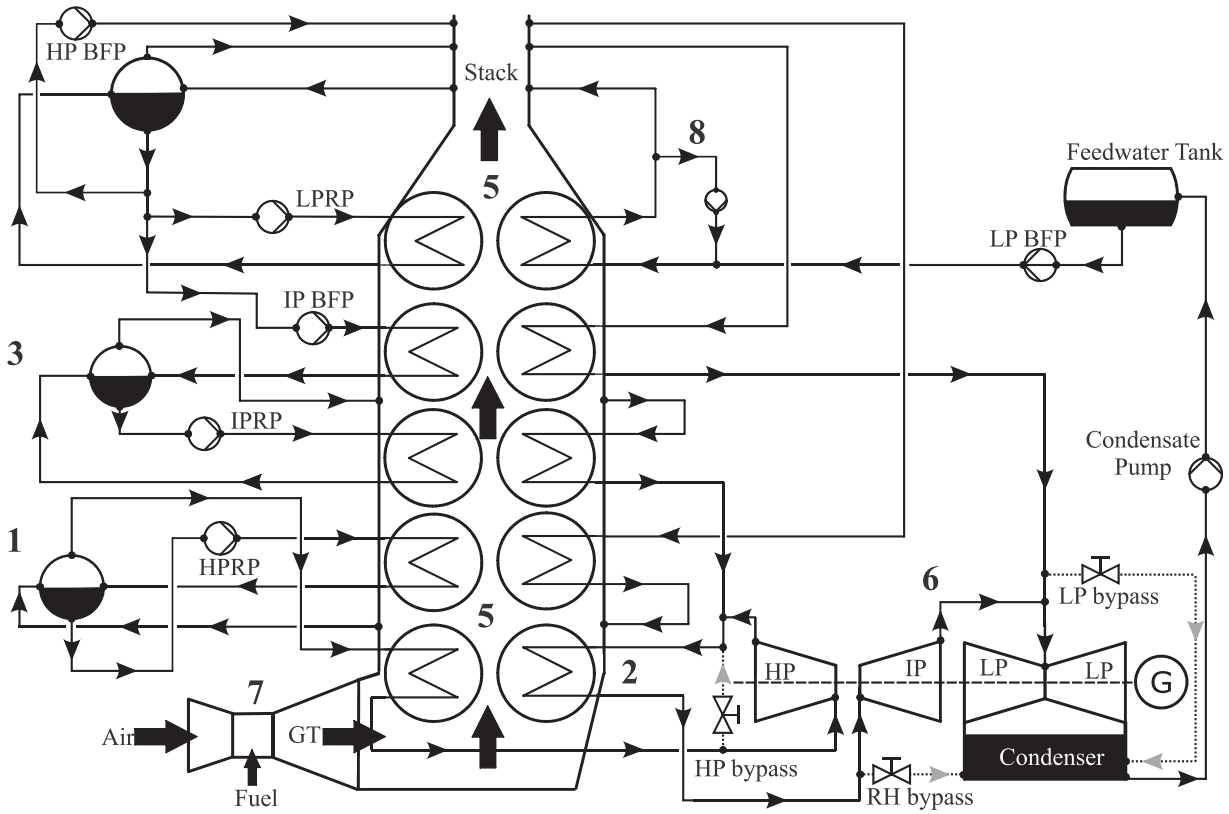

Figure 3.26 Simplified schematic diagram of Combined Cycle Power Plant

3.6.1 Gas Turbine Simulation

For the gas turbine process model, a natural gas turbine model verified using design data was adapted for use in the IGCC process. The adapted process model can be seen in Figure 3.27. The isentropic efficiencies of the compressor and turbine, pressure ratios, cooling air ratios, and air number were retained. Since the turbine inlet temperature (TIT) for syngas-fired turbines of running IGCC plants is in the range of 1200 °C to 1300 °C [115], this was lowered to 1250 °C in the model by increasing the cooling air flow. The syngas itself is diluted with the available nitrogen from the air separation unit to reduce the flame temperature to the value for natural gas combustion and avoid NOx formation. Table 3.11 summarizes the key parameters of the underlying natural gas turbine as well as the modeled syngas turbine when using syngas almost fully converted to hydrogen. As can be seen, when syngas is used instead of natural gas, both the turbine outlet temperature (TOT) decrease by about 70 °C, and the turbine efficiency decrease by about 3%. A lower turbine outlet temperature has the particular consequence that a downstream steam power process has to be adapted. The gas temperature can be raised again to the level of natural gas turbines using an additional burner. In the model, this is done by diverting a partial stream of the syngas diluted with nitrogen for post-combustion after the turbine. This lowers the efficiency by a further 3%. Alternatively, the same turbine outlet temperature can be achieved by changing the pressure ratio. In reality, this approach requires a new turbine and accordingly cannot be flexibly changed for different load points. The result for this approach is also shown in Table 3.11.

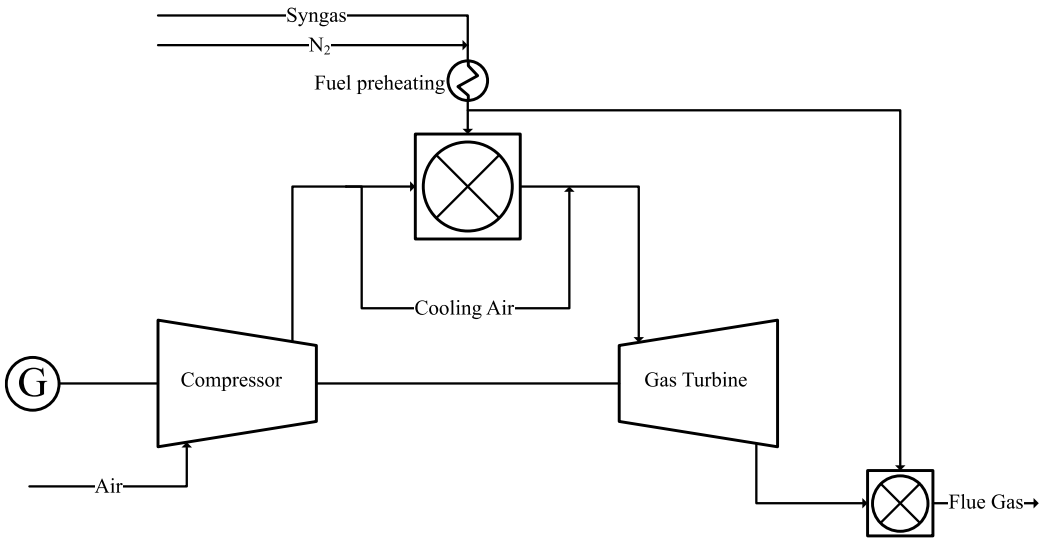

Figure 3.27 Gas Turbine process flow diagram

Table 3.11 Parameters of the gas turbine process models

	Pressure ratio	COT [°C]	TIT [°C]	TOT [°C]	Efficiency
Natural gas	17.6	1443	1360	625	38.40%
Syngas	17.6	1443	1250	555	35.20%
Syngas with post-combustion	17.6	1443	1250	625	32.10%
Syngas with different pressure ratio	12.8	1443	1250	625	33.00%

It is assumed for further evaluation that a multi-fuel power plant can also be operated flexibly with natural gas. Accordingly, the connection of the turbine with the post-combustion is considered.

3.6.2 HRSG Simulation

The model of the subcritical HRSG with the flue gas side and the water/steam side is developed using the operating data of the reference power plant. Figure 3.28 shows the model of the HRSG of the reference power plant. It includes the flue gas and water/steam sides with HP, IP, and LP stages. The flue gas enters the duct of the HRSG from the GT with a mass flow rate of 587.3 kg/s and a temperature of 628 °C. After flowing through the duct, the flue gas is cooled to 81 °C with a small pressure drop of about 15 mbar. The efficiency in relation to the lower heating value is 91.28%.

An overview of the water/steam path is presented in Figure 3.28. The LP circuit routes from the inlet of the LP-ECO to the outlet of the LP-SH. A supply of LP feedwater is provided to the LP-ECO by the condensate pump, which is modeled here as an inlet boundary condition. This feedwater flows with a temperature of 49.8 °C from the LP-ECO to the LP drum as a result of recirculation from the outlet to the inlet of the LP-ECO, independent of the power plant load. The water circulates from the LP drum through the LP evaporator tubes, raising the temperature due to heat transfer from the GT flue gas to the water in the evaporator tubes, yielding saturated steam. The majority of the saturated water is separated in the LP drum and fed into the LP circuit through the LP feedwater pump and into the HP circuit through the HP feedwater pump. The saturated

steam leaves the LP drum and passes through the LP-SH. After leaving the LP-SH, the superheated steam enters the LP turbine.

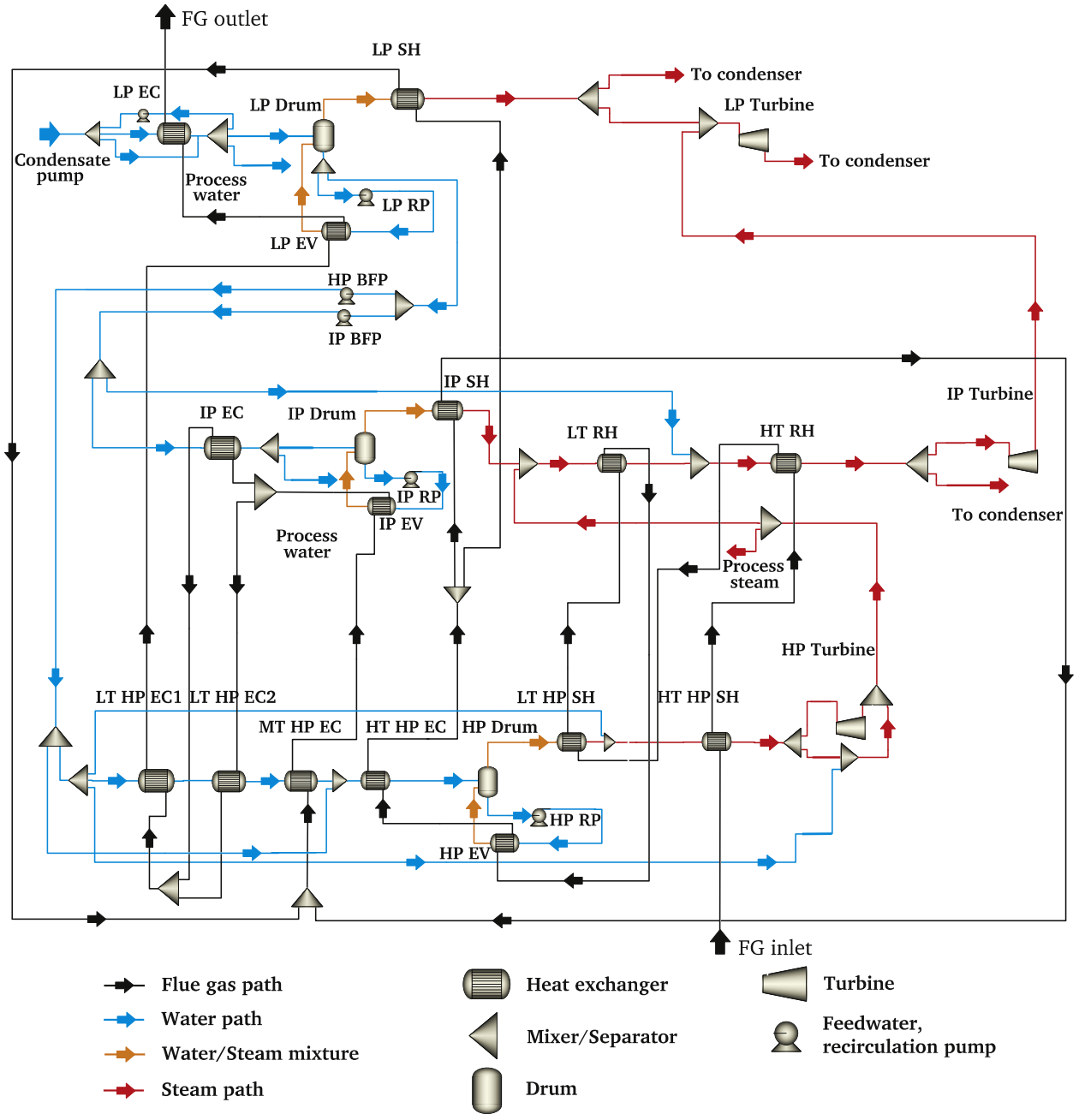

Figure 3.28 Aspen Plus flowsheet of HRSG model

The HP circuit as shown in Figure 3.28 begins at the inlet of the HP feedwater pump and ends at the outlet of the HP-SH. The HP feedwater pump ensures the flow of feedwater mass flow into the HP circuit. The feed water flows through the HP ECO (HPLT-ECO1, HPLT-ECO2, HPIT-ECO, and HPHT-ECO) into the HP drum. In the HP circuit, the process water is removed before entering the HP-ECO and is finally returned to the condenser. The water in the HP drum circulates through the HP evaporator with the help of the HP circulating pump, generating saturated steam in the HP drum. The drum acts as a separator here. While the liquid remains in the drum and is mixed with the water from the HP-ECO, the vapor leaves the drum and is fed to the HP-SH. The steam flows through the HP superheater (HPLT-SH and HPHT-SH), which continues to absorb heat from the

flue gas. At the inlet of the HPHT-SH is an HP temperature controller (attemperator), which regulates the temperature at the inlet of the HP turbine to 567 °C. The water for the HP steam cooler is taken after the HP feedwater pump. The superheated steam from the HP stage is expanded in the HP turbine and fed to the IP stage.

The IP circuit as presented in Figure 3.28 starts at the inlet of the IP feedwater pump and ends at the outlet of the IP-SH. It consists of the following heat exchangers: IP-ECO, IP-EVAP, and IP-SH. The IP feedwater pump supplies the IP feedwater mass flow. The IP feedwater flows through the IP-ECO into the IP drum and circulates through the IP evaporator, where it is converted by heat transfer from the flue gas into saturated steam before returning to the IP drum. The generated steam flows into the IP-SH where it is superheated. From the water heated in the ECO, 9 kg/s of process water is taken from the IP circuit to preheat the air in the GT combustor. Some of this process water is taken upstream of the IP-ECO to heat the fuel gas. Both water streams are returned to the system upstream of the condenser. The superheated IP steam mixes with the expanded steam from the HP turbine and is further heated in the RH (LT-RH and HT-RH). The attemperator regulates the temperature of the reheated steam to 567 °C by removing water before the IP-ECO. The reheated steam then enters the IP turbine. There it is expanded and then expanded to 82 mbar together with the superheated steam from the LP-SH in the LP turbine. Finally, the saturated steam is condensed again in the condenser and brought to a pressure of 12.5 bar with the aid of the condenser pump.

The validation of the model was performed at different load cases (100%, 80%, and 60%) using the measured data of steam mass flow, temperature, and pressure at the outlet of the HRSG because these parameters are affecting the performance of the HRSG. The comparison of these parameters among the model and the operating data of the reference power plant at the outlet of the HPHT-SH is presented in Table 3.12 which shows a very good agreement. The simulated superheated steam mass flow is in good agreement with the measurement data. The HP attemperator keeps the superheated steam temperature constant at 567 °C regardless of the plant load. In addition, the simulated superheated steam HP agrees with the given pressure at various loads. No parameter in the high-pressure circuit has a relative error of more than 1.82%, and even better, most parameters have relative errors of less than 0.73%.

Table 3.12 Parameters at the outputs of HPHT-SH at different load cases

Load		100%	80%	60%
Mass flow rate [kg/s]	Operational Data	78.20	66.90	58.30
	Simulation Results	77.63	65.81	57.34
	Relative Error	-0.73%	-1.63%	-1.65%
Temperature [°C]	Operational Data	567.00	566.80	566.90
	Simulation Results	567.00	567.00	567.00
	Relative Error	0.00%	0.04%	0.02%
Pressure [bar]	Operational Data	97.70	88.00	76.20
	Simulation Results	97.20	86.40	76.40
	Relative Error	-0.51%	-1.82%	0.26%

Table 3.13 shows the comparison between the measured data and the simulation results for the steam mass flow, pressure, and temperature at the outlet of the reheater section. Indeed, the

simulation results for the superheated steam mass flow and temperature at various partial loads agree very well with the measured values. Thereby, the maximum relative error is 2% for the superheated steam mass flow at 60% part load. As previously mentioned, the temperature of the superheated steam in the HP circuit is kept constant at 567 ℃ by the RH. The simulated reheat pressure shows good agreement with the measurements. However, the reheat pressure in the HRSG model exceeds the reheat pressure in the real plant at 60% part load by about 1.2 bar (relative error of 6.7%). The reason for this discrepancy is related to the simulated mass flow rate of the reheat steam, which is about 1.5 kg/s lower than the measured value.

Table 3.13 Parameters at the outputs of HT-RH at different load cases

Load		100%	80%	60%
Mass flow rate [kg/s]	Operational Data	83.2	74.7	64.9
	Simulation Results	83.53	74.86	63.31
	Relative Error	0.40%	0.21%	-2.45%
Temperature [℃]	Operational Data	567	567	566.9
	Simulation Results	567	567	567
	Relative Error	0.00%	0.00%	0.02%
Pressure [bar]	Operational Data	21.4	20.6	17.7
	Simulation Results	21.6	20.7	18.9
	Relative Error	0.93%	0.49%	6.78%

Table 3.14 compares the steam mass flow, temperature, and pressure at the outlet of the LP-SH with the measurement data and the simulation results. The simulation results show a very good agreement with the measured data. The calculated values for the reheat temperature and pressure have a maximum of about 1% and 2% relative errors, respectively. The mass flow rate of the superheated LP steam shows good agreement with the measurement at 100% load, with a relative error of about 1%. At 80% part load, the error increases to 7% before decreasing to 6% at 60% part load. Nevertheless, the good agreement between the simulated temperature and pressure at the outlet of the LP-SH for 80% and 60% part load (maximum relative error of 2.12%) indicates that the deviation of the simulated steam mass flow is due to the uncertainty of the LP steam mass flow measurement.

Table 3.14 Parameters at the outputs of LP-SH at different load cases

Load		100%	80%	60%
Mass flow rate [kg/s]	Operational Data	9.8	7.7	6.4
	Simulation Results	9.93	8.31	6.757
	Relative Error	1.33%	7.92%	5.58%
Temperature [℃]	Operational Data	293	289.9	281
	Simulation Results	292.52	289.91	282
	Relative Error	-0.16%	0.00%	0.36%
Pressure [bar]	Operational Data	4.1	3.9	3.3
	Simulation Results	4.1	3.82	3.23
	Relative Error	0.00%	-2.05%	-2.12%

The power generated in the steam turbine (ST) is compared between the simulation and the actual value of the reference power plant. Table 3.15 presents this comparison, which shows a very good agreement at the three load cases with a maximum relative error of about 2.31%.

Table 3.15 Comparison of Steam turbine power [MW_{el}]

Load	Operational Data	Simulation Results	Relative Error
100%	131.82	133.83	1.52%
80%	114.41	113.26	-1.01%
60%	96.08	93.86	-2.31%

3.6.2.1 Modification for Synthesis Gas Turbine

The steam power cycle is investigated within a CCPP operated by a gas turbine that uses natural gas fuel for combustion. Whereas the IGCC is operated by a synthesis gas turbine that uses syngas as fuel for the combustion. The impact of using syngas is discussed in section 3.6.1. Accordingly, the steam power process must be modified.

With synthetic gas turbines, the flue gas temperature is lower. However, the heat delivered to the HRSG is to remain constant. To calculate the heat delivered to the HRSG, equation 3.21 should be deployed.

$$\dot{Q} = \dot{m}_{flue\ gas}(h_{in} - h_{out}) \tag{3.21}$$

Therefore, model modification is considered in which the flue gas temperature at the HRSG inlet (Gas turbine outlet) is 600 °C. The transferred heat quantity of the model that was investigated is 364.676 MW_{th}. To achieve a constant heat flow into the HRSG, and by using equation 3.21 the flue gas mass flow must be increased by 4.313% which means from 587.33 kg/s to 612.66 kg/s. Moreover, it should be noted that due to the temperature decrease of 28°C, it is not possible to increase the temperatures to 567 °C after the HPHT-SH and the HT-RH, using the same (Terminal Temperature Difference) TTD. Therefore, a temperature of 551 °C is set for the synthetic gas turbine case. For this purpose, it is necessary to adjust the TTD of the heat exchangers due to the lower flue gas temperatures. The HPHT-SH was reduced by 12 °C and the HT-RH by 18 °C. The setpoint value of the controller must also be reduced. The setpoint of the controller must be set to 551 °C. Table 3.16 lists the comparison between ST with synthetic GT and ST with natural gas GT. It is clear that the output decreases slightly in full load and 80% partial load. In the 60% partial load case, there is an increase in the output. This is due to a low TTD in the HT-RH. A low degree of TTD is always associated with an improvement in performance, whereby this has a significant effect on the price of the heat exchanger.

Table 3.16 The outputs of the steam turbine combined with synthetic GT and natural gas GT [MW_{el}]

Load	With synthetic GT	With natural gas GT	Deviation
100%	128.27	133.83	-4.15%
80%	109.62	113.26	-3.21%
60%	94.57	93.86	+0.76

3.7 Heat Integration

The steam power process is based on an existing and already validated Aspen plus model of the water-steam cycle of a natural gas-fired combined cycle power plant in the previous section and published by Bany Ata et al. [137,179]. This model was transferred to EBSILON Professional where it was studied in detail. Key plant data are summarized in Table 3.2. Figure 3.26 shows the schematic diagram of plant design. The model included the flue gas path and the steam cycle with a steam turbine, heat exchangers, valves, and pumps.

For the adaptation of the steam power process to the polygeneration approach, the integration of heat and steam flows in the process model was investigated. Specifically, the integrations listed in Table 3.17 were carried out. The indicated pressures and temperatures represent minimum requirements for the respective steam or heat flow.

Table 3.17 Heat and steam integration for the steam power process

	Presser [bar]	**Temperature [°C]**
Steam extraction		
WTA drying	4.2	Sat. Steam
HTW gasifier	35	560
Water-gas shift	35	Sat. Steam
Heat consumers		
Acid gas removal (reboiler)	Sat. Steam	90
Preheating gas turbine		180
Heat suppliers		
Raw gas cooler	Sat. Steam	< 260
Methanol synthesis	Sat. Steam	< 260

In WTA drying, the pressure results from the required saturated steam temperature in the condenser. In the case of the HTW gasifier, as well as in a water-gas shift, the pressure must be above the process pressure so that the steam can be fed into the process. In the case of the HTW gasifier, it is also desirable to provide as high a temperature as possible so that the oxygen demand in the gasifier remains small. The necessary temperatures for the heat consumers, acid gas removal, and gas preheating of the gas turbine result from the temperature of the heated streams. In acid gas removal, the heat is utilized in the reboiler by condensation, which is why at least saturated steam is required here. For gas preheating, a tapping of intermediate pressure process water is usually used in combined cycle processes, which is already available in the validated model. The raw gas cooler and, in the case of parallel methanol and electricity production, the waste heat of the methanol synthesis are available as heat suppliers for the steam process. In both cases, saturated steam can be produced. The temperature of the heat input results from the gas-side temperature in the process. For the raw gas cooler, this corresponds to the outlet temperature of the synthesis gas at 265 °C. For the methanol synthesis, this corresponds to the temperature of the first reactor in the mega methanol process, since this is designed as an evaporator at 265 °C. Overheating is not possible with the usual design of the apparatus.

The required pressure of the steam as a gasification agent for the HTW gasifier places high demands on the steam power process. 35 bar can only be obtained in the steam power process of the reference plant in Malaysia by tapping the high-pressure turbine. However, a tap with the

corresponding pressure only has a temperature of approx. 420 °C in the investigated steam power process. However, tapping the superheated HP steam before it enters the turbine is unfavorable from an energy point of view, as this greatly reduces turbine output. It would therefore be desirable to tap the steam before the IP turbine. To achieve this, the intermediate pressure must be raised. It must also be taken into account that the pressure drops in the partial load case of the steam power process. For modeling purposes, the pressure at the turbine inlet is therefore increased to 42.3 bar. An increase in the intermediate pressure also requires an increase in the high pressure at the same time, since otherwise, the turbine outlet temperature from the HP turbine increases significantly compared to the reference design. This hot steam stream is then mixed in the process with only slightly superheated IP steam, resulting in a high exergy loss. To maintain the same turbine outlet temperature at the HP turbine, the inlet pressure of the HP turbine is increased to 178 bar in the model. The temperatures in the IP and HP superheaters are maintained, which is why these adjustments to the model result in only a minimal change in the efficiency.

After increasing the pressure level in the steam process, the tapping for the water-gas shift as well as for the gasification agent of the gasifier can take place at the IP steam after the reheater or the evaporator. The tapping for the WTA drying is realized at the IP turbine at 4.2 bar. The tapped steam is superheated and has a temperature of 259 °C. The heat for acid gas scrubbing is taken at the LP turbine at 0.8 bar and at a temperature of 110 °C. The two heat suppliers are integrated as additional evaporators in parallel to the IP evaporator in the process. In Figure 3.29, the taps in the steam power process are drawn in red.

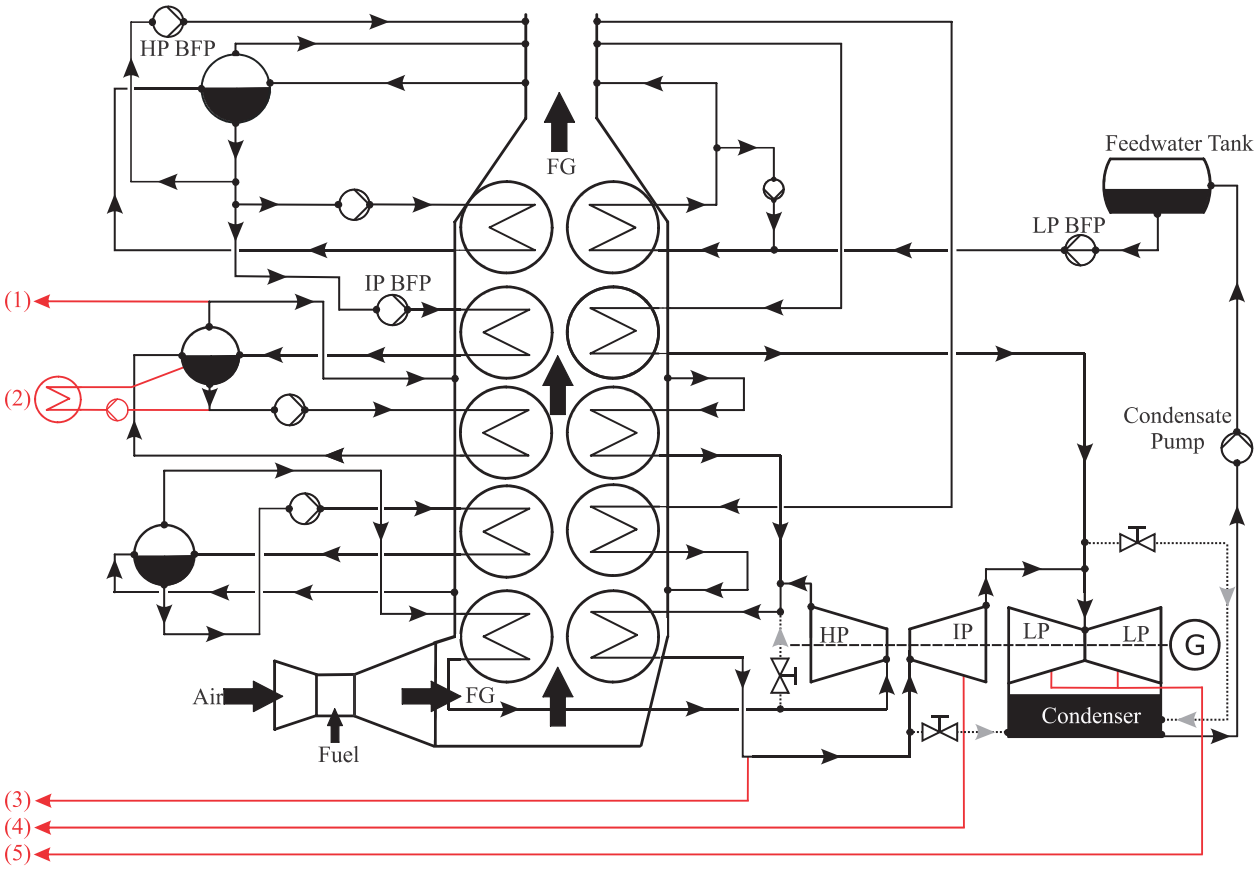

Figure 3.29 Steam power process with tapping and heat integration. ((1) Water-gas shift; (2) raw gas cooler and methanol synthesis; (3) HTW gasifier; (4) WTA drying; (5) Acid Gas Removal).

For the partial load operation of the plant, a sliding pressure control was implemented in the model for the power range from 60% to 100%. The pressure ratios from the reference plant were scaled according to the pressure increase. Below 60%, the plant must be operated in equal pressure mode, since otherwise, the taps of the IP steam have insufficient pressure to be fed into the gasifier or the conversion reactor.

The power of the steam turbine of the model in all load cases, after applying the heat integration, that is calculated numerically is shown in Table 3.18. These values are used as reference values for the following optimization of the extractions.

Table 3.18 Power of the steam turbine of the reference case in all load cases

Load	ST Power [MW_{el}]
100%	71.3
80%	54.6
60%	39.6

3.8 Simulation of Methanol Synthesis

For methanol synthesis, a simplified model was implemented according to the process flow diagram shown in Figure 3.30 based on Heinze [101]. The syngas, which leave the acid gas removal, is fed to a compressor via a condensate separator. The syngas, compressed to 55 bar, is then preheated via a regenerative heat exchanger and fed into a reactor. The reactor is implemented as an isothermal equilibrium model for methanol synthesis, considering reactions (R 2.6, R 2.28, and R 2.29). The reactor temperature is set at 210 °C so that a carbon conversion per reactor pass of about 60% is obtained. This value is not unusual for commercial methanol plants. Modern plants achieve up to 80% with optimal process control [135]. The recycle ratio, defined according to equation 3.22, is approx. 1 for a discard of 10 vol% purge.

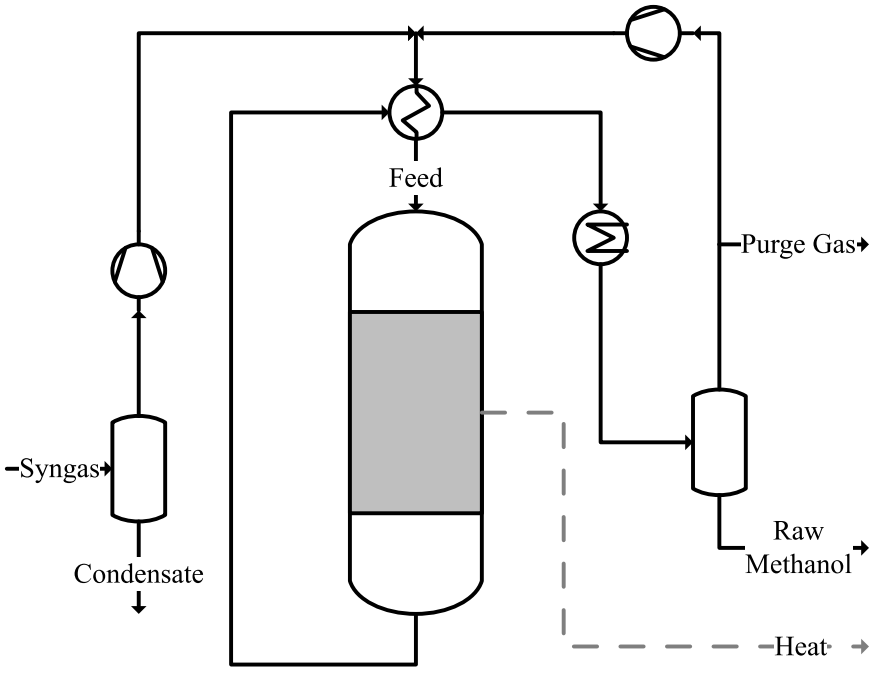

Figure 3.30 Methanol synthesis process flow diagram

$$Recycle\ ratio = \frac{\dot{n}_{Recycle}}{\dot{n}_{Syngas}} \tag{3.22}$$

Table 3.19 shows an overview of the results of the process model. Due to the relatively high proportion of methane and nitrogen in the synthesis gas stream, the inert gas content of more than 25% already results in a recycle ratio of approx. 1 in the synthesis reactor. The methanol produced has 60% of the calorific value of the synthesis gas stream. A further 22.1% is lost to the process as waste heat due to the exothermic reactions in the reactor. The remaining approx. 18% is found as methane, CO, and hydrogen in the purge gas stream. This stream can be used to further increase the exhaust gas temperature for the heat recovery steam generator downstream of the gas turbine.

Table 3.19 Results of Methanol Synthesis model [101]

Parameter	**Unit**	**Syngas**	**Recycle**	**Feed**	**Raw methanol**	**Waste heat**
H_2	Vol.-%	60.60%	25.80%	42.90%		
CO		30.30%	13.70%	21.90%		
CO_2		3.00%	14.20%	8.70%		
CH_4		5.10%	37.70%	21.70%		
CH_3OH		0.00%	0.40%	0.20%		
N_2		1.00%	8.30%	4.70%		
distribution	mol/mol_{gas}	100.00%	103.30%	203.30%	28.70%	
Calorific value	MJ/kg	22.46	21.27	21.73	19.92	
Calorific value of flow	$MW/MW_{Raw\ gas}$	100.00%	137.60%	226.90%	60.00%	22.10%

Chapter 4: **Results and Discussion**

In this chapter, the results of the process simulation are reported and discussed. The syngas composition in the main streams of the pilot plant process simulation model was presented. Then, an evaluation of the three different AGR processes was performed. Finally, a techno-economic assessment was carried out for the IGCC power plant for polygeneration of electricity and methanol under various availabilities and variable product prices.

4.1 Pilot Plant Simulation Results

The process simulation results of the pilot-scale model are presented in this section. Figure 4.1 shows the process block flow diagram with numbered streams. As introduced previously, all components of the gas treatment plant were modeled in Aspen Plus according to the specifications of ThyssenKrupp Industrial Solutions (TKIS). Therefore the results of this pilot plant model simulation are validated against the heat and mass balance (HMB) provided by TKIS.

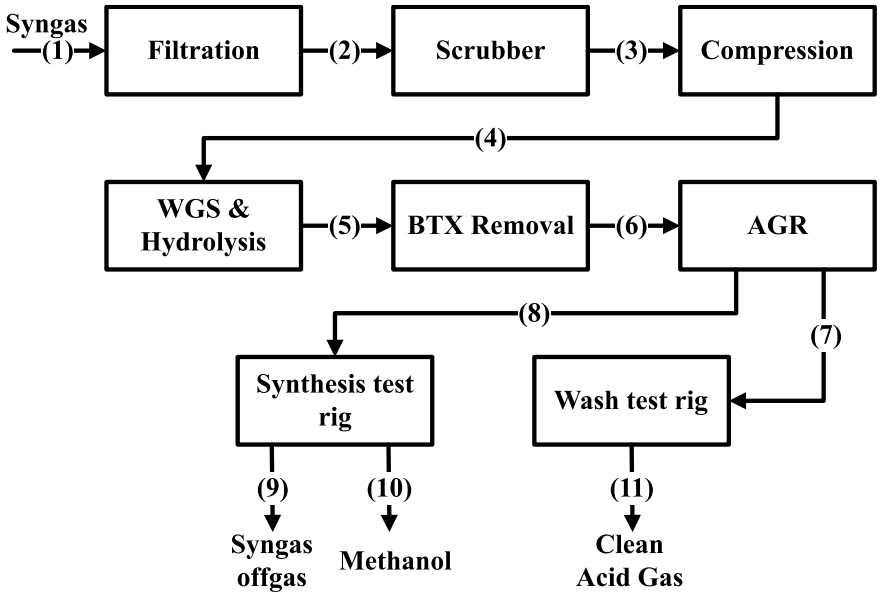

Figure 4.1 Block flow diagram of the pilot plant simulation

The simulation is conducted using an input stream 1 as shown in Table 4.1. Also, the composition of the syngas at each stream entering or leaving each syngas purification unit is presented in Table 4.1.

The raw gas scrubbing was modeled in Aspen Plus according to the specifications of TKIS. After the raw gas scrubbing the temperature decreases from 350 to 70 °C. For most components, the raw gas composition is essentially determined by the change in the water vapor partial pressure. This agrees with the HMB of TKIS, the exceptions are the water-soluble gas components (NH_3, HCN, HCl) and gas components with a high boiling point (benzene, naphtha), which can therefore partially condense out. The water-soluble constituents are precipitated by the Aspen Plus model in very comparable quantities to those in the HMB from TKIS. The Chan-Fair correlation yields results that are somewhat closer to the TKIS values than the Chen-Chuang correlation.

Table 4.1 Heat and material balance of the pilot plant simulation

Stream ID	Unit	1	2	3	4	5	6	7	8	9	10	11
Temperature	℃	350	350	70.01	10	70	30	30.8	35	28	20	30
Pressure	bar	1	0.975	0.89	5.4	3.8	3	3.1	1.3	37	37	1
Mole Flows	kmol/hr	7.632	7.632	8.615	5.584	5.584	5.122	3.479	1.766	0.004	0.103	1.844
Mass Flows	kg/hr	198.136	198.136	214.957	160.127	160.127	140.838	67.512	75.491	0.139	0.12	78.931
H_2	Mole-fraction	0.14817	0.14817	0.13126	0.2025	0.2025	0.22074	0.32464	0.00079	0.0036	0.62904	0.00075
CO		0.26459	0.26459	0.23439	0.3616	0.3616	0.39157	0.57582	0.00153	0.00357	0.31429	0.00144
CO_2		0.29016	0.29016	0.25636	0.39387	0.39392	0.35131	0.03566	0.94923	0.00487	0.02217	0.95254
CH_4		0.02646	0.02646	0.02344	0.03616	0.03616	0.0332	0.04879	0.0002	0.00089	0.03045	0.00019
H_2O		0.26459	0.26459	0.35081	0.00173	0.00168	0.00166	0.01509	0.04434	0.0175	0.00002	0.04311
H_2S		0.00115	0.00115	0.00101	0.00155	0.0016	0.00135	9.27 ppm	0.0039	0	0	0.00197
COS		0.00011	0.00011	0.0001	0.00016	0.00011	0	0	0	0	0	0
NH_3		0.00282	0.00282	0.00169	0.00100	0.00100	0	0	0	0	0	0
HCl		0.00001	0.00001	0	0	0	0	0	0	0	0	0
Benzene		0.00106	0.00106	0.00094	0.00144	0.00144	0.00009	0	0	0	0	0
Naphtalin		0.00088	0.00088	0	0	0	0	0	0	0	0	0
Methanol		0	0	0	0		0	0	0	0.96957	0.00403	0

The syngas leaves the compression process at stream 4. The raw gas composition is well matched for most components (deviation <5% relatively). Exceptions are the water content, the ammonia content, and the aromatics. The cause for the ammonia content may be the use of a simple flash as a knock-out drum since this does not simulate washing, which presumably takes place in the demister. The partial pressure of the water at 10 °C explains the reason for the low amount of water directly after the compression.

The steam 5 leaves the WGS and hydrolysis, the raw gas composition is well matched for all components (deviation <5% rel. for main components, <10% rel. for trace gases). It is striking that this time benzene and naphtha are also modeled very well.

In the BTX removal process, the syngas composition is well matched for most components (deviation <5% rel. for main components, <10% rel. for trace gases). The water content is estimated to be significantly lower compared to the TKIS calculation. However, this should have little influence on the process, since the water content is essentially determined by the steam partial pressure in the individual preparation steps. As with the halogen wash, the benzene and naphtha content is estimated to be significantly lower than TKIS. In the composition of the scrubbing oil, the main constituents are well represented. There are massive deviations in the CO_2 content of the scrubbing oil. This remains at a similarly high level for various property methods tested. In addition, significantly less benzene and naphtha are recycled.

At the amine AGR, the hydrogen sulfide is successfully removed together with the carbon dioxide. The magnitudes match the design specification of the basic engineering, where an H_2S concentration of 5-15 ppm has been expected and a CO_2 concentration of 1-3 vol%.

The simulation output gives an insight into the apparatus, such as profiles and the concentration of each species. The calculation methods display physical processes to cover a wide field of action and the simulation provides trustworthy results.

A simulation of the mobile washing test rig has been created, which is usable for gas-liquid absorptions accelerated by a chemical reaction. The oxidative agent can be substituted, e.g. with $KMnO_4$. After gaining more experience of the conversion depending on several influences, a suitable calculation method for the reaction can be set. By this, the simulation can be used to analyze additional conditions or it is used for module 100 or even a scale-up.

4.2 Enhancement of Predefined Extractions

In the following sections, the possibilities for optimizing the performance of the steam power process including the extractions are examined. The goal of the optimization is to adapt the steam of the extractions as exactly as possible to their boundary conditions since high-quality steam is extracted from the system, which is not required for the production of synthesis gas. The possibilities to optimize the model are to vary the extraction point and to adapt the mass flow of some extractions to the boundary conditions of the EBSILON Professional model. Another possibility is to modify the location of the heat input of the raw gas cooler in the HRGS. The ultimate option is the modification of the three pressures system to allow new variations of the extraction points.

4.2.1 Enhancement of Dryer Extraction

The steam used for the WTA dryer has a pressure of 4.2 bar. The Aspen plus value corresponds to the saturated steam temperature, which is 145.4 °C. In the EBSILON professional model, however, superheated steam with a temperature of 326.3 °C is removed from the turbine. A condenser is used for heat extraction in the WTA dryer. In the case of superheated steam, superheating and condensation heat are available consequently less steam mass flow is required to provide the heat demand. As a result, the steam requirement for superheated steam is reduced from 56.46 kg/s to 46.367 kg/s. Table 4.2 compares the output power of the system after adjusting the steam mass flow of the WTA dryer process to the reference values. Since the steam mass reduction is approx. 10 kg/s, more mass flow is expanded into the subsequent turbine stages; hence, the capacities increase significantly in all load cases.

Table 4.2 The Output of Steam Turbine with new WTA dryer mass flow rate

Load	Reference output	Modified Model output	Improvement
100%	71.31	78.46	+10.0%
80%	54.64	61.71	+12.9%
60%	39.67	46.74	+17.8%

4.2.2 Enhancement of Gas Preheating and Acid Gas Removal Extractions

Due to the reduction of the steam mass flow for the WTA dryer, more steam is available for the extractions of the gas preheating and the AGR. This issue solves the problem that appeared in the 60% partial load case, in which there is no sufficient steam available for the last extractions. Accordingly, the extractions can be installed in the low-pressure turbine without restrictions. As the steam for the gas preheating must always have a minimum temperature of 160 °C, it is taken from the low-pressure turbine at a pressure of 1.5 bar. The AGR reboiler extractions are installed at 0.8 bar in the turbine. The performance could be further improved slightly by reducing the extraction pressure of the AGR. However, if the pressure were to be lowered further, significantly larger pipe diameters would be required due to the pipe friction pressure losses, which would affect the economy and space. For the full load case, this optimization resulted in a performance improvement of the steam turbine of 12.8% in contrast to the new values from Table 4.2 (6.9% in the 80% load case and 9.5% at 60%). This significant performance improvement is due to the optimization of the gas preheating extractions since this high-quality steam was extracted before the intermediate-pressure turbine.

The effects on output of integrating the gas preheater extraction into the HRSG instead of extracting it from the turbine were also investigated. Saturated intermediate or high-pressure steam was used for the gas preheater mass flow. This means that less mass flow is required to be superheated, so more heat is available for evaporation. However, both cases have lower performance outputs compared to the model when it is integrated with the gas preheating extraction where installed in the low-pressure turbine. Since low-pressure steam has a major effect on the turbine output. Consequently, these ideas were discarded.

4.2.3 Enhancement of Gasifier and WGS Extractions

Due to the necessary boundary conditions, the extractions of the gasifier and the WGS shift reaction cannot be further optimized in the existing model. The steam for the gasifier must have maximum

temperatures. Saturated steam is required for the WGS. Both require a steam pressure of 35 bar. Since these boundary conditions are only present upstream or in the high-pressure turbine, the extractions must be installed there. In the present model, steam is extracted at a pressure of 97.7 bar for the gasifier and superheated steam at 35 bar and a temperature of about 400 °C for the WGS. Therefore, the goal should be to create possibilities to adapt these extractions to their boundary conditions by modifying the process. Modification of the intermediate pressure of the plant would be a viable option. The intermediate-pressure steam at the outlet of the HTRH is at the same temperature as the high-pressure steam at the outlet of the HPHTSH. If the intermediate pressure is modified at least 35 bar in each load case, the gasifier extraction can be installed there. This modification also provides a new extraction option for WGS extraction. Since the pressure of the intermediate-pressure steam at the outlet is always at least 35 bar, the steam at the outlet of the intermediate-pressure evaporator also has a minimum pressure of at least 35 bar. This means that the saturated steam for the WGS can be extracted at this point.

4.2.4 Modification of the Intermediate Pressure System

The modification aims to increase the intermediate pressure to a value of at least 35 bar in each load case. Since the pressure decreases at partial load, the lowest load case that investigated (60% partial load case) is considered. In this load case, the mean pressure of the EBSILON Professional model is 17.7 bar. This is now set to a value of 35 bar at the outlet of the HTRH. The intermediate pressure at 80% and 100% load cases can be calculated from the ratio of the pressures of the different load cases. This ratio can be calculated from the unmodified model. Accordingly, the intermediate pressure at 80% is 40.3 bar and for the 100% load case is 42.3 bar. The saturated steam at the outlet of the intermediate pressure drum has a pressure of 44.62 bar at full load. At 80%, the pressure is 42.83 bar, and at 60%, 37.14 bar. However, for a gas and steam power plant with three pressure stages, there is an optimum pressure ratio of the three pressure stages at which the maximum output is achieved. Here, the pressure ratio of the original model is optimal because it was modeled based on the design data, which is designed to maximize efficiency. Accordingly, a change in the average pressure results in a degradation of the plant's output. Table 4.3 compares the output of the synthesis model in Table 3.16 to the output after the pressure modification.

Table 4.3 Output of ST with the synthesis gas turbine before and after pressure modification [MW_{el}]

Load	Reference output	Modified Pressure Model output	Improvement [%]
100%	128.27	125.95	-1.04%
80%	109.62	98.79	-5.62%
60%	94.57	83.09	-9.85%

It is found that the output declines mainly at part load. This decline at part load is due to the throttling of the high-pressure steam before mixing with the intermediate-pressure steam. The outlet flow of the high-pressure turbine must always have a pressure of 44 bar. This is because the pressure of the high-pressure steam is always reduced to the pressure of the intermediate-pressure steam, which is 43.6 bar at full load. Since the pressure differences of the load cases are much larger after the modification, the pressure of the high-pressure steam must be reduced more in the partial load cases. In the 60% case, for example, the throttle reduces the pressure of the high-pressure steam by approximately 8.0 bar. This leads to a large pressure reduction without using it

energetically. In addition, the mass flow for WTA dryer extraction must be increased because the temperature of the superheated steam has dropped to 147 °C at 4.2 bar. A mass flow of 50.68 kg/s is now required.

4.2.5 Variation of the Gasifier and WGS Extractions

The modification that was carried out allows the positions for the WGS and gasifier extractions to be varied. The WGS extraction is varied starting with the WGS extraction. After the intermediate-pressure drum, the steam is extracted instead of the high-pressure turbine. A steam mass flow of 21.55 kg/s is required. This is provided in each load case as the intermediate pressure mass flow evaporates with the benefit of the raw gas cooler. Regardless of the load case, the raw gas provides 86.96 MW_{th} of heat to the heat exchanger, evaporating 50.20 kg/s of mass flow rate. This variation in WGS extraction resulted in a further 7.7% improvement in output at full load (12.0% at 80% part load and 12.8% at 60%), despite the drop in output due to the change in pressure. The gasifier extraction is then varied. This is now located after the HT-RH instead of the HPHT-SH since the steam has maximum temperatures there. However, this variation in extraction only resulted in a further output improvement of less than 1% in all load cases. This small improvement is due to more high-pressure steam mass flow being returned to the reheater section since the gas preheater extraction points no longer receive high-pressure steam. Consequently, more steam mass flow must be heated to the specified temperature in the reheaters, requiring more heating energy. In addition, the quality of the superheated intermediate-pressure steam is only slightly lower than that of the superheated high-pressure steam.

However, this modification of the intermediate pressure limits the plant to a partial load performance of 60%, since the pressure of 35 bar was defined for the 60% load case according to the HT-RH. If the plant were to run at less load, the pressure of the steam would drop below 35 bar, violating the boundary conditions of the gasifier extraction.

4.2.6 Enhancement the Heat Input of the Raw Gas Cooler

The high raw gas temperatures of 950 °C are the most effective to integrate the heat input of the raw gas cooler into the HRSG at the earliest possible stage. By integrating the heat of the raw gas cooler into HRSG at an early stage, more high- or intermediate-pressure steam can be generated, which has a profound influence on the output of the steam turbine. The heat from the raw gas was fed into the IP-EVAP in previous cases, as the raw gas could be cooled to the desired temperature in this heat exchanger. Since the raw gas is to be cooled to a temperature of 250-300 °C, all the heat can be removed. Now the heat input is transferred to the HP-EVAP. There is a pressure of 102.6 bar in the HP-EVAP and, accordingly, the evaporation temperature is 312.9 °C. This means that the raw gas cannot be cooled down to the required temperature, since the raw gas temperature must not drop below the evaporation temperature. Therefore, the raw gas is then passed through the HPIT-ECO, where the saturated water has an inlet temperature of 246.1 °C. This allows the flue gas to be cooled down to 250 °C. Due to the modification, the TTD of the heat exchangers should be adjusted. Since the raw gas should provide as much heat as possible to the HP-EVAP, the pinch point of the evaporator unit has been set to 4 °C. To achieve the outlet temperature of 250 °C for the flue gas in the HPIT-ECO, the TTD of this heat exchanger is set to 52 °C. As the flue gas from the steam turbine flows around the HP-EVAP, it has a temperature 100 °C higher upstream of the HPHT-ECO than in the previous model. To prevent the water in the economizer

from evaporating, the efficiency of the HPHT-ECO is increased by 100 °C. This applies analogously to the LP-SH, which is why the TTD of this heat exchanger has also been increased by 100 °C. The TTD of the IP superheater does not need to be adjusted because the intermediate pressure steam in the superheated system is superheated regardless. The hotter the steam is before the reheater system, the less heat is required for the reheater. The much higher temperature of the flue gas is finally converted to the IP-EVAP. The higher flue gas temperature means that more intermediate-pressure steam can be generated in the IP-EVAP.

Modification of the heat input of the raw gas cooler achieved only a performance improvement of less than 0.6% in all load cases compared to the performance of the already optimized model. However, in this case, the economics of the system should be considered. When the heat input is transferred to the HP-EVAP, new requirements arise for the raw gas cooler. This must be designed for high pressures. The large wall thicknesses that are required for this give a rise in the thermal stresses that have to be controlled. Since the performance of the steam turbine could be improved only slightly, the new technical and thus also economic requirements predominate. Therefore, an optimization of the heat input of the raw gas cooler is discarded and the heat flow continues to be integrated with the IP-EVAP.

4.2.7 Enhanced Model

This section summarizes the final optimized model. Since only the steam mass flow for the WTA dryer was adjusted, it is still installed in the intermediate pressure turbine at 4.2 bar. The heat flows for gas preheating and acid gas removal are removed from the low-pressure turbine (gas preheating at 1.5 bar and acid gas removal at 0.8 bar). The gasifier extraction is located downstream of the HT-RH, while the WGS reaction saturated steam is extracted from the HRSG downstream of the intermediate pressure evaporator. The heat input of the raw gas cooler remains unchanged for the IP-EVAP. Table 4.4 shows the output of the optimized model compared to the output of the reference case. For all load cases, a significant relative output increase of more than 30% was achieved. The output increase in the 60% load case of 45.9 % is possibly due to the adjustment of the intermediate pressure to the 60% load case.

Table 4.4 Steam turbine output in all load cases after optimization [MW_{el}]

Load	Reference output	Modified model output	Improvement
100%	71.3	95.7	+34.2%
80%	54.6	74.2	+35.9%
60%	39.6	57.8	+45.9%

4.2.8 Assessment of the Improvements

Finally, a sensitivity analysis was carried out for the improved model. Using the sensitivity analysis, the effects of a variation of the extraction mass flows can be presented. Thus, the effects of unpredictable deviations of the extraction mass flow, as well as a targeted variation of the mass flows, can be predicted. For the sensitivity analysis, the steam mass flow of the extractions was varied successively by ∓10% and the output of the steam turbine was calculated numerically. The power deviation per kg of varied steam mass flow is calculated according to equation 4.1.

$$Power\ Deviation = \left| \frac{P_{ST,ref} - P_{ST,\mp 10\%}}{\dot{m}_{extraction,\mp 10\%}} \right| \quad (4.1)$$

The absolute value is used because only the magnitude of the deviation is relevant. Figure 4.2 lists the output deviations of the different extractions in the three load cases. This clearly shows that the deviations are independent of the load case, as the values of the load cases of an extraction hardly change. The largest output deviation in MW_{el} of electrical output per kg/s of steam results for the gasifier extraction with a value of about 1.23 MW_{el}/kg/s. Since both the heat contribution of the raw gas cooler and the extraction for the WGS reaction reduce the saturated intermediate pressure mass flow, they have an equal influence on the output and a value of about 0.8 MW_{el}/kg/s. This is followed by a WTA dryer with a power deviation of 0.62 MW_{el}/kg/s, gas preheater extraction with 0.43 MW_{el}/kg/s, and finally extraction for the re-boilers with a value of 0.35 MW_{el}/kg/s.

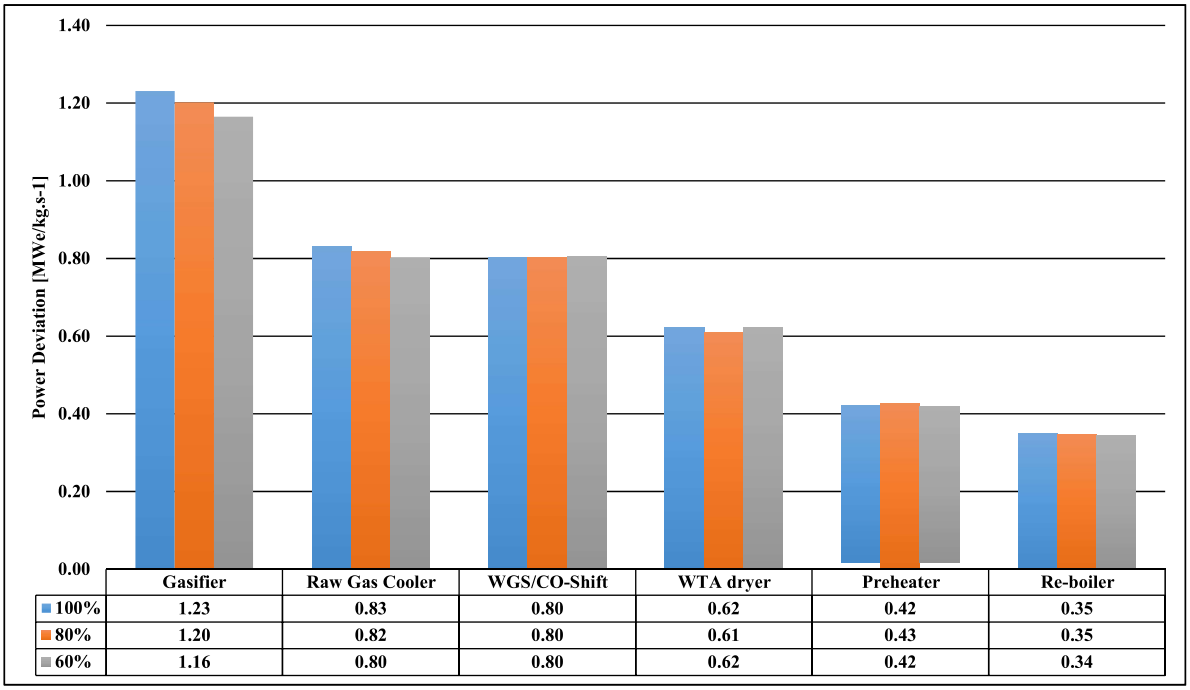

	Gasifier	Raw Gas Cooler	WGS/CO-Shift	WTA dryer	Preheater	Re-boiler
100%	1.23	0.83	0.80	0.62	0.42	0.35
80%	1.20	0.82	0.80	0.61	0.43	0.35
60%	1.16	0.80	0.80	0.62	0.42	0.34

Figure 4.2 The output deviations of the different extractions at the three load cases

For the evaluation of the process, the exergetic efficiency for the taps was also determined. The approach of the exergetic evaluation allows a statement about the influence of additional steam consumers and suppliers on the electrical power supply of the plant independent of a concrete integration of the water-steam cycle into the polygeneration process. The exergetic evaluation of the steam flows in the CCPP process is performed by deriving the gross electrical power of the plant according to the steam flow of the corresponding quality (equation 4.2). As a result, the specific electrical energy content of the steam flow can be determined.

$$e_{el}(p,T) = \frac{dP_{el}}{d\dot{m}_{steam}(p,T)} \quad (4.2)$$

$$\eta_{ex}(p,T) = \frac{e_{el}(p,T)}{e_{ex}(p,T)} \quad (4.3)$$

In the process model, the derivation was approximated by the finite difference method in a range of about ± 10% around the nominal values of the mass flows, which was performed for the 60% load case as well as for the 100% load case. The ambient pressure was set to standard conditions and the ambient temperature was 10 °C. The results can be seen in Figure 4.3. The exergetic efficiency for the taps is given by equation 4.3. For the tapping of the superheated steam at the intermediate pressure turbine, this is just under 80%. With decreasing steam quality, the realizable exergetic efficiency in the steam power process also decreases. Tapping the low-pressure steam for the reboiler of the acid gas scrubber has an exergetic efficiency of only 60 %.

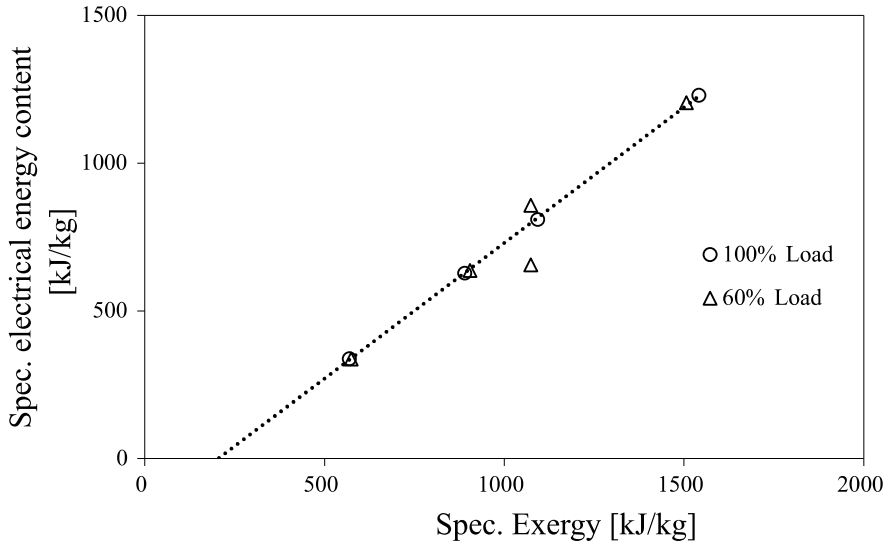

Figure 4.3 Specific electrical energy content of steam taps

It is noticeable that the higher the quality of the extracted steam, the greater the influence on the output of the gas turbine when the extraction steam mass flow is varied. This relation is shown in Figure 4.4. Here, the value of the power deviation per kg/s of steam was taken over the exergy of the respective steam. There is a linear relationship between the power deviation and the exergy and thus the quality of the steam.

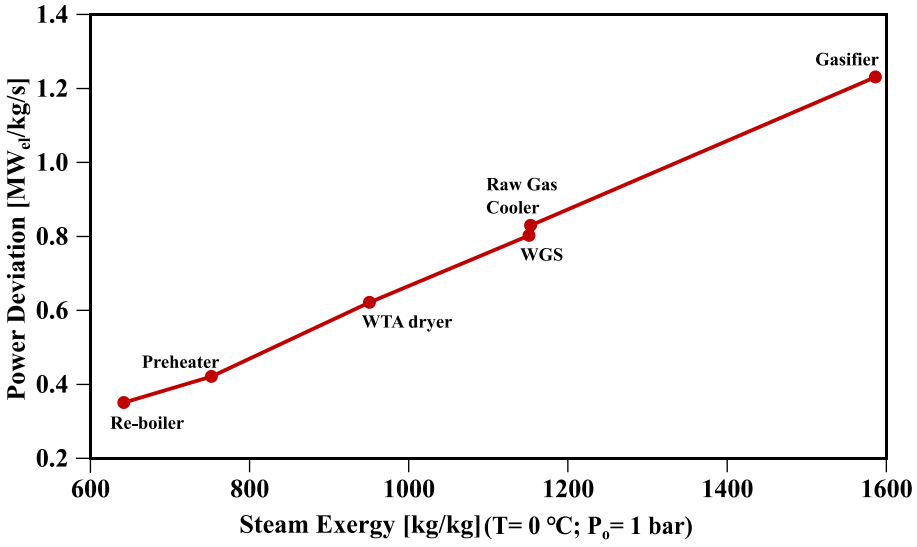

Figure 4.4 Correlation between Power deviation and steam exergy

4.3 Evaluation of Acid Gas Removal (AGR) Process

A dual-stage process model for pre-combustion AGR was developed using Aspen Plus software, and thermodynamic results derived from Aspen Plus were analyzed. The dimensions of the H_2S and CO_2 absorbers and H_2S strippers of the three AGR processes were calculated and applied to the RadFrac model in Aspen Plus. Other equipment for the operation and maintaining of the pre-combustion CO_2 capture process, such as the pumps, compressors, and heat exchangers, were developed using the model library provided by Aspen Plus. It was assumed that the property method of the dual-stage pre-combustion AGR process using the physical solvents (Selexol and Rectisol) is PC-SAFT (Perturbed Chain Statistical Associating Fluid Theory) while the property method used for the chemical solvent is Electrolyte NRTL.

The syngas characteristics that enter the WGS and leave it to the AGR are presented in Table 4.5. Here case 1 (80% coal and 20% RDF) of feedstock is taken as an example.

Table 4.5 Characteristics of Syngas streams entering the WGS and AGR

Parameter	Unit	From Gas scrubbing To WGS	From WGS To AGR
Temperature		156.07	40.00
Pressure	bar	29.00	27.00
Mole Flows	kmol/hr	12,783.28	11,292.83
Mass Flows	kg/hr	259,687.00	232,103.00
H_2		0.288477	0.432497
CO		0.287692	0.216893
CO_2		0.156846	0.282070
HCN		0.000001	0.000000
NH_3		0.000000	0.000000
H_2S		0.002381	0.002742
COS	Mole-fraction	0.000086	0.000001
HCl		0.000000	0.000000
H_2O		0.207196	0.002709
N_2		0.002678	0.003031
O_2		0.000000	0.000000
Argon		0.000053	0.000060
CH_4		0.054590	0.059997

Table 4.6 shows the simulation results of the three AGR processes using each solvent. The Rectisol process consumes the lowest amount of solvent flow for H_2S/COS removal and CO_2 capture. In comparison, the Rectisol process requires about 78.9% and 172% of solvent flow with respect to the Selexol process and the a-MDEA process, respectively. On the other hand, various results of modeling in terms of solvent loss were obtained: Solvent losses of 0.092 kg/h, 1526 kg/h, and 10.19 kg/h were determined for the Selexol, Rectisol, and a-MDEA processes, respectively. The highest solvent loss for the Rectisol process is due to the relatively high vapor pressure under normal process conditions [107] and the absence of the water wash process to avoid large amounts of solvent.

Table 4.6 Simulation result on each process

Parameter	Unit	Selexol	Rectisol	a-MDEA
Total recirculation solvent mass flow rate	kg/hr	1,683,959.272	1,231,767.244	2,194,475.431
Required solvent	kg/kg-CO_2	7.016	5.132	9.143
CO_2 removal rate	%	90.0%	90.0%	90.0%
H_2S+COS at exhaust stream	ppm	4.690	4.670	4.630
Hydrogen loss	%	0.143%	0.029%	0.176%
Solvent loss	kg/hr	0.092	1526.000	16.674
Power duty	MW_{el}	11.294	11.797	7.143
Cooling duty	MW_{th}	5.447	6.595	168.215
Heating duty	MW_{th}	27.238	28.390	295.744

The electrical and thermal energy consumption of the individual systems was also compared. The a-MDEA process required the lowest amount of 7.143 MW_{el} to be operated, while Selexol and Rectisol processes utilized 11.294 MW_{el} and 11.797 MW_{el}, respectively. The electrical energy consumption is high for the physical solvent AGR processes because they have a refrigeration load, while the a-MDEA process does not require refrigeration, which explains the difference in electricity consumption. The temperature of the lean solvent leaving the CO_2 absorber of the Rectisol process dropped to <10 ℃ due to the pressure drop during CO_2 capture caused by the pressure swing. Therefore, no energy is required to chill the CO_2 absorber feed solvent. However, a significant amount of electrical energy is being consumed in the H_2S absorber section for the CO_2 recovery compressor. The Rectisol process demands a relatively high amount of solvent in the first stage to comply with the system constraints for the dual-stage pre-combustion AGR process. The total amount of energy consumption increased due to the compression of a relatively high amount of absorbed CO_2 for recirculation. Heating duty was estimated at 27.238 MW_{th}, 28.390 MW_{th}, and 295.744 MW_{th} for the Selexol, Rectisol, and a-MDEA processes, respectively. Moreover, the cooling duty is 5.447 MW_{th}, 6.595 MW_{th}, and 168.215 MW_{th} for the Selexol, Rectisol, and a-MDEA processes, respectively. Figure 4.5 shows the energy consumption of each process.

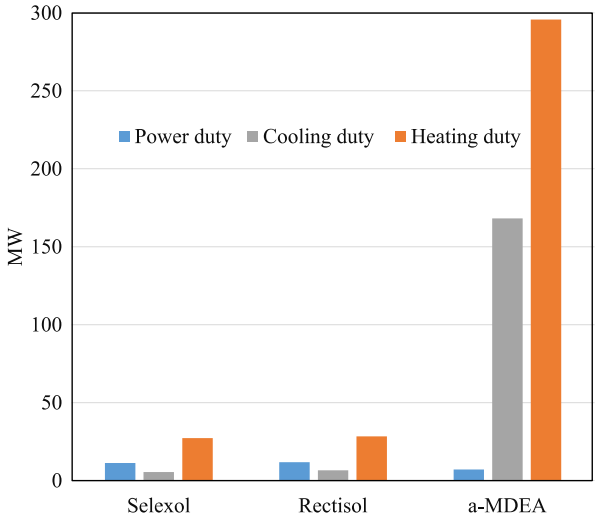

Figure 4.5 Electrical and thermal energy consumption on each process

4.3.1 Variation of the Design Parameters

4.3.1.1 Effect of WGS Conversion Rate

Produced syngas in the gasification process, composed primarily of CO and H_2. Therefore, a WGS reactor is essential to capture the CO_2 through pre-combustion and convert CO to CO_2 and H_2. The CO conversion rate to CO_2 depends on the operation conditions of the system, e.g., the solvent flow rate and the energy consumption. A quantitative evaluation of each system was performed, with a variation of the WGS conversion rate. As shown in Figure 4.6, which present a comparison between the total circulation flow rates of each system of the different solvents at different WGS conversion rate. The figure indicates that the solvent flow rate increases with the increasing percentage of WGS by a low slope linear function for all of the three solvents.

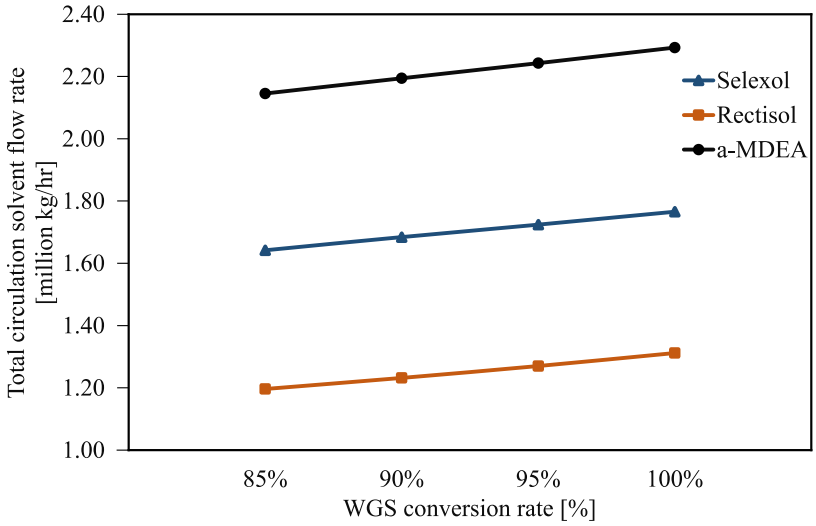

Figure 4.6 Comparison results of total solvent flow rate against WGS conversion rate

In Figure 4.7 the WGS conversion rate was changed from 85% to 100% to get the appropriate WGS conversion rate and heat demand of the reboiler for solvent regeneration. As a result, an increase in the WGS conversion rate occurred along with the flow rate and concentration of CO_2 fed to the dual-stage pre-combustion AGR process. Consequently, the amount of solvent fed to this process rose along with the heat load on the reboiler.

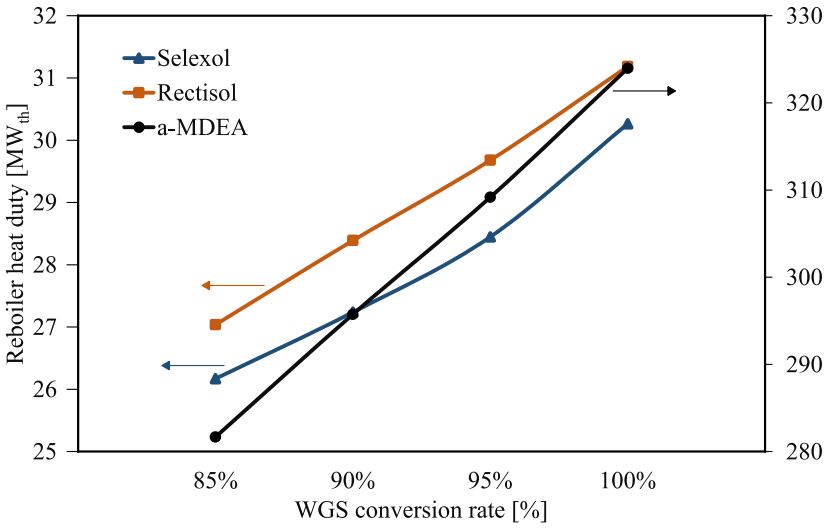

Figure 4.7 Comparison result of reboiler heat duty of AGR with WGS conversion rate

The impact of WGS conversion rate was also investigated quantitatively on electrical energy consumption in Figure 4.8. The fed solvent flow rate and the electrical energy consumption increased along with the WGS conversion rate. It is noticeable that the electrical energy increased significantly in the Rectisol process. This is a result of the large flow rate of fed solvent in the first stage to achieve the system constraint of 90% CO_2 capture and 5 ppm H_2S/COS emission. In addition, a study of the influence of the WGS conversion rate on the flow rate of CO_2 absorbed within the H_2S absorber was also performed. As a result of the relatively large increase in the flow rate observed during the Rectisol process, there is a concomitant and significant increase in the amount of CO_2 recirculated and electricity consumed.

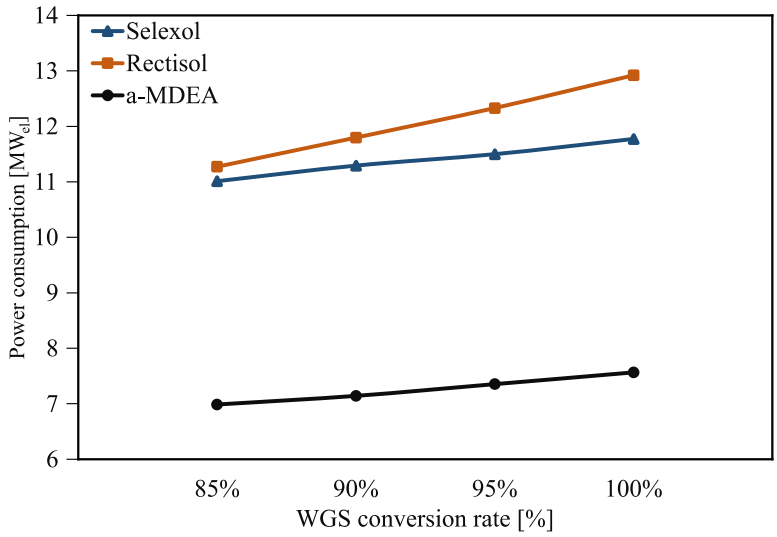

Figure 4.8 Electric energy consumption depending on WGS conversion rate

On the other hand, the relationship between hydrogen loss versus system efficiency and power consumption is illustrated in Figure 4.9. The WGS conversion rate affected the process efficiencies of Selexol, Rectisol, and a-MDEA differently: +0.003%, −0.013%, and −0.018%, respectively. For the Rectisol process, a hydrogen loss of about 0.76 kg/h was found, but the impact on the overall process is estimated to be relatively small.

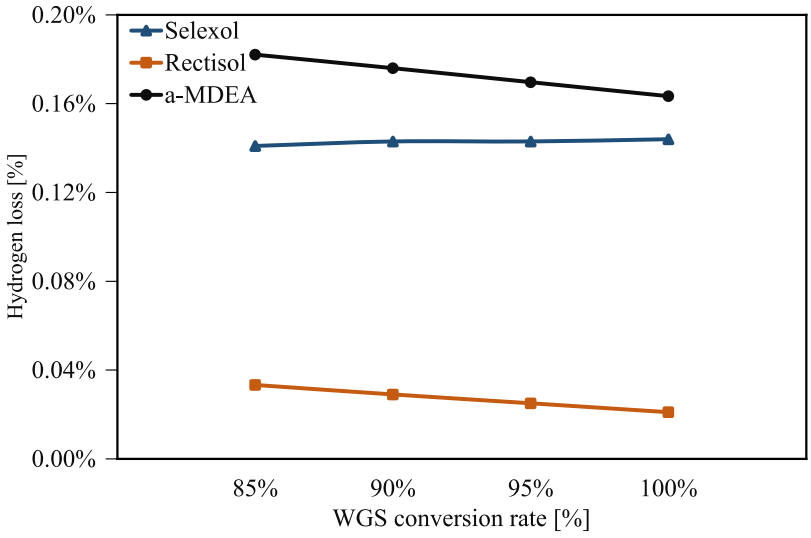

Figure 4.9 Hydrogen loss of each process relation with WGS conversion rate

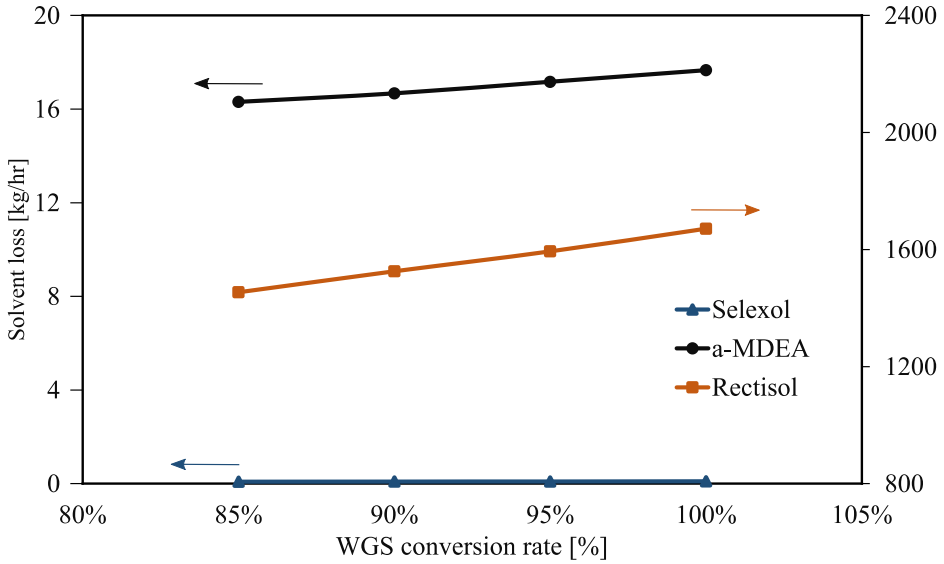

Figure 4.10 Solvent loss of each process relation with WGS conversion rate

4.3.1.2 The Impact of the CO_2 Capture Rate

Pre-combustion CO_2 capture processes are affected by the CO_2 capture rate in terms of solvent circulation flow rate and electrical/thermal energy consumption. Thus, modeling analyses were performed with a variety of parameters: Reboiler duty, electrical energy consumption, and hydrogen loss. As shown in Figure 4.11, the solvent flow rate shows an increment with CO_2 capture. Conversely, the heat duty for solvent regeneration decreased with the CO_2 capture rate as shown in Figure 4.12. The decrease in heat demand observed with the CO_2 capture rate is attributed to the design constraint of ≤5 ppm H_2S/COS set in the modeling. Thus, the regeneration heat duty decreases with the CO_2 capture rate. For example, the amount of solvent added in the first stage of the Selexol process decreases significantly, and the heat duty of the reboiler is affected in proportion compared to other processes.

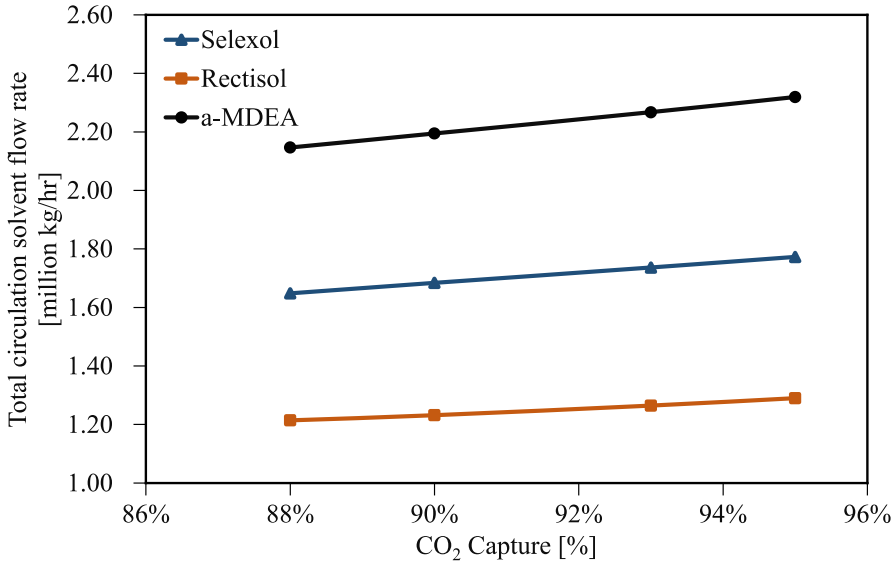

Figure 4.11 Relation of total solvent circulation flow rate depending on CO_2 capture rate

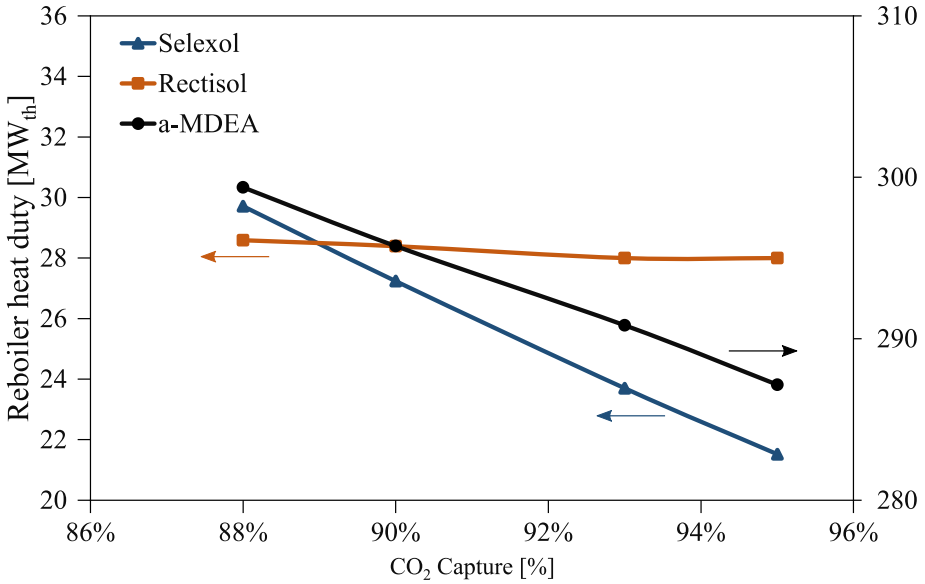

Figure 4.12 Relation of reboiler heat duty depending on CO_2 capture rate

The CO_2 capture rate also influences the power consumption of each process, as illustrated in Figure 4.13. In consideration of this, the total power consumption decreased with the recirculating CO_2 flow rate and the temperature of the gas supplied to the absorber. Conversely, the power consumption of the a-MDEA process increased with the CO_2 capture rate. The general operating parameters analyzed previously concerning the Selexol and Rectisol processes have little effect on the a-MDEA process. A larger flow rate of the a-MDEA process increases the power consumption of the CO_2 absorber that chills the solvent. Accordingly, the total power consumption increases with the CO_2 capture rate.

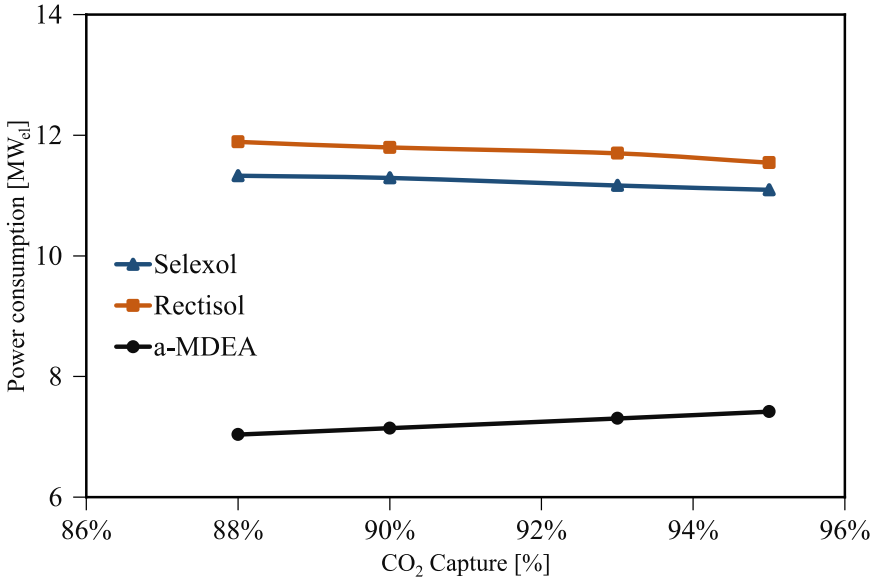

Figure 4.13 Electric energy consumption depending on CO_2 capture rate

Finally, Figure 4.14 shows the hydrogen loss versus CO_2 capture rate plot. In principle, the hydrogen loss increases with increasing CO_2 capture rate. For the Rectisol process, hydrogen loss

varies only slightly with CO_2 capture rate, but the estimated 8% increase is comparable to the 6.5% increase in solvent rate.

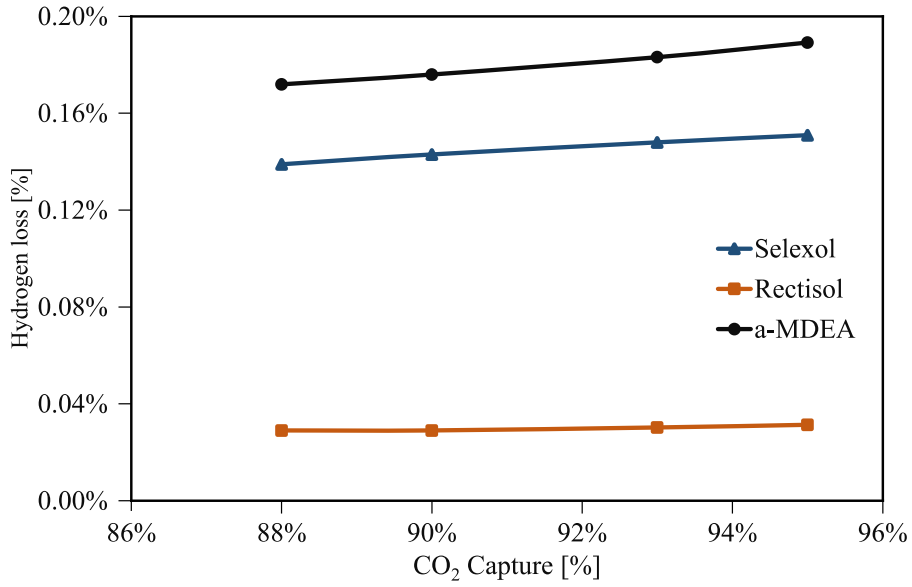

Figure 4.14 Hydrogen loss depending on CO_2 capture rate

Also, Figure 4.15 shows the amount of solvent loss in the process along with the CO_2 capture rate. The estimated amount of solvent loss in the Rectisol process is greater for all processes, but only a slight increase of 4.6% is found as the CO_2 capture rate increases. While the estimated amount of solvent losses in the Selexol process is minimum, an increase in solvent content of 13.6% is measured, which is the largest value of all three processes.

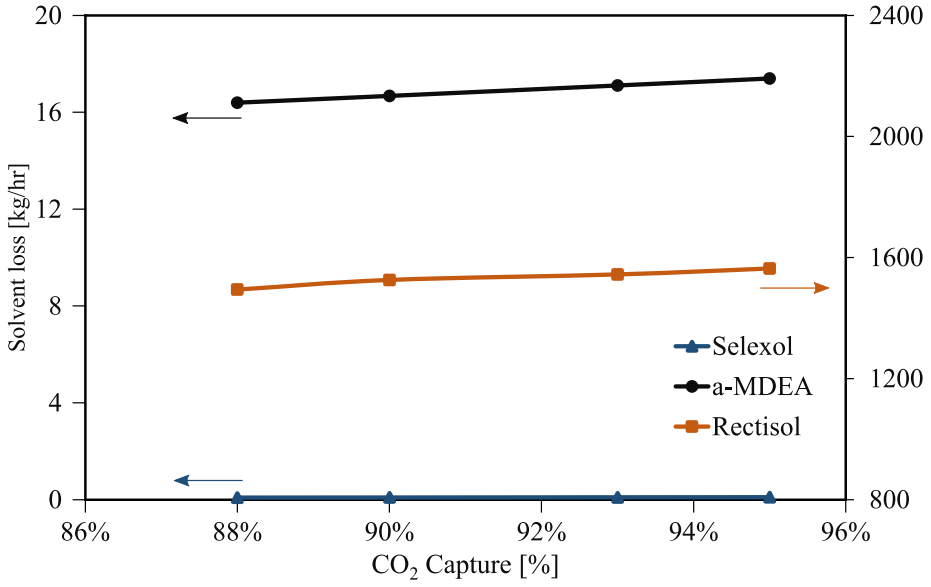

Figure 4.15 Comparison result for solvent loss of each case depending on CO_2 capture rate

Additional solvent comparisons are available in the literature. Doctor et al. [180], referring to a technical report, compared Selexol and Rectisol processes for an IGCC application which found that the Selexol process was more cost-effective than the Rectisol process for CO_2 sequestration in the fuel cycle. Also, Burr and Lyddon [107] offered a comparison of Selexol, Purisol, Rectisol, and Fluor Solvent and found that Selexol had an advantaged performance in applications that

involved removal of both H_2S and CO_2. They also determined that all of the physical solvents could be successfully used to remove CO_2 in large quantities.

4.4 Thermo-economic Evaluation of Polygeneration

Flowsheets for 100% electricity production as the base case and polygeneration of electricity and methanol were developed by using Aspen Plus software. The co-gasification of lignite coal and RDF is considered in this study at different mixing ratios. Various scenarios were then developed and simulated, including variations in electricity and methanol polygeneration and carbon capture levels. Simulation results, such as electricity and methanol production and product value, were used to perform the economic analysis of the polygeneration plant under unsteady economic parameters, i.e., selling prices for electricity and methanol. The capital cost was not evaluated because this is a thermodynamic analysis.

As market prices for chemicals and electricity may fluctuate in the future. Electricity prices may fluctuate daily, weekly, or seasonally. However, it is difficult to predict the fluctuations in the prices of the chemicals. The market price and demand volatility will lead the management to change the decision for polygeneration. How much of a particular product (electricity, methanol) to produce depends on market prices and demand for these products. The decision to use a particular product can be made by changing the split ratio of syngas toward methanol and power generation, while also taking into account the effects of carbon capture.

Different scenarios were created for polygeneration by determining the proportion of syngas used for methanol production (see Table 4.7). First, six different values of syngas splitting were taken into consideration: 0, 4, 8, 12, 16, and 20 %. On the other hand, carbon capture levels of 80, 85, 90, and 95% were also considered, as shown in Table 4.7. The ranges of these variants were amended after analyzing the simulated results. The production rates and total product value were evaluated for all of these scenarios.

Table 4.7 Scenarios of polygeneration

Case No.	Scenario No.	Carbon Capture (%)	Syngas Split for Methanol Production (%)
1	1-6	95	0,4,8,12,16,20
2	7-12	90	0,4,8,12,16,20
3	13-18	85	0,4,8,12,16,20
4	19-23	80	0,4,8,12,16,20

Since the operating choices are flexible, the choice that corresponds to the maximum output will be the optimal choice within the 23 scenarios for the market prices given. These choices will be highly dependent on the selling prices of each product. Thus, the impact of the product selling price uncertainty is discussed. Thus, the impact of the product selling price uncertainty will be discussed, but the impact of capital cost change, as well as the carbon emissions penalties, will not be investigated during this study but is deferred for future work.

The total selling price for all products is evaluated in this analysis based on the simulation results of the 23 scenarios are discussed, taking into account the market prices for electricity and methanol. Three scenarios were considered for each product price, resulting in a total of nine scenarios, which

are listed in Table 4.8. The economic analysis conducted for all of these scenarios was evaluated based on total fuel benefits, i.e., total product value. The prices are taken based on the historical price variations as reported by Statistica based on the European market [181,182].

Table 4.8 Electricity and methanol market price scenarios

Scenario No.	Electricity price (€/kWh)	Methanol Price (€/kg)
1	0.18	0.4
2	0.2	0.4
3	0.22	0.4
4	0.18	0.45
5	0.2	0.45
6	0.22	0.45
7	0.18	0.5
8	0.2	0.5
9	0.22	0.5

4.4.1 Energy Analysis

Initially, a base case was simulated considering full load power generation and a 90% carbon capture rate. The simulation results of the IGCC power plant are presented in Table 4.9.

Table 4.9 IGCC power plant performance indicators

Main plant data	Unit	Case 1	Case 2	Case 3
Solvent of AGR		Selexol		
Coal and RDF flowrate	kg/hr	149,997.52		
Coal/RDF LHV	MJ/kg	21.85/26.03		
Coal/RDF ratio	-	0.8/0.2	0.5/0.5	0.2/0.8
Feedstock thermal energy – LHV (A)	MW_{th}	945.234	997.484	1,049.733
Thermal energy of the syngas (B)	MW_{th}	796.265	843.971	893.113
Cold gas efficiency (B/A ×100)	%	84.24	84.61	85.08
Thermal energy of syngas exit AGR (C)	MW_{th}	710.348	753.244	797.817
Syngas treatment efficiency (C/B ×100)	%	89.21	89.25	89.33
Gas turbine output	MW_{el}	264.10	280.05	296.62
Steam turbine output	MW_{el}	178.20	188.96	200.14
Expander power output	MW_{el}	1.26	1.34	1.42
Gross electric power output (D)	MW_{el}	443.56	470.35	498.18
ASU consumption + O_2 compression	MW_{el}	40.20	42.62	45.15
Gasification island power consumption	MW_{el}	6.93	7.35	7.79
AGR+CO_2 drying and compression	MW_{el}	28.04	29.73	31.49
Power island power consumption	MW_{el}	16.02	17.03	17.98
Total ancillary power consumption (E)	MW_{el}	91.19	96.73	102.41
Net electric power output (F = D − E)	MW_{el}	352.38	373.62	395.78
Gross electrical efficiency (D/A ×100)	%	46.93	47.15	47.46
Net electrical efficiency (F/A ×100)	%	37.28	37.46	37.70
Carbon capture rate	%	90.33	90.48	91
CO_2 specific emissions	kg/MWh	19.27	18.90	18.06

For the three cases of co-gasification and using the Selexol AGR, the IGCC net efficiency average is 37.48%. This shows a reasonable consistency with the literature. In addition, it is noted the net power generation for the third Case is the highest because the bulk of the feedstock is the RDF, which has a high LHV, which explains this situation. Also, the specific emissions are low, which indicates that this IGCC is environment friendly with lower emissions than the natural gas CCPP.

4.4.2 Energy Analysis for Polygeneration

For variable polygeneration of electricity and methanol, a carbon capture rate of 90% was kept by adjusting the lean solvent amount, i.e., Selexol. Production decisions were made based on the percentage of syngas used for methanol production. All production scenarios with four different carbon capture rates (95%, 90%, 85%, and 80%) as indicated in Table 4.7 were simulated at the syngas composition of the co-gasification Cases 1, 2, and 3, and the results for electricity and methanol are shown in Figure 4.16.

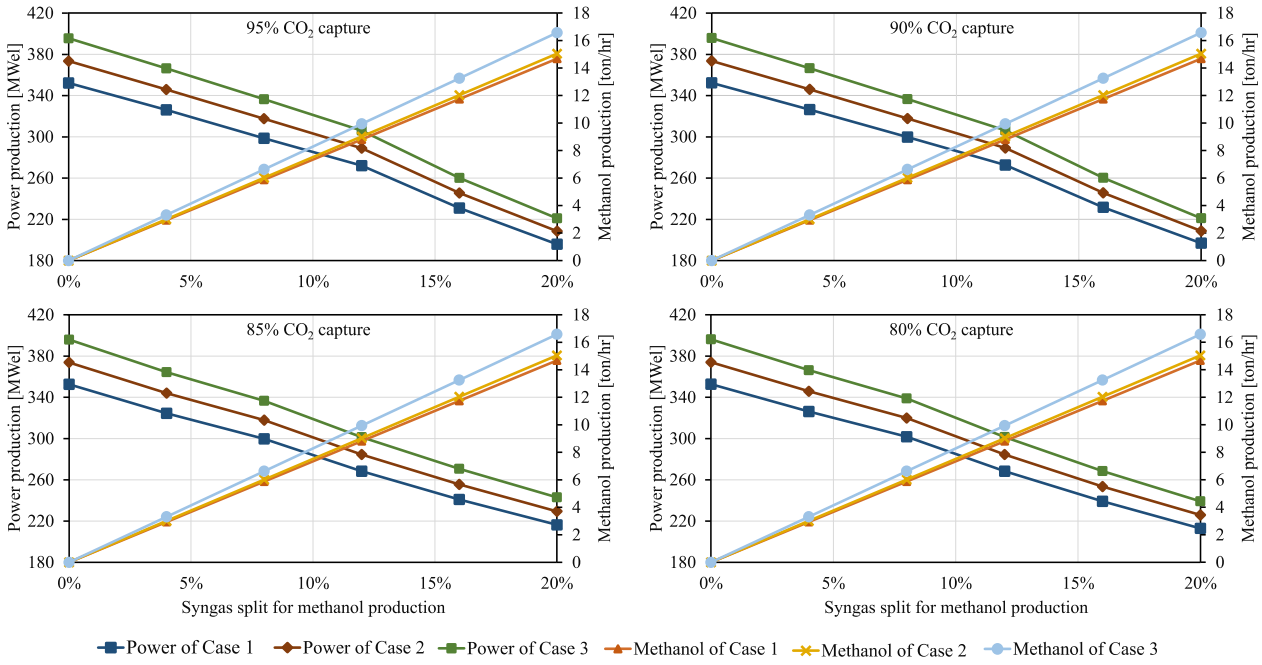

Figure 4.16 Power and methanol production at a different CO_2 capture rate

As the percentage of syngas used for methanol production is increased, electricity generation decreases, as shown in Figure 4.16 for different values of CO_2 capture rates. It can also be seen that for a given syngas split ratio, the electricity generation decreases more when the methanol generation is increased since the reduction of hydrogen for electricity generation has a greater impact than the reduction of syngas. On the other hand, electricity generation was detected to slightly increase when the level of carbon capture is reduced. However, considering that more than 95% of the electricity consumption comes from the ASU, which is constant for all scenarios, there is no thermal power consumption in either the H_2S purification or carbon capture units. Consequently, 90% capture was assumed in the following sections.

4.4.3 Economic Analysis for Polygeneration

The total product value or selling price for nominal market prices under different production scenarios is shown in Figure 4.17. IGCC availability for production is also considered by applying four availability values. The selling price decreased with the increase of syngas share for methanol production. The highest value of selling price was obtained for case 3 at all availability levels. It is obvious from this that the optimal production level choices are very important and are expected to depend on the market prices of the products, as will be elaborated in the following section. It should be noted that no penalty was applied to CO_2 emissions.

As market prices for electricity and methanol are expected to fluctuate over time, this type of market compels the plant operator to have flexibility in operating the plant. Thus, the impact of fluctuating market prices should be considered in planning and operating strategies. In this type of IGCC power plant, the flexibility of the plant is not only limited to varying the output by using a lower amount of feedstock for gasification, but also to the variable degree of carbon capture and the variable production of electricity and methanol. During periods of low electricity demand/prices, most of the syngas and hydrogen from the polygeneration plant are used for methanol production. In contrast, to meet energy demand during peak periods, carbon capture and methane production can be reduced. The impact of market prices on making optimized choices has been discussed in this section. However, it should be remarked that the total product value for the nominal scenario was discussed at different capture levels and production decisions.

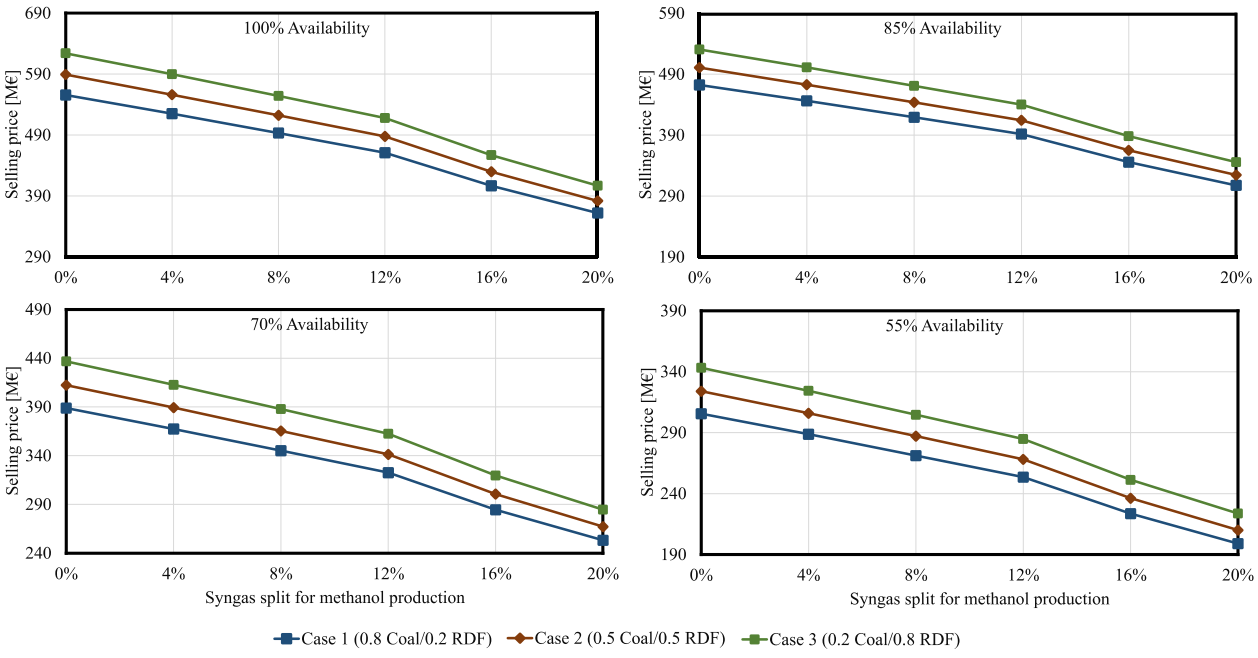

Figure 4.17 Selling price of the IGCC products at different shares of syngas for methanol production and different availability levels of the IGCC

All scenarios for the different cases of co-gasification and availability of the IGCC plant are shown in Figure 4.18 for the 100%, Figure 4.19 for 85%, Figure 4.20 for 70%, and Figure 4.21 for 55% availability. From the figures, it can be seen that with the increase of the split ratio for methanol production, the trend of the total selling price decreases in all scenarios, which leads to the result that the volatility of electricity prices has a great influence on the total selling price of the products, while the volatility of methanol prices has a very small influence on the total selling price.

Therefore, the production of electricity is preferable when it is in demand, and the production of methanol could be done during off-peak periods. Therefore, it is clear that the choice of the optimal production level is very important and probably depends on the market prices of the products.

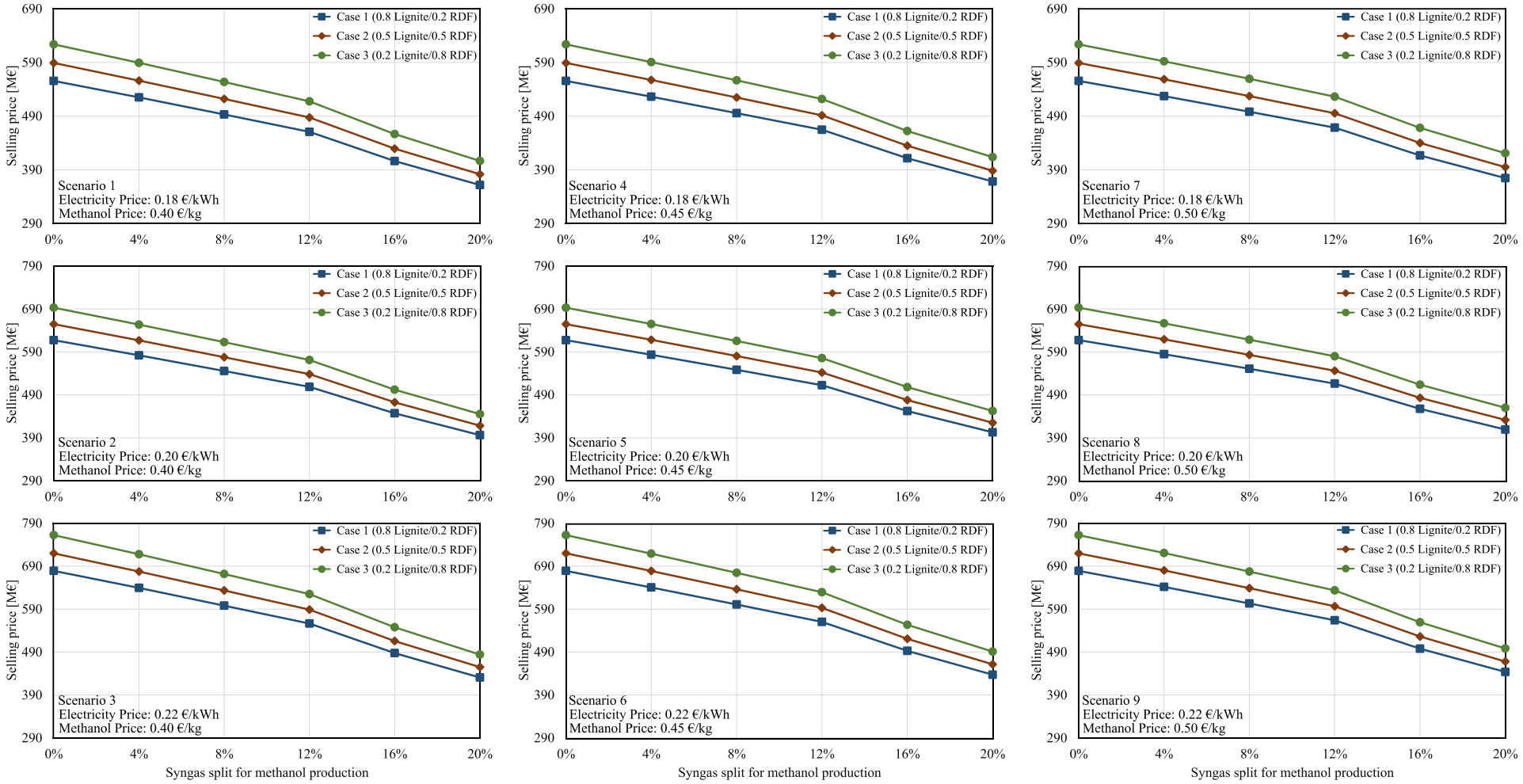

Figure 4.18 Effect of market price change at 100% availability of IGCC

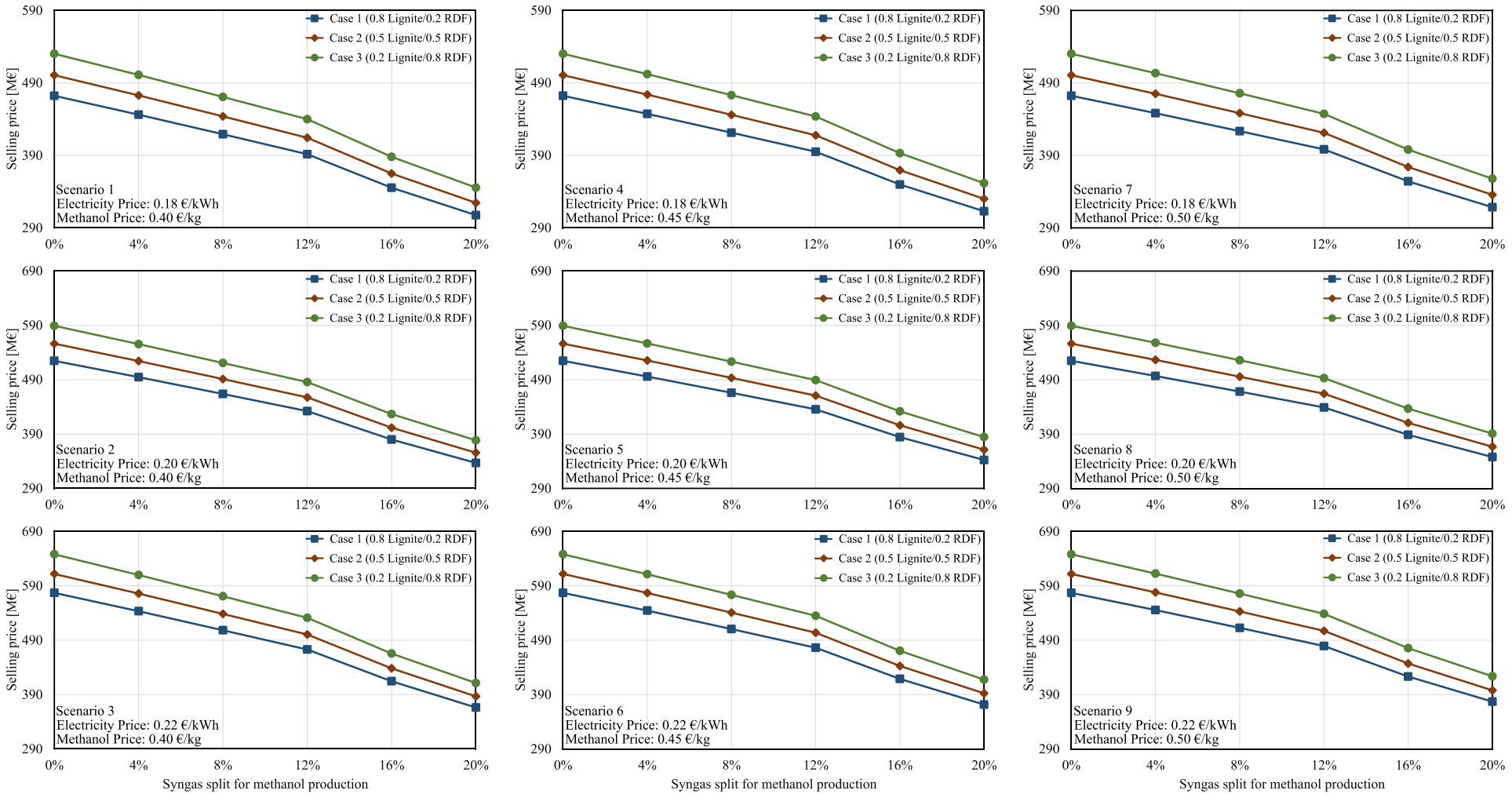

Figure 4.19 Effect of market price change at 85% availability of IGCC

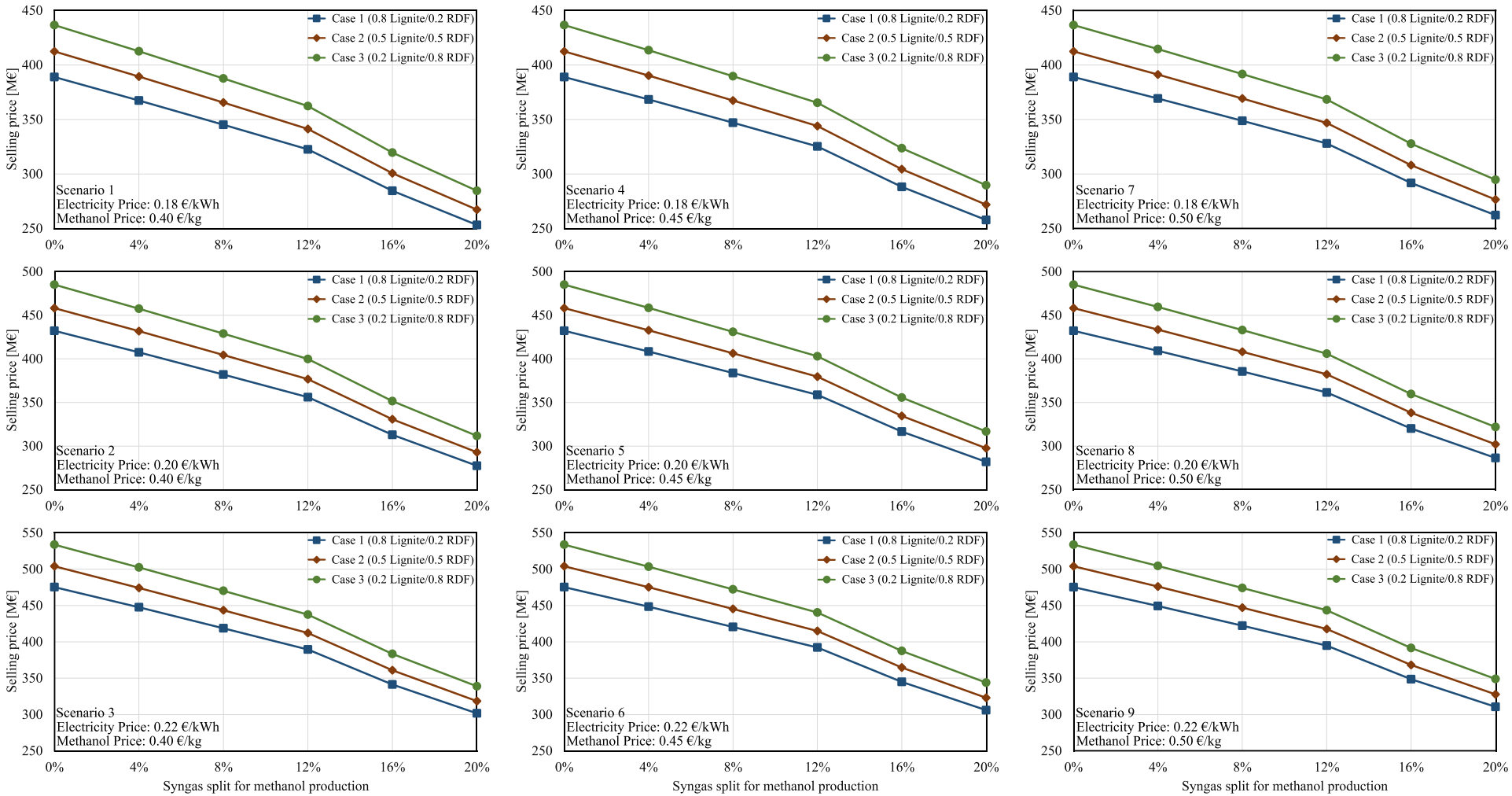

Figure 4.20 Effect of market price change at 70% availability of IGCC

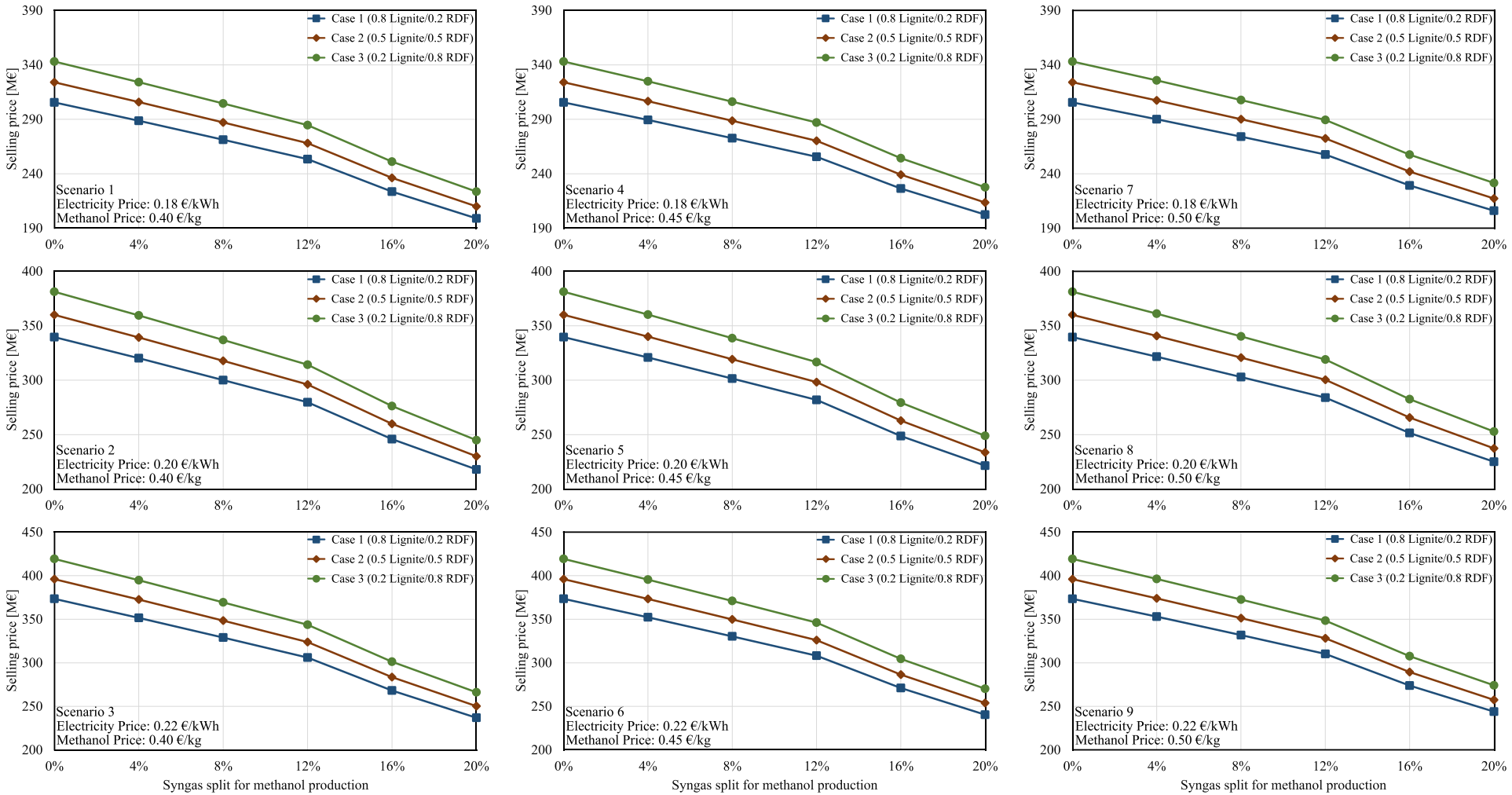

Figure 4.21 Effect of market price change at 55% availability of IGCC

Chapter 5: **Conclusion and Outlook**

The concept of flexible IGCC power plants with carbon capture for polygeneration to produce electricity and chemicals in parallel on-demand is a promising approach to compensate for the fluctuating power generation from wind power and photovoltaics and to reduce CO_2 emissions in the energy and industrial sectors. The investigated approach allows the CO_2 produced to be made available as a pure material stream for storage or other uses. Also, besides coal, anthropogenic and biogenic residues can be used as feedstock for the process. Furthermore, established and proven technologies can be used for the essential process steps. A process simulation model for the flexible IGCC power plant was developed using Aspen Plus in this work using a polygeneration approach.

As part of this work, a process simulation model of the pilot-scale gasification and purification plant was developed based on the pilot plant installed at TU Darmstadt. This model has been validated based on the heat and material balances as well as the design data and specifications provided by ThyssenKrupp. It was intended to investigate the behavior of the gas purification stages. Also, it was aimed at providing a good basis for the modeling of an industrial scale gas treatment plant. The results showed good agreement with the data used to validate this model. Furthermore, the results pointed the way to a better understanding of the process behavior and the interacting variables, as a supplement to the literature. Subsequently, an industrial-scale gasification and gas cleaning plant is developed and integrated into a 360 MW_{el} CCPP model. This CCPP process simulation model was developed based on the operating data of a CCPP in Malaysia. The simulation results, such as electrical power, pressure, temperature, and mass flow rate, were validated against actual measurements and showed good agreement, highlighting the reliability of the process simulation model in predicting process behavior.

The evaluation of the IGCC power plant model for flexible polygeneration developed as part of this thesis using HTW gasification technology shows a promising electrical efficiency of about 37.48% with a carbon capture rate of 90%. In addition, co-gasification of lignite and RDF at different mixing ratios is simulated, which shows high performance due to the high calorific value of RDF. Therefore, this will contribute to better use of resources and waste management solutions using flexible IGCC technology with carbon capture to protect both the environment and the planet. In addition, the IGCC model was used for a thermo-economic evaluation to assess the potential of the technology, the expected operating conditions, and load transients, and to identify open research questions.

5.1 Heat Integration Enhancement

The improvement of the steam power process has a significant impact on the overall performance of the plant. Within this work, the heat integration between HRSG and the gas treatment process was implemented in the Aspen Plus model. The results of this model needed to be optimized to achieve better performance. Therefore, the model of the steam cycle was created in EBSILON Professional software. This was then validated at 100% full load case as well as an 80% and 60% partial load case based on measurement data of the real plant. The validated model was modified to use synthesis gas since an IGCC is fired with synthesis gas. This was followed by the integration

of the predefined extractions and their optimization concerning the performance of the steam turbine. The following essential points resulted from this study:

1. The numerical model created in EBSILON Professional can quantitatively represent the real plant in the different load cases. Especially for the values of pressure and temperature, relative errors below 1% were found. For the mass flow, there were somewhat higher deviations from the measured data. For this reason, the performance of the steam turbine of the model was compared to the performance of the steam turbine under the conditions of the measurements. This resulted in relative errors below 5% in all load cases. Thus, the model is considered validated.

2. The model was successfully modified to use synthesis gas, and the predefined extractions were integrated. The output of the steam turbine of the model is 71.3 MW_{el} at 100% load, 54.6 MW_{el} at 80% load, and 39.6 MW_{el} at 60% load. These values were selected as reference values for the optimization.

3. The optimization allowed the output of the steam turbine to be significantly increased in all three load cases. In the 100% load case, there was a relative increase in output of the steam turbine of 34.2% with an output value of 95.7 MW_{el}. The output increase at 80% load was 35.9% (74.2 MW_{el}) and at 60% load 45.9% (57.8 MW_{el}).

Based on this work, it is interesting to examine the system in terms of economic efficiency. The optimization of the entire IGCC plant with the boundary conditions of the optimized HRSG model is also a topic of further research.

5.2 AGR Evaluation

In this study, the process redesign modeling was performed on dual-stage pre-combustion CO_2 capture processes for application to 360 MW_{el} IGCC system employing HTW gasifier, using Aspen Plus. The process performance was also an important design specification for redesign modeling.

1. The Selexol process was found to be the most efficient process in terms of electricity and thermal energy consumption, while the Rectisol process was quite efficient in terms of electricity and thermal energy consumption. On the other hand, the a-MDEA process has the lowest power consumption but consumes a significant amount of thermal energy for the regeneration process in the reboiler.

2. The WGS conversion rate is not significantly affecting the electrical and thermal energy consumption associated with the Selexol process. In contrast to the Selexol process, the solvent loss is much larger in other processes using Rectisol and a-MDEA. The Selexol process was found to be the most efficient and economical process in terms of WGS conversion rate.

3. The solvent property specifies the operating temperature for the Rectisol process. This is advantageous for the solvent cycle with a lower flow rate, reduced thermal requirements of the reboiler, and hydrogen loss. Considering this, the Rectisol process proved to be more economical due to the low solvent loss and smaller plant size.

4. The total effect of CO_2 capture rate on both the individual hydrogen and solvent loss has been 8-10% and 6-13%, respectively, whereas the solvent flow rate was linearly dependent

on the CO_2 capture rate. Considering the thermal and electrical energy consumption, the Selexol process was evaluated as a more efficient process for CO_2 capture at a high level with physical solvents.

5.3 Energy and Economical Analysis

IGCC power plant with polygeneration approach at various carbon capture levels, different feedstock mixing rates, and production shares was simulated using Aspen Plus. A mixture of coal and RDF was used as the feedstock to an HTW gasifier. The plant's performance was evaluated with respect to the product price, comprising electricity and methanol for different production shares. Subsequently, this information was used to assess the impact of product price fluctuations on the overall product price. A total of nine scenarios were considered regarding market price fluctuations. However, the carbon emissions penalty that occurs when the carbon capture rate decreases below 90% was not included in the calculation of the total product value. As this was a thermodynamic analysis, the detailed design and therefore the capital costs were not considered in this study.

A preliminary analysis was conducted to evaluate the economic performance of the IGCC power plant using the Aspen Plus thermodynamic model in flexible mode, followed by an economic analysis. However, the analysis can be further improved by including the capital cost. The following conclusions can be drawn from the results.

1. For the power generation mode only, the efficiency of the IGCC power plant was 37.48%.
2. As methanol production increased, electricity production decreased and so did the efficiency of the plant. The effects of hydrogen splitting for methanol production were rather adverse to electricity production.
3. When the electricity price increases, the optimal point moves to lower methanol production. This indicates that electricity production should be increased to obtain the maximum total output value for the nominal scenario.
4. Electricity price volatility has the largest impact on the total value of the product, while methanol price volatility has a smaller impact on the total value of the product.

For future work, I will recommend considering the results presented in this dissertation as a preliminary analysis of a comprehensive techno-economic analysis under conditions of uncertainty. Also, More details about the design and economic data can be used in an extension of this work. Such as, calculating the capital cost and thus performing the profitability analysis. On the other hand, the penalty for carbon emission to the atmosphere may also change the optimal proportions of operation. And finally, the results open up good opportunities to develop an Artificial Intelligence (AI) algorithm to control the operation strategy for the best performance and product value.

Bibliography

[1] Klare MT. Rising powers, shrinking planet : the new geopolitics of energy. Henry Holt and Co; 2009.

[2] Lambert JG, Hall CAS, Balogh S, Gupta A, Arnold M. Energy, EROI and quality of life. Energy Policy 2014;64:153–67. doi:10.1016/j.enpol.2013.07.001.

[3] Commission on the Geopolitics of Energy Transformation GI. A new world: The geopolitics of the energy transformation. 2019.

[4] Newell R, Raimi D, Aldana G. Global energy outlook 2019: the next generation of energy. 2019.

[5] Cozzi L, Gould T, Bouckart S, Crow D, Kim T-Y, McGlade C, et al. World Energy Outlook 2020 2020;2050:1–461.

[6] Arto I, Capellán-Pérez I, Lago R, Bueno G, Bermejo R. The energy requirements of a developed world. Energy for Sustainable Development 2016;33:1–13. doi:10.1016/j.esd.2016.04.001.

[7] Ammari H, Bany Ata A. Economic comparison between PV powered vapor compression refrigeration system and solar thermal powered absorption refrigeration system. 5th Jordanian IIR International Conference on Refrigeration and Air Conditioning., Aqaba, Jordan: 2015, p. 9.

[8] IEA. Electricity Market Report. 2020. doi:10.1787/f0aed4e6-en.

[9] IRENA, IEA, REN21. Renewable Energy Policies in a Time of Transition: Heating and Cooling. 2020.

[10] Arto I, Dietzenbacher E. Drivers of the growth in global greenhouse gas emissions. Environmental Science and Technology 2014;48:5388–94. doi:10.1021/es5005347.

[11] UNFCC. Adoption of the Paris Agreement. Paris: 2015.

[12] Dröge S. The Paris Agreement 2015: turning point for the international climate regime. vol. 4/2016. Berlin: Stiftung Wissenschaft und Politik -SWP- Deutsches Institut für Internationale Politik und Sicherheit; 2016.

[13] Global historical CO2 emissions 1750-2020 | Statista n.d. https://www.statista.com/statistics/264699/worldwide-co2-emissions/ (accessed September 22, 2021).

[14] European Commission. Climate Action - Building a world we like, with a climate we like. 2014. doi:10.2775/83031.

[15] Masson-Delmotte V, Zhai P, Pörtner H-O, Roberts D, Skea J, Shukla PR, et al. Global warming of 1.5°C An IPCC Special Report on the impacts of global warming of 1.5°C above pre-industrial levels and related global greenhouse gas emission pathways, in the context of strengthening the global response to the threat of climate change, . 2019.

[16] Consoli C. Bioenergy and carbon capture and storage. 2019.

[17] Edenhofer O, Sokona Y, Minx JC, Farahani E, Kadner S, Seyboth K, et al. Climate Change 2014 Mitigation of Climate Change Working Group III Contribution to the Fifth Assessment Report of the Intergovernmental Panel on Climate Change Edited by. 2014.

[18] Lee RP, Keller F, Meyer B. A concept to support the transformation from a linear to circular

carbon economy: net zero emissions, resource efficiency and conservation through a coupling of the energy, chemical and waste management sectors. Clean Energy 2017;1:102–13. doi:10.1093/CE/ZKX004.

[19] Emissions by sector – Greenhouse Gas Emissions from Energy: Overview – Analysis - IEA n.d. https://www.iea.org/reports/greenhouse-gas-emissions-from-energy-overview/emissions-by-sector (accessed September 22, 2021).

[20] IEA. Net Zero by 2050 - A Roadmap for the Global Energy Sector. 2021.

[21] Lund H. Large-scale integration of wind power into different energy systems. Energy 2005;30:2402–12. doi:10.1016/j.energy.2004.11.001.

[22] Verzijlbergh RA, De Vries LJ, Dijkema GPJ, Herder PM. Institutional challenges caused by the integration of renewable energy sources in the European electricity sector. Renewable and Sustainable Energy Reviews 2017;75:660–7. doi:10.1016/j.rser.2016.11.039.

[23] Alshahrani A, Omer S, Su Y, Mohamed E, Alotaibi S. The Technical Challenges Facing the Integration of Small-Scale and Large-scale PV Systems into the Grid: A Critical Review. Electronics 2019;8:1443. doi:10.3390/electronics8121443.

[24] IEA (2020). Key World Energy Statistics 2020. Paris: OECD Publishing; 2020. doi:https://doi.org/https://doi.org/10.1787/295f00f5-en.

[25] Petroleum B. Statistical Review of World Energy - Global. 2020.

[26] bp. bp Statistical Review of World Energy 2020. 2020.

[27] Ellen MacArthur Foundation. The New Plastics Economy: Rethinking the future of plastics. 2016.

[28] Tavoni M, Zwaan B van der. Nuclear Versus Coal plus CCS: a Comparison of Two Competitive Base-Load Climate Control Options. Environmental Modeling & Assessment 2011 16:5 2011;16:431–40. doi:10.1007/S10666-011-9259-1.

[29] Wang T, Stiegel G. Integrated gasification combined cycle (IGCC) technologies. Elsevier Inc.; 2016. doi:10.1016/c2014-0-00849-0.

[30] Vermeiren W, Gilson J-P. Impact of Zeolites on the Petroleum and Petrochemical Industry. Topics in Catalysis 2009 52:9 2009;52:1131–61. doi:10.1007/S11244-009-9271-8.

[31] Davidson RM. Pre-combustion capture of CO 2 in IGCC plants 2011.

[32] Berstad D, Anantharaman R, Nekså P. Low-temperature CCS from an IGCC Power Plant and Comparison with Physical Solvents. Energy Procedia 2013;37:2204–11. doi:10.1016/j.egypro.2013.06.100.

[33] Chen C, Rubin ES. CO2 control technology effects on IGCC plant performance and cost. Energy Policy 2009;37:915–24. doi:10.1016/J.ENPOL.2008.09.093.

[34] DESCAMPS C, BOUALLOU C, KANNICHE M. Efficiency of an Integrated Gasification Combined Cycle (IGCC) power plant including CO2 removal. Energy 2008;33:874–81. doi:10.1016/j.energy.2007.07.013.

[35] Padurean A, Cormos CC, Agachi PS. Pre-combustion carbon dioxide capture by gas-liquid absorption for Integrated Gasification Combined Cycle power plants. International Journal of Greenhouse Gas Control 2012;7:1–11. doi:10.1016/j.ijggc.2011.12.007.

[36] Cormos CC. Evaluation of energy integration aspects for IGCC-based hydrogen and electricity co-production with carbon capture and storage. International Journal of Hydrogen Energy 2010;35:7485–97. doi:10.1016/J.IJHYDENE.2010.04.160.

[37] Gaspar J, Cormos AM. Dynamic modeling and absorption capacity assessment of CO2 capture process. International Journal of Greenhouse Gas Control 2012;8:45–55. doi:10.1016/J.IJGGC.2012.01.016.

[38] Lee JC, Lee HH, Joo YJ, Lee CH, Oh M. Process simulation and thermodynamic analysis of an IGCC (integrated gasification combined cycle) plant with an entrained coal gasifier. Energy 2014;64:58–68. doi:10.1016/J.ENERGY.2013.11.069.

[39] Lee C, Lee SJ, Yun Y. Effect of air separation unit integration on integrated gasification combined cycle performance and NOx emission characteristics. Korean Journal of Chemical Engineering 2007 24:2 2007;24:368–73. doi:10.1007/S11814-007-5047-7.

[40] Gharaie M, Jobson M, Panjeshahi MH, Zhang N, Smith R. Techno-economic optimization of IGCC integrated with utility system for CO2 emissions reduction—Simultaneous heat and power generation from IGCC. Chemical Engineering Research and Design 2015;94:428–39. doi:10.1016/J.CHERD.2014.08.019.

[41] Frey* HC, Zhu Y. Improved System Integration for Integrated Gasification Combined Cycle (IGCC) Systems. Environmental Science and Technology 2006;40:1693–9. doi:10.1021/ES0515598.

[42] Zhang X, Zhang R, Liu H, Gao H, Liang Z. Evaluating CO2 desorption performance in CO2-loaded aqueous tri-solvent blend amines with and without solid acid catalysts. Applied Energy 2018;218:417–29. doi:10.1016/j.apenergy.2018.02.087.

[43] Mondol JD, McIlveen-Wright D, Rezvani S, Huang Y, Hewitt N. Techno-economic evaluation of advanced IGCC lignite coal fuelled power plants with CO2 capture. Fuel 2009;88:2495–506. doi:10.1016/j.fuel.2009.04.019.

[44] Majoumerd MM, Raas H, Jana K, De S, Assadi M. Coal Quality Effects on the Performance of an IGCC Power Plant with CO2 Capture in India. Energy Procedia 2017;114:6478–89. doi:10.1016/J.EGYPRO.2017.03.1784.

[45] Li Z, Liang X, Xue Y. Techno-economic comparison of IGCC systems employing bituminous and lignite. Zhongguo Dianji Gongcheng Xuebao(Proceedings of the Chinese Society of Electrical Engineering), vol. 32, Chinese Society for Electrical Engineering; 2012, p. 39–47.

[46] Bonalumi D, Ciavatta A, Giuffrida A. Thermodynamic Assessment of Cooled and Chilled Ammonia-based CO2 Capture in Air-Blown IGCC Plants. Energy Procedia 2016;86:272–81. doi:10.1016/j.egypro.2016.01.028.

[47] Sheikh HM, Ullah A, Hong K, Zaman M. Thermo-economic analysis of integrated gasification combined cycle (IGCC) power plant with carbon capture. Chemical Engineering and Processing - Process Intensification 2018;128:53–62. doi:10.1016/J.CEP.2018.04.007.

[48] Sofia D, Coca Llano P, Giuliano A, Iborra Hernández M, García Peña F, Barletta D. Co-gasification of coal–petcoke and biomass in the Puertollano IGCC power plant. Chemical Engineering Research and Design 2014;92:1428–40. doi:10.1016/J.CHERD.2013.11.019.

[49] Thallam Thattai A, Oldenbroek V, Schoenmakers L, Woudstra T, Aravind P V. Experimental model validation and thermodynamic assessment on high percentage (up to 70%) biomass co-gasification at the 253 MWe integrated gasification combined cycle power plant in Buggenum, The Netherlands. Applied Energy 2016;168:381–93. doi:10.1016/J.APENERGY.2016.01.131.

[50] Cormos CC. Integrated assessment of IGCC power generation technology with carbon capture and storage (CCS). Energy 2012;42:434–45. doi:10.1016/J.ENERGY.2012.03.025.

[51] Zhang X, Gundersen T, Roussanaly S, Brunsvold AL, Zhang S. Carbon chain analysis on a coal IGCC — CCS system with flexible multi-products. Fuel Processing Technology 2013;108:146–53. doi:10.1016/J.FUPROC.2012.05.012.

[52] Kanniche M, Bouallou C. CO2 capture study in advanced integrated gasification combined cycle. Applied Thermal Engineering 2007;27:2693–702. doi:10.1016/j.applthermaleng.2007.04.007.

[53] Cau G, Tola V, Deiana P. Comparative performance assessment of USC and IGCC power plants integrated with CO2 capture systems. Fuel 2014;116:820–33. doi:10.1016/j.fuel.2013.06.005.

[54] Asif M, Bak CU, Saleem MW, Kim WS. Performance evaluation of integrated gasification combined cycle (IGCC) utilizing a blended solution of ammonia and 2-amino-2-methyl-1-propanol (AMP) for CO2 capture. Fuel 2015;160:513–24. doi:10.1016/j.fuel.2015.08.008.

[55] Urech J, Tock L, Harkin T, Hoadley A, Maréchal F. An assessment of different solvent-based capture technologies within an IGCC-CCS power plant. Energy 2014;64:268–76. doi:10.1016/j.energy.2013.10.081.

[56] Ordorica-Garcia G, Douglas P, Croiset E, Zheng L. Technoeconomic evaluation of IGCC power plants for CO2 avoidance. Energy Conversion and Management 2006;47:2250–9. doi:10.1016/j.enconman.2005.11.020.

[57] Kunze C, Riedl K, Spliethoff H. Structured exergy analysis of an integrated gasification combined cycle (IGCC) plant with carbon capture. Energy 2011;36:1480–7. doi:10.1016/j.energy.2011.01.020.

[58] Siefert NS, Litster S. Exergy and economic analyses of advanced IGCC-CCS and IGFC-CCS power plants. Applied Energy 2013;107:315–28. doi:10.1016/j.apenergy.2013.02.006.

[59] Field RP, Brasington R. Baseline flowsheet model for IGCC with carbon capture. Industrial and Engineering Chemistry Research 2011;50:11306–12. doi:10.1021/ie200288u.

[60] Kapetaki Z, Brandani P, Brandani S, Ahn H. Process simulation of a dual-stage Selexol process for 95% carbon capture efficiency at an integrated gasification combined cycle power plant. International Journal of Greenhouse Gas Control 2015;39:17–26. doi:10.1016/j.ijggc.2015.04.015.

[61] Moioli S, Giuffrida A, Gamba S, Romano MC, Pellegrini L, Lozza G. Pre-combustion CO2 capture by MDEA process in IGCC based on air-blown gasification. Energy Procedia 2014;63:2045–53. doi:10.1016/j.egypro.2014.11.220.

[62] Skorek-Osikowska A, Janusz-Szymańska K, Kotowicz J. Modeling and analysis of selected carbon dioxide capture methods in IGCC systems. Energy 2012;45:92–100. doi:10.1016/j.energy.2012.02.002.

[63] Boerrigter H, Van Der Drift B, Van Der Meijden CM, Van Paasen SVB, Pels JR, Rabou LPLM, et al. INTEGRATED BIOMASS GASIFICATION AND GAS CLEANING FACILITY; ECN PILOT-PLANT FOR BIOMASS RESEARCH 2004.

[64] Kolb T, Eberhard M, Dahmen N, Leibold H, Neuberger M, Sauer J, et al. BtL-The bioliq ® Process at KIT. New Technologies and Alternative Feedstocks in Petrochemistry and Refining DGMK Conference, Dresden, Germany: 2013.

[65] Viguié J-C, Ullrich N, Porot P, Bournay L, Hecquet M, Rousseau J. BioTfueL project : targeting the development of second-generation biodiesel and biojet fuels n.d.

[66] Buttler A, Kunze C, Spliethoff H. IGCC-EPI: Decentralized concept of a highly load-flexible IGCC power plant for excess power integration. Applied Energy 2013;104:869–79. doi:10.1016/j.apenergy.2012.11.066.

[67] Meerman JC, Ramírez A, Turkenburg WC, Faaij APC. Performance of simulated flexible integrated gasification polygeneration facilities. Part A: A technical-energetic assessment. Renewable and Sustainable Energy Reviews 2011;15:2563–87. doi:10.1016/J.RSER.2011.03.018.

[68] Meerman JC, Ramírez A, Turkenburg WC, Faaij APC. Performance of simulated flexible integrated gasification polygeneration facilities, Part B: Economic evaluation. Renewable and Sustainable Energy Reviews 2012;16:6083–102. doi:10.1016/J.RSER.2012.06.030.

[69] Wolfersdorf C, Boblenz K, Pardemann R, Meyer B. Syngas-based annex concepts for chemical energy storage and improving flexibility of pulverized coal combustion power plants. Applied Energy 2015;156:618–27. doi:10.1016/J.APENERGY.2015.07.039.

[70] Todd D, Sorensen J, Higman C, Kubek D, Marasigan J. Design options for enhancing IGCC flexible operations performance and economics, Palo Alto, CA, (3002003742): 2014.

[71] Higman C, van der Burgt M. Gasification. Elsevier Inc.; 2008. doi:10.1016/B978-0-7506-8528-3.X0001-6.

[72] Wagner NJ, Coertzen M, Matjie RH, Van Dyk JC. Coal Gasification. Applied Coal Petrology 2008:119–44. doi:10.1016/B978-0-08-045051-3.00005-1.

[73] Spliethoff H. Power generation from solid fuels. springer science & business media; 2010.

[74] Kunii D, Octave L. Fluidization Engineering. Elsevier; 1991. doi:10.1016/C2009-0-24190-0.

[75] Hermann H, Reinhard R, Klaus B, Koch RB, Kraftwerk GGMBH. Biomass CHP Plant Güssing-A Success Story n.d.

[76] Lavoie J-M, Marie-Rose S, Lynch D. Non-homogeneous residual feedstocks to biofuels and chemicals via the methanol route. Biomass Conversion and Biorefinery 2012 3:1 2012;3:39–44. doi:10.1007/S13399-012-0050-6.

[77] Toporov D, Abraham R. Gasification of low-rank coal in the High-Temperature Winkler (HTW) process. Journal of the Southern African Institute of Mining and Metallurgy 2015;115:589–97. doi:10.17159/2411-9717/2015/V115N7A5.

[78] Renzenbrink W, Wischnewski R, Engelhard J, Mittelstädt A, Ag R. High Temperature Winkler (HTW) Coal Gasification A Fully Developed Process For Methanol and Electricity Production. n.d.

[79] Herdel P, Krause D, Peters J, Kolmorgen B, Ströhle J, Epple B. Experimental investigations in a demonstration plant for fluidized bed gasification of multiple feedstock's in 0.5 MWth scale. Fuel 2017;205:286–96. doi:10.1016/J.FUEL.2017.05.058.

[80] Toporov D. Production of Biofuels using thyssenkrupp Gasification Technologies. in Gasification, Delhi, India: 2016.

[81] Adlhoch W, Sato H, Wolff J, Radtke K. High-temperature Winkler gasification of municipal solid waste. Gasification Technologies Conference, 2000, p. 1–15.

[82] Zhou Z, Yu G, Gong X, Wang F, Liu H, Wang Y. Development, Demonstration and Application of Opposed Multi-Burner Coal Gasification Process. 5th International Freiberg Conference on IGCC & XtL Technologies, Leipzig, Germany: 2011.

[83] Gong Y, Yu G, Guo Q, Wang Y, Chen X, Wang F. Progress on Opposed Multi-Burner (OMB) Coal-Water Slurry Gasification Technology and Its Industrial Applications. Energy Procedia 2017;142:1089–94. doi:10.1016/J.EGYPRO.2017.12.361.

[84] Buschsieweke F. Dampfwirbelschichttrocknung von Braunkohle. Universit¨at Stuttgart, 2006.

[85] Fantozzi F, Bartocci P. Biomass feedstock for IGCC systems. Integrated Gasification Combined Cycle (IGCC) Technologies, Woodhead Publishing; 2017, p. 145–80. doi:10.1016/B978-0-08-100167-7.00004-4.

[86] Lozza G. Syngas cooling in IGCC systems. Integrated Gasification Combined Cycle (IGCC) Technologies, Woodhead Publishing; 2017, p. 357–71. doi:10.1016/B978-0-08-100167-7.00009-3.

[87] Amick P. Case study: Wabash River Coal Gasification Repowering Project, USA. Integrated Gasification Combined Cycle (IGCC) Technologies, Woodhead Publishing; 2017, p. 699–714. doi:10.1016/B978-0-08-100167-7.00017-2.

[88] Schoenmakers L. Case study: Nuon–Buggenum, The Netherlands. Integrated Gasification Combined Cycle (IGCC) Technologies, Woodhead Publishing; 2017, p. 715–52. doi:10.1016/B978-0-08-100167-7.00018-4.

[89] Woolcock PJ, Brown RC. A review of cleaning technologies for biomass-derived syngas. Biomass and Bioenergy 2013;52:54–84. doi:10.1016/J.BIOMBIOE.2013.02.036.

[90] Kurkela E, Kurkela M. Advanced Biomass Gasification for High-Efficiency Power. Publishable Final Activity Report of BiGPower Project. 2009.

[91] Zwart RWR, Drift A Van der, Bos A, Visser HJM, Cieplik MK, Könemann HWJ. Oil-based gas washing—Flexible tar removal for high-efficient production of clean heat and power as well as sustainable fuels and chemicals. Environmental Progress & Sustainable Energy 2009;28:324–35. doi:10.1002/EP.10383.

[92] Thielert H, WOZNY G, Richter D. Removal of aromatic hydrocarbons from coking gas by absorption. EP2162511B1, 2008.

[93] Müller MT, Thielert H, Richter D, Repke J-U, Wozny G. EXPERIMENTAL INVESTIGATIONS ON BIODIESEL AS AN ALTERNATIVE ABSORBENT FOR THE RECOVERY OF AROMATIC HYDROCARBONS UNDER INDUSTRIAL CONDITIONS. Distillation Absorption 2010, 2010.

[94] Ratnasamy C, Wagner JP. Water Gas Shift Catalysis. Catalysis Reviews 2009;51:325–440. doi:10.1080/01614940903048661.

[95] Levalley TL, Richard AR, Fan M. The progress in water gas shift and steam reforming hydrogen production technologies – A review. International Journal of Hydrogen Energy 2014;39:16983–7000. doi:10.1016/J.IJHYDENE.2014.08.041.

[96] J BSR, Loganathan M, Shantha MS. A Review of the Water Gas Shift Reaction Kinetics. International Journal of Chemical Reactor Engineering 2010;8. doi:10.2202/1542-6580.2238.

[97] De La Osa AR, De Lucas A, Valverde JL, Romero A, Monteagudo I, Sánchez P. Performance of a sulfur-resistant commercial WGS catalyst employing industrial coal-derived syngas feed. International Journal of Hydrogen Energy 2011;36:44–51. doi:10.1016/J.IJHYDENE.2010.08.127.

[98] Carbo MC, Boon J, Jansen D, van Dijk HAJ, Dijkstra JW, van den Brink RW, et al. Steam demand reduction of water–gas shift reaction in IGCC power plants with pre-combustion

CO2 capture. International Journal of Greenhouse Gas Control 2009;3:712–9. doi:10.1016/J.IJGGC.2009.08.003.

[99] Martelli E, Kreutz T, Carbo M, Consonni S, Jansen D. Shell coal IGCCS with carbon capture: Conventional gas quench vs. innovative configurations. Applied Energy 2011;88:3978–89. doi:10.1016/J.APENERGY.2011.04.046.

[100] Kohl AL, Nielsen RB. Physical Solvents for Acid Gas Removal. Gas Purification 1997:1187–237. doi:10.1016/B978-088415220-0/50014-8.

[101] Heinze C. Konzeption einer Pilotanlage auf Grundlage einer technoökonomischen Bewertung von flexiblen Polygenerationsprozessketten. Technische Universität Darmstadt, 2021.

[102] Mumford KA, Wu Y, Smith KH, Stevens GW. Review of solvent based carbon-dioxide capture technologies. Frontiers of Chemical Science and Engineering 2015 9:2 2015;9:125–41. doi:10.1007/S11705-015-1514-6.

[103] Rackley SA. Absorption capture systems. Carbon Capture and Storage 2017:115–49. doi:10.1016/B978-0-12-812041-5.00006-4.

[104] Bhattacharyya D, Turton R, Zitney SE. Acid gas removal from syngas in IGCC plants. Integrated Gasification Combined Cycle (IGCC) Technologies 2017:385–418. doi:10.1016/B978-0-08-100167-7.00011-1.

[105] Huang W, Zheng D, Xie H, Li Y, Wu W. Hybrid physical-chemical absorption process for carbon capture with strategy of high-pressure absorption/medium-pressure desorption. Applied Energy 2019;239:928–37. doi:10.1016/j.apenergy.2019.02.007.

[106] Miller B. Greenhouse gas – carbon dioxide emissions reduction technologies. Fossil Fuel Emissions Control Technologies 2015:367–438. doi:10.1016/B978-0-12-801566-7.00008-7.

[107] Burr B, Lyddon L. A comparison of physical solvents for acid gas removal. Gas Processors' Association Convention, Grapevine, TX, Bryan, Texas, U.S.A.: 2008.

[108] Higman C. Gasification process technology. Advances in Clean Hydrocarbon Fuel Processing: Science and Technology 2011:155–85. doi:10.1533/9780857093783.2.155.

[109] Cantrell J, McIntyre G, Daniels C, Stewart E. OPERATIONAL CONSIDERATIONS OF SIDE REACTIONS IN GAS SWEETENING SYSTEMS. Laurance Reid Gas Conditioning Conference, Norman, Oklahoma USA: 2017.

[110] Ying J, Raets S, Eimer D. The Activator Mechanism of Piperazine in Aqueous Methyldiethanolamine Solutions. Energy Procedia 2017;114:2078–87. doi:10.1016/J.EGYPRO.2017.03.1342.

[111] Polasek J, Bullin J. Selecting amines for sweetening units. ENERGY PROGRESS 1984;4:146–9.

[112] Gadde S, Wu J, Gulati A, McQuiggan G, Koestlin B, Prade B. Syngas capable combustion systems development for advanced gas turbines. Proceedings of the ASME Turbo Expo, vol. 4, American Society of Mechanical Engineers Digital Collection; 2006, p. 547–54. doi:10.1115/GT2006-90970.

[113] Daniel Brdar R, Jones RM. GE Power Systems GE IGCC Technology and Experience with Advanced Gas Turbines. 2000.

[114] Wang T. An overview of IGCC systems. Integrated Gasification Combined Cycle (IGCC)

Technologies, Woodhead Publishing; 2017, p. 1–80. doi:10.1016/B978-0-08-100167-7.00001-9.

[115] Wolfersdorf C, Meyer B. The current status and future prospects for IGCC systems. Integrated Gasification Combined Cycle (IGCC) Technologies, Woodhead Publishing; 2017, p. 847–89. doi:10.1016/B978-0-08-100167-7.00024-X.

[116] Barnes I. Recent Operating Experience And Improvement Of Commercial IGCC. 2013.

[117] Chiesa P, Lozza G, Mazzocchi L. Using hydrogen as gas turbine fuel. Journal of Engineering for Gas Turbines and Power 2005;127:73–80. doi:10.1115/1.1787513.

[118] Nord LO, Bolland O. Carbon dioxide emission management in power generation. Carbon Dioxide Emission Management in Power Generation 2020:1–310. doi:10.1002/9783527826667.

[119] Shukla AK, Singh O. Performance evaluation of steam injected gas turbine based power plant with inlet evaporative cooling. Applied Thermal Engineering 2016;102:454–64. doi:10.1016/j.applthermaleng.2016.03.136.

[120] Wang T. The gas and steam turbines and combined cycle in IGCC systems. Integrated Gasification Combined Cycle (IGCC) Technologies, Woodhead Publishing; 2017, p. 497–640. doi:10.1016/B978-0-08-100167-7.00028-7.

[121] Alobaid F, Mertens N, Starkloff R, Lanz T, Heinze C, Epple B. Progress in dynamic simulation of thermal power plants. Progress in Energy and Combustion Science 2017;59:79–162. doi:10.1016/j.pecs.2016.11.001.

[122] Keim W. C1 chemistry: potential and developments. Pure and Applied Chemistry 1986;58:825–32.

[123] Kopyscinski J, Schildhauer TJ, Biollaz SMA. Production of synthetic natural gas (SNG) from coal and dry biomass – A technology review from 1950 to 2009. Fuel 2010;89:1763–83. doi:10.1016/J.FUEL.2010.01.027.

[124] Götz M, Lefebvre J, Mörs F, McDaniel Koch A, Graf F, Bajohr S, et al. Renewable Power-to-Gas: A technological and economic review. Renewable Energy 2016;85:1371–90. doi:10.1016/J.RENENE.2015.07.066.

[125] Stockwell DM, Kelkar CP. Liquefaction of Coal. Studies in Surface Science and Catalysis 2004;150:181–267. doi:10.1016/S0167-2991(04)80009-0.

[126] Thiébaut D. Supercritical Fluid Chromatography of Petroleum Products. Supercritical Fluid Chromatography: Handbooks in Separation Science 2017:381–417. doi:10.1016/B978-0-12-809207-1.00013-6.

[127] Kandiyoti R, Herod AA, Bartle KD. Liquefaction: Thermal Breakdown in the Liquid Phase. Solid Fuels and Heavy Hydrocarbon Liquids 2006:161–98. doi:10.1016/B978-008044486-4/50005-2.

[128] VAN DER LAAN GP, BEENACKERS AACM. Kinetics and Selectivity of the Fischer–Tropsch Synthesis: A Literature Review. Catalysis Reviews 1999;41:255–318. doi:10.1081/CR-100101170.

[129] Speight JG. Coal gasification processes for synthetic liquid fuel production. Gasification for Synthetic Fuel Production: Fundamentals, Processes and Applications, Woodhead Publishing; 2015, p. 201–20. doi:10.1016/B978-0-85709-802-3.00009-6.

[130] Zannis TC, Hountalas DT. DI diesel engine performance and emissions from the oxygen enrichment of fuels with various aromatic content. Energy and Fuels 2004;18:659–66.

doi:10.1021/ef0301598.

[131] Olah GA. Towards oil independence through renewable methanol chemistry. Angewandte Chemie - International Edition 2013;52:104–7. doi:10.1002/anie.201204995.

[132] Riaz A, Zahedi G, Klemeš JJ. A review of cleaner production methods for the manufacture of methanol. Journal of Cleaner Production 2013;57:19–37. doi:10.1016/j.jclepro.2013.06.017.

[133] Bussche KM Vanden, Froment GF. A steady-state kinetic model for methanol synthesis and the water gas shift reaction on a commercial Cu/ZnO/Al2O3Catalyst. Journal of Catalysis 1996;161:1–10.

[134] Cryogenics & Lurgi Technologies. METHANOL AND DERIVATIVES PROVEN TECHNOLOGIES FOR OPTIMAL PRODUCTION. 2017.

[135] Haid J, Koss U. Lurgi's Mega-Methanol technology opens the door for a new era in down-stream applications. Studies in Surface Science and Catalysis, vol. 136, Elsevier; 2001, p. 399–404. doi:10.1016/s0167-2991(01)80336-0.

[136] Gootz M, Pardemann R, Meyer B. Flexible operation and control of methanol production from fluctuating syngas feed. 7th International Freiberg/Inner Mongolia conference; Huhhot, Inner Mongolia, China, 2015.

[137] Bany Ata A, Alobaid F, Heinze C, Almoslh A, Sanfeliu A, Epple B. Comparison and validation of three process simulation programs during warm start-up procedure of a combined cycle power plant. Energy Conversion and Management 2020;207:112547. doi:10.1016/j.enconman.2020.112547.

[138] Anantharaman R, Bolland O, Booth N, Van Dorst E, Ekstrom C, Fernandes ES, et al. Enabling advanced pre-combustion capture techniques and plants. 2011.

[139] Krause D, Herdel P, Ströhle J, Epple B. HTW^{TM}-gasification of high volatile bituminous coal in a 500 kWth pilot plant. Fuel 2019;250:306–14. doi:10.1016/j.fuel.2019.04.014.

[140] Thielert D, Richter H. Process for the removal of aromatic hydrocarbons from Kokereigas with biodiesel as a washing liquid and apparatus for carrying out the method. DE102012107336A1, 2012.

[141] Bailer O, Spiegel L, Von Scala C. Structured packings for Distillation, Absorption and Reactive Distillation. Structured Catalysts and Reactors 2005:539–50.

[142] Aspen Technology Inc. Aspen Plus | Leading Process Simulation Software. Aspen Technology, Inc 2020.

[143] Microsoft. Microsoft Excel | Spreadsheet software. MicrosoftCom 2016. https://www.microsoft.com/en-us/microsoft-365/excel (accessed August 6, 2021).

[144] Lewis GN. The Law of Physico-Chemical Change. Proceedings of the American Academy of Arts and Sciences 1901;37:49. doi:10.2307/20021635.

[145] Lewis GN, Randall M, Pitzer KS, Brewer L, Kestin J. Thermodynamics. Journal of Applied Mechanics 1962;29:221–221. doi:10.1115/1.3636482.

[146] Redlich O, Kwong JNS. On the thermodynamics of solutions. V. An equation of state. Fugacities of gaseous solutions. Chemical Reviews 1949;44:233–44. doi:10.1021/cr60137a013.

[147] Smith R, Peters C, Inomata H. Equations of state and formulations for mixtures.

Supercritical Fluid Science and Technology, vol. 4, Elsevier; 2013, p. 333–480. doi:10.1016/B978-0-444-52215-3.00006-4.

[148] Winterbone DE. Equations of State. Advanced Thermodynamics for Engineers, Butterworth-Heinemann; 1997, p. 121–34. doi:10.1016/b978-034067699-8/50009-0.

[149] Soave G. Equilibrium constants from a modified Redlich-Kwong equation of state. Chemical Engineering Science 1972;27:1197–203. doi:10.1016/0009-2509(72)80096-4.

[150] Renon H, Prausnitz JM. Local compositions in thermodynamic excess functions for liquid mixtures. AIChE Journal 1968;14:135–44. doi:10.1002/aic.690140124.

[151] Chen CC, Song Y. Generalized electrolyte-NRTL model for mixed-solvent electrolyte systems. AIChE Journal 2004;50:1928–41. doi:10.1002/aic.10151.

[152] Savuto E, Di Carlo A, Gallucci K, Di Giuliano A, Rapagnà S. Steam gasification of lignite and solid recovered fuel (SRF) in a bench scale fluidized bed gasifier. Waste Management 2020;114:341–50. doi:10.1016/j.wasman.2020.07.016.

[153] RWE. Die WTA-Technik ein modernes Verfahren zur Aufbereitung und Trocknung von Braunkohle. 2009.

[154] Lewis WK, Whitman WG. Principles of Gas Absorption. Industrial and Engineering Chemistry 1924;16:1215–20. doi:10.1021/ie50180a002.

[155] Bottoms RR. Process for Separating Acidic Gases. US Patent 1930;7:1783901 (to Gridler Corp.).

[156] Aaron D, Tsouris C. Separation of CO2 from flue gas: A review. Separation Science and Technology, vol. 40, Taylor & Francis; 2005, p. 321–48. doi:10.1081/SS-200042244.

[157] Edwards TJ, Maurer G, Newman J, Prausnitz JM. Vapor-liquid equilibria in multicomponent aqueous solutions of volatile weak electrolytes. AIChE Journal 1978;24:966–76. doi:10.1002/AIC.690240605.

[158] Bates RG, Pinching GD. Acidic Dissociation Constant and Related Thermodynamic Quantities for Monoethanolammonium Ion in Water From 00 to 50 0 C. Journal of Research of the National Bureau of Standards 1951;46.

[159] Athanassios Vrachnos, Epaminondas Voutsas *,†, Kostis Magoulas † and, Lygeros A. Thermodynamics of Acid Gas−MDEA−Water Systems. Industrial and Engineering Chemistry Research 2004;43:2798–804. doi:10.1021/IE030769V.

[160] Pinsent BRW, Pearson L, Roughton FJW. The kinetics of combination of carbon dioxide with hydroxide ions. Transactions of the Faraday Society 1956;52:1512–20. doi:10.1039/TF9565201512.

[161] Li BH, Zhang N, Smith R. Simulation and analysis of CO2 capture process with aqueous monoethanolamine solution. Applied Energy 2016;161:707–17. doi:10.1016/J.APENERGY.2015.07.010.

[162] Graaf GH, Stamhuis EJ, Beenackers AACM. Kinetics of low-pressure methanol synthesis. Chemical Engineering Science 1988;43:3185–95. doi:10.1016/0009-2509(88)85127-3.

[163] Lim H-W, Park M-J, Kang S-H, Chae H-J, Bae JW, Jun K-W. Modeling of the Kinetics for Methanol Synthesis using Cu/ZnO/Al2O3/ZrO2 Catalyst: Influence of Carbon Dioxide during Hydrogenation. Industrial and Engineering Chemistry Research 2009;48:10448–55. doi:10.1021/IE901081F.

[164] Spliethoff H. Coal-Fuelled Combined Cycle Power Plants. Power Systems, vol. 21, Springer, Berlin, Heidelberg; 2010, p. 469–628. doi:10.1007/978-3-642-02856-4_7.

[165] Gross J, Sadowski G. Perturbed-chain SAFT: An equation of state based on a perturbation theory for chain molecules. Industrial and Engineering Chemistry Research 2001;40:1244–60. doi:10.1021/ie0003887.

[166] Field RP, Brasington R. Baseline Flowsheet Model for IGCC with Carbon Capture. Ind Eng Chem Res 2011;50:11306–12. doi:10.1021/ie200288u.

[167] Dyment J, Watanasiri S. Acid Gas Cleaning using DEPG Physical Solvents : Validation with Experimental and Plant Data. 2015.

[168] James III PhD RE, Kearins D, Turner M, Woods M, Kuehn N, Zoelle A. Cost and Performance Baseline for Fossil Energy Plants Volume 1: Bituminous Coal and Natural Gas to Electricity. 2019. doi:10.2172/1569246.

[169] Ahn H. Process Simulation of a Dual-stage Selexol Process for Pre-combustion Carbon Capture at an Integrated Gasification Combined Cycle Power Plant. Process Systems and Materials for CO 2 Capture, Chichester, UK: John Wiley & Sons, Ltd; 2017, p. 609–28. doi:10.1002/9781119106418.ch24.

[170] Ahn H, Kapetaki Z, Brandani P, Brandani S. Process simulation of a dual-stage selexol unit for pre-combustion carbon capture at an IGCC power plant. Energy Procedia, vol. 63, Elsevier Ltd; 2014, p. 1751–5. doi:10.1016/j.egypro.2014.11.182.

[171] Luberti M, Friedrich D, Brandani S, Ahn H. Design of a H2 PSA for cogeneration of ultrapure hydrogen and power at an advanced integrated gasification combined cycle with pre-combustion capture. Adsorption 2014;20:511–24. doi:10.1007/s10450-013-9598-0.

[172] MCJANNETT J. Using physical solvent in multiple applications. Petroleum Technology Quarterly 2012. https://www.digitalrefining.com/article/1000359/using-physical-solvent-in-multiple-applications#.YRTUNYgzaUk (accessed August 12, 2021).

[173] Sun L, Smith R. Rectisol wash process simulation and analysis. Journal of Cleaner Production 2013;39:321–8. doi:10.1016/j.jclepro.2012.05.049.

[174] Gao N, Zhai C, Sun W, Zhang X. Equation oriented method for Rectisol wash modeling and analysis. Chinese Journal of Chemical Engineering 2015;23:1530–5. doi:10.1016/j.cjche.2015.03.010.

[175] Gatti M, Marechal F, Martelli E, Consonni S. Thermodynamic analysis, energy integration and flowsheet improvement of a methanol absorption acid gas removal process. Chemical Engineering Transactions, vol. 35, 2013, p. 211–6. doi:10.3303/CET1335035.

[176] Munder B, Grob S, Fritz P, Keresteciogl u, Meier H, Prelipceanu A, et al. Selection of Wash Systems for Sour Gas Removal. 4 th International Freiberg Conference on IGCC & XtL Technologies, Dreseden, Germany: 2010.

[177] Padurean A, Cormos CC, Agachi PS. Pre-combustion carbon dioxide capture by gas–liquid absorption for Integrated Gasification Combined Cycle power plants. International Journal of Greenhouse Gas Control 2012;7:1–11. doi:10.1016/J.IJGGC.2011.12.007.

[178] Lee WS, Lee JC, Oh HT, Baek SW, Oh M, Lee CH. Performance, economic and exergy analyses of carbon capture processes for a 300 MW class integrated gasification combined cycle power plant. Energy 2017;134:731–42. doi:10.1016/j.energy.2017.06.059.

[179] Bany Ata A, Seufert PM, Heinze C, Alobaid F, Epple B. Optimization of Integrated Gasification Combined-Cycle Power Plant for Polygeneration of Power and Chemicals. Energies 2021;14:7285. doi:10.3390/en14217285.

[180] Doctor RD, Molburg JC, Thimmapuram P, Berry GF, Livengood CD, Johnson RA. Gasification combined cycle: Carbon dioxide recovery, transport, and disposal. Energy Conversion and Management 1993;34:1113–20. doi:10.1016/0196-8904(93)90060-N.

[181] Preis für Methanol auf dem europäischen Markt bis 2021 | Statista n.d. https://de.statista.com/statistik/daten/studie/730823/umfrage/durchschnittlicher-preis-fuer-methanol-auf-dem-europaeischen-markt/ (accessed September 23, 2021).

[182] Industrial electricity prices including tax Germany 1998-2021 | Statista n.d. https://www.statista.com/statistics/1050448/industrial-electricity-prices-including-tax-germany/ (accessed September 23, 2021).